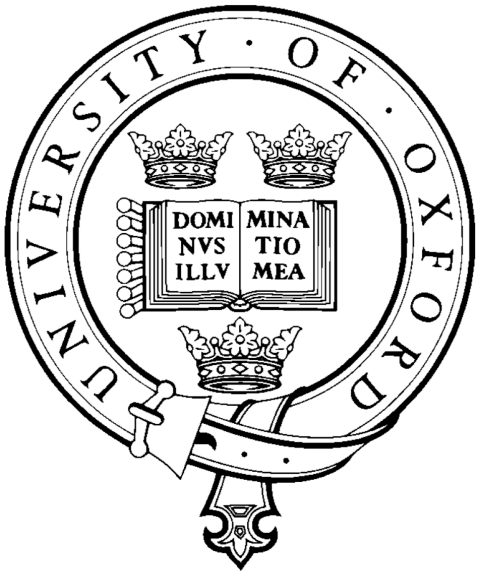
Cell therapy: enhancing the therapeutic potential of a cardiac stromal cell population for delivery after myocardial infarction using miR-210



Rita Alonaizan

St Catherine's College

Department of Physiology, Anatomy & Genetics

University of Oxford

A thesis submitted for the degree of *Doctor of Philosophy*

Michaelmas 2020

Acknowledgments

This four-year journey would not have been possible without the support and contribution of a number of people, to whom I am very grateful.

Firstly, I would like to thank my supervisors: Professor Carolyn Carr for her guidance and support throughout this rewarding and challenging learning experience and for always being available to discuss scientific ideas; and Professor Nicola Smart for her valuable scientific input and for always being keen to offer help when I needed extra support. I would like to thank Professor Kieran Clarke for her support and welcoming me into the Cardiac Metabolism Research Group. I also owe a thank you to my transfer and confirmation of status examiners Professors Manuela Zaccolo, Shankar Srinivas and Duncan Sparrow, as well as my final viva examiners Professors Paul Riley and Sian Harding for their valuable contribution.

Secondly, a huge thank you to past and present members of the CMRG for making my DPhil journey enjoyable and for their friendship and advice: Dr. Cher-Rin Chong, Javier Gilbert-Jaramillo, Ujang Purnama, Claudia Montes, Dr. Matthew Kerr, Dr. Heba Al-Siddiqi, Dr. Sophia Malandraki-Miller, Azrul Abdul Kadir, David Dearlove, Dr. Kerstin Timm, Andrew Tyler, Tony Zhou, Mala Gunadasa-Rohling, Dr. Justin Lau, Dr. Adrian Soto Mota, Dr. Colleen Lopez, Dr. Arne Bruyneel, Dr. Maria de Luz Fialho, Dr. Dragana Savic, Dr. Jack Miller, Dr. Andrew Lewis, Dr. Michael Dodd, Vicky Ball, Nicola Dixon, Yvonne Green, Professor Lisa Heather, Dr. Rhys Evans and Professor Damian Tyler. In particular, to my friend Cher-Rin for all the times she helped me during tough phases and for always encouraging me and being an amazing travel companion! To Javier for all the dinners he cooked for us and for being my Oxford family during Christmas. To Ujang, the reigning queen of the lab, for keeping me company in the culture room, always making me smile, and for experimental help when I was finishing up. To Claudia, for teatime chats and bringing joy to the office.

I would like to thank collaborators and everyone who provided tools for this research to be achieved: Dr. Michela Noseda for collaborating on the single-cell qRT-PCR experiment, Mala Gunadasa-Rohling for performing the MI surgery, Dr. Andrew Lewis for help with the echocardiography, Smart group for providing me with technical guidance when needed, Dr. Tara Caffrey (Wade-Martins group) for help with the retroviral transduction, Riley group for the *R26R-EYFP* mice, Poulton group for the *RFP-MIT;EGFP-LC3* MEFs, Martelli group (University of Milan) for the miR-210 retrovirus, Ferreira group (University of Coimbra) for the NP170, Michal Maj and Line Eriksen at the Dunn School FACS Facility, Dr. Alan Wainman at the Dunn School Bioimaging Facility, and the administration and support team at DPAG including Talitha Smith, Sean Alderson, Gary Mort and Lee Brown. I would like to thank my students: Emma Smith, Jack Oldbury, Junyan Wang and Esra Şengül for assisting me in my experiments. I am also thankful to one of the most helpful individuals at DPAG, Sarah Noujaim.

I am grateful to my funders, the King Faisal Specialist Hospital and Research Centre, and the Saudi Arabian Cultural Bureau and Ministry of Education for their continuous support.

Finally, a very special thank you to my family.. thank you for always believing in me. To my parents Maryam Alhumaidan and Khalid Alonaizan, your sacrifices to support me throughout all my endeavours and your unconditional love and encouragement are incomparable; I wouldn't be here without all you have done for me. To my brothers Mohammad and Abdulnasser, thank you for all the happiness (and Maltesers) you bring into my life. I am very lucky to have you.

Dedication

To my role model and late uncle

Ali Alonaizan

Abstract

Cardiovascular diseases are the number one cause of death globally and are a major contributor to reduced quality of life. Despite the development of improved pharmacological therapy and surgical interventions, myocardial infarction (MI) still has a poor prognosis. Therefore, the search for new treatment strategies is becoming increasingly urgent. Many avenues have been under investigation, but this thesis addressed the use of cardiac cell therapy to repair the heart after MI. Cell therapy using cardiac stromal or progenitor populations emerged about two decades ago. However, the identity of these populations has been under debate and the field has been hindered by limitations that include low cell retention following transplantation.

Firstly, this thesis aimed to characterise a slowly adhering population of unsorted stromal cells isolated from adult mouse atrial appendages using a collagenase and trypsin protocol (CTs). CTs were compared to other atrial stromal populations including the cardiosphere-derived cells (CDCs), which have been shown to have a therapeutic effect in pre-clinical models of MI. Single-cell qRT-PCR revealed that CTs resembled CDCs in the expression of cardiogenic transcription factors but were also enriched for *Tcf21* and the macrophage-associated genes *Mrc1* and *Csf1r*.

Secondly, I investigated the overexpression of miR-210, as a pro-survival miRNA, in our population of interest, the CTs. *In vitro* studies showed that miR-210 has an anti-apoptotic effect and a role in downregulating mitochondrial autophagy and fission. Moreover, miR-210 partially rescued the gene expression profile of CTs that shifted following starvation and enhanced their paracrine potential. Finally, we tested the ability of miR-210 to enhance the retention of CTs *in vivo* in a mouse MI model but did not find a significant improvement.

In summary, this thesis provides valuable insights into the heterogeneity of cardiac stromal populations, the mechanisms of action of miR-210, and the use of this miRNA to enhance the therapeutic potential of cells for cardiac cell therapy.

Research outcomes

Publications:

1. Malandraki-Miller, S., Lopez, C., **Alonaizan, R.**, Purnama, U., Perbellini, F., Pakzad, K., Carr, C., **2019**. Metabolic flux analyses to assess the differentiation of adult cardiac progenitors after fatty acid supplementation. Stem Cell Research. https://doi.org/10.1016/j.scr.2019.101458
2. Constantinides, C., McNeill, E., Carnicer, R., Zen, A.A.H., Urruela, R.S., Shaw, A., Patel, J., Swider, E., **Alonaizan, R.**, Potamiti, L., Hadjisavvas, A., et al., **2018**. Improved cellular uptake of perfluorocarbon nanoparticles for in vivo murine cardiac 19F MRS/MRI and temporal tracking of progenitor cells. Nanomedicine: Nanotechnology, Biology and Medicine. https://doi.org/10.1016/j.nano.2018.10.014
3. Lopez, C.*, Al-Siddiqi, H.*, Purnama, U., Iftekhar, S., Bruyneel, A., Kerr, M., Nazir, R., da Luz Fialho, M., Malandraki-Miller, S., **Alonaizan, R.**, Kermani, F., Heather, L., Czernuszka, J., Carr, C. Physiological and pharmacological stimulation for in vitro maturation of substrate metabolism in human induced pluripotent stem cell-derived cardiomyocytes (in review).

Scientific presentations:

Oral:

- BHF CRM Imperial Meeting 2019
- Oxford Sherrington talks 2019

Posters:

- Society for Developmental Biology Annual Meeting, Boston 2019
- BHF CRM Joint Centre Annual Meeting, Oxford 2019
- Development and Cell Biology Theme Day, Oxford 2019
- Young Embryologists Network meeting, London 2019
- MitOX annual meeting, Oxford (**poster prize**) 2019
- ISHR-ES meeting, Amsterdam (**published abstract**) 2018
- BHF Centre of Research Excellence Annual Symposium, Oxford 2018
- Mitochondrial Biology & Selective Autophagy Keystone Symposium, Kyoto 2018
- International Society of Stem Cell Research, Boston 2017
- BHF CRM Joint Centre Annual Meeting, Nottingham 2017
- BHF Centre of Research Excellence Annual Symposium, Oxford 2017
- Regeneration Nature Conference, Milan 2017
- MitOX annual meeting, Oxford 2017

Table of contents

1 INTRODUCTION 2

1.1 MYOCARDIAL INFARCTION 2
1.2 HEART DEVELOPMENT 3
1.3 HEART REGENERATION 6
1.4 CAN HEART REGENERATION BE ACHIEVED BY CELL THERAPY? 8
1.4.1 Mesenchymal stem cells 8
1.4.2 Fibroblasts 10
1.4.3 Proposed populations of adult mammalian cardiac progenitors 12
1.5 CELL THERAPY – MECHANISMS OF ACTION AND CURRENT LIMITATIONS 18
1.5.1 MicroRNAs 22
1.6 HYPOTHESIS AND PROJECT AIMS: 28
1.6.1 Hypothesis: miR-210 overexpression enhances the therapeutic potential of cardiac stromal cells for transplantation after MI. 28
1.6.2 Project aims: 28

2 MATERIALS AND METHODS 31

2.1 MICE 31
2.1.1 Tg(CAG-EGFP)1Osb/J mouse model 31
2.1.2 Sarcolipin$^{Cre/+}$ mouse model 31
2.2 ISOLATION AND EXPANSION OF MOUSE CARDIAC STROMAL CELLS 31
2.2.1 Collagenase trypsin cells (CTs) 32
2.2.2 Cardiosphere-derived cells (CDCs) 32
2.3 CELL CULTURE CONDITIONS 33
2.3.1 CTs and CDCs 33
2.3.2 HL-1 cardiomyocytes 34
2.3.3 Adult cardiac fibroblasts 34
2.3.4 Human umbilical vein endothelial cells (HUVECs) 34
2.3.5 RFP-MIT;EGFP-LC3 mouse embryonic fibroblasts 35
2.4 IMMUNOHISTOCHEMISTRY 35
2.4.1 Tissue cryosectioning 35
2.5 IMMUNOCYTOCHEMISTRY 36
2.5.1 Sample preparation and blocking 36
2.5.2 Antibody staining, DAPI, and mounting 36
2.6 MIRNA AND SIRNA TRANSFECTION USING DHARMAFECT 36
2.7 QUANTITATIVE REVERSE TRANSCRIPTION POLYMERASE CHAIN REACTION (QRT-PCR) 37
2.7.1 Primer design 37
2.7.2 RNA extraction and cDNA synthesis 37

2.7.3 qRT-PCR reaction and analysis 38
2.8 SINGLE-CELL QRT-PCR 39
2.9 ASSESSING MITOCHONDRIAL COPY NUMBER BY QPCR 40
2.10 ASSESSING MIR-210 LEVELS BY QRT-PCR 40
2.11 FAM-FLICA POLY CASPASE ACTIVITY ASSAY 41
2.12 TERMINAL DEOXYNUCLEOTIDYL TRANSFERASE DUTP NICK END LABELLING ASSAY (TUNEL) ASSAY 42
2.13 MITOTRACKER RED CMXROS STAINING 42
2.14 METABOLIC ANALYSES 43
2.14.1 ^{14}C-glucose oxidation measurement 43
2.14.2 ^{3}H glucose measurement of glycolytic flux 44
2.15 GROWTH FACTOR ARRAY 46
2.16 NANOPARTICLE CELL TRANSFECTION 46
2.17 MIR-210 OVEREXPRESSION USING RETROVIRAL TRANSDUCTION 47
2.17.1 Bacterial transformation 47
2.17.2 Miniprep, maxiprep, and restriction digests 48
2.17.3 Retroviral packaging using Phoenix-Ampho cells 49
2.17.4 CT retroviral transduction 49
2.18 MOUSE INFARCT SURGERY 50
2.19 ECHOCARDIOGRAPHY 51
2.20 HEART DISSOCIATION AND FLOW CYTOMETRY 51
2.21 SERUM PREPARATION AND CARDIAC TROPONIN I ELISA 52
2.22 STATISTICAL ANALYSIS 52
2.23 ILLUSTRATIONS 52

3 RESULTS CHAPTER 1 54

3.1 INTRODUCTION 54
3.1.1 The identity of proposed populations of adult mammalian cardiac progenitors 54
3.1.2 A novel protocol for the isolation of cardiac stromal cells 55
3.1.3 Aims 57
3.2 RESULTS 59
3.2.1 Immunophenotypic analysis of CTs 59
3.2.2 Characterisation of CT morphology and gene expression profile in comparison to CDCs and CFs 62
..... 72
3.2.3 Growth factor release by CTs in comparison to CDCs and CFs 73
3.2.4 CTs have a superior survival potential compared to CFs, but not CDCs, following serum starvation 76
3.3 DISCUSSION 77

3.3.1 Characterisation of CT morphology and gene expression profile in comparison to CDCs and CFs 77
3.3.2 Growth factor release by CTs in comparison to CDCs and CFs 84
3.3.3 CTs have a superior survival potential compared to CFs, but not CDCs, following serum starvation 86

4 RESULTS CHAPTER 2 97

4.1 INTRODUCTION 97
4.1.1 Cell death pathways 97
4.1.2 Aims 104
4.2 RESULTS 105
4.2.1 Optimisation of miR-210 delivery into CTs 105
4.2.2 miR-210 inhibits apoptotic cell death and has a role in the regulation of mitochondrial fission and autophagy in CTs 112
4.3 DISCUSSION 139
4.3.1 Optimisation of miR-210 delivery into CTs 139
4.3.2 miR-210 inhibits apoptotic cell death 140
4.3.3 miR-210 has a role in the regulation of mitochondrial fission and autophagy in CTs 141

5 RESULTS CHAPTER 3 152

5.1 INTRODUCTION 152
5.1.1 Harnessing advances in the field of microRNA therapeutics for cell therapy 152
5.1.2 Mouse heart LAD ligation as an MI model 153
5.1.3 Aims 155
5.2 RESULTS 156
5.2.1 miR-210 transfection partially reversed the effect of serum starvation on the CT gene expression profile 156
5.2.2 The effect of miR-210 on the paracrine potential of CTs 164
5.2.3 The effect of miR-210 transfection on CT retention 24 hours post MI 172
5.2.4 Echocardiography and serum cTnI levels 24 hours post MI 175
5.3 DISCUSSION 178
5.3.1 miR-210 transfection partially reversed the effect of serum starvation on the CT gene expression profile 178
5.3.2 The effect of miR-210 on the paracrine potential of CTs 180
5.3.3 The effect of miR-210 transfection on CT retention 24 hours post MI 183

6 CONCLUSION 186

6.1 STUDY LIMITATIONS AND CHALLENGES 191

7 APPENDICES 194

8 BIBLIOGRAPHY 206

List of figures

Figure 1.1 Differential regenerative capacities of the hearts of different organisms 8
Figure 1.2 Cell types of the healthy adult heart 12
Figure 1.3 Proposed mechanisms of action of cardiac cell therapy using CPCs 21
Figure 1.4 The canonical miRNA biogenesis pathway 24
Figure 2.1 Schematic of the use of radiolabelled substrates in metabolic assays 45
Figure 3.1 Isolation method of the three cardiac stromal populations, CTs, CDCs and CFs 57
Figure 3.2 Overview of the single-cell qRT-PCR experiment used to characterise the three cardiac stromal populations, in comparison to HL-1 cardiomyocytes 58
Figure 3.3 CTs are positive for fibroblast-associated markers 60
Figure 3.4 No α sarcomeric actinin detected in CTs 61
Figure 3.5 CDCs and CFs are positive for fibroblast-associated markers 62
Figure 3.6 Morphological analysis of the three cardiac stromal populations 63
Figure 3.7 Single-cell analysis reveal an enrichment of *Tcf21* and low expression of *Tbx5* in CTs, compared to CDCs and CFs 67
Figure 3.8 PCA of the three cardiac stromal population and HL-1 cardiomyocytes 69
Figure 3.9 Statistical analysis of the single-cell qRT-PCR data 71
Figure 3.10 Gene correlation plot derived from the single-cell qRT-PCR data 72
Figure 3.11 Growth factor array comparing the three cardiac stromal populations 74
Figure 3.12 CTs demonstrate superior survival potential to that of CFs 76
Figure 4.1 The extrinsic and intrinsic pathways of apoptosis 99
Figure 4.2 Mitophagy pathways 104
Figure 4.3 Delivery of miR-210 into CTs using NP170 106
Figure 4.4 Retroviral transduction of miR-210 in comparison to the DharmaFECT reagent 108
Figure 4.5 miR-210 levels in CTs over 3 days following transfection using the DharmaFECT reagent 109
Figure 4.6 Dy547-miRNA levels in CTs over 3 days following transfection using the DharmaFECT reagent 111
Figure 4.7 miR-210-transfected CTs show decreased Casp8ap2 mRNA levels and poly-caspase activity following serum starvation 112
Figure 4.8 miR-210-transfected CTs show decreased TUNEL+ cells following serum starvation 113
Figure 4.9 miR-210 downregulates the expression of glycerol-3-phosphate dehydrogenase 1-like (*Gpd1l*), a regulator of HIF1α stability 116
Figure 4.10 Hypoxic culture upregulates the mRNA levels of mitophagy-associated genes in CTs 117
Figure 4.11 Validation of *Bnip3* siRNAs 118
Figure 4.12 *Bnip3* knockdown in miR-210-transfected CTs TUNEL assay 119
Figure 4.13 miR-210-transfected CTs show decreased *Nix*, but not *Bnip3*, mRNA levels 122
Figure 4.14 miR-210-transfected CTs show decreased mRNA levels of mitophagy-associated genes 125
Figure 4.15 Attempts at visualising mitophagy using LC3 as a marker of autophagosomes 127
Figure 4.16 Mitotracker retention in miR-210-transfected CTs 129
Figure 4.17 miR-210-transfected CTs show increased mitochondrial copy number 131

Figure 4.18 miR-210-transfected CTs show decreased mitochondrial fission 133
Figure 4.19 The effect of miR-210 on the metabolic profile of CTs 134
Figure 4.20 mRNA levels of hypoxia-associated genes in miR-210-transfected CTs 137
Figure 5.1 Overview of the in vivo experiment used to assess CT retention following miR-210 transfection in a mouse MI model 155
Figure 5.2 Single-cell gene expression profiles of CTs following miR-210 transfection and/or serum starvation 160
Figure 5.3 Statistical analysis of the single-cell qRT-PCR data 161
Figure 5.4 PCA and statistical analysis of serum starved CTs transfected with a negative miRNA or miR-210 in comparison to an untransfected control 163
Figure 5.5 Growth factor array on the conditioned media of miR-210-transfected CTs 165
Figure 5.6 Conditioned media of normoxic miR-210-overexpressing CTs enhances HUVEC proliferation 167
Figure 5.7 Optimisation of simulated ischaemia/reperfusion in HL-1 cardiomyocytes 169
Figure 5.8 Conditioned media of normoxic miR-210-overexpressing CTs has an anti-apoptotic effect in HL-1 cardiomyocytes subjected to simulated ischaemia/reperfusion 170
Figure 5.9 The effect of miR-210 transfection on CT retention 24 hours post MI 174
Figure 5.10 Echocardiography measurements in the infarcted mice used in this study 176
Figure 5.11 Serum cardiac troponin I levels in the infarcted mice used in this study 177
Figure 6.1 Overview of the effect of miR-210 overexpression on CTs 190

List of tables

Table 2.1 DharmaFECT-miRNA and -siRNA transfection solutions 37
Table 2.2 Components of the qRT-PCR reaction 38
Table 2.3 Components of the pre-amplification reaction 40
Table 2.4 Components of the miR-210 qRT-PCR reaction 41
Table 3.1 The markers used in the single-cell qRT-PCR characterisation 89
Table 3.2 The growth factors assessed in cell conditioned media using antibody arrays and their relevant functions 94
Table 4.1 Summary of the different parameters measured in response to miR-210 transfection, hypoxic culture and/or serum starvation 150

Abbreviations

AGO	Argonaute
APAF-1	Apoptotic protease activating factor 1
AR	Amphiregulin
Atg	Autophagy-related gene
B2m	Beta-2 microglobulin
bFGF	Basic fibroblast growth factor
BH domain	BCL2 homology domain
BHF	British Heart Foundation
BID	BH3-interacting death domain agonist
Bim	Bcl-2-like protein 11
BMP	Bone morphogenetic protein
Bnip3	BCL2 interacting protein
BSA	Bovine serum albumin
Casp8ap2	Caspase 8 associated protein 2
Caspase	Cysteine aspartyl-specific protease
CCCP	Carbonyl cyanide m-chlorophenyl hydrazone
CD	Cluster of differentiation
CDC	Cardiosphere-derived cell
Cdh5	Cadherin 5
CEM	Complete explant medium
CF	Cardiac fibroblasts
CFU-F	Colony-forming unit-fibroblastic cell
CGM	Cardiosphere growth medium
Cnn1	Calponin 1
Col1a1	Collagen, type I, alpha 1
Colec11	Collectin subfamily member 11
COX10	Cytochrome c oxidase assembly protein
CPM	Counts per minute
Csf1r	Colony-stimulating factor 1 receptor
CT	Collagenase-trypsin cell
CTCF	Corrected total cell fluorescence
cTnI	Cardiac troponin I
cTnT	Cardiac troponin T
Cx3cr1	CX3C chemokine receptor 1
DAMP	Danger-associated molecular pattern
Ddr2	Discoidin domain receptor tyrosine kinase 2
DGCR8	DiGeorge syndrome chromosomal (or critical) region 8
DISC	Death-inducing signalling complex
DPBS	Dulbecco's phosphate-buffered saline
Drp1	Dynamin related protein 1
E	Embryonic day
EDC	Explant-derived cell
Efna3	Ephrin A3
EGF	Epidermal growth factor
EGM	Endothelial cell growth medium
ELISA	Enzyme-linked immunosorbent assay

EMT	Epithelial-to-mesenchymal-transition
EPDC	Epicardium-derived cell
ESC	Embryonic stem cell
EXP5	Exportin 5
FBS	Foetal bovine serum
FCF-C	Fibroblast colony-forming cell
FDA	US Food and Drug Administration
FHF	First heart field
FSP	Fibroblast surface protein
Gapdh	Glyceraldehyde 3-phosphate dehydrogenase
Gata4	GATA binding protein 4
GCSF	Granulocyte-colony stimulating factor
Glut1	Glucose transporter type 1
GM-CSF	Granulocyte-macrophage colony-stimulating factor
Gpd1l	Glycerol-3-phosphate dehydrogenase 1-like
GRK2	G protein-coupled receptor kinase 2
Hand	Heart- and neural crest derivatives-expressed protein
HF	Heart failure
HGF	Hepatocyte growth factor
HIF	Hypoxia-inducible factor
HLA-DR	Human Leukocyte Antigen – DR isotype
HRE	Hypoxia responsive element
HRPT	Hypoxanthine-guanine phosphoribosyltransferase
HSP47	Heat shock protein 47
HUVEC	Human umbilical vein endothelial cell
I/R	Ischaemia/reperfusion
IACUC	Institutional Animal Care and Use Committee
IGF	Insulin-like growth factor
IGFBP	Insulin-like growth factor-binding protein
IL	Interleukin
IMM	Inner mitochondrial membrane
ISCU	Iron sulphur scaffold protein
Isl1	Islet1
ISO	Isoproterenol
Kcna1	Potassium voltage-gated channel subfamily A member 1
Kcnj8	Potassium inwardly-rectifying channel, subfamily J, member 8
Kdr	Kinase insert domain receptor
KIT	Stem cell growth factor receptor, also known as proto-oncogene KIT or CD117
Klf4	Kruppel like factor 4
LAD artery	Left anterior descending artery
LC3	Microtubule-associated protein light chain 3
LIR	LC3 interacting region
Ly6a	Lymphocyte antigen 6 complex
M-CSF	macrophage colony- stimulating factor
Medag	Mesenteric oestrogen-dependent adipogenesis protein
MEF	Mouse embryonic fibroblast
Mef2	Myocyte enhancer factor-2
Mesp1	Mesoderm posterior bHLH transcription factor 1
Mfn	Mitofusin

MI	Myocardial infarction
miRNA/ miR	Micro-Ribonucleic Acid
MOMP	Mitochondrial outer membrane permeabilisation
Mrc1	Mannose receptor C-type 1
MRI	Magnetic resonance imaging
Ms4a4d	Membrane-spanning 4-domains subfamily A member 4D
MSC	Mesenchymal stem cells
Mt-Nd1	Mitochondrial NADH dehydrogenase 1
Myh	Myosin heavy chain
Myl	Myosin light chain
Ng2	Neuron-glial antigen 2
NK cells	Natural killer cells
NKX2-5	NK2 homeobox 5
NP	Nanoparticle
Nppa	Natriuretic peptide A
Oct4	Octamer-binding transcription factor 4 or Pou5f1
OMM	Outer mitochondrial membrane
Opa1	Mitochondrial dynamin like GTPase
PCA	Principle component analysis
PCD	Programmed cell death
Pdgfr	Platelet-derived growth factor receptor
Pdk1	Pyruvate dehydrogenase kinase 1
PE	Phosphatidylethanolamine
PFA	Paraformaldehyde
PFCE	Perfluoro-1,5-crown ether
Phds	Prolyl hydroxylases
Pink1	PTEN-induced kinase 1
PLGA	Poly(lactic acid-co-glycolic acid)
Plp1	Proteolipid protein 1
Pol II	RNA polymerase II
Pre-miRNA	Precursor miRNA
Prg4	Proteoglycan 4
Pri-miRNA	Primary miRNA
PS	Protamine sulphate
PSC	Pluripotent stem cell
PSG	Penicillin, Streptomycin, L-Glutamine
Ptprc	Protein tyrosine phosphatase, receptor type, C
qRT-PCR	Quantitative reverse transcription polymerase chain reaction
RAC	Rapidly adhering cell
Raldh2	Retinaldehyde dehydrogenase 2
RISC	RNA-induced silencing complex
ROS	Reactive oxygen species
RT	Room temperature
SAC	Slowly adhering cell
SCA1	Stem cell antigen 1 or lymphocyte antigen 6 complex Ly6a
SCF	Stem cell factor
SHF	Second heart field
SHH	Sonic hedgehog
SLN	Sarcolipin
Sox2	SRY (sex determining region Y)-box 2

SP	Side population
SR	Sarco(endo)plasmic reticulum
tBID	Truncated BH3-interacting death domain agonist
Tbx	T-box
Tcf21	Transcription factor 21
Tert	Telomerase reverse transcriptase
TGFβ	Transforming growth factor beta
TIMPs-1	Tissue inhibitor of metalloproteinases-1
TNF	Tumour necrosis factor
TUNEL assay	Terminal deoxynucleotidyl transferase dUTP nick end labelling assay
Ubc	Ubiquitin C
VEGF	Vascular endothelial growth factor
VEGF-R	Vascular endothelial growth factor receptor
Vim	Vimentin
Vwf	Von Willebrand factor
Wif1	WNT inhibitory factor 1
WNT	Wingless-related integration site
Wt1	Wilms tumour 1
αSA	Sarcomeric α-actinin
αSMA	Alpha smooth muscle actin

CHAPTER 1

Introduction

1 Introduction

1.1 Myocardial infarction

Myocardial infarction (MI) is a leading cause of morbidity and mortality worldwide (WHO). In the UK there are nearly 100,000 hospital visits each year due to MIs (BHF). With advances in MI treatments, that include pharmacological agents and mechanical assist devices, more patients survive the MI, and therefore have an increased risk of developing heart failure (HF), a debilitating and deadly chronic disease. There are more than 900,000 people living with HF in the UK (BHF). This number will continue to rise due to improved survival rates following MI, an ageing population and the lack of a viable cure.

In the late 19th century, it was noted that there was an association between thrombotic occlusion of a coronary artery and MI[1]. However, a later autopsy study demonstrated the lack of coronary occlusion in 31% of deceased patients with an MI[2]. Hence, the controversy around the definition of MI over the years. According to the 2018 Expert Consensus Document by the European Society of Cardiology, MI is defined as prolonged ischaemia-induced cardiomyocyte death as a result of an imbalance between oxygen supply and demand[3]. This can be detected clinically using biomarkers (e.g. cardiac troponins) or using cardiac imaging by echocardiography or MRI. Sarcolemmal disruption, relaxed myofibrils, reduced cellular glycogen, and mitochondrial defects are the first structural changes to occur in an MI[4,5].

As the adult mammalian heart lacks sufficient regenerative capacity, myocardial healing is dependent on the formation of a collagen-based scar where inflammation is an important endogenous response. The healing process has been described in three overlapping phases: the inflammatory phase, the proliferative phase, and the maturation phase[6,7]. In the initial phase, the release of members of the danger-associated molecular patterns (DAMPs) family is triggered by the sudden cardiomyocyte death[8]. Other cell types including resident endothelial

cells, fibroblasts, and mast cells; and newly recruited neutrophils, monocytes and platelets have also been implicated in the activation of the inflammatory response. However, their relative contributions remain unclear. This phase serves the key role of clearing the wound of dead cells and extracellular matrix debris and is subsequently actively suppressed to initiate the proliferative phase of healing.

During the proliferative phase, mononuclear cells and macrophages secrete growth factors to recruit and activate mesenchymal reparative cells, mainly myofibroblasts. Myofibroblasts express contractile proteins, such as α-smooth muscle actin, and secrete extracellular matrix proteins to retain the structural integrity of the heart[9,10]. They are generated by the transdifferentiation of resident cardiac fibroblasts, bone marrow-derived fibroblast progenitors, endothelial cells, smooth muscle cells, and pericytes[11–13]. It has been shown that transforming growth factor β (TGFβ) signalling and active repression of the inflammatory phase are essential for myofibroblast activation[14,15]. Finally, reparative cells undergo apoptotic cell death to end the proliferative phase and the scar matures as cross-linked collagen is formed[6,7].

Currently, heart transplantation is the only long-term cure available to HF patients. However, this is limited by an inadequate number of available donor hearts, the risks associated with the procedure, and the need for chronic immunosuppressants. Therefore, the search for an alternative solution is becoming increasingly more urgent.

1.2 Heart development

Insights into the regulatory mechanisms of heart development can be harnessed to promote heart regeneration and repair. This is based on the concept that developmental paradigms are recapitulated during repair in postnatal tissue.

The heart is the first organ to form during mammalian embryonic development. It is derived from the mesoderm, the middle layer of the early trilaminar embryo germ layers originating from the primitive streak during gastrulation. The basic helix-loop-helix (bHLH) transcription

factor MESP1 is the earliest protein detected in cardiac precursors, where the two mouse MESP paralogs are redundantly required for the specification of cardiac mesoderm[16]. The cardiac crescent emerges at embryonic day 7.5 (E7.5) from the first population of cells to migrate to the heart-forming region, known as the first heart field (FHF). This migration of mesodermal cells is driven by MESP1-induced epithelial-to-mesenchymal-transition (EMT)[17,18] and cardiogenic markers are first detected at this stage[19,20]. It has been shown that spontaneous asynchronous Ca^{2+}-oscillations occur in the forming cardiac crescent at E7.75 prior to the initiation of contraction at E8[21].

The cardiac crescent subsequently expands and migrates to the midline, then fuses to form the linear heart tube. This is followed by a second wave of migrating cells, known as the second heart field (SHF), which induces the heart tube to undergo looping and elongation. The FHF gives rise to the left ventricle, atrioventricular canal, sinus venosus and atria, whereas the SHF contributes to the outflow tract, the right ventricle and portions of the atria[17]. The SHF also gives rise to the proepicardial organ which protrudes into the pericardial cavity and eventually forms the epicardial layer at E9.5[22].

Heart tube looping (E8.5) occurs as a consequence of uneven growth and remodelling leading to the positioning of the venous pole anteriorly and the formation of primitive cardiac chambers. Once formed, the cardiac chambers undergo a complex maturation process involving septation and valve formation by E15. This allows the transition from a smooth heart tube containing immature endocardial and myocardial layers to generate the mature mammalian heart[23]. It has been shown that cardiac neural crest cells, which migrate from the neural tube into the cardiac outflow tract, are not only required for septation[24] but also for normal heart tube looping[25].

The FHF and SHF lineages are regulated by complex regulatory networks involving components of the bone morphogenetic protein (BMP), sonic hedgehog (SHH), fibroblast

growth factor (FGF), wingless-related integration site (WNT), and Notch pathways. For example, BMP arising from the adjacent endoderm induces cardiomyocyte specification, whereas WNT signals from the underlying neural tube and notochord repress it[20]. Both the FHF and SHF lineages are responsive to epicardial- and endocardial-derived signals such as retinoic acid and neuregulin, respectively[26]. Ultimately, a core set of evolutionary conserved transcription factors (NK2, MEF2, GATA, TBX, and HAND) is activated to control cardiac morphogenesis, cell fate, and the expression of genes encoding contractile proteins. These transcription factors also regulate each other to stabilise the cardiogenic program. Other cardiogenic factors that interact with the core set have also been described[19,27].

The upstream input signals activating the core cardiac transcriptional paradigm differ between the FHF and SHF. In the FHF, this is driven by NKX2-5 (NK2 homeobox 5) and GATA4. However, it is driven by the LIM-homeodomain transcription factor Islet1, and the forkhead transcription factor Foxh1 in the SHF. It has been suggested that this is due to the evolutionary addition of the SHF which is unique to amniotes[27]. GATA4 and NKX2-5 are therefore central transcription factors in both the FHF and SHF[20].

The MADS box transcription enhancer factor MEF2 is a key component of muscle gene regulatory networks as it is required for the specification of all muscle cell types. In cardiomyocytes, MEF2 interacts with the other components of the core set to regulate gene expression, whereas in skeletal muscle it interacts with the MyoD family[28]. The vertebrate MEF2 family comprises 4 members where MEF2c is required for the specification of cardiac structures in the SHF[27,29].

Other factors that are differentially expressed between the heart fields include members of the TBX (T-box) family. TBX5 plays an important role in the development of the FHF, whereas TBX1 is a central regulator of the SHF as it is necessary for proper development of the outflow tract[30]. SHH indirectly maintains *Tbx1* expression by inducing forkhead-containing

transcription factors[31]. On the other hand, TBX20 is required for the expansion of cells from both heart fields[32]. Moreover, the bHLH transcription factors HAND1 and HAND2 are preferentially enriched in the FHF and SHF, respectively[33].

1.3 Heart regeneration

During development, cardiomyocytes arise from cardiomyocyte proliferation[34]. In the postnatal mammalian heart, cardiomyocytes undergo a final round of DNA synthesis without cytokinesis making the majority binucleated and heart growth is mainly achieved through hypertrophy. Hence, the postnatal mammalian heart was once believed to be a post-mitotic organ.

Anversa and colleagues reported evidence of cardiomyocyte renewal in the adult heart, challenging the dogma of cardiomyocyte terminal differentiation[35–37]. A key study provided evidence for human cardiomyocyte renewal by taking advantage of the incorporation of carbon-14 (^{14}C) that was released during atomic bomb testing into DNA[38]. It was found that cardiomyocytes renewed at a rate of 0.5 to 2 %, and this rate declined with age. Multiple studies have attempted to determine the frequency of cardiomyocyte renewal. A study by the Anversa group on cancer patients who had received an infusion of iododeoxyuridine showed a renewal frequency of around 22%[39]. However, studies by the Anversa group have been under scrutiny (see 1.4.3) and cardiomyocyte renewal rates of around 1% were most commonly reported[38,40,41].

Unlike mammals, certain species possess a robust ability to regenerate their hearts and zebrafish (*Danio rerio*) is a classic example. In 2002, Poss *et al*. demonstrated that resection of up to 20% of the adult zebrafish ventricle resulted in complete regeneration within 2 months post injury without fibrotic scar formation[42]. It was later shown that zebrafish heart regeneration is dependent on cardiomyocyte dedifferentiation and proliferation[43,44]. Therefore, regenerative processes have been studied extensively in the zebrafish heart with the ultimate

goal of ‘unlocking’ them in humans. Several factors have been proposed to explain the differences in regenerative capacity including polyploidisation[45], epicardial and endocardial signalling[46,47], oxygen-rich environments[48], and the immune response[49,50].

Not all teleost fish possess this remarkable ability of heart regeneration. For example, Japanese Medaka fish (*Oryzias latipies*) form a fibrotic scar instead[51] and *Astyanax mexicanus* cavefish lost this ability in comparison to their river-dwelling counterparts[52]. Investigating differential responses to cardiac injury provides a unique prospect to pinpoint targets in cardiac regeneration. Another promising model system is the neonatal mouse which retains regenerative capacity for around 7 days following birth[53–57]. Heart regeneration in neonatal mice is also dependent on cardiomyocyte proliferation, suggesting this may be evolutionarily conserved. A regenerative window has also been proposed in human new-borns based on the analysis of post-mortem tissue in the 1920-30s[58,59]. Indeed, case studies demonstrated functional recovery following corrective heart surgeries in infants[60], and MI in a new-born child[61,62] (figure 1.1).

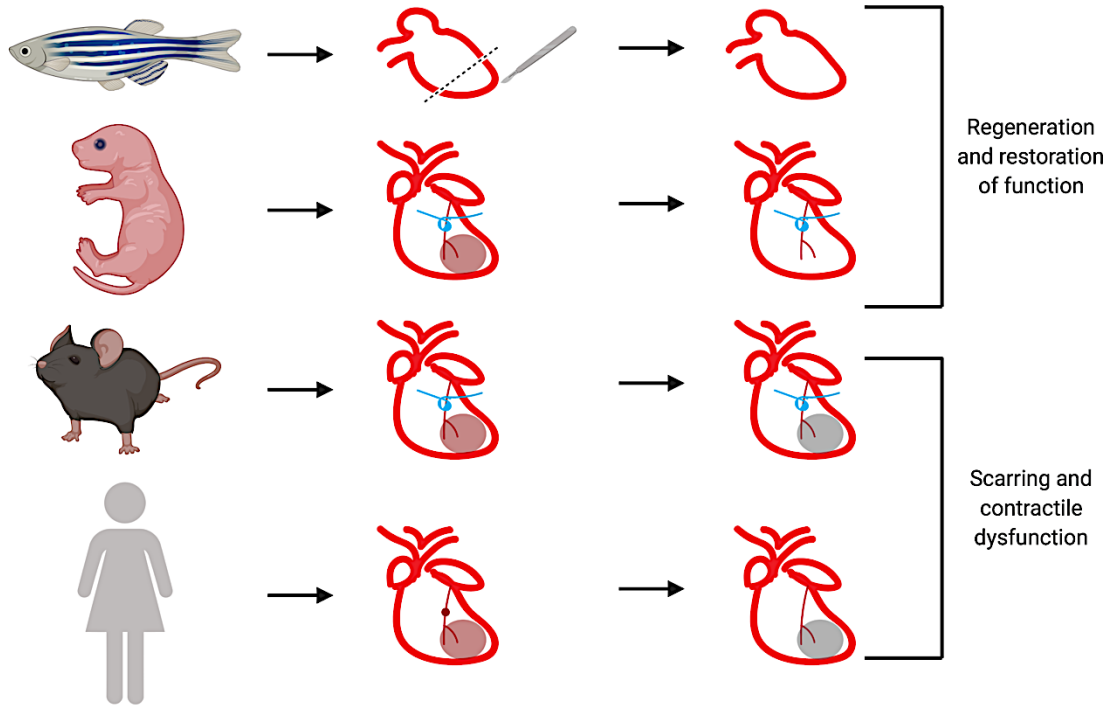


Figure 1.1 Differential regenerative capacities of the hearts of different organisms

Adult zebrafish and neonatal mice undergo robust regeneration in response to cardiac injury through cardiomyocyte proliferation. Models of cardiac injury include, but are not limited to, the shown ventricular apex resection and MI induction by LAD ligation in zebrafish and mice, respectively. Adult mice and humans show scarring in response to an MI injury.

1.4 Can heart regeneration be achieved by cell therapy?

Multiple cell populations have been investigated for therapeutic delivery post MI, including pluripotent stem cell (PSC)-derived cardiomyocytes, and stromal cells such as mesenchymal stem cells, fibroblasts, and cardiac cells. This sub-chapter will discuss the delivery of stromal cells, which is most relevant to this study.

1.4.1 Mesenchymal stem cells

The term 'mesenchymal stem cells' (MSCs) was first coined in 1991 by US biologist Caplan to describe a population of cells isolated from bone marrow[63]. The cells were shown to adhere to plastic and differentiate into osteocytes, chondrocytes, and adipocytes. Since then, cells with similar characteristics have been described in cultures of other foetal and adult tissue including the heart[64,65]. The origin of MSCs is debated but it has been suggested that most are derived

from perivascular cells, pericytes. Pericytes isolated from a variety of tissues give rise to MSCs as identified by their cell surface markers and *in vitro* multipotency. Indeed, MSCs have been isolated from a variety of vascularised tissue including menstrual blood[66].

In addition to the ability of MSCs to differentiate into osteocytes, chondrocytes, and adipocytes, it has been reported that MSCs also give rise to endothelial cells[67,68], cardiomyocytes[69], insulin-producing cells[70], and renal tubular epithelial-like cells[71], among others. MSCs have also been claimed to be hypoimmunogenic[72] and safe for allogeneic transplantation, though this was later challenged[73]. This made MSCs an attractive tool for allogenic cell therapy and since their identification in 1991, research on MSCs has been on the rise with more than 32,000 Medline-indexed articles published so far[74].

However, different markers are used to characterise MSCs which limits the reproducibility of these studies. In 2014, a study showed that proposals submitted to the US Food and Drug Administration (FDA) for MSC-based products did not agree on the tissue sources, manufacturing processes, and molecular characterisation of MSCs[75]. Moreover, it has been shown that MSCs isolated from different tissue varied considerably in their gene expression profile and differentiation potential. This emphasises the need to resolve the MSC identity and to discern standardised criteria which define an MSC, although attempts to do this by the International Society for Cellular Therapy (ISCT) in 2006 had limited success[76].

Moreover, there is controversy about the stemness and functional mechanisms of MSCs due to the lack of evidence of direct regeneration following transplantation. Indeed, Caplan called for a name change from ‘mesenchymal stem cells’ to ‘medicinal signalling cells’ to highlight their paracrine mechanism of action rather than direct contribution to tissue[77]. The pro-angiogenic and anti-apoptotic properties of MSC secretome have been demonstrated in many studies[78,79]. Mouse, rat, and porcine adipose-derived MSC transplantation accelerated angiogenesis and improved heart function following cardiac damage[78,80,81]. MSCs have been shown to be safe

and demonstrated encouraging results in clinical trials[82] and there are currently over 30 ongoing clinical trials of MSC transplantation for cardiac repair. Nonetheless, there is a need for large-scale clinical trials to support the efficacy of this approach, allowing for an allogenic off-the-shelf treatment.

1.4.2 Fibroblasts

The heart is lined by a single-cell epithelial layer called the epicardium forming the inner layer of the pericardium, a double-layered membranous sac covering the heart and root of the large vessels. During development, the epicardium is a source of progenitors that undergo EMT to form cells of different cardiac lineages including coronary smooth muscle cells, and fibroblasts[83–88]. In the adult heart, fibroblasts originate from pre-existing fibroblasts, the epicardium, and endocardium[11,85,88–91], where the contribution of haematopoietic cells was excluded[89,92,93]. Fibroblasts constitute 27% of the total cell population in the adult mouse heart, 67% in the rat heart, and 60-70% in the human heart[94–96] (figure 1.2). This highlights the variability between species in cardiac cellular makeup, which may play a role in cardiac physiological, reparative, and remodelling processes.

Fibroblasts contribute to the synthesis of extracellular matrix proteins, such as collagen, to provide structural tissue support (see 1.1. Myocardial infarction - proliferative phase). They also exhibit functional pluralism, by contributing to immunoregulation, cytoprotection, and angiogenesis[97]. It has been suggested that fibroblasts may have a role in regulating cardiomyocyte survival. Administration of neonatal cardiac fibroblast secretome reduced infarct size in a mouse MI model via paracrine mechanisms involving tissue inhibitor of metalloproteinases-1 (TIMPs-1)[98]. Fibroblasts may also extend ischaemic injury, augmenting cardiomyocyte death, following MI by GRK2 (G protein-coupled receptor kinase 2) signalling which activates pro-inflammatory actions[99]. It remains unknown if different functions are performed by different subtypes of cardiac fibroblasts.

Fibroblasts were first isolated from bone marrow and described by Friedenstein in the 1960s as adherent, clonogenic, and highly proliferative cells that he named fibroblast colony-forming cells (FCF-C), and later colony-forming unit-fibroblastic cells (CFU-F)[100–102]. When transplanted under the kidney capsule of guinea-pigs, fibroblasts formed bone tissue[103]. It was later shown that fibroblasts could also differentiate into fat and cartilage[102]. All these characteristics are very similar to those of MSCs that were later described by Caplan.

Fibroblasts and MSCs are morphologically indistinguishable. Moreover, MSCs are defined by their expression of *CD105*, *CD73*, and *CD90* and lack of expression of *CD45*, *CD34*, *CD14*, *CD9α*, and *HLA-DR*[76]. Multiple studies have shown that fibroblasts follow an almost identical expression pattern of these markers and that MSCs also express fibroblast-associated genes that encode proteins such as vimentin, α smooth muscle actin (αSMA), fibroblast surface protein (FSP), and heat shock protein 47 (HSP47)[104,105]. Nonetheless, a study by Ghazanfari *et al*. in 2016 demonstrated that $CD271^{pos}/CD140a^{low/neg}$ MSCs maintain self-renewal and differentiation into the three lineages in a serial transplantation setting suggesting that they meet stringent stem cell criteria *in vivo*[106]. Other studies suggested that fibroblasts and MSCs can be differentiated by mechanisms by which they modulate immune responses, and their DNA methylation patterns[107].

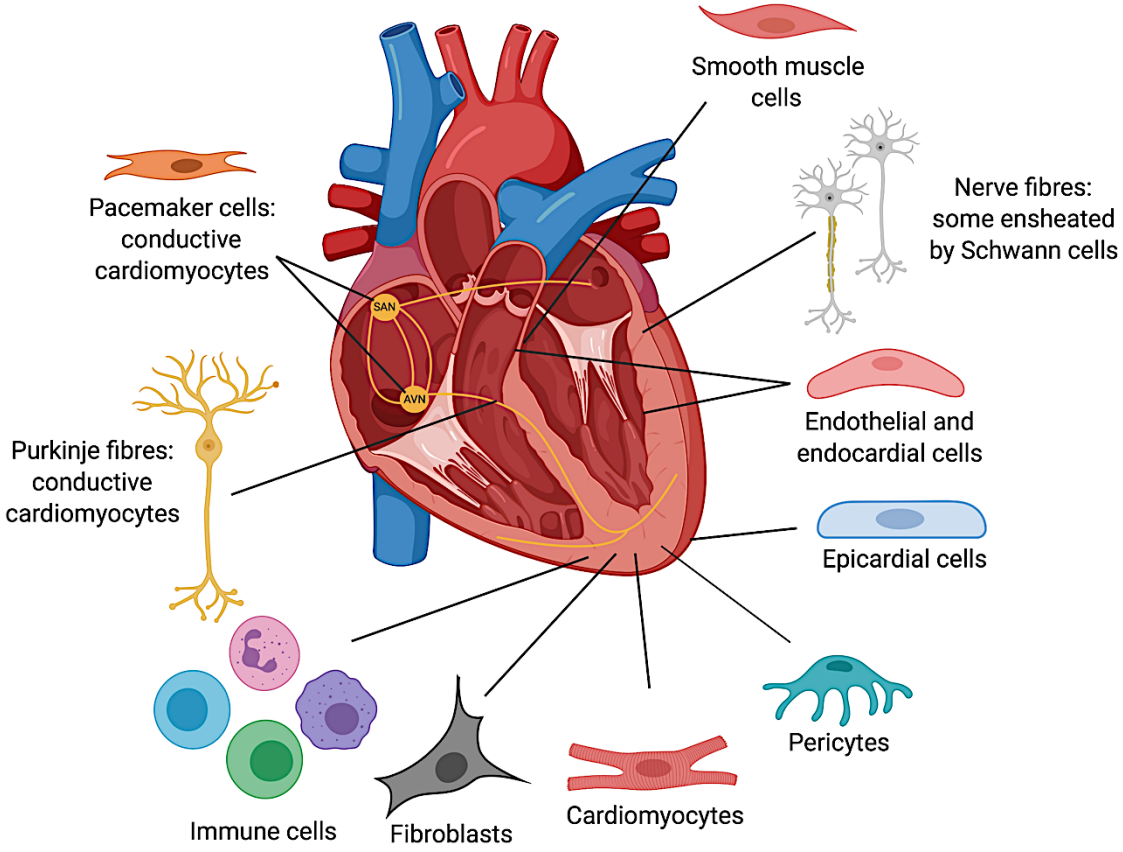


Figure 1.2 Cell types of the healthy adult heart

The main cell types of the heart are the cardiomyocytes, fibroblasts, smooth muscle cells, epicardial cells, pericytes and endothelial cells, which form the endocardium and interior lining of vasculature and valves. The heart contains a network of nerve bundles and nerve fibres, some of which are encapsulated by Schwann cells[108]. Pacemaker and Purkinje cells are specialised cardiomyocytes that form the conduction system of the heart. The sinoatrial node (SAN) and the atrioventricular node (AVN) are formed by groups of pacemaker cells which generate electrical impulses and conduct them from the atria to the ventricles, respectively. Immune populations are found in the healthy adult heart including resident macrophages[109–111]. (adapted from Xin *et al*. 2013[20])

1.4.3 Proposed populations of adult mammalian cardiac progenitors

It has been described by multiple research groups that *de novo* cardiomyocytes arise from endogenous cardiac progenitor cells (CPCs) in the adult mammalian heart. Therefore, attempts have been undertaken to identify these progenitor populations as a potential candidate for heart regeneration. Multiple CPC isolation methods have been described that depend on the expression of genes encoding proteins such as stem cell antigen 1 (SCA1), stem cell growth

factor receptor KIT (KIT), Wilms tumour 1 (WT1) or islet1 (ISL1), or the ability to form colonies, form 3D multicellular clusters called cardiospheres, or to actively efflux dyes. These will be described in the following sub-chapters.

The cardiac side population and SCA1$^+$ cells

The first attempt to describe an endogenous myocardial stem cell was made by Hierlihy *et al*. who isolated a side population (SP) from the hearts of 8-week old mice based on their ability to efflux the DNA-binding dye Hoechst through an ATP-binding cassette transporter[112]. The SP assay has been extensively used to identify stem cell and progenitor populations in different tissues, including umbilical cord blood[113], skeletal muscle[114], kidney[115], mammary gland[116], and lung[117]. The cardiac Hoechst-effluxing SP represented around 1% of the total cell numbers in the adult heart as identified by flow cytometry and were initially described as negative for the proteins KIT, SCA1 (encoded by *Ly6a*), and CD90. However, Pfister *et al*. showed that a subset of mouse SP cells that was CD31$^-$ and SCA1$^+$ exhibited functional cardiomyogenic differentiation capacity[118]. It was later shown that SP cells significantly overlapped with the SCA1$^+$ population[119].

The Schneider group demonstrated that SCA1$^+$ cells transplanted into injured mouse hearts differentiated into cardiomyocytes[119]. Another study showed that a subset of SCA1$^+$ cells contributed to the cardiomyocyte lineage during aging, while mostly contributing to smooth muscle cells and potentially endothelial cells[120]. Moreover, the *in vitro* colony-forming assay first used by Friedenstein (see 1.4.2. Fibroblasts) to characterise bone-marrow-derived fibroblasts was utilised to isolate similar cells from the heart[121]. The resulting cardiac colony-forming unit-fibroblast (cCFU-F) were shown to be of epicardial origin and perivascular, but based on their lack of *Ng2* expression to be non-pericytes. More importantly, the CFU-F ability was determined by the PDGFRα$^+$ SP$^+$ CD31$^-$ subset of SCA1$^+$ cells.

Noseda *et al*. revealed that PDGFRα^{+} SP^{+} CD31^{-} cells produced by preparative cell sorting identified the clonogenic cardiogenic subset of SCA1^{+} cells[122]. Transplantation of the clonal progeny of a single SCA1^{+} PDGFRα^{+} SP^{+} CD31^{-} cell showed cardiomyocyte, endothelial and smooth muscle lineage potential, and enhanced cardiac function. However, as with most cell transplantation studies, low cell retention was described. Single-cell qRT-PCR analysis of the cardiac SCA1^{+} PDGFRα^{+} SP population revealed enrichment for the cardiogenic genes *Gata4/6, Mef2a/c, Tbx5/20 and Hand2*.

Although an ortholog of SCA1 is absent in humans, SCA1-like cells have been isolated from the adult human heart using the mouse antibody[123]. Moreover, cardiac SP cells were identified in the human left, but not the right, atrium where it accounted for around 0.2% of nonmyocytes[124].

KIT

In 2003, a landmark study was published by the Anversa group describing a resident KIT^{+} progenitor population[125]. The KIT^{+} cells were described as self-renewing, clonogenic, negative for haematopoietic lineage markers (Lin^{-}), and regenerated the myocardium once transplanted in a rat MI model. However, *Kit* expression is not unique to this progenitor population as it has been described in postnatal cardiomyocytes[126], dedifferentiated adult cardiomyocytes[127,128], coronary endothelial cells[129], and heart-resident cells co-expressing *CD45* indicating a bone marrow origin[130].

Studies by the Anversa group demonstrated the therapeutic effect of KIT^{+} cells in dogs[131] and described them in mouse[132] and human hearts[133,134]. A key functional study was also published by Ellison *et al*. in 2013 where a model of diffuse cardiomyopathy induced by bolus injection of isoproterenol (ISO) was used to examine the *in vivo* activation of KIT^{+} cells[135]. Bromodeoxyuridine^{+} mononuclear cardiomyocytes were formed to replace the lost cardiomyocytes and were shown to originate from KIT^{+} cells. Ablation of dividing KIT^{+} cells

(and other dividing cells) using 5-fluorouracil abolished regeneration and functional recovery after ISO. However, this was reversed by transplantation of the progeny of a single KIT^+ cell. This was later challenged by a study showing that only around 0.03% of cardiomyocytes were of the KIT lineage and KIT^+ cells abundantly generated cardiac endothelial cells[136]. Additional studies generated more sensitive methods to characterise the identity of KIT^+ cells and their progeny by inserting conditional Cre and/or marker cassettes directly into the start codon of the first *Kit* coding exon[137,138]. KIT^+ cells were found to be consistent with an endothelial phenotype as suggested by their co-expression of *CD31*, and their localisation within the endocardium and coronary endothelium. Following MI, they retained their endothelial phenotype, and only a very rare subset co-expressed the cardiogenic markers *Nkx2-5* or cardiac troponin T *(cTnT)*.

The phase I SCIPIO (Stem Cell Infusion in Patients with Ischaemic Cardiomyopathy; NCT00474461) clinical trial demonstrated the safety of intracoronary delivery of autologous KIT^+ cells and showed reduced infarct size and improved left ventricular contractility. A follow-up phase II CONCERT-HF (Combination of Mesenchymal and KIT^+ Cardiac Stem Cells as Regenerative Therapy for Heart Failure; NCT02501811) clinical trial was initiated to compare the effects of MSCs, KIT^+ cells and a combination thereof. However, studies by the Anversa group have been under scrutiny over the past few years. More recently, Harvard Medical School and Brigham and Women's Hospital determined that 31 papers from the Anversa lab must be retracted, including the SCIPIO trial results. The CONCERT-HF clinical trial was also paused by the National Heart, Lung, and Blood Institute (NHLBI).

ISL1

Isl1 expression is detected in cardiac mesodermal progenitors of the FHF[139] and SHF[140], and in cardiac neural crest cells[141]. In the developing heart, $ISL1^+$ progenitors have been shown to contribute to the formation of cardiomyocytes, endothelial cells and smooth muscle cells[142]. In

2005, Laugwitz *et al*. showed that ISL1$^+$ cells give rise to a minor proportion of cardiomyocytes in the postnatal murine heart[143]. Although, ISL1$^+$ cells have been described in adult human and murine hearts, they are very rare and unlikely to play a role in myocardial regeneration[144,145]. Indeed, it was shown that the distribution and numbers of ISL1$^+$ cells are not altered following MI in the murine heart[144]. Weinberger *et al.* used thymosin β4 to test its potential in reactivating *Isl1* expression in adult mouse ventricles[146]. However, this did not yield an amplification in the number of ISL1$^+$ cells. More recently, transplantation of embryonic stem cell (ESC)-derived ISL1$^+$ progenitors was shown to improve cardiac function following MI[147]. The ESCORT clinical trial (Transplantation of Human Embryonic Stem Cell-derived Progenitors in Severe Heart Failure; NCT02057900) demonstrated the safety of transplanting hESC-derived ISL1$^+$ cells embedded in a fibrin patch[148]. Clinically silent alloimmunisation reactions were described but resolved over time. The authors reported improved systolic wall motion of cell-treated regions. However, the study is limited by the small sample size of six patients only and the lack of a control group.

Cardiosphere-derived cells

In 2004, Messina *et al*.[149] isolated and expanded cardiosphere-derived cells (CDCs) as a monolayer originating from cardiospheres. CDCs isolated from human and murine hearts were described as clonogenic, self-renewing and a heterogeneous population expressing *KIT*, high levels of *CD90*, *CD105* with low expression of *CD31* and *CD34* and lack expression of the haematopoietic lineage markers *CD133* and *CD45*[149,150]. The first CDC functional study was published in 2007 by the Marbán group where CDCs expanded from adult human biopsies were shown to promote cardiac regeneration and improve function in a mouse MI model[150]. Many studies by the Marbán group demonstrated a therapeutic effect of CDCs in different settings including: pig model of MI[151,152], mouse model of non-ischaemic dilated cardiomyopathy[153], and rat model of heart failure with preserved ejection fraction[154].

Other groups have also showed a therapeutic effect of CDCs[155–158] including a study in Rhesus monkeys[159], and a study by the Carr group where neonatal CDCs were injected into infarcted rat hearts and improved cardiac function and increased capillary density[160]. Further studies from the Carr group demonstrated that CDCs can be isolated from patients with chronic ischaemic heart disease[161], and murine models of different morbidities[162,163].

With a growing body of evidence, CDCs entered clinical trial in 2009 as the CADUCEUS (CArdiosphere-Derived aUtologous stem CElls to reverse ventricULar dysfunction; NCT00893360) trial was initiated to assess the safety of intracoronary administration of autologous CDCs in MI patients[164]. Results did not raise significant safety concerns and indicated a decrease in scar size (12.3% at 12 months), though changes in left ventricular ejection fraction were not detected[164]. More recently, the follow-up phase II ALLSTAR (Allogenic Heart Stem Cells to Achieve Myocardial Regeneration; NCT01458405) clinical trial was terminated in February 2019 for failing to meet the primary end point of scar size. CDCs are currently being investigated as a therapy for dilated cardiomyopathy in end-stage Duchenne muscular dystrophy[165].

Epicardium-derived cells

During development, the epicardium secretes trophic factors required for myocardial maturation, and undergoes EMT to directly contribute precursors of numerous cardiac cell types: coronary vascular smooth muscle cells, and interstitial and perivascular fibroblasts. It has also been suggested, though controversial, that epicardium-derived cells (EPDCs) contribute to the endothelial and cardiomyocyte lineages[166,167]. These EPDCs are detected through the expression of the transcription factors *Wt1*, *Tbx18*, *Tcf21* and *Raldh2*, whose protein product is involved in retinoic acid synthesis[168].

Following development, the epicardium enters a state of quiescence in the healthy mammalian heart. However, this state of quiescence is lost upon cardiac injury and the embryonic gene

programme is activated as evident by an organ-wide epicardial upregulation of WT1, TBX18 and RALDH2 and subsequent epicardial expansion[169]. Epicardial activation leads to fibrosis and scar formation in the mammalian heart. Conversely, this activation is necessary for regenerative processes in the zebrafish heart[47,170].

Smart *et al*. showed that thymosin β4 induced epicardial neovascularisation[171], and that thymosin β4 priming prior to MI induced a sub-population of $WT1^+$ EPDCs towards a cardiomyocyte lineage[172]. Moreover, $WT1^+$ progenitors transplanted into infarcted hearts formed *de novo* cardiomyocytes. However, the contribution of EPDCs to both vasculature and cardiomyocytes is currently insufficient for effective myocardial regeneration. A recent study showed that co-transplantation of hESC-derived epicardial cells and cardiomyocytes resulted in the epicardial cells forming persistent fibroblast grafts and increased the size of cardiomyocyte grafts[173].

1.5 Cell therapy – mechanisms of action and current limitations

Many clinical trials of cell therapies for MI patients have shown limited efficacy in comparison to pre-clinical studies. A main limitation in pre-clinical studies is the use of young, homogenous and healthy small animals. Aging in mice is associated with increased adverse cardiac remodelling after MI[174]. CDCs isolated from mice were demonstrated to have lower proliferation capacity, expression of *Kit* and *Sca1* and *in vitro* cardiogenic differentiation potential with increased age[162]. This highlights the need for the use of aged animal models in pre-clinical studies[175]. Unfortunately, this limitation is somewhat challenging to overcome due to the time and cost associated with the use of aged animal models. Moreover, patients in clinical trials typically present with comorbidities and a variation in existing treatment regimens. Therefore, stratifying patients into more homogenous subgroups is required for robust analysis of clinical trial results. Cell therapy clinical trials are also limited by the lack of standardisation of a number of parameters including handling and characterisation of the

used cells, cell delivery route and timing of delivery. Efforts to organise large-scale clinical trials with enhanced standardisation and to better define cell therapy mechanisms of action are required.

Mechanisms responsible for the observed beneficial effects following administration of cardiac stromal cells or CPCs in both animal models and clinical trials have been under debate (figure 1.3). Due to the significantly limited cell retention and differentiation *in vivo*, it has been suggested that the observed improvement is mostly due to the production of paracrine factors that may stimulate endogenous regeneration or alter the tissue's response to injury[176]. A variety of cell types, including the proposed CPC populations, have been shown to secrete paracrine factors such as growth factors, cytokines, and microRNAs (miRNAs) in naked forms or in membrane vesicles such as exosomes[177]. For example, administration of extracellular vesicles isolated from human CDCs significantly repressed apoptosis, stimulated angiogenesis, and improved cardiac function in a rat MI model[178]. More recent studies by the Marbán group focused on the therapeutic potential of CDC-secreted extracellular vesicles in multiple pathologies such as MI, stroke, and Duchenne Muscular Dystrophy[179–181]. Other studies have demonstrated that the delivery of the secretome of stem cells or CPCs is sufficient to induce cardiac repair following MI[182–184]. Furthermore, it has been recently suggested that the therapeutic benefit of cardiac cell therapy is mediated through an acute immune response, which further challenged the idea of direct differentiation of stromal populations following transplantation[185]. This was demonstrated by showing that injection of bone marrow mononuclear cells, either viable or freeze/thaw-killed, induced $CCR2^{+}$ and $CX3CR1^{+}$ macrophages and enhanced cardiac function in a mouse MI model.

The lack of direct differentiation of delivered CPCs into cardiomyocytes has shed some doubt on the identity of the proposed CPC populations. Indeed, the Cardiomyocyte Regeneration Consensus Statement published in 2017 noted that: (1) CPCs may contribute to the formation

of cardiomyocytes in adult homeostasis, albeit at very low levels and that (2) the mechanism behind cardiomyocyte renewal in the adult mammalian heart is cardiomyocyte proliferation suggesting evolutionary conservation[186]. This is based on studies utilising different pulse-chase approaches and fate mapping experiments that identified a sub-population of cycling cardiomyocytes as the dominant source of cardiomyocyte renewal in both homeostasis and following injury[40,187,188]. A more recent study utilised a dual genetic lineage tracing strategy in which cardiomyocytes and nonmyocytes of the developing heart could be simultaneously labelled by two orthogonal recombination systems[189]. It was shown that nonmyocytes do not give rise to cardiomyocytes, at or beyond E11.5 to E12.5, and in the neonatal heart in both homeostasis and following injury.

Despite the lack of *in vivo* differentiation of delivered CPCs into cardiomyocytes and the controversy surrounding their identity, cardiac cell therapy has shown some promising results. Therefore, efforts have been made to address the challenges hindering further advancement in the field. Indeed, it has been suggested that these CPCs can act as a "paracrine factors factory" following transplantation[190]. As mentioned earlier, one of the main challenges is the extremely low cell retention. Following MI, harsh events such as ischaemia, oxidative stress and increased inflammation limit the survival and engraftment of transplanted cells. Massive loss of the transplanted cells has been reported, as typically 90% of the cells are lost within the first week[191–194]. Enhancing the survival of the cells may provide a mechanism by which the window of beneficial paracrine signalling may be prolonged. Hence, the move towards using improved delivery strategies including biomaterials[195,196], simultaneous delivery of growth factors[197,198], and preconditioning techniques such as cell glycoengineering[199], hypoxic conditioning[200–203], and electromechanical conditioning[204] to enhance cell retention.

Previous work by the Carr group had investigated the use of MRI-detectable nanoparticles (NPs) that could be utilised for cell tracking *in vivo*, and that were capable of delivering

microRNAs (miRNAs) into the cell[205]. With the aim of labelling cells with NPs bearing a miRNA that would enhance cell retention and therapeutic effect, an appropriate pro-survival miRNA was sought. S. Malandraki-Miller (thesis) showed that cells transfected with the hypoxia miRNA, miR-210, had increased survival following serum starvation by assessing cell numbers in comparison to cells transfected with a negative miRNA. Parts of this thesis will therefore build on these findings by further investigating the use of miR-210 as a pro-survival agent. miRNAs and their role in the healthy and injured heart are introduced in the following subchapters with a focus on miR-210.

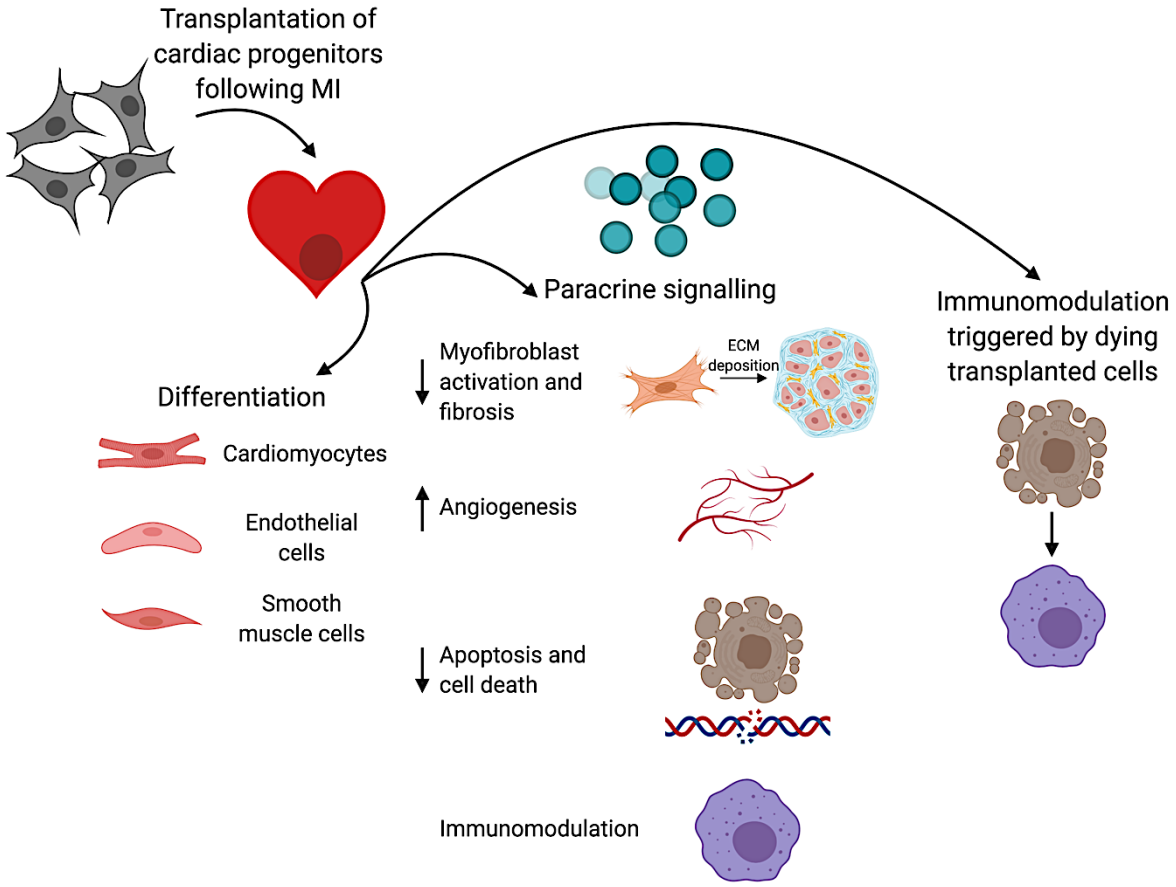


Figure 1.3 Proposed mechanisms of action of cardiac cell therapy using CPCs

Transplantation of CPCs following MI may contribute to cardiac repair via differentiation into cardiovascular cell types or via the secretion of paracrine factors that modulate the host tissue's response to injury.

1.5.1 MicroRNAs

miRNAs are short (~22 nucleotides) single-stranded non-coding RNAs that play a key regulatory role in gene expression at the post-transcriptional level. miRNAs function by degrading target mRNAs, repressing their translation, or rare endonucleolytic cleavage of target mRNAs if a high level of complementary is present[206]. This occurs via an interaction between the miRNA "seed region" and the 3'-UTR, or more rarely the 5'-UTR, of target mRNAs[207]. The miRNA seed region is usually at the 5′ end spanning from nucleotide position 2 to 8. miRNAs with an identical sequence at nucleotides 2–8 of the mature miRNA are generally considered of the same family[207]. The downstream nucleotides of miRNAs can also contribute to the interaction with target mRNAs[208].

The significance of miRNAs had been overlooked, due to methodology limitations, until it was shown that the miRNAs lin-4 and let-7 have a key role in *C. elegans* development [209,210]. Following that, many miRNAs and their binding targets have been identified experimentally and computationally in animals, plants, and viruses[211]. A considerable number of miRNAs are highly conserved in sequence among different organisms, suggesting their involvement in critical cellular processes[212]. It is estimated that more than 60% of human protein-coding genes contain at least one conserved miRNA-binding site. Therefore, the majority of protein-coding genes may be under miRNA control, as many non-conserved sites also exist[213]. This highlights the significance of miRNA regulation. Indeed, miRNA dysregulation is frequently associated with physiological and pathological conditions, including cancer[214] and neurodevelopmental disorders[215].

1.5.1.1 miRNA biogenesis

miRNAs are transcribed by RNA polymerase II (Pol II) producing a long primary transcript with a local stem–loop structure where miRNA sequences are embedded[208] (figure 4.1). This primary miRNA (pri-miRNA) undergoes maturation in the nucleus by a complex called

Microprocessor, which cleaves the stem–loop to release the precursor miRNA (pre-miRNA), a small hairpin-shaped RNA of ~65 nucleotides[216]. The Microprocessor complex consists of the nuclear RNase III Drosha and its essential cofactor DGCR8[217]. Following cleavage, the pre-miRNA hairpin is transported to the cytosol, where maturation is completed. Exportin 5 (EXP5) forms a transport complex with the GTP-binding nuclear protein RAN•GTP and the pre-miRNA[218,219]. Following transportation through the nuclear pore complex, the GTP is hydrolysed, allowing the release of the pre-miRNA into the cytosol. The pre-miRNA is then cleaved by the RNase III Dicer releasing a small miRNA duplex[220–222]. The RNA duplex is subsequently loaded onto an Argonaute (AGO) protein forming an effector complex known as RNA-induced silencing complex (RISC), followed by the removal of the passenger strand to generate a mature miRNA[223,224].

Each pre-miRNA produces two mature strands of miRNA: one from the 5′ and one from the 3′ side (e.g. miRNA-210-5p and miRNA-210-3p). The ‘guide’ or ‘lead’ strand is usually more abundant (96–99%), and more biologically active than the ‘passenger’ strand (miRNA*)[208]. This is because the passenger strand is degraded quickly after release from AGO, resulting in higher abundance of the guide strand. The guide strand is determined during the AGO loading step by the thermodynamic properties, and hence stability, of the strand[225,226], thus determining the degree to which each strand participates in the RNAi pathway[226].

Other non-canonical miRNA biogenesis pathways have also been described, where miRNAs are produced independently of Dicer or Drosha. However, most non-canonical pathways are low in prevalence, and are poorly conserved, where the majority of miRNA follow the canonical pathway of biogenesis[208].

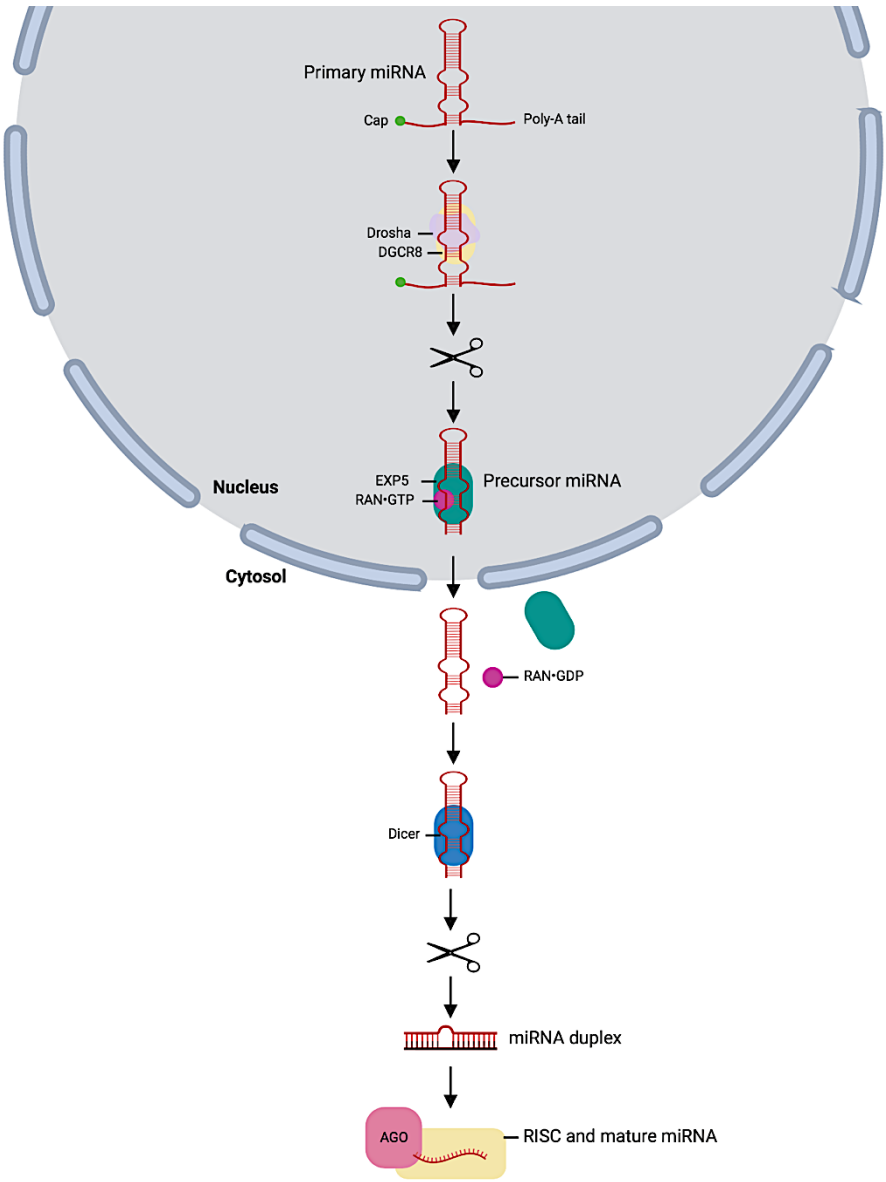


Figure 1.4 The canonical miRNA biogenesis pathway

Generation of a mature miRNA strand using the canonical miRNA biogenesis pathway. (Adapted from[227] and [208])

1.5.1.2 Computational analysis of miRNA targets

Each miRNA targets more than one mRNA and miRNA-mRNA interactions are not entirely complimentary making target identification challenging. Bioinformatics tools attempt to predict potential miRNA-mRNA interactions for experimental validation. The most frequently used miRNA target prediction tools include TargetScan, miRanda, miRBase, and DIANA microT. However, these vary in their prediction algorithms and the biological elements used

for target recognition. The biological elements considered include the seed region, conservation status, and pairing stability. Other tools take into consideration the expression pattern of the miRNA and the mRNA, and physical configurations that may hinder pairing[228].

1.5.1.3 miRNAs in the heart and their role following MI

miRNAs have been shown to be important regulators of cardiac development, and cardiomyocyte differentiation and proliferation. *Dicer* knockout mice exhibit defective cardiac development and embryonic lethality[229]. Cardiac-specific knockout of *Dgcr8* leads to dilated cardiomyopathy and heart failure[230].

The most abundant miRNAs in the heart are miR-1, miR-133, miR-208, and miR-499[231], which are known as MyomiRs, a term used to describe miRNAs enriched in muscle tissue[232]. Indeed, these MyomiRs have been implicated not only in cardiac development and proliferation but also cardiac diseases such as cardiac hypertrophy and MI. miR-499 regulates myosins and is increased in cardiomyopathy[233,234]. Moreover, miRNAs have been classed into positive and negative regulators of cardiomyocyte survival[235]. Both the miR-15 and miR-34 families have been shown to contribute to cardiomyocyte death *in vivo*[236,237]. For example, targeting the seed region of members of the miR-15 family using antimiRs protects against cardiac ischaemic injury[236]. An example of a positive regulator is miR-24, where its overexpression reduced infarct size and improved cardiac function following MI. This is attributed to its targeting action of *Bim* (encoding pro-apoptotic BCL2-like protein 11)[238]. Moreover, inhibition of anti-angiogenic miRNAs, such as miR-92a, has also been shown to enhance outcome following MI in mice, demonstrating the significant role miRNAs play in cardiac ischaemia[239].

miRNAs have also been utilised in cell therapy applications. Overexpression of miR-126 in MSCs delivered into the heart enhanced the cells' angiogenic potential[240,241]. Moreover, a pro-survival cocktail containing miR-21, miR-24, and miR-221 was used to enhance the survival and engraftment of transplanted CPCs in infarcted mouse hearts[242]. miRNAs have also been

injected directly into the heart. Improved cardiac function following MI was shown after miR-210 injection, where miR-210 promoted angiogenesis and survival by targeting *Efna3* and *Ptp1b*, which encode an anti-angiogenic receptor and a pro-apoptotic protein, respectively[243]. miR-210 has, therefore, been proposed as a potential therapeutic approach for ischaemic heart disease.

1.5.1.4 miRNA-210: the hypoxamiR

miR-210 is an hypoxia-inducible miRNA, also known as an hypoxamiR. Its hypoxic regulation was first identified in 2007 using a miRNA microarray[244]. Unlike many other hypoxamiRs, miR-210 is consistently and robustly induced under hypoxic conditions in all systems[245]. The stem–loop of miR-210 is located in an intron of a noncoding RNA, which is transcribed from *AK123483* on chromosome 11p15.5[245]. miR-210 is regulated by hypoxia-inducible factor 1α (HIF1α)[246–249] when it binds to an hypoxia responsive element (HRE) on the proximal miR-210 promoter[248]. The miR-210 HRE site was found to be highly conserved, indicating the importance of hypoxia in regulating miR-210 expression[245]. miR-210 has also been shown to be regulated by HIF2α[250].

miR-210 has been implicated in the regulation of many cellular functions and processes including angiogenesis[251–253], cell cycle regulation[250,254], DNA damage repair[246], mitochondrial metabolism inhibition[255], and stem cell survival[249]. The crucial role of miR-210 in the cell response to hypoxia has been demonstrated pre-clinically and clinically. miR-210 is upregulated in a variety of ischaemic conditions, including hindlimb ischaemia in mice[256], atherosclerotic plaques[257] and the failing diabetic heart in humans[258], ischaemic wounds[259], and following MI in mice[243] and humans[260]. This comes as a part of an articulate response to hypoxia aimed at relieving the effects of decreased oxygen levels[261]. A study by the Martelli group using the TetOn technology to conditionally overexpress miR-210 showed that miR-210 decreased tissue damage and increased blood perfusion in a hindlimb ischaemia model[261]. Another study

showed that inhibiting miR-210 using LNA-antisense oligonucleotides increased tissue apoptosis and necrosis in the ischaemic limb[256]. Although a miR-210 knockout mouse has been generated, ischaemic disease was not explored in this model[262].

Given miR-210's cytoprotective and pro-angiogenic role in ischaemic disease, particularly post MI[243], this study examined its effect on cell survival *in vitro* and retention *in vivo* following injection into a mouse MI model. The guide strand of the miRNA-210 duplex, miR-210-3p, was selected for this study. S. Malandraki-Miller initiated this study during her DPhil by optimising overexpression of miR-210 using the commercial transfection agent DharmaFECT formulation 1 in unsorted stromal cells isolated from adult mouse atrial appendages as a slowly adhering population (named CTs). She also showed that miR-210-transfected CTs had increased survival following 72 hours of serum starvation by assessing cell numbers in comparison to CTs transfected with a negative miRNA. Finally, miR-210-transfected CTs were shown to have increased VEGF-A secretion in comparison to CTs transfected with a negative miRNA. The CT isolation protocol was developed in an attempt to optimise cardiac stromal cell isolation due to the variability we observe in CDC expansion time[161]. More detail on how the isolation method of CTs was developed and why atrial appendages were selected for their isolation is provided in chapter 3 (see 3.1.2).

1.6 Hypothesis and project aims:

1.6.1 Hypothesis: miR-210 overexpression enhances the therapeutic potential of cardiac stromal cells for transplantation after MI.

- Unsorted stromal cells isolated from adult mouse atrial appendages as a slowly adhering population (CTs) are more homogenous and display greater survival potential, compared to other cardiac stromal populations.
- Overexpressing miR-210 in CTs protects from apoptotic cell death *in vitro* and, as an hypoxia miRNA, miR-210 has a role in targeting mitochondrial dynamics.
- miR-210 enhances the paracrine potential of CTs and rescues their gene expression profile following *in vitro* stress.
- The pro-survival effect of miR-210 translates *in vivo* in a mouse MI model.

1.6.2 Project aims:

Objective 1: To characterise a slowly adhering population of unsorted stromal cells isolated from adult mouse atrial appendages using a collagenase and trypsin protocol developed by our group (CTs).

- Compare CTs to different unsorted populations isolated from adult mouse atrial appendages: (1) CDCs and (2) 'Cardiac fibroblasts' purchased from Cell Biologics (CFs).
- Use immunocytochemistry and single-cell qRT-PCR to characterise the CTs, CDCs and CFs.
- Examine if differences in the gene expression profile of the different populations may be reflected on the paracrine potential, using cytokine arrays.
- Assess the survival potential of the different populations in an *in vitro* starvation model.

Objective 2: Investigate miR-210 mechanisms of action and its effect on apoptosis and mitochondrial dynamics in CTs.

- Investigate the pro-survival effect of miR-210 in CTs following serum starvation.
- Assess the role of miR-210 on mitochondrial dynamics in CTs using a siRNA knockdown system, qRT-PCR, immunocytochemistry, and radio-labelled substrate metabolism assays.

Objective 3: Assess miR-210 as a conditioning agent for cell therapy by examining its effect on CT gene expression profile and paracrine potential and determine if it has a positive effect on CT survival and retention in a mouse MI model.

- Examine if miR-210 rescues the gene expression profile of CTs following serum starvation by single-cell qRT-PCR.
- Use cytokine arrays, and *in vitro* co-culture with HL-1 cardiomyocytes and HUVECs to assess the paracrine potential of CTs following miR-210 transfection.
- Use echocardiography and measure serum cardiac troponin I (cTnI) levels by ELISA to assess the consistency of mouse MI surgery.
- Quantify the retention of $EGFP^+$ CTs transfected with either a negative miRNA or miR-210 in a mouse MI model following 24 hours by flow cytometry.

CHAPTER 2

Materials and methods

2 Materials and methods

2.1 Mice

Mice were kept under controlled conditions of temperature, light and humidity, with free access to water and chow. All the procedures involved in this study were reviewed and approved by the Institutional Animal Care and Use Committee (IACUC) and the Home Office, and conformed to UK government regulations (Project Licence number 30/3322). This study used 2-3-month-old wild type C57BL/6 mice (Envigo UK), and transgenic mice, as specified below.

2.1.1 Tg(CAG-EGFP)1Osb/J mouse model

EGFP-transgenic mice, *C57BL/6-Tg (CAG-EGFP) 10sb/J*, were obtained from The Jackson Laboratory (Bar Harbor, ME, USA). This transgenic line expresses EGFP cDNA under the control of a chicken beta-actin promoter and cytomegalovirus enhancer making all tissues, except for erythrocytes and hair, appear green after excitation[263].

2.1.2 Sarcolipin$^{Cre/+}$ mouse model

The *Sarcolipin$^{Cre/+}$* mouse model was a gift from Dr. Atsushi Nakano (University of California, San Diego). The mouse model was generated by Nakano *et al*. where exon 2 of the *Sarcolipin* locus including the 1st ATG was replaced with Cre recombinase cDNA by homologous recombination[264]. *Sarcolipin$^{cre/+}$* heterozygotes were crossed with *R26R-TdTomato*[265] and *R26R-EYFP*[266] reporter lines (a gift from the Riley group, University of Oxford).

2.2 Isolation and expansion of mouse cardiac stromal cells

Mice were terminally anesthetized with isoflurane to allow tissue removal. Hearts were isolated and washed with DPBS containing 50mg of primocin (antimicrobial agent; InvivoGen ant-pm-2) then placed in ice-cold 10ml falcon tubes containing 2ml of sterile CEM for immediate isolation of cardiac stromal cells.

2.2.1 Collagenase trypsin cells (CTs)

Mouse atrial appendages were dissected, transferred into Petri dishes containing DPBS and primocin, and washed thoroughly to remove excess blood. The appendages were minced into 1 - 2 mm^3 pieces with tweezers then transferred into 0.5ml of the digestion mix (0.1% trypsin and 0.1% Collagenase II (Calbiochem, 286U/mg) in DPBS) and incubated in a water bath at 37°C for a total of 40 minutes. Every 10 minutes the digestion-solution containing the tissue pieces was mechanically triturated by pipetting, left on ice for 1 minute to settle and the supernatant was collected. Fresh digestion mix was added again to the tissue pieces for a total of 4 digestions. At the final digestion step, sterile 19G needles and 1ml syringes were used to triturate the tissue. After each digestion, the supernatant was neutralised, and the cell suspension was resuspended in fresh complete explant medium (CEM)[150] to be plated in a 12-well plate through a 40µm cell strainer. The wells were pre-coated with 50µl per cm^2 of fibronectin bovine plasma (2µg/ml in DPBS; Sigma-Aldrich). Cells were allowed to attach for 72 hours without media changes.

2.2.2 Cardiosphere-derived cells (CDCs)

2.2.2.1 Explants

Mouse CDCs were isolated using a protocol adapted from that of Smith *et al.* (2007). Mouse atrial appendages were dissected, transferred into Petri dishes containing DPBS and primocin and washed thoroughly to remove excess blood then minced mechanically as described before (2.2.1). The tissue pieces were digested in 0.05% Trypsin-EDTA (ThermoFisher) for 4 minutes at 37°C then neutralised with CEM. Processed tissue pieces were plated on fibronectin-coated (3µg/ml in DPBS) 6-well plates containing 500µl of CEM and incubated for 60 minutes at RT to allow sufficient adhesion of the explants to the fibronectin. An additional 1ml of CEM was then added and explants were cultured for 25-30 days at 37°C in 5% CO_2 with media changes every 2-3 days.

2.2.2.2 Generation of cardiospheres and CDCs

When explant-derived cell (EDCs) reached 70-80% confluency, they were harvested by washing once with 2ml DPBS, and once with 1ml 0.53mM Versene (ThermoFisher) before a trypsin digestion. EDCs were counted and resuspended in Cardiosphere Growth Medium (CGM), comprising 65% Dulbecco's modified eagle medium (DMEM/F12), 35% IMDM, 7% foetal bovine serum (FBS), 2% B27 (ThermoFisher), 25ng/ml cardiotrophin (Peprotech EC), 10ng/ml epidermal growth factor (EGF; Peprotech EC), 20ng/ml basic fibroblast growth factor (FGF; Promega) and 5 units thrombin (Sigma-Aldrich), at a concentration of 2 x 10^4 cells/ml and seeded as 25µl droplets on an un-coated lid of a 150 x 15mm Petri dish. DPBS was added to the Petri dishes to keep the hanging drops humid throughout 3 days of culture at 37°C in 5% CO_2 allowing the spherical multicellular clusters, known as cardiospheres, to form. Cardiospheres were collected by elution and gentle pipetting with DPBS and were plated in fibronectin-coated 24-well plates with CEM allowing them to spontaneously release CDCs.

2.3 Cell culture conditions

2.3.1 CTs and CDCs

Isolated cardiac stromal cells were routinely cultured in CEM with media changes every 2-3 days. CEM comprised of Iscove's modified Dulbecco's medium (IMDM; ThermoFisher) with 20% foetal bovine serum (FBS) (ThermoFisher), 100U/ml penicillin, 100µg/ml streptomycin and 2mM L-glutamine (ThermoFisher). Cells were passaged when reached 90% confluency using 0.05% Trypsin-EDTA (ThermoFisher) for 3-4 minutes at 37°C. Cells were maintained in a normoxic incubator at 5% CO_2, unless otherwise indicated. Cells were seeded at a density of 1 x 10^3 per cm^2 and allowed to attach overnight prior to transfection or running an assay.

2.3.2 HL-1 cardiomyocytes

HL-1 cardiomyocytes[267] were routinely maintained in Claycomb medium (Sigma-Aldrich), supplemented with 100U/ml penicillin, 100µg/ml streptomycin and 2mM L-glutamine (ThermoFisher), 100µM norepinephrine (Sigma-Aldrich) in 30mM L-ascorbic acid (Sigma-Aldrich), and 10% FBS (ThermoFisher). At confluency, the cells were passaged in a split ratio of 1:3. Cells were plated in culture flasks, precoated with 0.02% (wt/vol) gelatin (Sigma-Aldrich) containing 5µg/ml fibronectin. Cells were maintained in a normoxic incubator at 5% CO_2, unless otherwise indicated.

2.3.3 Adult cardiac fibroblasts

C57BL/6 adult mouse primary cardiac fibroblasts isolated from the atria only were obtained from Cell Biologics (USA). Cells were cultured following accompanying instructions. Briefly, cells were routinely maintained in complete fibroblast medium (Cell Biologics – USA) supplemented with the provided supplement kit: FGF, hydrocortisone, L-glutamine, Antibiotic-Antimycotic Solution, and 10% FBS. At confluency, the cells were passaged in a split ratio of 1:2 or 1:3. Cells were plated in culture flasks, precoated with 0.02% (wt/vol) gelatin. Cells were maintained in a normoxic incubator at 5% CO_2.

2.3.4 Human umbilical vein endothelial cells (HUVECs)

Primary HUVECs were obtained from Lonza (USA). Cells were cultured following accompanying instructions. Briefly, cells were routinely maintained in complete EGM-Plus (Endothelial Cell Growth Media-Plus; Cell Biologics – USA) supplemented with the provided supplement BulletKit: Endothelial Growth Supplement, L-glutamine, ascorbic acid, hydrocortisone hemisuccinate, human epidermal growth factor, heparin, gentamicin/amphotericin-B, and 2% FBS. At confluency, the cells were passaged in a split ratio of 1:3. Cells were maintained in a normoxic incubator at 5% CO_2.

2.3.5 RFP-MIT;EGFP-LC3 mouse embryonic fibroblasts

Primary mouse embryonic fibroblasts (MEFs) isolated from an *RFP-MIT;EGFP-LC3* mouse model[268] were a gift from Prof. Jo Poulton (University of Oxford). Cells were routinely maintained in complete DMEM (ThermoFisher) supplemented 100U/ml penicillin, 100µg/ml streptomycin, 2mM L-glutamine and 10% FBS. At confluency, the cells were passaged in a split ratio of 1:3. Cells were maintained in a normoxic incubator at 5% CO_2.

2.4 Immunohistochemistry

2.4.1 Tissue cryosectioning

Hearts were fixed in 4% PFA for 2 hours at RT, rinsed with DPBS, then equilibrated in 30% sucrose in DPBS pH 7.4 overnight at 4°C. Hearts were embedded in optimal cutting temperature compound (OCT; Sakura Tissue-Tek, 4583) and frozen at -80°C. Frozen tissue were sliced into 10µm cryosections at -20°C using a cryostat (Bright 5040) and stored at -80°C. Slides were allowed to reach RT and dry (10 minutes on the bench) and OCT was rinsed with DPBS. Sections were permeabilised with 0.5% Triton X-100 (Sigma-Aldrich) for 10 minutes at RT and washed twice with DPBS. Immedge pen was used to draw around the sections and slides were placed in foil-covered humid box. Sections were incubated with blocking solution (1% BSA, 10% serum from species in which secondary antibody was raised, ± 0.1% Triton X-100 in DPBS) for 1 hour at RT. Sections were incubated with the primary antibody (Appendix B) in blocking solution overnight at 4°C then washed with DPBS. The secondary antibody was added for 30 minutes at RT then the slides were washed with DPBS and nuclei were stained with DAPI (0.5µg/ml in DPBS; D1306) for 10 minutes at RT. Slides were mounted with 1:1 DPBS:Glycerol on cover glass and stored in the dark at 4°C.

2.5 Immunocytochemistry

2.5.1 Sample preparation and blocking

1 x 10^4 cells per well were seeded on fibronectin-coated cover glasses in 24-well plates and allowed to attach prior to fixation. Culture media was removed and cells were fixed with 4% PFA (Santa Cruz) for 10 minutes at RT. Cells were then washed twice with DPBS and stored in DPBS at 4°C. For intracellular staining, cells were permeabilised with 0.5% Triton X-100 (Sigma-Aldrich) for 10 minutes at RT and washed twice with DPBS. Cells were incubated in blocking solution (1% BSA, 10% serum from species in which secondary antibody was raised, ± 0.05% Triton X-100) for 1 hour at RT.

2.5.2 Antibody staining, DAPI, and mounting

Cells were incubated with the primary antibody in blocking solution for 1 hour at RT or overnight at 4°C then washed with DPBS. The secondary antibody was added for 30 minutes at RT then slides were washed with DPBS and nuclei were stained with DAPI for 10 minutes at RT. Slides were mounted with 1:1 DPBS:Glycerol on cover glass and stored in the dark at 4°C. Samples were scanned using an Inverted Olympus FV1000 Confocal system and acquired images were processed using Fiji software.

2.6 miRNA and siRNA transfection using DharmaFECT

Cells were seeded in fibronectin-coated 6-well plates (1 x 10^5 cells per well) and incubated overnight. DharmaFECT Transfection Reagent #1 (ThermoFisher) was used according to manufacturer's instructions. Briefly, miRNA or siRNA oligonucleotides and DharmaFECT were diluted in antibiotics/serum-free IMDM (table 2.1) separately and incubated for 5 minutes at RT. The two solutions were then combined, mixed by gentle pipetting, and incubated for 20 minutes at RT before adding antibiotics-free CEM to the mix. The final concentration of

oligonucleotides was 100nM, unless otherwise indicated. Cells were incubated with the DharmaFECT-oligonucleotide solution for 48 hours.

Table 2.1 DharmaFECT-miRNA and -siRNA transfection solutions

		Tube 1: diluted oligonucleotide		Tube 2: diluted DharmaFECT			
Plating format	Surface area (cm^2/ well)	Volume of 10µM oligonucle-otide (µl)	Antibiotic/ FBS-free medium (µl)	Volume of DharmaFECT reagent (µl)	Antibiotic/ FBS-free medium (µl)	antibiotics-free CEM (µl/ well)	Total volume (µl/ well)
96	0.3	1	9	0.2	9.8	80	100
24	2	5	45	1	49	400	500
12	4	10	90	2	98	800	1000
6	10	20	180	4	196	1600	2000

2.7 Quantitative reverse transcription polymerase chain reaction (qRT-PCR)

2.7.1 Primer design

Primers were designed using the NCBI Primer-Blast online tool (www.ncbi.nlm.nih.gov/tools/primer-blast/). For optimal primer design for SYBR Green qRT-PCR, the following criteria were followed:

- GC content of 50-60%
- Primers ending in G or C
- Melting temperature of 65-75°C
- Primer length of 18-25 nucleotides
- Primers must flank the exon-exon border of the gene to avoid genomic DNA amplification

2.7.2 RNA extraction and cDNA synthesis

Cell pellets were collected and stored at -80°C. Total RNA was extracted using RNeasy Mini Kit (Qiagen), according to manufacturer's instruction. RNA yield and purity were determined using the NanoDrop spectrophotometer with a ratio of $A_{260/280}$ = 1.8-2.0 considered as

acceptable RNA purity. Complementary cDNA was synthesised using High-Capacity cDNA Reverse Transcription Kit (ThermoFisher), according to manufacturer's instruction.

2.7.3 qRT-PCR reaction and analysis

Real time PCR was performed using the Applied Biosystems StepOnePlus Real-Time PCR System (Applied Biosystems, ThermoFisher). Relative mRNA levels were normalised to the housekeeping gene *Hprt*. The housekeeping gene was chosen by S. Malandraki-Miller (thesis) by performing an initial comparative analysis of several reference genes (geNorm Kit; Primerdesign) and analysing the output with geNorm software, using "qBase^{+}" (Biogazele, Belgium). SYBR Green fluorescent intercalating dye was used as a detection system for the reaction (SYBR Green PCR mastermix, ThermoFisher) according to table 2.2. Melting curves were used to determine the specificity of PCR products. Relative quantification of target gene expression was performed using the ΔΔCt Livak method[269], plotting the data as $2^{-\Delta\Delta Ct \pm SE}$, which is calculated with the following steps:

- Calculate the average Ct value per target gene and housekeeping gene
- Calculate ΔCt = Ct of target gene - Ct of housekeeping gene
- Calculate ΔΔCt = ΔCt of test sample - ΔCt of control sample
- Calculate the fold change $2^{-\Delta\Delta Ct}$

Table 2.2 Components of the qRT-PCR reaction

Component	**Volume (µl)**
AB Slow mix (dNTPS, DNA polymerase, SYBR fluorescent dye)	5
Primer forward	0.5
Primer reverse	0.5
RNase/DNase Free H_2O	1.5
Template cDNA (12.5ng)	2.5
Total	10/ reaction

2.8 Single-cell qRT-PCR

The single-cell qRT-PCR experiments were performed in the Schneider lab at Imperial College London in collaboration with Dr. Michela Noseda. The sorting was performed by Dr. Patricia Chaves-Guerrero. The pre-amplification and array chips were run with the help of Dr. Patricia Chaves-Guerrero and Sara Samari.

Single cells were sorted directly (FACSAria II) into 96-well plates containing 10µl per well of the reaction mixture for pre-amplification (table 2.3), using CellsDirect One-Step qRT–PCR Kits (ThermoFisher). Pre-amplification was performed in a Veriti Thermal Cycler (Applied Biosystems) for 22 cycles. As negative controls, at least 3–5 non-template samples were included in each run at the pre-amplification stage. Quantitative amplification was performed using Dynamic Array chips for 48 assays x 48 samples, the BioMark HD system (Fluidigm) and TaqMan probes (Appendix D) according to manufacturer's instructions. Each sample was normalised to ΔCt using the expression of *Ubc*.

As described in Noseda *et al*. 2015[122], data were plotted in colour-coded heatmaps of inverted ΔCt values (blue is low or absent; red is high). Samples were ordered based on cell type, and the genes grouped by a hierarchical clustering algorithm based on the underlying co-expression pattern. Differences between samples were investigated using PCA. PCA applies multiple linear transformations (singular value decomposition) to the expression profiles (standardised ΔCt values) of individual samples and identifies a series of PCs that elucidate the most distinguishing features between the samples. The linear projections (PC scores) attempt to maximise the variation between the samples, whereas the coefficients of those projections (PC loadings) measure the importance of genes in defining the underlying variability associated with each component.

Table 2.3 Components of the pre-amplification reaction

Component	Volume (µl)
CellsDirect 2X Reaction Mix	5
SUPERase	0.1
TE Buffer	1.2
0.2X Taqman Assay Mix	2.5
SuperScript III RT/Platinum Taq Mix	1.2
Total	10/ reaction

2.9 Assessing mitochondrial copy number by qPCR

DNA was extracted from cells using the DNeasy Blood & Tissue Kit (Qiagen) and SYBR Green fluorescent intercalating dye was used as a detection system for the reaction (as described in table 2.2). The gDNA:mtDNA ratio was calculated by normalising the mitochondrial gene NADH dehydrogenase 1 (*mt-Nd1*) to the nuclear gene beta-2 microglobulin (*B2m*) using the ΔΔCt Livak method, plotting the data as $2^{-\Delta\Delta Ct \pm SE}$.

2.10 Assessing miR-210 levels by qRT-PCR

Cell pellets were collected and stored at -80°C. Total RNA was extracted using miRNeasy Mini Kit (Qiagen), according to manufacturer's instruction. RNA yield and purity were determined using the NanoDrop spectrophotometer with a ratio of $A_{260/280}$ = 1.8-2.0 considered as acceptable RNA purity. cDNA was synthesised using miScript II RT Kit (ThermoFisher), according to manufacturer's instruction. qRT-PCR was performed using the Applied Biosystems StepOnePlus Real-Time PCR System (Applied Biosystems, ThermoFisher). Relative miR-210 levels were normalised to the housekeeping gene *Snord68* using the miR-210_2 and SNORD68_11 miScript Primer Assays. miScript SYBR Green PCR Kit (ThermoFisher) was used as a detection system for the reaction (table 2.4) according to

manufacturer's instructions. Relative quantification of target gene expression was performed using the ΔΔCt Livak method, plotting the data as $2^{-\Delta\Delta Ct \pm SE}$.

Table 2.4 Components of the miR-210 qRT-PCR reaction

Component	Volume (µl)
2x QuantiTect SYBR Green PCR Master Mix	12.5
10x miScript Universal Primer	2.5
10x miScript Primer Assay	2.5
RNase/DNase Free H_2O	5
Template cDNA (12.5ng)	2.5
Total	25/ reaction

2.11 FAM-FLICA Poly Caspase activity assay

The FAM-FLICA Poly Caspase activity kit measures apoptosis by detecting active caspases in cells via a cell-permeable reagent called the Fluorochrome Inhibitor of Caspases (FLICA), which comprises a caspase inhibitor sequence linked to a green (Carboxyfluorescein, FAM) fluorescent label. 5 x 10^3 cells were plated in Falcon 96-well black microplates with clear flat bottom and allowed to reach 70-80% confluency. 30X FAM-FLICA reagent was added at 1:30 after experimental manipulation of the plated cells, incubated for 45 minutes at 37°C while mixing gently every 10 minutes, washed with media and incubated for 60 minutes at 37°C allowing unbound excess FLICA to diffuse out of the cells. Cells were washed with fresh media and endpoint fluorescence was measured using an excitation wavelength of 488nm and emission filter of 530nm on the Fluostar OPTIMA Microplate Reader (BMG Labtech, Germany).

2.12 Terminal deoxynucleotidyl transferase dUTP nick end labelling assay (TUNEL) assay

Cells were cultured on fibronectin-coated coverslips in 24-well plates and the experimental treatment was carried out. At the indicated time-point, cells were fixed with 4% PFA. The TUNEL assay was performed using Click-iT TUNEL Alexa Fluor 594 Imaging Assay (ThermoFisher), as per the manufacturer's instructions. DNase-I treated slides were used for positive control. Samples were imaged using an Inverted Olympus FV1000 Confocal system. The percentage of cell apoptosis was determined by quantifying cells visualised in 3 random fields. Acquired images were processed using the Fiji software plugin JACoP[270] to calculate Mander's colocalisation coefficient, which represented the fraction of Hoechst33342 (DNA) overlapping Alexa Fluor 594 (apoptosis). A normalised threshold was used when analysing images of the same experiment.

2.13 MitoTracker Red CMXRos staining

MitoTracker Red CMXRos (ThermoFisher) is a red-fluorescent dye that stains mitochondria in live cells and its accumulation is dependent upon membrane potential. The dye is well-retained after aldehyde fixation. CTs were seeded on fibronectin-coated cover glasses in 24-well plates at a density of 1 x 10^4 per well and allowed to attach overnight. Following the experimental manipulation of the cells, a working solution of 200nM MitoTracker Red CMXRos, in antibiotics/serum-free IMDM, was added to the cells and incubated for 40 minutes. Cells were washed with DPBS and fixed with 4% PFA for 10 minutes at RT. Cells were then washed with DPBS, stained with DAPI for 10 minutes at RT. Cover glasses were mounted with 1:1 DPBS:Glycerol on slides and stored in the dark at 4°C. MitoTracker Red CMXRos fluorescence was imaged using an Inverted Olympus FV1000 Confocal system at the excitation/emission wavelengths of 579/599 nm. Fluorescence intensity was quantified

using Fiji software by assessing cells visualised in 3 random fields and measuring stained and background areas. Corrected total cell fluorescence (CTCF) was calculated using the following formula[271]:

$$\text{CTCF} = \text{integrated density} - (\text{area of selected cell} \times \text{mean fluorescence of background})$$

2.14 Metabolic analyses

Both metabolic analyses were performed by Ujang Purnama, a DPhil student in the Carr group.

2.14.1 ^{14}C-glucose oxidation measurement

Glucose oxidation was measured using the method of Collins *et al*.[272], with some modifications as described in Malandraki-Miller *et al*.[273], which is dependent on the release of CO_2 during the passage of acetyl-CoA through the citric acid cycle (figure 2.1). CTs were seeded on fibronectin-coated 24-well plates and the experimental treatment was carried out. Subsequently, CTs were washed with DPBS then incubated for 3 hours in no-glucose basal DMEM (ThermoFisher) supplemented with radiolabelled glucose at 12mM containing 0.185 MBq D-U-^{14}C-glucose (PerkinElmer). Wells with DMEM alone were assessed as negative controls and wells without cells containing DMEM with ^{14}C-glucose were used to measure background radioactivity. The $^{14}CO_2$ produced by the glucose oxidation was trapped using 40% KOH-soaked filter papers placed in the wells of a 24-well plate used as a lid of the apparatus. A perforated rubber gasket, with holes corresponding to each well, separated the two plates. To ensure the system was sealed and avoid $^{14}CO_2$ leakage, the plates were wrapped tightly with Parafilm and screwed into a metal frame. 70% perchloric acid was added to the wells to kill the cells and trigger the release of $^{14}CO_2$ after a 2-hour incubation. It was injected through the top holes in the top plate, through the seal and into the well. The holes were instantly resealed with new parafilm. Subsequently, the samples were allowed to sit for 1 hour to allow the complete release of $^{14}CO_2$ that was dissolved in the media as HCO^-_3. The filter papers containing trapped $^{14}CO_2$ were placed in scintillation vials filled with 10mls of scintillation

fluid (MP Biomedicals) and analysed using the Tri-Carb 2800TR Liquid Scintillation Analyzer, which measured radiation counts per minute (CPM).

Glucose oxidation rates (nMoles/ min/ 10^5 cells) were calculated using the following equation:

$$(\text{Sample CPM at 3} - \text{hour timepoint} - \text{Sample CPM at 0} - \text{hour timepoint}) \times \text{CPM per nMole of glucose} / \textit{cell count} / \textit{incubation time}$$

2.14.2 ^{3}H glucose measurement of glycolytic flux

Glycolytic flux was measured as described in Malandraki-Miller *et al*.[273], which was adapted from studies on isolated working hearts[274–276]. Glycolytic rates were determined through the conversion of ^{3}H-glucose to ^3H_2O via enolase which converts 2-phosphoglycerate to phosphoenolpyruvate and releases H_2O as a by-product during glycolysis (figure 2.1). CTs were seeded on fibronectin-coated 24-well plates and the experimental treatment was carried out. Subsequently, CTs were washed with DPBS then incubated for 6 hours in no-glucose basal DMEM supplemented with radiolabelled glucose at 12mM containing 0.118 MBq ^{3}H-glucose (PerkinElmer). Wells with DMEM alone were assessed as a negative control. Following incubation, the culture media contained both released ^3H_2O and remaining ^{3}H-glucose. Therefore, ^3H_2O was separated from ^{3}H-glucose using a Dowex 1×4 chloride form (Sigma-Aldrich) anion exchange column, which binds the ^{3}H-glucose and elutes ^3H_2O. To prepare the columns, 250g of Dowex resin was added to a 1.25M NaOH and 1.61M boric acid solution and washed with distilled H_2O until the pH reached 7.5. The prepared solution was then added to glass Pasteur pipettes (VWR) plugged with glass wool. Scintillation vials were filled with 10mls of scintillation fluid (MP Biomedicals) and placed underneath the columns to collect the eluted samples. Subsequently, 200µl of each culture media sample was added to a column allowing for the ^{3}H-glucose to bind to the column for 15 minutes before washing each column with 2mls of distilled H_2O for ^3H_2O to be eluted into the scintillation vials. The samples were analysed using the Tri-Carb 2800TR Liquid Scintillation Analyzer (PerkinElmer), which

measured radiation counts per minute (CPM). Glycolytic rates (nMoles/ min/ 10^5 cells) were calculated using the following equation:

$$(\text{Sample CPM at 6} - \text{hour timepoint} - \text{Sample CPM at 0} - \text{hour timepoint}) \times \text{CPM per nMole of glucose} / \textit{cell count} / \textit{incubation time}$$

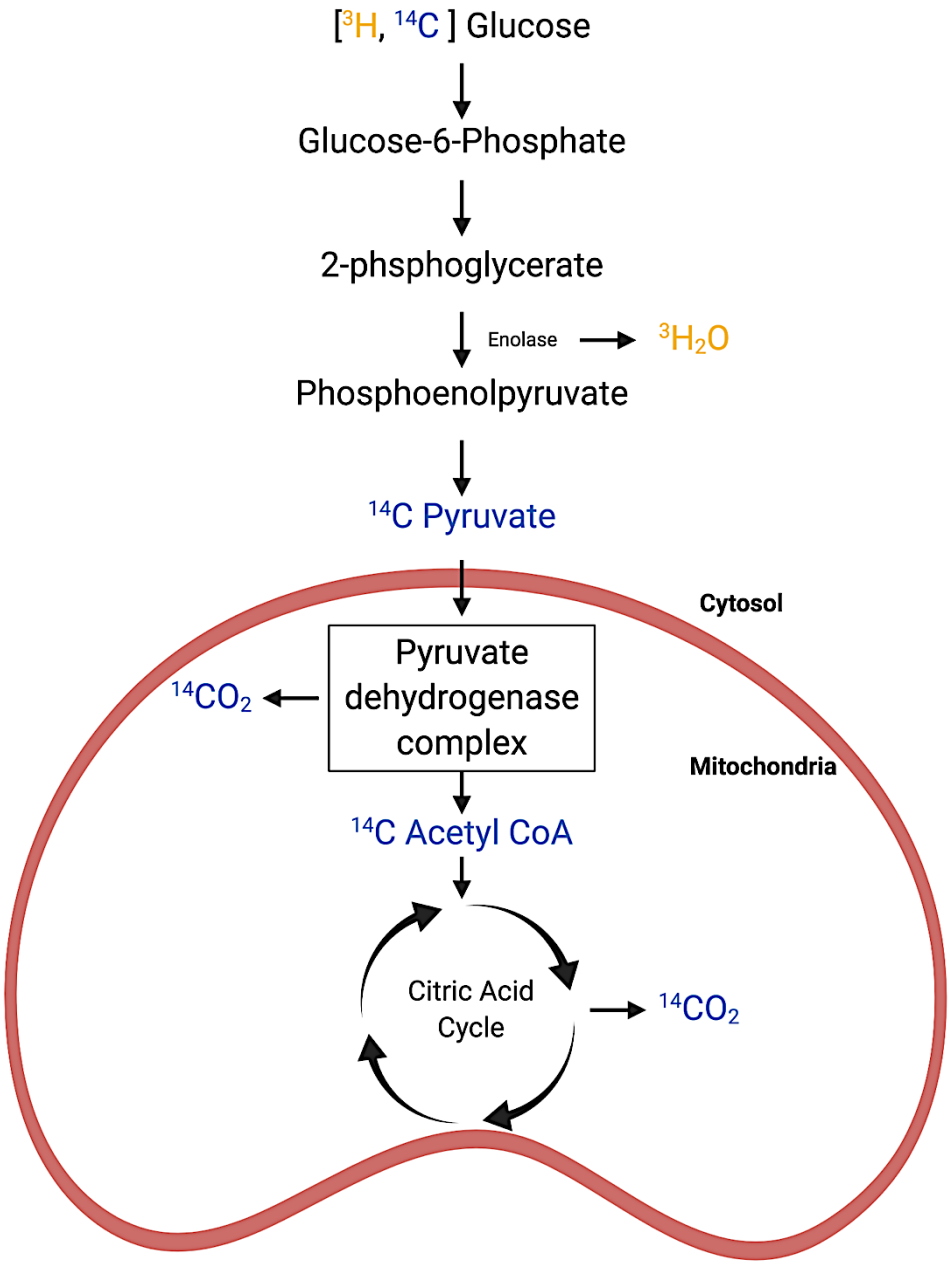


Figure 2.1 Schematic of the use of radiolabelled substrates in metabolic assays

Tracking radiolabelled substrates through glycolysis and glucose oxidation. (adapted from Barr *et al*. 2000[277])

2.15 Growth factor array

Cells were cultured on fibronectin-coated plates in basal IMDM. Culture medium was collected after 48 hours and stored at -80°C. Before use, culture medium was spun down to remove cell debris then run undiluted. RayBiotech C-Series Mouse Growth Factor Antibody Array Kit was used to detect 20 mouse growth factors in cell conditioned media and was performed according to manufacturer's instructions. The arrays were imaged using a LI-COR scanner. The spots were analysed using a pixel counting programme (ImageStudioLite) and the pixel counts normalised to the average of the positive control spots of each array.

2.16 Nanoparticle cell transfection

The NP170 used in this study were designed by R.S.M. Gomes[205] during her PhD project with the Ferreira group (University of Coimbra) and the Carr group. The engineered NP170s are biodegradable, with a 170nm diameter, and consist of poly(lactic acid-co-glycolic acid) (PLGA), a biocompatible and versatile polymer approved for human use, encapsulating a fluorine-based compound perfluoro-1,5-crown ether (PFCE) core, which allows *in vivo* cell tracking by ^{19}F MRI. The NP170s are coated with protamine sulphate (PS), a polycationic peptide that facilitates cell internalisation and the complexation of the miRNA. The NP170s are labelled with Rhodamine B isothiocyanate (Sigma-Aldrich) to enable fluorescence imaging. For transfection, CTs were seeded in fibronectin-coated 6-well plates (1 x 10^5 cells per well) and allowed to attach overnight. NP170s were sterilised under UV light for 30 minutes and used at a concentration of 1.25 mg/ 10^6 cells (standard dose). NP170s were then dissolved in 1ml of pre-warmed DPBS, and ultra-sonicated for 30 seconds twice. miRNA mimics were prepared at the required concentration of 100nM in antibiotics/serum-free IMDM. The miRNA solution was incubated for 5 minutes at RT then conjugated with the NP170s on a shaker at 100rpm for 1 hour at RT. The NP170-miRNA mixture was then added to antibiotics-free 1%-FBS IMDM. Cells were washed twice with DPBS before adding the NPs and

incubated for 6 hours. An incubation period of 6 hours was reported by S. Malandraki-Miller as the optimum for maximum transfection for CTs (thesis). After the incubation, cells were washed 3 times gently with DPBS then incubated with CEM before analysis.

2.17 miR-210 overexpression using retroviral transduction

The retroviral transduction was performed under the guidance of Dr. Tara Caffrey, a postdoctoral research scientist at the Wade-Martins group.

2.17.1 Bacterial transformation

The plasmids were received blotted on filter paper and therefore were resuspended in 100µl of TE buffer overnight at 4°C. LB agar and broth were dissolved in distilled water and autoclaved. The following day, LB agar was microwaved for 20 minutes to liquefy it and it was allowed to cool down before adding ampicillin at 1:500. The LB agar was then plated in petri dishes and allowed to solidify before adding the bacterial transformations.

One Shot Stbl3 chemically competent *E. coli* (ThermoFisher) were used to clone the resuspended plasmid DNA according to manufacturer's instructions. Briefly, the bacterial cells were defrosted on ice and then a volume of 5µl of each plasmid DNA was added to a vial of cells and incubated for 30 minutes on ice. The bacterial cells were heat shocked at 42°C for 45 seconds and allowed to recover on ice for 2 minutes and then 250µl of S.O.C. medium (ThermoFisher) was added to each vial. The vials were shaken horizontally at 37°C for 1 hour at 200 rpm in a shaking incubator. Finally, working under a laminar hood, three different volumes (10, 50, 100µl) of each transformation were plated on the LB agar dishes using sterile spatulas. The dishes were inverted and incubated overnight at 37°C then checked for colonies the following day and stored at 4°C until the following step.

2.17.2 Miniprep, maxiprep, and restriction digests

To grow bacterial colonies for the miniprep, 5mg of ampicillin was added to 50ml of LB broth then added at 1.5ml per glass tube. Large isolated colonies were selected, as random bacteria may grow next to large colonies that use up the ampicillin. We selected 6 colonies per plasmid. A pipette tip was used to pick the colonies which were transferred to the glass tubes. A negative control glass tube with no colony was also prepared. The tubes were incubated overnight at 200rpm and 37°C. The LB broth were cloudy the next day, except the negative control. Bacterial miniprep was performed using the QIAprep Spin Miniprep Kit (Qiagen) following manufacturer's instructions. To verify that we had the correct plasmid DNA in the selected colony minipreps, a restriction digest was performed using the restriction enzymes XhoI (NEB), which should linearize the retrovirus and give a band at 6349bp, and PvuI-HF (R3150), which should give bands at 896bp and 5453bp. A volume of 8µl of the miniprep was added to 1.5µl 10x CutSmart high fidelity buffer (B7204), 0.2µl of the enzyme, and 5.5µl of water for a total of 15µl. The restriction digest reaction was incubated for 2 hours at 37°C. A 1% agarose gel containing ethidium bromide was prepared. Following the 2-hour incubation, 5µl of 5x DNA Loading Buffer Blue (Bioline) was added to the minpreps and the entire 20µl was loaded into the gel. HyperLadder 1Kb (Bioline) was loaded into the gel for reference. Bacterial maxiprep was performed on one of the selected colonies for the miniprep after ensuring that the colony contains the correct plasmid DNA by the giving the right size band on the gel. One colony for each plasmid was chosen and picked using a pipette tip then added to a flask containing 250ml of LB media and 500µl of ampicillin. The flask was covered with foil and incubated overnight at 200rpm and 37°C. The maxiprep was performed using the NucleoBond Xtra Maxi kit (Macherey-Nagel) and the NucleoBond Finalizer Large Plus kits (Macherey-Nagel) following manufacturer's instructions. Both the minipreps and maxipreps can be stored at 4°C.

2.17.3 Retroviral packaging using Phoenix-Ampho cells

Phoenix-Ampho cells at were seeded at $3x10^6$ cells in $10cm^2$ plates in growth media (DMEM containing PSG, and 10% FBS). The plates were gently shaken to distribute the cells evenly in the plate then allowed to attach overnight. The cells must be at 2/3 confluence, as they are most transfectable at subconfluence giving the highest titer virus possible. The next day, a FuGENE HD mix was prepared by adding 600µl of OptiMEM (ThermoFisher) without antibiotics to 20µl of FuGENE HD (Promega) and incubated for 5 minutes at RT. A DNA mix was prepared by adding 2µg of VSVG plasmid to 8µg of miR-210, backbone, or pmax GFP positive control vector (Lonza). The FuGENE Mix was added drop by drop to the DNA mix, mixed gently, and incubated for 30 minutes at RT. This was then added to the cells and topped up with 2.5ml of growth media and incubated for 4 hours at 37°C. After 4 hours, 7.5ml of growth media was added to each plate and incubated overnight. The next day, the transfection control plate incubated with pmax GFP positive control vector was checked for transfection efficiency. If successful, the media, now containing viruses, was collected, centrifuged for 5 minutes at 330×g, and filtered using a 0.45µm filter to remove any cells.

Fresh growth medium was added to the cells and the same process was repeated the next day. The media containing viruses was snap-frozen in dry ice and stored at -80°C.

2.17.4 CT retroviral transduction

To determine the concentration and cell density at which puromycin is 100% lethal to CTs, CTs were seeded at 50, 80, and 100 x 10^3 cells per well in a 6-well plate and treated with either 1µg/ml of puromycin. Cell survival was examined daily and seven days were found to induce complete cell death.

2.18 Mouse infarct surgery

The left anterior descending (LAD) coronary artery of wildtype female C57Bl/6 (20 - 25 g) was occluded using the method of Lygate *et al.*[278]. The surgery was performed by Mala Gunadasa-Rohling.

Prior to surgery, the animal was weighed, anaesthetised using 4% isoflurane in O_2, and injected with buprenorphine (0.06mg/kg) for analgesia and 200µl of saline. The mouse was suspended on a platform by the upper molars for intubation. Once intubated, the ventilator was set to 200bpm and 200 units of volume, a rectal probe was used to monitor temperature, and Lacri-lube eye gel was applied before securing the mouse limbs onto a heated surgical mat. Isoflurane levels were then reduced to 2% in O_2 and the chest was shaved and disinfected with Hibiscrub Antibacterial Skin Cleanser. An incision was made halfway through the ribcage in parallel to the ribs and blunt forceps were used to separate the skin and pectoral muscles. An opening was made in the 4th intercostal muscle for access to the heart. An 8-0 ethilon suture was tied around the middle left ventricular wall to occlude the LAD. Once the heart had settled around a minute after ligation, EGFP$^+$ CTs were injected to the infarct region at one or two points using an insulin syringe (30G). The ribs and then the skin were closed using a 7.0 prolene suture. The mouse was injected again with 300µl saline. The isoflurane was switched off gradually and the mouse was recovered in a warm incubator at around 33°C. Vetergesic jelly was provided for pain relief and the mice were monitored for 24 hours post-surgery.

2.19 Echocardiography

Echocardiographic imaging and analysis was performed by Prof. Carolyn Carr and Dr. Andrew Lewis. Briefly, mice underwent imaging 24 hours following LAD surgery and cell injection. Mice were anaesthetised using 2% isoflurane in $O_{2,}$ positioned on a heated stand and scanned by transthoracic echocardiography using the Visualsonics Vevo 1100 system. Parasternal long-axis and three short-axis B-mode images were acquired. The ventricular length at systole and diastole were measured from the long axis view and the LV area was measured in the three short axis images. Measurements of left ventricular function, comprising ejection fraction and stroke volume were calculated using Simpson's rule.

2.20 Heart dissociation and flow cytometry

Hearts were collected in ice-cold CEM before digestion using the Multi Tissue Dissociation Kit 2 (Miltenyi Biotec) to obtain single cells. The kit is optimised for a high yield of viable non-myocytes. The enzyme mix was prepared according to manufacturer's instructions. Hearts were transferred into Petri dishes containing DPBS with primocin and washed thoroughly to remove excess blood. Tissue was minced into 1 - 2 mm^3 pieces with tweezers then transferred into 500µl of the enzyme mix in 15ml falcon tubes and incubated in the water bath for 40 minutes. The reaction was neutralised by adding 7.5ml of CEM then applied through a 70µm strainer which was then washed with 3ml of CEM. The suspension was centrifuged at 600×g for 5 minutes and the supernatant discarded. Each sample was stained with 500µl of Zombie Violet Fixable Viability Kit dye (Biolegend) diluted in DPBS (1:500) for 20 minutes at RT then diluted with DPBS and centrifuged as before to discard the supernatant. The samples were fixed in 500µl 4% PFA for 30 minutes at 4°C then diluted with DPBS and centrifuged as before to discard the supernatant. The samples were resuspended in 1ml of DPBS and kept at 4°C to be run the next day. Negative and single-colour controls were also used where an uninjected heart was dissociated and divided into 4: unstained, stained with Zombie Violet only, mixed

with EGFP$^+$ CTs, mixed with EGFP$^+$ CTs and stained with Zombie Violet. The samples were run using the Cytek DxP8 flow cytometer. Non-viable cells, which tend to have greater autofluorescence, and doublets increase false positives and therefore were excluded. The gating strategy is shown in figure 5.9.B.

2.21 Serum preparation and cardiac troponin I ELISA

Blood was collected by cardiac puncture using a 19G needle and transferred into an Eppendorf tube where it was allowed to clot by leaving it incubated at RT for 15 minutes. The samples were then centrifuged at 1,000–2,000×g for 10 minutes at 4°C. Following centrifugation, blood serum formed as a supernatant and was transferred into clean Eppendorf tubes and kept on ice before storage at -80°C before running the cardiac troponin I ELISA. Serum samples were thawed and diluted 4-fold in the provided diluent. The ELISA was performed according to manufacturer's instructions (Life Diagnostics). Optical density was measured at 450nm using the Fluostar OPTIMA Microplate Reader (BMG Labtech, Germany).

2.22 Statistical analysis

Results are presented as mean ± standard deviation. All statistical analysis was performed using Graphpad Prism. Data were analysed using unpaired two-tailed Student's t-test, one-way or two-way analysis of variance (ANOVA). The statistical analysis used is mentioned in the legend of each results figure. A value of $P < 0.05$ was considered statistically significant and represented as * = $P < 0.05$, ** = $P < 0.01$, *** = $P < 0.001$, **** = $P < 0.0001$.

2.23 Illustrations

Illustrations were created with Biorender.com.

CHAPTER 3

Characterisation of CTs in comparison to CDCs and CFs

3 Results chapter 1

3.1 Introduction

3.1.1 The identity of proposed populations of adult mammalian cardiac progenitors

Evidence stemming from fate mapping studies of cardiomyocyte renewal in the adult mammalian heart challenged the dogma considering the heart as a post-mitotic organ[40,187,188]. Therefore, multiple research groups attempted to characterise endogenous cardiac populations that may have a role in the cardiac regenerative process. Identifiers of the proposed CPC populations include SCA1 and the SP dye-efflux phenotype, KIT, ISL1, cardiosphere- and colony-forming assays, or re-activation of the embryonic epicardial programme and WT1 upregulation (discussed in more detail in Introduction 1.4.3). More recent evidence has suggested that the mechanism behind cardiomyocyte renewal in the adult mammalian heart is cardiomyocyte proliferation and that contribution of CPCs is minimal[40,186–189]. Despite this, and the low cardiomyogenic potential of CPCs following transplantation, the therapeutic functionality of these cell types has been demonstrated in pre-clinical studies[122,150,151,160,172].

Numerous studies have questioned the differences between the various cardiac stromal cell populations including mesenchymal cells, fibroblasts, pericytes, and CPC populations[102,105,107,279,280]. This is based on the overlap in their morphology and gene expression profile. For example, as observed in CPCs, cardiac fibroblasts have also been shown to express cardiogenic transcription factors, which contribute to cardiac development and repair[281]. Both cardiac and tail fibroblasts share a highly similar molecular signature to that which has been previously described for MSCs[282]. Substantial efforts have been made to determine the identity of these cardiac stromal cells and differentiate between different cell types. To further confuse the situation, single-cell transcriptional profiling of mouse ventricular nonmyocytes revealed subpopulation heterogeneity within the cardiac fibroblast population[283].

In addition, the commonly-used markers to identify pericytes (e.g. *Pdgfrβ* and *Ng2*) are relatively non-specific, although genes that show higher expression in pericytes relative to other cell types expressing them have been identified[283].

3.1.2 A novel protocol for the isolation of cardiac stromal cells

Certain research groups have relied on sorting cardiac stromal populations based on surface marker expression followed by clonogenic selection. These include the clonogenic derivation of $SCA1^+$ $PDGFR\alpha^+$/SP cells researched by the Schneider group, and of KIT^+ cells researched by the Ellison, Nadal-Ginard and Torella groups[122,284]. Both methods resulted in homogenous self-renewing cardiogenic populations that showed promise. However, these cell types are found at very low rates in the adult mouse heart and both studies reported a cloning efficiency of around 1-2%. Ideally, the optimal cell isolation protocol would generate a robust large population of cells in the shortest possible duration.

The Carr group has worked extensively on CDCs, a heterogenous stromal population (see Introduction 1.4.3). Although CDCs have shown some promise in pre-clinical studies[150,151,160], unpublished work from the group has shown that the CDC isolation protocol produces a highly variable population of cells (F. Perbellini, thesis, University of Verona). When considering cell therapy, especially for clinical studies, it is important to assure a robust and reproducible isolation protocol. The isolation of CDCs involves culturing cardiac explants to harvest EDCs that are later induced to form cardiospheres. It was noted that these EDCs vary in their morphology and the time required to achieve confluent culture[161]. Considerable variation was also observed in CDC expansion time that can range from 5-84 days[161]. This variation may have been due to the expansion of CDCs from patients with chronic ischaemic heart disease who varied in age and in the existence of co-morbidities[161] but was also evident to a lesser extent in cells expanded from young healthy mice (F. Perbellini, thesis, University of Verona). In an attempt to optimise cardiac stromal cell isolation, S. Malandraki-Miller (thesis) developed

a collagenase-trypsin (CT) protocol adapted from a study by Gharaibeh *et al*.[285] and Okada *et al*.[286] for isolating slowly adhering cells (SACs) from skeletal muscle. These SACs had higher differentiation, survival, and therapeutic potential in comparison to rapidly adhering cells (RACs). The CT protocol was found to generate a population with less variation in cell yield and expansion time in comparison to CDCs but retaining a similar gene expression profile (S. Malandraki-Miller – thesis).

We have shown that CTs can be induced to differentiate into the cardiomyocyte lineage *in vitro*[273] using the published TGFβ1 protocol[123,287]. We have examined metabolic manipulation as a means to enhance the cardiomyocyte differentiation of CTs. Fatty acid supplementation triggered a metabolic switch as evident by an upregulation in glucose and fatty acid oxidation, as well as glycolytic flux. This was accompanied by an increased expression of cardiomyocyte markers in CTs following differentiation using the TGFβ1 protocol. These results are concordant with the observed metabolic switch from glucose to fatty acid oxidation that ensues during heart development and cardiomyocyte maturation. Moreover, S. Malandraki-Miller (thesis) found that CTs can be cultured for more than 40 passages. CTs were also found to contain a population of "strongly-adherent" cells that required at least three rounds of trypsinisation to harvest. These strongly-adherent cells had higher expression of the pluripotency-associated marker *Pou5f1* (encodes Oct4) in comparison to the total population but are lost within a couple of passages due to their strongly-adherent phenotype.

Another key factor to consider in cardiac cell therapy is the cardiac compartment from which cells are to be isolated. With the exception of epicardial-derived $WT1^+$ cells, CPC populations have been isolated from the whole heart[149,158,288,289], ventricles[119,150], or atrial appendages[123,290]. Interestingly, a study by the Carr group showed that EDCs could be expanded from all atrial biopsies but from fewer than half of ventricular biopsies obtained from patients with chronic ischaemic heart disease[161]. Moreover, the KIT^+ and $SCA1^+$ cell niches have been described as

the atria and apex of the adult mouse heart[291–293]. Based on this, and the relative ease of obtaining a biopsy from the atrial appendage, our group selected the atria as the compartment from which cardiac stromal cells (both CDCs and CTs) were to be isolated.

3.1.3 Aims

As this thesis is based on the unsorted cardiac stromal CT population, this chapter is dedicated to further characterising these cells. This was achieved by comparing them to CDCs and primary cardiac fibroblasts (CFs) purchased from Cell Biologics using immunofluorescence, single-cell qRT-PCR, cytokine arrays, and assessing their survival potential. All three populations were isolated from adult mouse atria. Figure 3.1 demonstrates the method by which each cardiac stromal cell population was isolated. However, some details regarding the isolation of CFs could not be attained from the selling company. The markers used and the design of the single-cell qRT-PCR characterisation experiment are described in table 3.1 and figure 3.2, respectively.

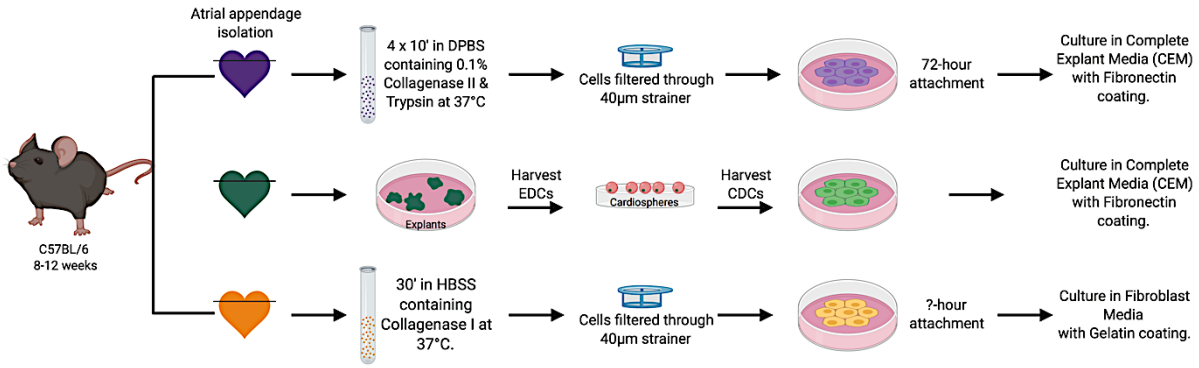


Figure 3.1 Isolation method of the three cardiac stromal populations, CTs, CDCs and CFs

Schematic showing the protocol used to isolate CTs, CDCs, and CFs. The isolation protocol of CTs and CDCs is detailed in the Methods chapter. As CFs were purchased and not isolated in our lab, some information are lacking e.g. age of mice, duration of cell attachment, and composition of the accompanying media.

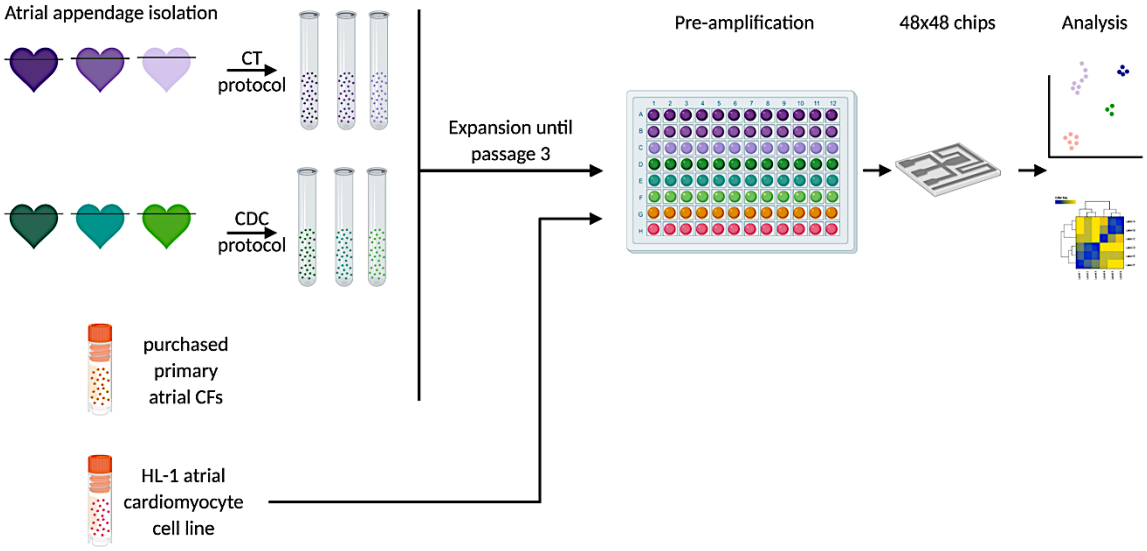


Figure 3.2 Overview of the single-cell qRT-PCR experiment used to characterise the three cardiac stromal populations, in comparison to HL-1 cardiomyocytes

Schematic showing the steps involved in the single-cell qRT-PCR experiment. The protocol is detailed in the Methods chapter. CTs and CDCs represented biological replicates, whereas CFs and HL-1 cardiomyocytes represented technical replicates.

3.2 Results

3.2.1 Immunophenotypic analysis of CTs

3.2.1.1 Expression profile of CTs at different passages

Immunofluorescence was used to phenotypically characterise CTs at passage 1 and passage 7 in an attempt to answer the following questions: Do CTs express fibroblast-associated markers? Do all the cells express those markers? Are these markers expressed by all cells uniformly or do some cells have higher or lower expression of a given marker?

Three biological replicates of CTs at each passage number were examined and three random fields were imaged of each replicate. We examined the expression of the fibroblast-associated genes *Cd44*, *Pdgfrβ*, *Acta2* (encodes αSMA), *Vim* (encodes vimentin) and *Wt1*. At passage 1, we found that CTs were positive for CD44, PDGFRβ, αSMA and vimentin. Although these proteins were detected in all of the cells, some heterogeneity in the expression level of some of the markers was detected between cells (arrows). The CTs were negative for WT1. Immunofluorescent staining of CTs at passage 7 showed that CTs retained their expression of the same markers tested. Some heterogeneity was also detected at later passages (figure 3.3).

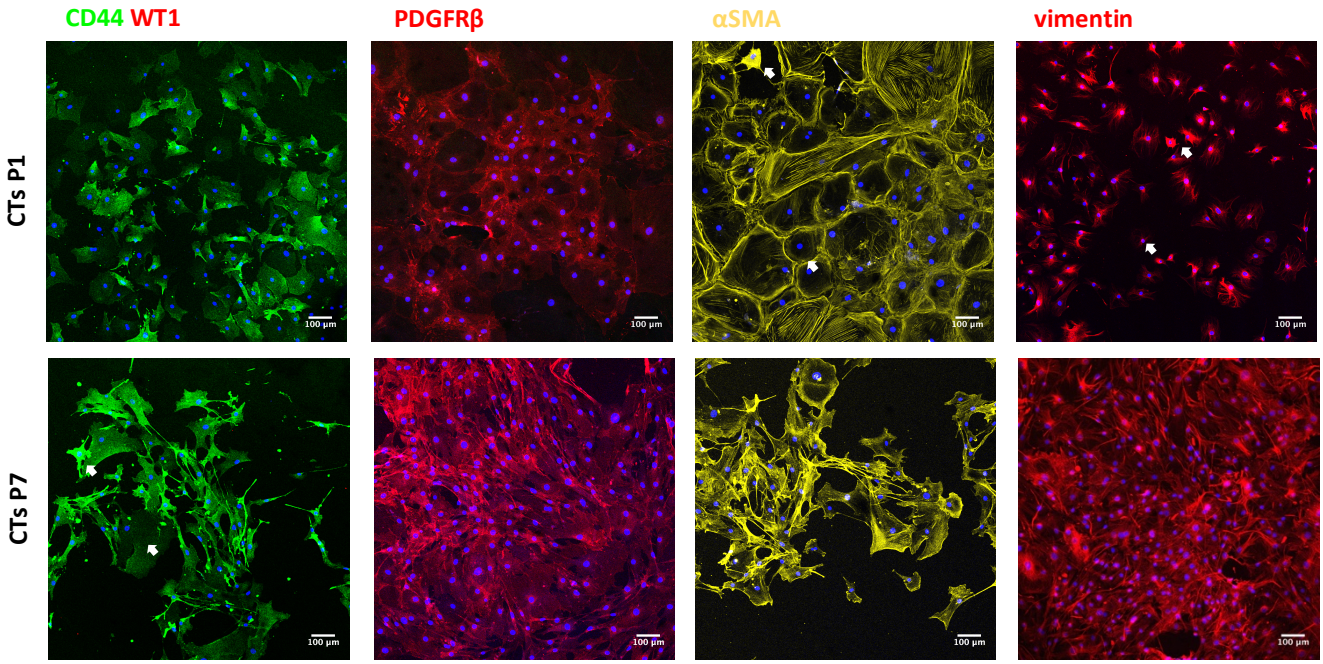


Figure 3.3 CTs are positive for fibroblast-associated markers

CTs at passages 1 and 7 stained with anti- CD44, WT1, PDGFRβ, αSMA and vimentin antibodies and DAPI, representative of n=3. Heterogeneity in expression levels is highlighted by white arrows. Cells were imaged using an FV1000 confocal microscope. Scale bar = 100μm.

3.2.1.2 The CT population does not contain cardiomyocytes

Staining the CT population with an antibody against the cardiac marker cTnT revealed cells positive for this protein. The number of cTnT+ cells among the CT population was unexpectedly high, we therefore sought to validate the specificity of the antibody. Whole mouse embryo sections (a gift from the Smart group) were stained with the cardiomyocyte antibodies cTnT, myosin light chain 2 (MYL2), myosin heavy chain 6 (MYH6), and sarcomeric α-actinin (αSA) to confirm their specificity to the heart. While all four antibodies strongly labelled the myocardium, the cTnT antibody labelled several domains outside the heart, including a large population of cells in the region of the septum transversum (indicated by the star in figure 3.4.G). Septum transversum mesenchyme is highly heterogeneous, containing precursors for a multitude of lineages, ranging from cardiomyocytes[294] to haematopoietic cells[295]. The differential labelling suggests that cTnT may be expressed in cardiomyocyte progenitors, whereas αSA is restricted to mature cardiomyocytes. As we found that αSA expression is restricted to mature cardiomyocytes, the αSA antibody was used to stain CTs. αSA^+ cells were not detected in the CT population and we thus concluded that there may be immature cardiomyocyte progenitors within the CT population but no mature cardiomyocytes (figure 3.4).

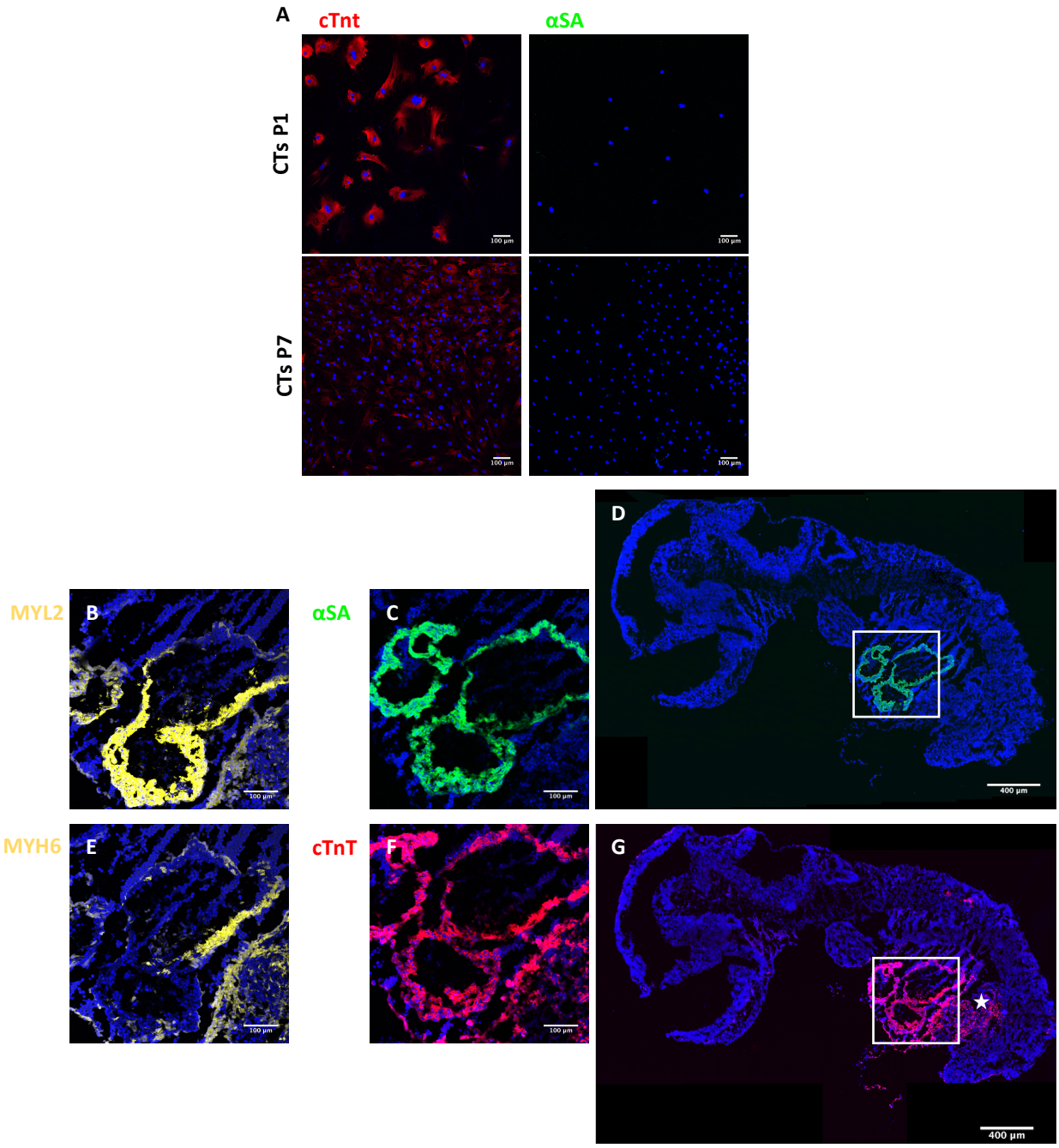


Figure 3.4 No α sarcomeric actinin detected in CTs

(A) CTs at passages 1 and 7 stained with anti- cTnT and αSA antibodies, representative of n=3 **(B,C,E,F)** Heart sections of mouse embryos at E10.5 stained with anti- MYL2, αSA, MYH6 and cTnT antibodies, representative of n=1 (scale bar = 100µm). C and F represent high power inserts which are shown by white boxes in whole mouse embryo sections (D and G, respectively; scale bar = 400µm). The septum transversum region is indicated by the star. Sections were imaged using an FV1000 confocal microscope.

3.2.2 *Characterisation of CT morphology and gene expression profile in comparison to CDCs and CFs*

3.2.2.1 *Immunofluorescence*

For further phenotypic characterisation of CTs, immunofluorescent staining was performed on other primary cardiac stromal populations isolated from adult mouse atrial appendages: CDCs (Methods 2.2.2) and CFs at passage 1. Three biological replicates of CDCs were examined and three random fields were imaged of each replicate. As CFs were purchased, it was not possible to use biological replicates, thus only technical replicates were used. Both CDCs and CFs were also positive for CD44, PDGFRβ, αSMA and vimentin. However, unlike CTs and CDCs, some CFs were positive for the epicardial- and fibroblast-associated marker WT1 (figure 3.5).

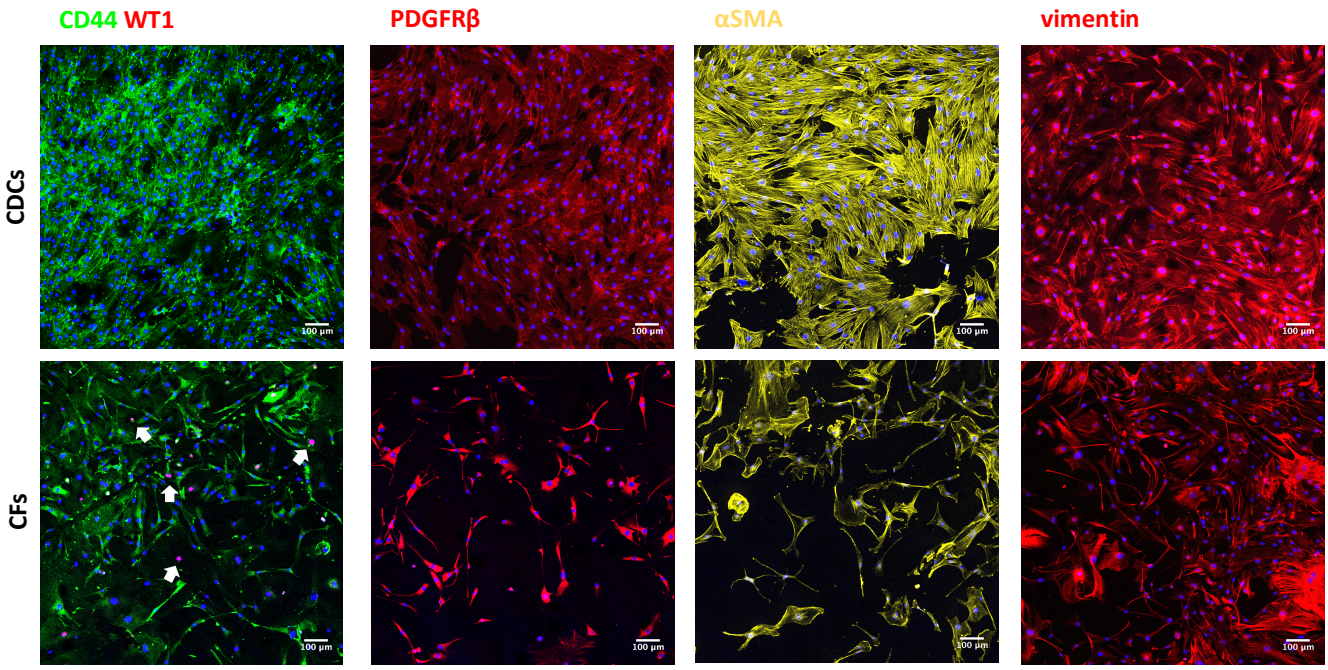


Figure 3.5 CDCs and CFs are positive for fibroblast-associated markers

CDCs and CFs at passages 1 and 7 stained with anti- CD44, WT1, PDGFRβ, αSMA and vimentin antibodies, representative of n=3. WT1 expression in CFs is highlighted by white arrows. Cells were imaged using an FV1000 confocal microscope. Scale bar = 100µm

3.2.2.2 Morphology

The three cardiac stromal populations were compared morphologically. They all appeared spindle-shaped, resembling fibroblast cultures. Heterogeneity in cell size was detected at passage 1 in all stromal populations, although CTs and CDCs appeared large in comparison to CFs at passage 1 (figure 3.6). Both CTs and CDCs decreased in cell size at passage 7 in comparison to passage 1. This was also evident by the increase in the required cell number to attain a confluent flask. In a 25cm^2 flask, around 200,000 passage 7 CTs or CDCs were required to achieve confluency whereas fewer than 50,000 cells were required at passage 1. Culturing CFs beyond passage 4-5 was not possible as they underwent cell death with successive passaging. This is consistent with Cell Biologics' specifications of the cell type and marks an interesting difference between the CFs, and CTs and CDCs.

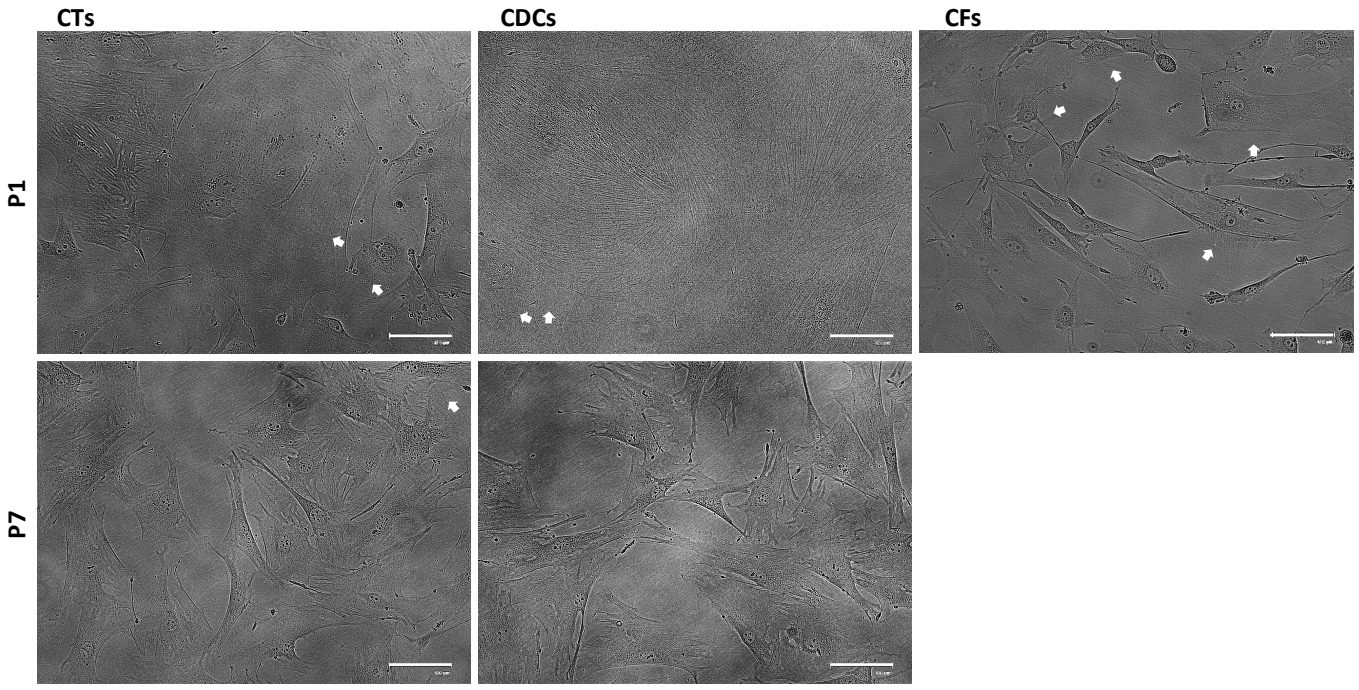


Figure 3.6 Morphological analysis of the three cardiac stromal populations

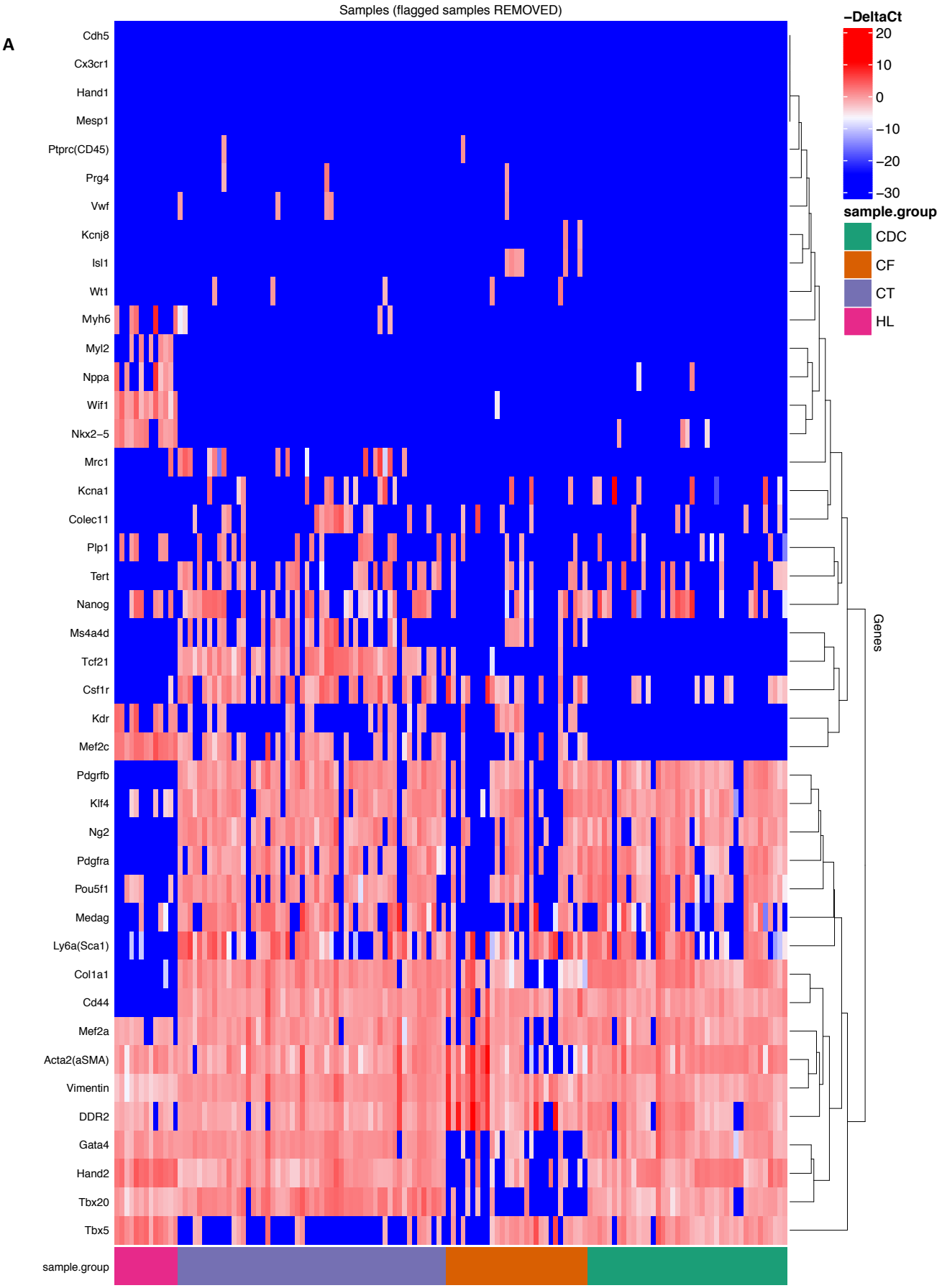
Representative images of CTs and CDCs at passages 1 and 7 and CFs at passage 1. Heterogeneity in cell size is highlighted by white arrows. Cells were imaged using an EVOS fluorescent microscope. Scale bar = 125µm.

3.2.2.3 Single-cell qRT-PCR

As immunofluorescent staining was only used for qualitative analysis and due to the innate heterogeneity of the cells, single-cell qRT-PCR was performed on CTs, CDCs, and CFs at passage 3, and compared with the HL-1 cardiomyocyte line which was used as a control. It was not possible to perform the single-cell qRT-PCR experiment at passage 1, as with the immunofluorescent staining, because it was performed using the BioMark HD system at Imperial College London, in collaboration with Dr. Michela Noseda, and we needed to make sure that the cells were robust enough to be transported as they are sensitive during the first couple of passages. Genes selected for this experiment included those that were assessed using immunofluorescent staining, in addition to genes encoding cardiogenic transcription factors and other genes that were deferentially expressed in the SCA1 subpopulations according to the Noseda *et al*. study. Moreover, we attempted to assess the existence of different cardiac subpopulations including pericytes, endothelial cells and macrophages using genes that were described by the Skelly *et al*. study. Genes selected for this experiment are detailed in table 3.1 and described in more detail below. Consistent with the immunofluorescence data, the cardiac stromal populations expressed *Cd44*, *Pdgfrβ*, *Acta2* (encodes αSMA), and *Vim*, albeit the CFs had less consistent expression of *Pdgfrβ*, and *Acta2*. Additional fibroblast-associated markers were also examined. CFs co-expressing *Wt1* and *Tcf21* (n=2/29) were detected which is consistent with the immunofluorescence data. Interestingly, CTs co-expressing *Wt1* and *Tcf21* were also detected (n=3/55). *Ly6a* (encodes SCA1) and *Pdgfrα* were expressed in all three populations. The three cardiac stromal populations expressed little or no *Prg4* and *Wif1* but displayed expression of *Ddr2*, *Medag* and *Col1a1*. *Ms4a4d* expression was detected in CTs and some CFs only. In regards to pericyte-associated marker, *Kcnj8* showed little or no expression in all populations. *Colec11* showed sporadic expression, whereas *Ng2* showed high expression in all three cardiac stromal populations (figure 3.7).

In CTs and CDCs, the most prevalent cardiogenic transcription factors were *Gata4*, *Tbx20*, *Hand2*, and *Mef2a* with little or no expression of *Hand1*, *Isl1*, and *Nkx2-5*. In contrast, CFs had less uniform expression of *Gata4*, *Tbx20*, and *Hand2*. Unlike CDCs, both CTs and CFs expressed *Mef2c* heterogeneously. The expression of *Tbx5* in CFs followed a similar pattern to CDCs, but was more sporadic in CTs. Interestingly, only CFs showed expression of *Isl1*. The three cardiac stromal populations had very little or no expression of markers of cardiomyocytes (*Nppa*, *Myh6*, and *Myl2*), haematopoietic (*Cd45*) and endothelial cells (*Cdh5* and *Vwf*), with the exception of *Kdr* expression, which was detected in the CTs, CFs and HL-1 cardiomyocytes. The three cardiac stromal populations also had very little or no expression of markers of smooth muscle cells (*Myh11* and *Cnn1*), but these could not be included in this analysis unfortunately due to technical difficulties with the R script used, which we are currently trying to resolve. Expression of stem cell-related markers (*Pou5f1*, *Nanog*, *Klf4*, and *Tert*) was found in the three cardiac stromal populations. Interestingly, *Pou5f1*, *Nanog*, and *Klf4*, but not *Tert*, were expressed in HL-1 cardiomyocytes as well. As expected, HL-1 cardiomyocytes had a distinctly different expression profile and displayed expression of most cardiogenic transcription factors (*Gata4*, *Hand2*, *Mef2a/c*, *Nkx2-5* and *Tbx5/20*), and cardiomyocyte markers (*Nppa*, *Myh6*, and *Myl2*). HL-1 cardiomyocytes also expressed *Vim*, *Ddr2* and *Acta2*.

Expression of Schwann cell-related markers (*Plp1* and *Kcna1*) was found sporadically in all populations, with the exception of HL-1 cardiomyocytes where only *Plp1*, but not *Kcna1*, was expressed. We also assessed the expression of the macrophage-associated genes *Mrc1*, *Csf1r* and *Cx3cr1*. *Cx3cr1* showed no expression in all population, whereas *Mrc1* was only expressed in CTs. *Csf1r* was expressed in all three stromal populations but showed a more uniform pattern in CTs.


A
Samples (flagged samples REMOVED)
−DeltaCt
20
10
0
−10
−20
−30
sample.group
CDC
CF
CT
HL
Cdh5
Cx3cr1
Hand1
Mesp1
Ptprc(CD45)
Prg4
Vwf
Kcnj8
Isl1
Wt1
Myh6
Myl2
Nppa
Wif1
Nkx2−5
Mrc1
Kcna1
Colec11
Plp1
Tert
Nanog
Ms4a4d
Tcf21
Csf1r
Kdr
Mef2c
Pdgrfb
Klf4
Ng2
Pdgfra
Pou5f1
Medag
Ly6a(Sca1)
Col1a1
Cd44
Mef2a
Acta2(aSMA)
Vimentin
DDR2
Gata4
Hand2
Tbx20
Tbx5
sample.group
Genes

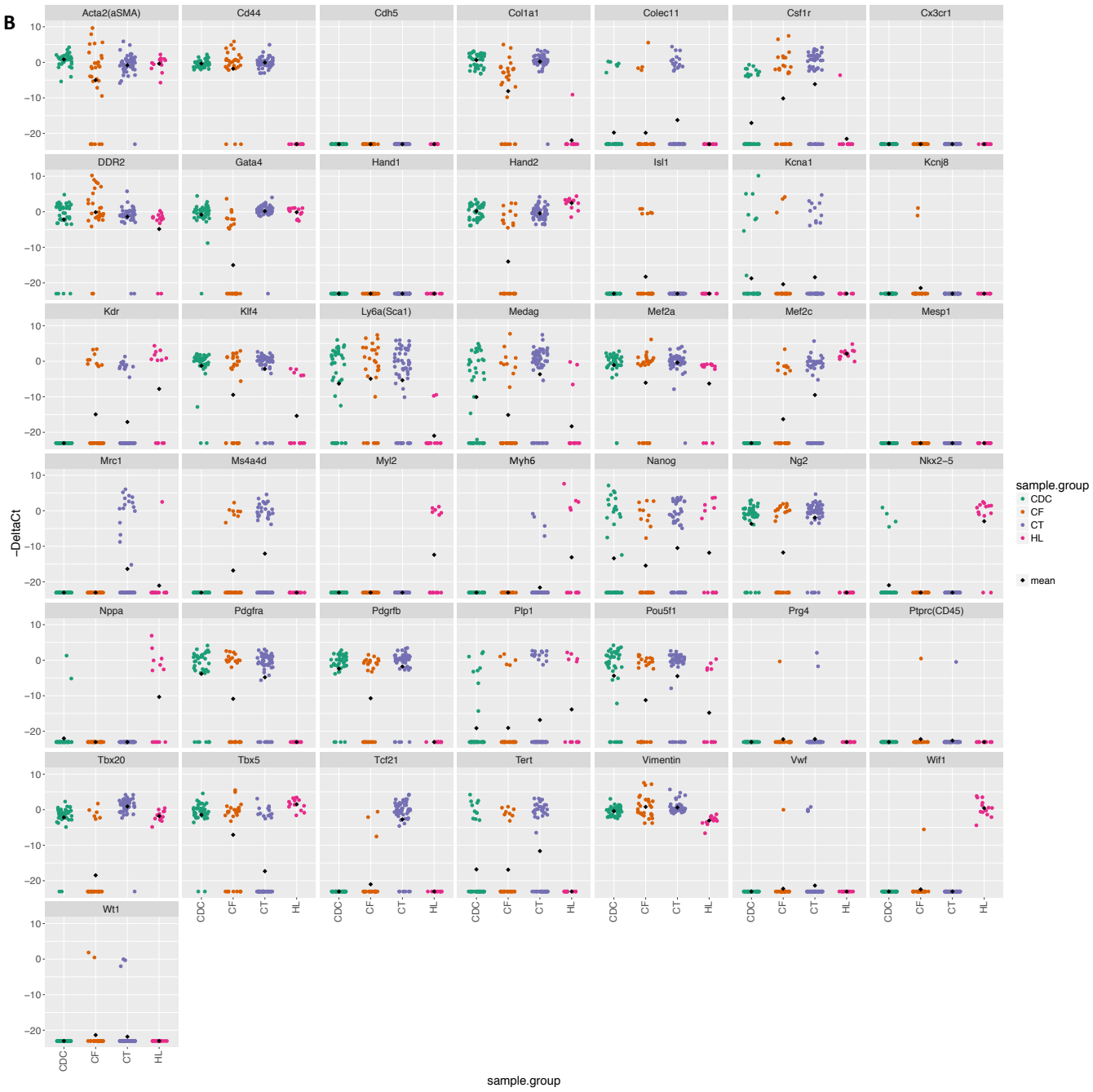


Figure 3.7 Single-cell analysis reveal an enrichment of *Tcf21* and low expression of *Tbx5* in CTs, compared to CDCs and CFs

(A) Expression of 43 genes was analysed at the single-cell level in the four cell populations shown: CTs (n=55), CDCs (n=41) and CFs (n=29) at passage 3, in addition to HL-1 cardiomyocytes (n=13). Both CTs and CDCs represent 3 biological replicates. The heatmap illustrates expression as -ΔCT values (blue is low or absent; red is high). Samples were ordered based on cell type, and the genes grouped by a hierarchical clustering algorithm based on the underlying co-expression pattern. **(B)** Single-cell expression of the 43 genes tested, represented individually in the four cell populations shown.

By principal component analysis (PCA), cardiac stromal cells and HL-1 cardiomyocytes were resolved as discrete groups, which is consistent with their distinct phenotypes. Gene loadings contributing to each dimension (Dim) suggest that a small subset of genes explain the cross-group variability captured by Dim.1 and Dim.2. The separation of HL-1 cardiomyocytes was attributable to *Wif1*, *Nkx2-5*, *Mef2c*, *Nppa*, *Myl2*, and *Myh6* (figure 3.8.A). Some separation of CFs from CTs with the CDCs clustering between the other two populations was also revealed and can be seen more clearly in the PCA of the stromal populations alone (figure 3.8.B). The separation of CTs was attributable to *Tcf21* and *Csf1r*, while the separation of CDCs and CFs was mainly attributable to *Tbx5*. CFs appeared more spread out suggesting higher heterogeneity, in comparison to CTs and CDCs, which is more apparent in the PCA of stromal populations only.

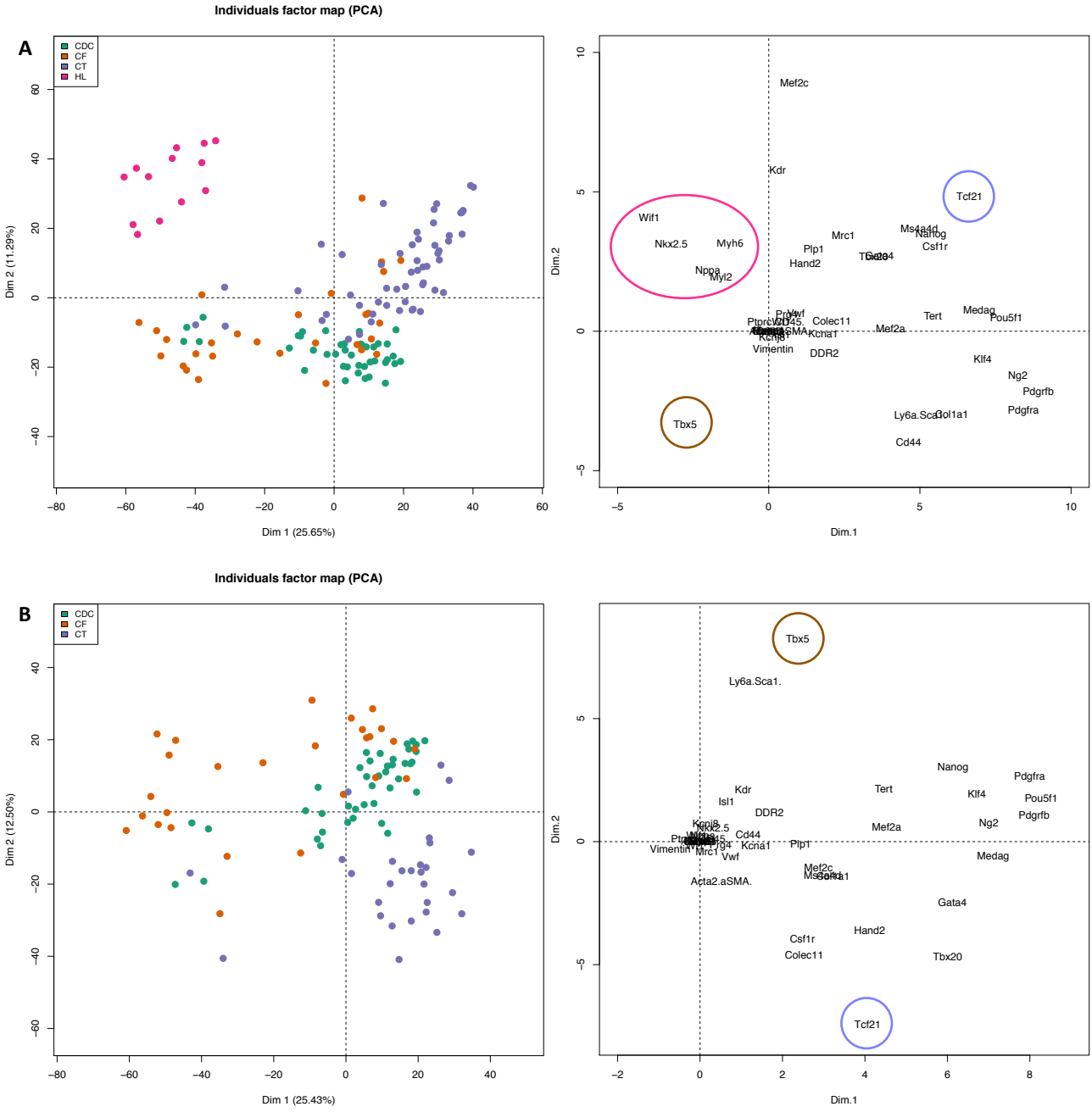


Figure 3.8 PCA of the three cardiac stromal population and HL-1 cardiomyocytes

(A) PCA of the four cell populations shown: CTs (n=55), CDCs (n=41) and CFs (n=29) at passage 3, in addition to HL-1 cardiomyocytes (n=13). Both CTs and CDCs represent 3 biological replicates. Dim.1 separates the cardiac stromal populations, whereas Dim.2 shows a distinct separation between cardiac stromal and myocyte populations. Gene loadings contributing to each Dim suggest that a small subset of genes explain the cross-group variability captured by Dim.1 and Dim.2. *Tcf21* is associated with CTs (emphasised in the blue circle), whereas *Tbx5* is associated with CDCs and CFs (emphasised in the brown circle). The separation between cardiac stromal and myocyte populations is reflected by clustering of cardiogenic and cardiomyocyte genes (*Nkx2.5*, *Wif1*, *Nppa*, *Myl2* and *Myh6*), which are emphasised in the pink circle **(B)** PCA of the three cardiac stromal populations alone: CTs (n=28), CDCs (n=41), CFs (n=27). Both CTs and CDCs represent 3 biological replicates. Gene loadings contributing to each Dim show that *Tcf21* is associated with CTs, whereas *Tbx5* is associated with CDCs and CFs.

Statistical analysis comparing the three cardiac stromal population revealed that CTs were more similar to CDCs than CFs with CTs showing significantly higher expression of *Vim* ($P < 0.05$), *Kdr* ($P < 0.05$), *Mrc1* ($P < 0.001$), *Tcf21* ($P < 0.0001$), *Ms4a4d* ($P < 0.0001$), *Tbx20* ($P < 0.0001$), *Csf1r* ($P < 0.0001$), *Mef2c* ($P < 0.0001$), and *Medag* ($P < 0.05$), but lower expression of *Tbx5* ($P < 0.0001$) and *Acta2* ($P < 0.01$), compared to CDCs. In comparison to the CFs, CTs showed significantly higher expression of *Col1a1* ($P < 0.0001$), *Pdgfrβ* ($P < 0.0001$), *Hand2* ($P < 0.0001$), *Pou5f1* ($P < 0.05$), *Mrc1* ($P < 0.001$), *Tcf21* ($P < 0.0001$), *Tbx20* ($P < 0.0001$), *Ng2* ($P < 0.01$), *Mef2c* ($P < 0.05$), *Medag* ($P < 0.001$), and *Gata4* ($P < 0.0001$), but lower expression of *Isl1* ($P < 0.0001$) and *Tbx5* ($P < 0.01$) (figure 3.9).

Correlation plot analysis based on data collected from both stromal and cardiomyocyte populations (figure 3.10) showed a polarisation between the expression of some fibroblast-associated markers and cardiogenic transcription factors and a positive correlation between the expression of cardiogenic transcription factors and cardiomyocyte markers. Moreover, *Tcf21* expression showed a positive correlation with the expression of *Tbx20*, *Csf1r*, *Ms4a4d* and *Mrc1*. This is attributed to the high expression of these genes in CTs. *Ly6a* with *Cd44* and *Ddr2*; *Acta2* with *Hand2*; *Pou5f1* and *Klf4* with *Mef2a*, *Medag*, *Ly6a* and *Nanog*. In addition, *Kcnj8* expression showed a positive correlation with the expression of *Isl1* due to their co-expression pattern in CFs. *Wt1* and *Tert* expression did not show any correlation with the tested genes.

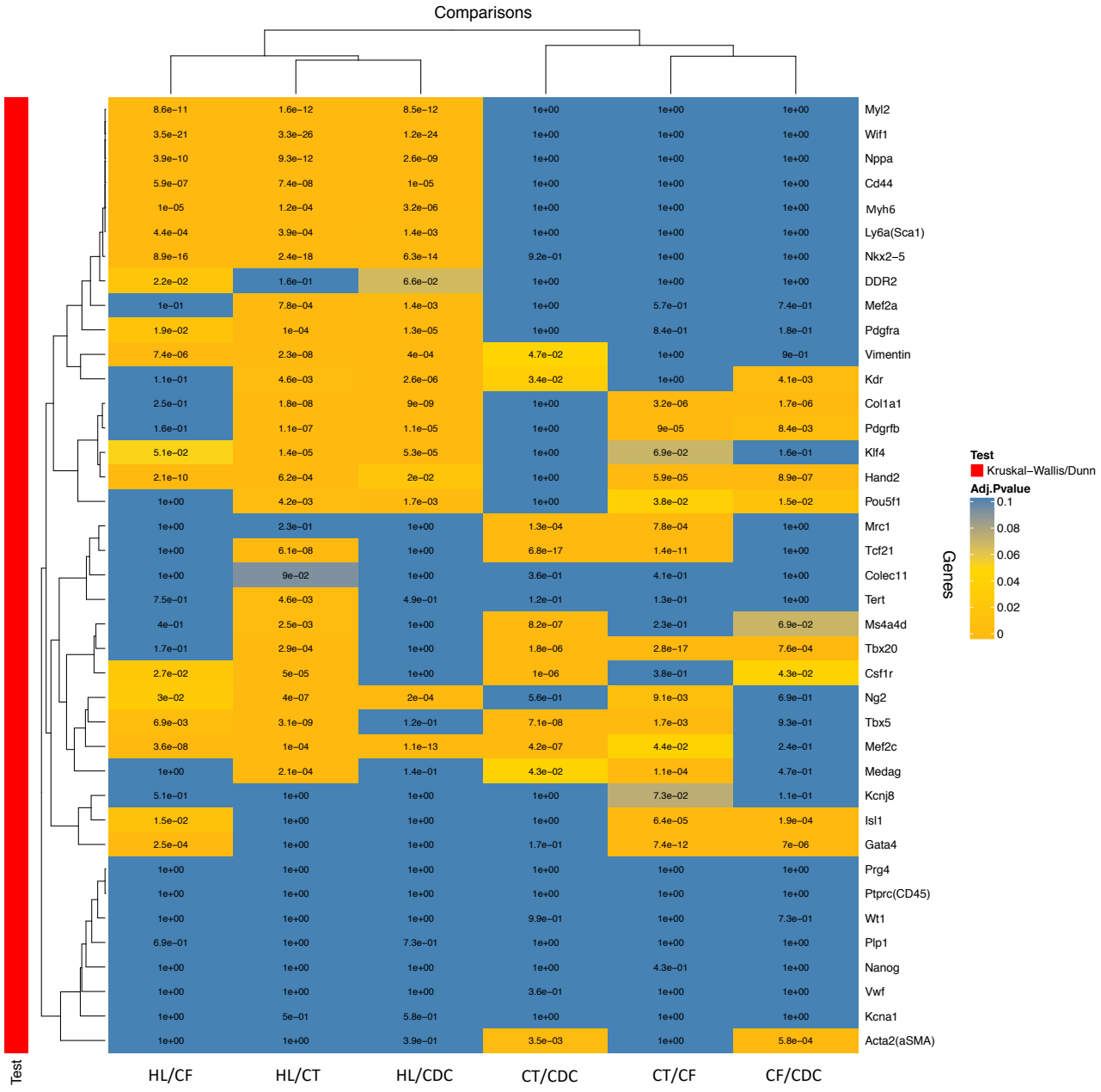


Figure 3.9 Statistical analysis of the single-cell qRT-PCR data

Statistical analysis of the four cell populations shown: CTs (n=55), CDCs (n=41) and CFs (n=29) at passage 3, in addition to HL-1 cardiomyocytes (n=13). Both CTs and CDCs represent 3 biological replicates. The heatmap illustrates P values from 0 to 0.1 (orange to blue is low to high). The genes were grouped by a hierarchical clustering algorithm based on the underlying co-expression pattern.

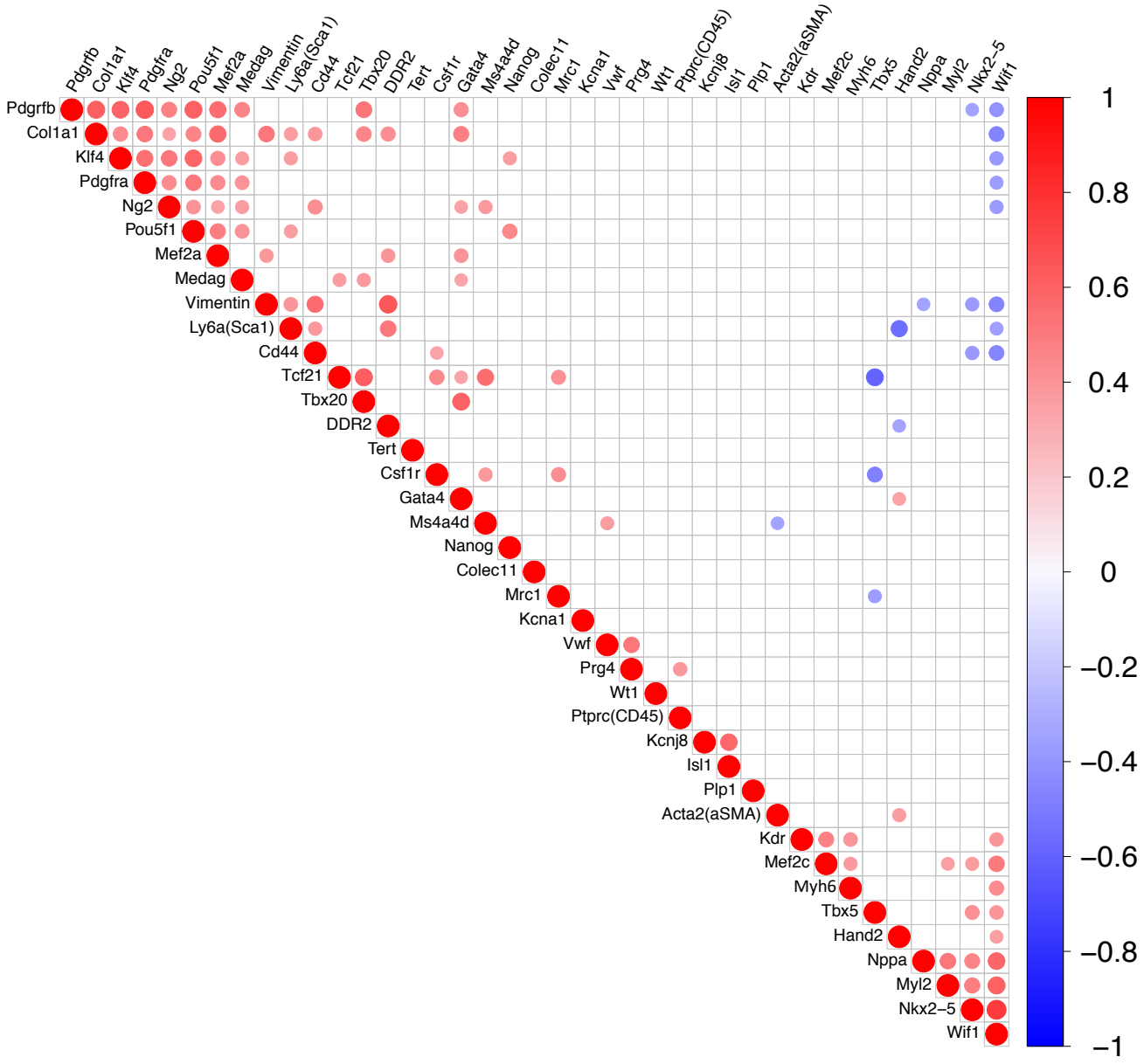


Figure 3.10 Gene correlation plot derived from the single-cell qRT-PCR data

Gene correlation plot derived from the single-cell qRT-PCR data of the four cell populations: CTs, CDCs, CFs and HL-1 cardiomyocytes. Gene correlation is represented by the colour of the dots (blue is negative; red is positive). Both the diameter and colour intensity of each dot are proportional to the level of correlation.

3.2.3 Growth factor release by CTs in comparison to CDCs and CFs

Due to the important role paracrine mechanisms play in cardiac repair, we examined the growth factors secreted by CTs in comparison to CDCs and CFs using an antibody array. Cells were cultured in serum-free media (as required by the manufacturer) for 48 hours prior to collection of the conditioned media. The conditioned media was assessed by a mouse growth factor array that detects 20 growth factors, many of which had been implicated in cardiac repair (see table 3.2). CTs, CDCs, and CFs showed a similar pattern in their secretion of the tested growth factors. Figure 3.11.A shows a heatmap of the spot intensities of all the assessed factors, whereas figure 3.11.B shows individual representation of the factors that were significantly differentially secreted by the stromal populations. Statistical analysis revealed that CTs secreted lower levels of IGF-1 (CTs, 0.61 ± 0.16; CDCs, 1.2 ± 0.09; $P < 0.01$; n=3), M-CSF (CTs, 0.45 ± 0.07; CDCs, 0.95 ± 0.06; $P < 0.01$; n=3), VEGF-A (CTs, 0.19 ± 0.04; CDCs, 0.58 ± 0.03; $P < 0.01$; n=3) but higher levels of VEGF-R1 (CTs, 0.25 ± 0.02; CDCs, 0.11 ± 0.02; $P < 0.05$; n=3) in comparison to CDCs. In comparison to CFs, CTs secreted lower levels of IGF-2 (CTs, 0.19 ± 0.01; CFs, 0.41 ± 0.14; $P < 0.05$; n=3), IGFBP-6 (CTs, 0.14 ± 0.02; CFs, 0.50 ± 0.19; $P < 0.05$; n=3), M-CSF (CTs, 0.45 ± 0.07; CFs, 1.2 ± 0.18; $P < 0.001$; n=3), and VEGF-A (CTs, 0.19 ± 0.04; CFs, 0.69 ± 0.11; $P < 0.001$; n=3). This shows that cardiac stromal populations may vary in their paracrine potential. With the exception of IGFBP-6 and VEGF-R1, all of the differentially secreted factors have potentially desirable effects in the context of cardiac repair (see table 3.2).

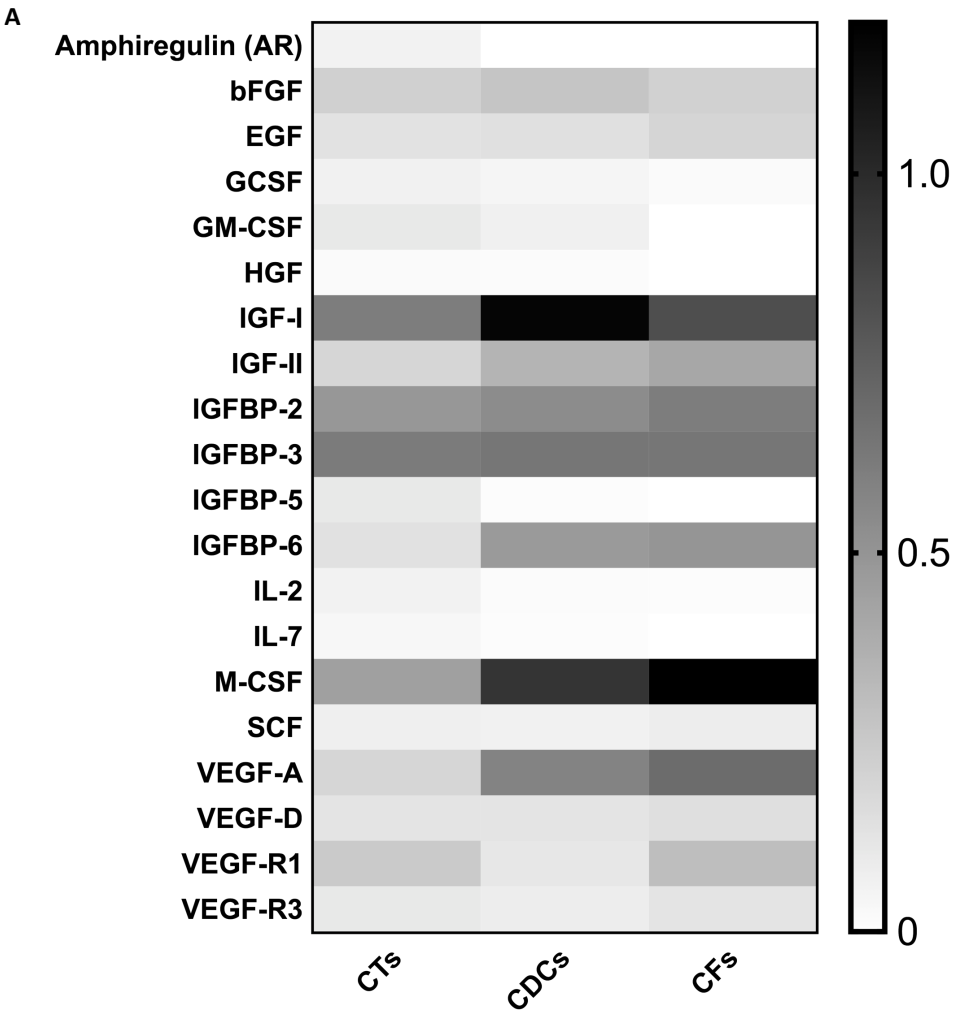
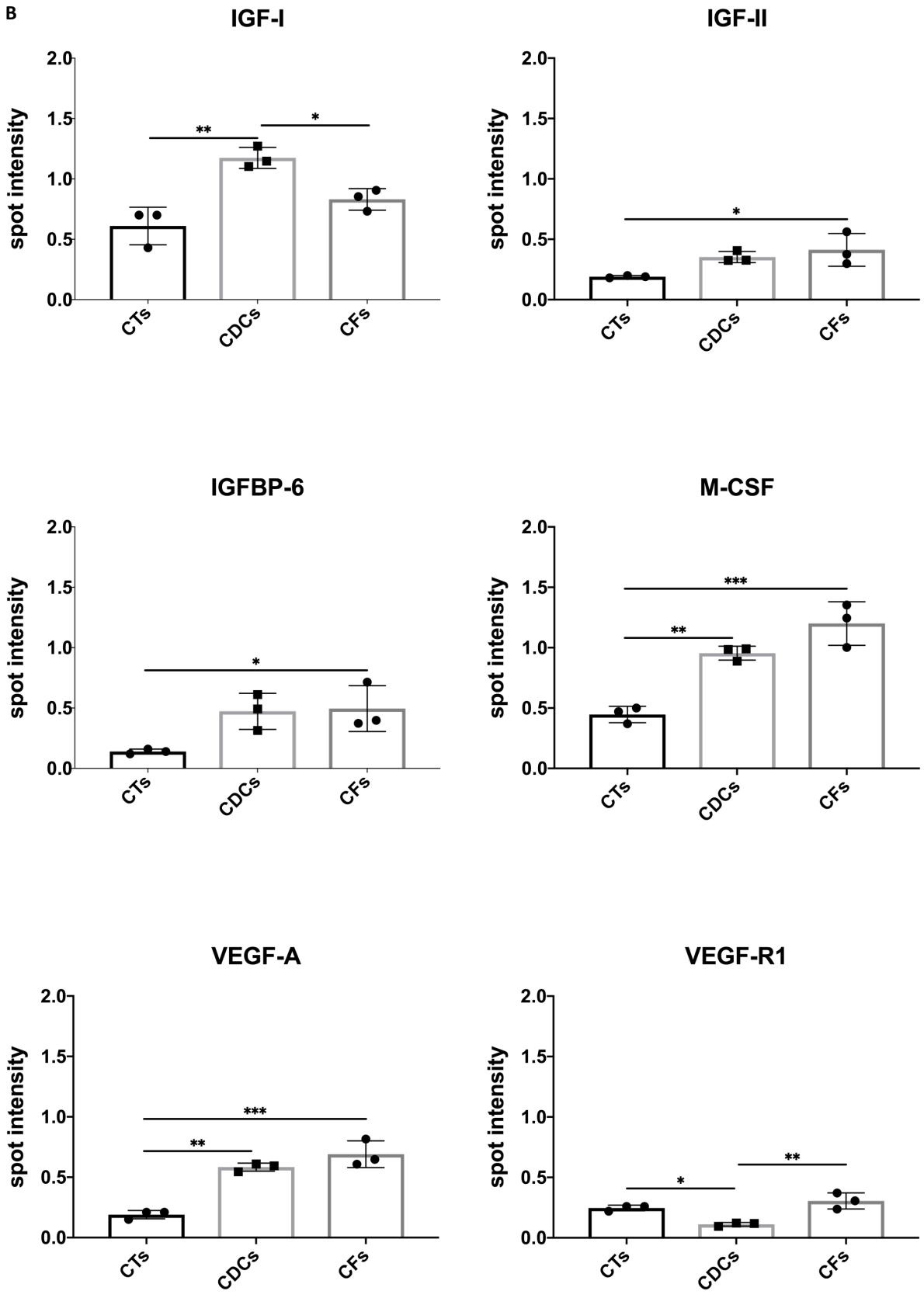


Figure 3.11 Growth factor array comparing the three cardiac stromal populations

The secretion of 20 growth factors was assessed in the conditioned media of CTs, CDCs and CFs using an array. Spot intensity of the samples was normalised to the average of the positive control spots of each array. **(A)** The heatmap illustrates spot intensity (white is low or absent; black is high). **(B)** Individual representation of growth factors that were significantly differentially secreted by the stromal populations. Analysed using a one-way ANOVA with Tukey's multiple comparisons test to determine statistical significance (n=3).

B


IGF-I
IGF-II
IGFBP-6
M-CSF
VEGF-A
VEGF-R1
spot intensity
2.0
1.5
1.0
0.5
0.0
CTs
CDCs
CFs
**
*
***

3.2.4 CTs have a superior survival potential compared to CFs, but not CDCs, following serum starvation

We assessed the survival potential of CTs in comparison to CDCs and CFs as this may be an indication of how robust the cells would be following transplantation. Serum starvation was used to challenge the cells in culture for 3 days and 10 days. CTs, CDCs, and CFs continued to grow following serum starvation with no significant difference in cell numbers detected at day 3 (CTs, 108,000 ± 34,448; CDCs, 125,500 ± 12,152; CFs 138,500 ± 48,370; $P > 0.05$; n=4). At day 10, CT cell numbers were significantly higher than CFs but not CDCs (CTs, 70,000 ± 5,598; CDCs 51,475 ± 8,898, CFs, 23,875 ± 1,315; $P < 0.05$; n=4), suggesting that CTs have a superior survival potential in comparison to CFs (figure 3.12).

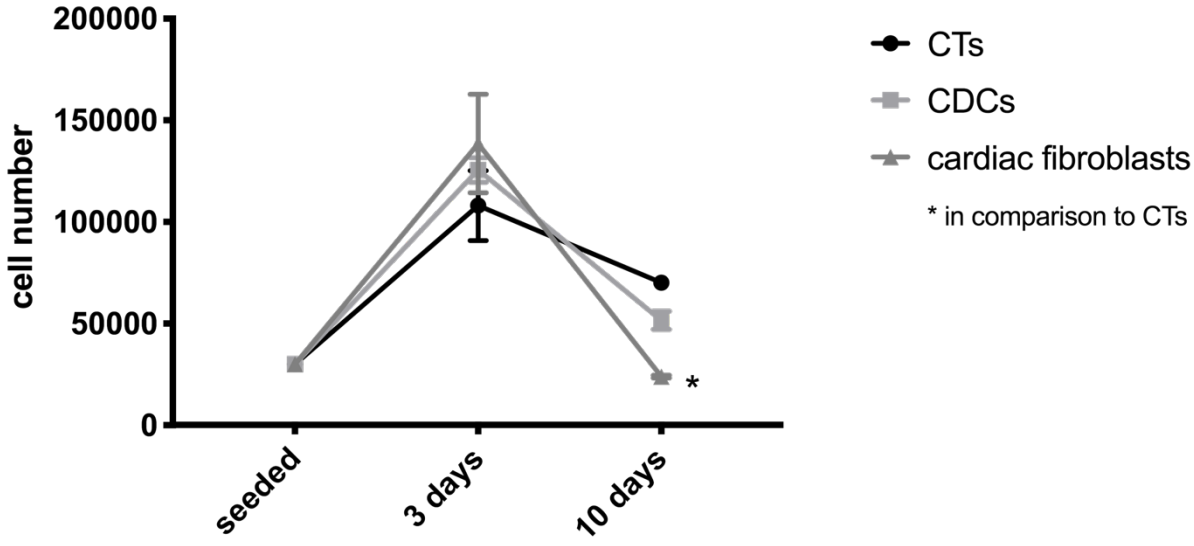


Figure 3.12 CTs demonstrate superior survival potential to that of CFs

Cell Survival following serum starvation for 3 or 10 days, as assessed by cell counting, in CTs, CDCs and CFs. Analysed using a two-way ANOVA with Tukey's multiple comparisons test to determine statistical significance (n=4).

3.3 Discussion

3.3.1 Characterisation of CT morphology and gene expression profile in comparison to CDCs and CFs

Fibroblasts have been described in the literature as morphologically flat, spindle-shaped, with processes arising from the main cell body[296]. Visualising the morphology of the three cardiac stromal populations would have been improved by the use of cell plasma membrane dyes. Although heterogeneity in cell size was detected at passage 1 in all stromal populations, CTs and CDCs appeared larger in comparison to CFs. However, both CTs and CDCs decreased in cell size at later passages. This may be due to a phenotypic drift with *in vitro* passaging and highlights the need for single-cell analysis of the populations at passage 1 in comparison to later passages. The morphological similarities between CTs and CDCs are consistent with them being more closely related in their gene expression profile.

In addition to morphological observations, the gene expression profile of the three cardiac stromal populations was also compared. A study by Skelly *et al*. 2018 examined the single-cell transcriptional profile of mouse ventricular nonmyocytes to identify distinct cell populations[283]. Subpopulation heterogeneity within the cardiac fibroblast population was described where the majority of fibroblasts "fibroblasts 1" were characterised by high expression of *Medag, Ms4a4d, Pdgfrα* and *Tcf21*, while a smaller distinct cluster "fibroblasts 2" expressed higher levels of *Tbx20*, *Wif1* and *Prg4*. Although we found that *Tbx20* was highly expressed in both CTs and CDCs, *Wif1* and *Prg4* showed little to no expression in all stromal populations. Moreover, *Medag* and *Pdgfrα* expression was detected in all three populations, whereas *Ms4a4d* and *Tcf21* was only found in CTs and CFs. However, CFs showed less consistent expression of *Ms4a4d* compared to CTs. This suggests that none of the three stromal populations fit the expression pattern of "fibroblasts 2" and that CTs were the best match to the expression pattern of "fibroblasts 1". However, an important consideration to make is that

the study by Skelly *et al*. examined ventricular rather than atrial nonmyocytes and used freshly isolated cells rather than passaged cells which may undergo phenotypic drift *in vitro*. Therefore, our data may not be directly comparable to the Skelly *et al*. data and further analysis of freshly isolated and/or ventricular CTs, CDCs and CFs may be required for more conclusive characterisation.

Additional mesenchymal- and fibroblast-associated genes were assessed including *Vim*, *Ddr2*, *Acta2*, *Cd44*, and *Col1a1*. αSMA is a protein commonly used to identify smooth muscle cells, pericytes and myofibroblasts, which acquire a contractile phenotype similar to that of smooth muscle cells upon differentiation[297]. *Vim* was the only gene expressed in all of the screened cells of all populations. Vimentin is an intermediate filament protein that has been widely used as a reliable marker of mesenchymal cells, highly migratory cells derived by EMT. It has been recently shown that vimentin has a protective role against nuclear rupture and DNA damage during migration[298]. None of these markers showed specificity to a certain population. *Vim*, *Ddr2* and *Acta2* were also expressed in HL-1 cardiomyocytes, an adult immortalised atrial cell line that has been shown to be similar to a mitotic embryonic cardiomyocytes rather than a mature adult cell[267], as reflected by their immature energy metabolism[299]. The expression of mesenchymal- and fibroblast-associated genes in HL-1 cardiomyocytes may be a reflection of the lack of specificity of these markers in *in vitro* cultures, the immature phenotype of HL-1 cardiomyocytes and/or their dedifferentiation in culture. Genomic instability is a common setback associated with the use of cell lines in research[300]. Unfortunately, we did not test the genomic stability of any of the three stromal populations or the used HL-1 cardiomyocytes.

As mentioned earlier (see Introduction 3.1.1), commonly-used markers to identify pericytes (e.g. *Pdgfrβ* and *Ng2*) are relatively non-specific. However, Skelly *et al*. 2018[283] identified *Kcnj8* and *Colec11*, among others, as genes that show higher expression in pericytes relative to other cell types expressing them. We found little or no expression of *Kcnj8* in all populations.

Colec11 showed sporadic expression, whereas *Ng2* and *Pdgfrβ* showed high expression in all three cardiac stromal populations. The expression of *Kcnj8* was positively correlated with *Isl1*, but not *Colec11* which did not show a positive correlation with other tested genes. Therefore, there is no conclusive evidence to suggest that these stromal populations are pericytes in their phenotype.

The three cardiac stromal populations had very little or no expression of markers of cardiomyocytes (*Nppa*, *Myh6*, and *Myl2*), haematopoietic (*Cd45*), smooth muscle cells (*Myh11 and Cnn1*) and endothelial cells (*Cdh5* and *Vwf*). Expression of *Nppa* and *Myh6* was found in few CDCs (2 *Nppa*$^+$ cells, n=41) and CTs (4 *Myh6*$^+$ cells, n=55). Given that these cells are at passage 3, it is highly unlikely that the cell expressing *Nppa* or *Myh6* cells are cardiomyocytes that survived the isolation protocol. This expression may be a result of spontaneous differentiation in culture or may reflect some progenitor status as suggested by the cTnT staining in figure 3.4 (3.2.1.2). In addition, *Kdr* expression, a marker of endothelial cells, was detected in the CTs, CFs and HL-1 cardiomyocytes. During development, KDR$^+$ progenitors deriving from MESP1$^+$ mesodermal lineage have a cardiovascular tri-lineage potential[301,302]. It has, more recently, been shown by lineage tracing that precursors expressing *Gata5* and *Wt1* give rise to the adult SCA1$^+$ SP$^+$ population (PDGFRα$^+$ /CD31$^-$), whereas the adult SCA1$^+$ SP$^-$ population (PDGFRα$^-$ /CD31$^+$) is mainly derived from precursors expressing *Kdr*[122]. However, our cells lack the expression of other endothelial markers as observed in the SCA1$^+$ SP$^-$ population. *Kdr* expression has also been described in coronary adventitial progenitors with cardiogenic potential[303] and in endothelial progenitors[304].

Cells co-expressing *Wt1* and *Tcf21* were detected in both the CF and CT populations. The existence of CFs expressing *Wt1* was consistent with the immunofluorescence data, whereas I did not observe any WT1$^+$ CTs using immunofluorescence. This may be a reflection of translational regulation of WT1 or protein degradation, which influence the correlation

between protein and transcript levels[305], or the observed extremely low transcript levels. In the developing heart, EPDCs are identified through the expression of *Wt1*, *Tbx18*, *Tcf21*, and *Raldh2*[168] (more detail in 1.4.3.). In the adult mammalian heart, the epicardium is in a state of quiescence, which is lost upon injury and the embryonic gene programme is activated by an upregulation of WT1, among others[169]. It has been demonstrated that the majority of $TCF21^+$ epicardial cells are committed to the cardiac fibroblast lineage prior to EMT initiation and that *Tcf21* expression persists in the adult heart[306–308]. Although WT1 is downregulated following gestation[309,310], its expression is still detected in the epicardium and a subset of coronary endothelial cells in the healthy adult heart[308,311]. In a study by Furtado *et al*. 2014, an enrichment of the epicardial markers *Wt1* and *Tcf21* was shown in adult cardiac fibroblasts[312]. It was also observed that *Wt1* was enriched in atrial fibroblasts as opposed to an enrichment of *Tcf21* in ventricular fibroblasts, showing that the cardiac fibroblast identity may be influenced by regional specification. More recent studies showed that *Wt1* is expressed in more cell types than previously appreciated with a study describing a $Wt1b^+$ macrophage subpopulation that plays an essential role in zebrafish heart and fin regeneration[313]. In our study, *Wt1* expression did not show a correlation with *Mrc1* or *Kdr* but all cells expressing *Wt1* were also positive for *Tcf21* suggesting a fibroblast phenotype.

Noseda *et al*. revealed an enrichment for *Tcf21* and *Pdgfrα*, the cardiogenic genes *Gata4, Mef2a/c, Tbx5/20 and Hand2*, and a lack of *Cdh5* and *Kdr* in the $SCA1^+$ SP^+ population in comparison to total $SCA1^+$ and $SCA1^+$ SP^- populations. In our study, a lack of *Cdh5* expression was observed in all cardiac stromal populations. Both CTs and CDCs showed high expression of the cardiogenic transcription factors *Gata4*, *Tbx20*, *Hand2*, and *Mef2a* with CTs expressing *Mef2c* and CDCs expressing *Tbx5*. Interestingly, among these transcription factors, *Tbx5* showed the lowest expression in the $SCA1^+$ SP^+ population. Moreover, these results are consistent with the observations of Furtado *et al*. showing an enrichment of cardiogenic genes

in cardiac fibroblasts[312]. In contrast, CFs had less uniform expression of *Gata4*, *Tbx20*, and *Hand2*. The PCA analysis showed an interesting polarisation between *Tcf21* and *Tbx5*, which was also reflected on the correlation plot showing a strong negative correlation between the two genes. Indeed, the separation in clustering of CTs and CFs can be attributed to their expression. Although it is unclear what this polarisation means, it is an interesting observation that warrants further investigations in future studies as it may reflect potential functional heterogeneity. *Tbx5* expression was not discussed in the Skelly *et al*. study[283].

Moreover, although *Isl1* expression is detected in the developing heart and ISL1$^+$ progenitors play an important role in giving rise to cardiac lineages during development[142], ISL1$^+$ cells are very rare in adult human and murine hearts[144,145] (more detail in 1.4.3.). In the Skelly *et al*. study, *Isl1* expression was very rare and was dispersed across various cardiac cell populations[283]. In our study, the expression of *Isl1* was detected in 6 CFs (n=29), but not other stromal populations.

Expression of stem cell-related markers (*Pou5f1*, *Nanog*, *Klf4*, and *Tert*) was found in all three cardiac stromal populations. In addition, *Pou5f1*, *Nanog*, and *Klf4*, but not *Tert*, showed expression in HL-1 cardiomyocytes as well. The expression of these stem cell-associated genes (*Pou5f1*, *Klf4*, *Nanog*) was observed in cardiac stromal populations by Noseda *et al*. 2015[122]. A sporadic expression of these markers was also observed in primary neonatal cardiomyocytes[122]. Indeed *Pou5f1*, *Klf4, Nanog* and *Sox2* expression was reported in rat CDCs by a previous member in the Carr group[203]. Other studies have also reported the expression of *Pou5f1*[314,315], *Klf4*[316], *Nanog*[317,318] in adult differentiated cells. As stem cell-associated genes have been implicated in tumorigenesis and proliferation[319,320], it is not surprising to observe their expression in the HL-1 cell line. Furthermore, *Tert* is activated in human and mouse primary fibroblasts to protect against malignant transformation[321]. The lack of *Tert* expression

in the Noseda study might be due to the use of freshly isolated cells that were not expanded *in vitro*, which is not the case in our study.

Macrophage-associated genes were examined including *Mrc1*, *Csf1r* and *Cx3cr1*. No expression of *Cx3cr1* was detected in any of the populations. *Csf1r*, which is enriched in M2-polarised macrophages[322], was expressed in all stromal populations, albeit at higher levels in CTs. *Csf1r* expression has also been used as an indicator of embryonic myeloid lineage commitment[323]. *Mrc1* was only expressed in CTs. *Mrc1* has been reported to show higher expression in macrophages, relative to other cell types expressing them in the heart[283]. This suggests that macrophages may exist within the CTs, and perhaps the CDCs and CFs as well. However, cells expressing *Mrc1* or *Csf1r* showed co-expression of fibroblast markers and did not show clear separation in clustering. Cells expressing *Mrc1* or *Csf1r* may therefore represent the transdifferentiation of macrophages in the stromal isolations into fibroblasts or *vice versa*. Indeed, the transdifferentiation of macrophages to fibroblast cells has been described *in vivo*[324]. Moreover, hybrid mesenchymal phenotypes have been previously described where fibroblast-associated genes are expressed in minor subpopulations of macrophage or endothelial cells[283]. However, due to the lack of *Cd45* expression, it is more likely that macrophage-associated genes were upregulated in a subset of fibroblasts rather than *vice versa*.

Plp1 and *Kcna1* were shown to be expressed at a higher level in Schwann cells relative to other cell types expressing them in the heart[283]. *Plp1* showed expression in all populations we tested, whereas *Kcna1* showed sporadic expression in the three stromal populations only. *Plp1* is not highly specific to Schwann cells as its expression has been described in endothelial, smooth muscle, pericyte and macrophage populations according to the PanglaoDB database[325]. Our results did not show a correlation between the expression of *Plp1* and *Kcna1*. Moreover, Schwann cells have been shown to transdifferentiate into myofibroblasts, and to originate from

fibroblasts[326–328]. Therefore, there is no conclusive evidence to suggest that cells expressing *Plp1* or *Kcna1* cells are Schwann cells.

Our results demonstrated how the isolation protocol may enrich for specific cell subpopulations. Although the isolation protocols of CTs and CFs seemed to be more similar to each other in comparison to CDCs, CTs more closely resembled CDCs than CFs. It is also worth noting that the culture media composition may have had an effect on the gene expression profile of the cardiac stromal populations. Although both CTs and CDCs were cultured using the same media, CFs were cultured in the manufacturer's recommended media with unknown composition. Moreover, CTs and CDCs were cultured on fibronectin-coated flasks, whereas CFs were cultured on gelatin-coated flasks. The effect of cell culture media composition on gene expression has been previously reported in both cells and embryos maintained *in vitro*[329–331]. Therefore, the phenotype of the cells may have been determined by both the isolation method and culture conditions.

This is the first study, to our knowledge, to examine the transcriptional profile of CDCs at the single-cell level. Our results suggest that (1) CTs, CDCs, and CFs resembled "fibroblasts 1", which are the predominant fibroblast subtype in the adult murine heart; (2) CTs and CDCs highly expressed cardiogenic factors and appeared to be more homogenous in comparison to CFs; (3) CDCs clustered between CTs and CFs which separated based on their expression of *Tcf21* and *Tbx5*, respectively; (4) CTs were enriched for the macrophage-associated genes *Mrc1* and *Csf1r*, which may be attributed to the upregulation of macrophage-associated genes in a subset of CTs; (5) PCA analysis revealed a transcriptional gradient suggesting that heterogeneity exists within fibroblast subtypes which may reflect functional heterogeneity. Overall, our findings highlight the heterogeneity of the stromal compartment of the heart and how the isolation protocol, and perhaps culture conditions, may enrich for specific cell subpopulations, which may ultimately affect the therapeutic potential of the cells.

3.3.2 Growth factor release by CTs in comparison to CDCs and CFs

Studies have reported that the secretome of stem cells and cardiac stromal populations is sufficient to improve cardiac function[182–184]. This is due to the existence of constituents such as cytokines, growth factors and genetic material that are capable of supporting cardiomyocyte survival and proliferation, and angiogenesis, while limiting inflammatory and pro-fibrotic processes[176].

Insulin Growth Factor-1 (IGF-1) and Hepatocyte Growth Factor (HGF) have been studied extensively in the context of cardiac repair. MSCs genetically modified to overexpress IGF-1 and HGF promoted angiogenesis and reduced inflammation in ischaemic tissue in a pig MI model[332] and IGF-1 reportedly induced *in vitro* cardiogenesis of PSCs[333]. Intracoronary administration of IGF-1 and HGF during coronary reperfusion in a pig MI model improved cardiomyocyte survival and KIT^+ cell numbers, as well as reducing fibrosis[334]. IGF-1 and HGF administration also increased the retention of $SCA1^+$ cells, reduced infarct size, and attenuated post-MI remodelling, compared to transplantation of $SCA1^+$ cells alone[335]. In addition to IGF-1 and HGF, basic Fibroblast Growth Factor (bFGF) and Vascular Growth Factor-A (VEGF-A) have also been implicated in inducing angiogenesis in the infarcted heart[336]. Indeed, both bFGF and VEGF-A have been tested in clinical trials where they were delivered as recombinant protein or via gene transfer but showed limited therapeutic benefit in patients[337]. It has been suggested that the limited efficacy of these trials may be due to the short half-life of the recombinant protein or low gene transfer efficiency, respectively. However, VEGF-A mRNA has been proposed as an alternative for regenerative angiogenesis where the mRNA is chemically modified to promote stability and evasion of the innate immune response[338,339].

Following MI, monocytes, precursors of macrophages, are abundantly recruited to initiate a biphasic monocyte/macrophage response and mediate both tissue destruction and repair. This is characterised by a pro-inflammatory response peaking at day 3 and involving the M1

macrophage subtype mainly aimed at debris clearance. The inflammatory phase is followed by a proliferative phase, on days 4-7, which is characterised by a peak in the M2 macrophage subtype. The M2 subtype has an immunosuppressive capacity and a role in extracellular matrix deposition, contributing to tissue remodelling and scar maturation[340]. This explains the increased risk of infarct rupture following pan-macrophage depletion[341]. Therefore, manipulating macrophage polarisation provides a better strategy to enhance cardiac repair. Granulocyte macrophage colony-stimulating factor (GM-CSF) and M-CSF belong to the CSF family and are key growth factors that mediate M1 and M2 polarisation, respectively[342]. Indeed, GM-CSF has been shown to impair healing following MI by stimulating the inflammatory response[343]. Moreover, stimulation of cardiac lymphangiogenesis by VEGF-C administration enhanced early resolution of the inflammatory response and functional outcome following MI[344]. CDC conditioned media has been shown to mediate macrophage polarisation towards a cardioprotective phenotype[345].

Based on the above discussed implications of paracrine signalling, the secretion of 20 cytokines and growth factors from CTs, CDCs, and CFs was evaluated using a cytokine array to evaluate their paracrine potential as a cell therapy product. Table 3.2. provides a summary of the relevant functions of the assessed factors in the context of cardiac repair. Our screening revealed that the three cardiac stromal populations are capable of secreting multiple different cytokines and growth factors. Although CTs, CDCs, and CFs showed a similar pattern in their secretion of the tested growth factors, statistical analysis revealed, disappointingly, that CTs secreted lower levels of IGF-1 in comparison to CDCs, IGF-2 and IGFBP-6 in comparison to CFs, and M-CSF and VEGF-A in comparison to both CDCs and CFs. In addition, CTs secreted higher levels of VEGF-R1 in comparison to CDCs. This shows that cardiac stromal populations may vary in their paracrine potential. With the exception of IGFBP-6 and VEGF-R1, all of these factors have potentially desirable effects in the context of cardiac repair. Interestingly, the

Marbán group had previously reported that cardiospheres were capable of secreting VEGF-A, IGF-1 and HGF whereas only VEGF-A and HGF release was detected in CDC conditioned media[346]. This is inconsistent with our results where all three factors were detected in all of the tested populations. The inconsistency may be due to the isolation of CDCs from a different mouse strain, use of poly-D-lysine in cardiosphere generation or the use of a different mode of detection (ELISA) in the Marbán study. Comparison of the pro-survival or angiogenic effect of stromal cell conditioned media in co-culture systems, with e.g. endothelial cells or cardiomyocytes, or after injection into infarcted hearts would give us a better understating of how these populations differ in their paracrine potential.

3.3.3 CTs have a superior survival potential compared to CFs, but not CDCs, following serum starvation

Low survival and retention of transplanted cells following ischaemic events is mainly due to the harsh conditions within the infarct region that include hypoxia, inflammation, and nutrient restriction. This complex environment can be difficult to mimic *in vitro*. However, acute hypoxic culture and/or serum starvation have been previously used as an *in vitro* assay of ischaemia[205,242,347]. Serum in cell culture media provides amino and fatty acids and its withdrawal is therefore considered a form of nutrient restriction. Serum starvation does not mimic the complex *in vivo* environment that occurs following MI or an ischaemic event but is an effective way of inducing cell apoptosis[348]. Previous work in collaboration with the Carr group used a combination of 0.1% O_2 and serum starvation to examine the pro-survival effect of miR-132 on mouse endothelial cells against hindlimb ischaemia[205]. Moreover, the viability of $SCA1^+$ cardiac cells following serum starvation was used to determine the pro-survival capacity of a miRNA cocktail[242].

Oxygen deprivation can result in a drop in ATP levels where cellular functions cannot be maintained, eventually causing cell death[349]. Hypoxia can also induce cell death via HIF1α

targets[350–352] and P53[353]. As cardiac stromal cells are less metabolically active in comparison to cardiomyocytes[354], higher tolerance to hypoxic conditions may be expected. Indeed, both CDCs[203] and CTs (data not shown) not only tolerate hypoxic conditions of 2-5% O_2, but also proliferate at higher rates than in normoxia. This tolerance to hypoxic conditions has also been described in MSCs[355,356]. It was not possible to test acute hypoxic conditions of less than 1% O_2 due to the limitations of the available incubator. Therefore, serum starvation alone was used in this study, as it is sufficient for apoptosis induction[348]. It was previously shown by S. Malandraki Miller (thesis) that 3 days of serum starvation was sufficient to induce apoptosis in both CTs and CDCs.

Here, we found that all three cardiac stromal populations continued to grow following serum starvation with no significant difference in cell numbers detected at day 3. However, CF cell numbers at day 10 were similar to the cell number seeded initially suggesting substantial cell death. At day 10, CT cell numbers were significantly higher than CFs but not CDCs, suggesting that CTs have a superior survival potential to that of CFs and is consistent with the single-cell qRT-PCR results showing that CTs and CDCs share a more similar gene expression profile in comparison to the CFs. Tolerance to serum starvation has also been observed in MSCs under both normoxic and hypoxic culture conditions[357,358].

Reduced robustness was noticed during routine culture of CFs in comparison to CTs and CDCs as shown by increased time to reach confluency and higher numbers of floating dead cells in culture. The CFs displayed reduced recovery following single-cell sorting for the single-cell qRT-PCR experiment, in comparison to CTs and CDCs. Moreover, the CFs could not be maintained in culture beyond 4-5 passages, in contrast to CTs and CDCs which have been previously shown to be maintained for more than 30 passages (S. Malandraki-Miller, thesis). It is difficult to pinpoint what is responsible for this reduced robustness. Our single-cell qRT-PCR reveal that CFs mostly differ from CTs and CDCs by expression of Isl1 and a reduced

expression of cardiogenic factors, though the genes explored were limited. Moreover, other factors such as media composition could have affected the robustness of CFs. As discussed earlier, unlike CTs and CDCs which were cultured in CEM (IMDM supplemented with 20% FBS), the CFs were cultured in the manufacturer's recommended media with unknown composition supplemented with FGF, hydrocortisone and 10% FBS. Moreover, CTs and CDCs were cultured on fibronectin-coated flasks, whereas CFs were cultured on gelatin-coated flasks. Differential effects of various culture coating substrate types on cell proliferation have been shown[359]. However, standardising the culture conditions of all cell types would have been counterproductive as our aim was to compare the populations as they would be cultured in other labs based on in their recommended and published culture conditions. Ideally, the survival potential of these different stromal population should be compared following transplantation into infarcted hearts or in *in vitro* conditions that more closely mimic the *in vivo* environment following MI. Overall, our data suggested that CTs and CDCs were more robust than CFs, both in long-term cell expansion and survival under serum starvation, and that the survival potential of cardiac stromal populations may differ in response to stress *in vitro*, which can be an indication of their *in vivo* behaviour following transplantation.

Table 3.1 The markers used in the single-cell qRT-PCR characterisation

Gene	Full name of encoded protein	Type	Relevant expression pattern	Relevant function	References
Cd44	Cluster of differentiation 44	Transmembrane glycoprotein	Fibroblasts, macrophages, endothelial cells	Cellular adhesion; angiogenesis; release of cytokines; regulates inflammation and fibrosis	325,360–362
Cdh5	Cadherin 5 or VE-cadherin	Member of the cadherin family of calcium-dependent glycoproteins	Endothelial cells	Calcium-dependent cell adhesion; cell proliferation and migration	325,363
Col1a1	Collagen, type I, alpha 1	Member of group I collagen	Fibroblasts, smooth muscle cells	Collagen type I synthesis	325,364
Colec11	Collectin subfamily member 11	Member of the collectin family of C-type lectins	Pericytes, endothelial cells	Collectins are initiators of the lectin complement pathway, which is integral to the innate immune response; embryogenesis	283,325,365,366
Csf1r	Colony-stimulating factor 1 receptor	Receptor tyrosine kinase	Macrophages (used as an M2 marker)	Growth and differentiation of macrophages; maintenance of the intestinal stem cell niche	322,367
Cx3cr1	CX3C chemokine receptor 1	Member of the 7-transmembrane G protein-coupled receptor family	Macrophages	Macrophage survival and function	325,368–370
Ddr2	Discoidin domain receptor tyrosine kinase 2 or CD167b	Receptor tyrosine kinase	Fibroblasts, smooth muscle cells, pericytes	Activated by collagen binding; cell proliferation; adhesion and migration; ECM degradation	325,371,372
Gata4	GATA binding factor 4	Transcription factor of the zinc-finger GATA family	Cardiomyocytes, cardiac fibroblasts	Cardiogenesis	20,281,282,373,374

Hand1	Heart- and neural crest derivatives-expressed protein 1	Transcription factor of the basic helix-loop-helix family	FHF, reported to be undetectable in adult mouse hearts	Cardiogenesis; epicardial development and coronary vessel formation	375–378
Hand2	Heart- and neural crest derivatives-expressed protein 2	Transcription factor of the basic helix-loop-helix family	SHF, cardiomyocytes, endothelial cells, fibroblasts	Cardiogenesis; epicardial development and coronary vessel formation	122,282,325,375–377
Isl1	Insulin gene enhancer protein 1	Transcription factor of the LIM/homeodomain family	CPCs, cardiac neural crest, endothelial cells	Cardiogenesis	139,140,142–145
Kcna1	Potassium voltage-gated channel subfamily A member 1	Member of the 6-TM family	Schwann cells	Regulator of membrane excitability	283,325,379
Kcnj8	Potassium inwardly-rectifying channel, subfamily J, member 8	The inward-rectifier potassium channel family (also known as 2-TM channels)	Pericytes	Regulator of vascular tone and cardiac adaptive response to systemic metabolic stressors	283,325,380–382
Kdr	Kinase insert domain receptor or foetal liver kinase 1 (FLK1); VEGFR2; CD309	Receptor tyrosine kinase	Endothelial cells, Kdr^{+} developmental cardiovascular progenitor	Transduction of VEGF-A effects	301,302,325,383
Kit	Stem cell growth factor receptor, proto-oncogene KIT or CD117	Receptor tyrosine kinase	HSCs, endothelial cells, CPCs, postnatal and dedifferentiated adult cardiomyocytes	Tumourigenicity; cell survival, proliferation and migration; angiogenesis	125–128,325,384,385
Klf4	Kruppel like factor 4	Member of the Kruppel-like family of transcription factors	Stem cells, endothelial cells, fibroblasts	Pluripotency; angiogenesis; embryonic vasculogenesis; myofibroblast differentiation	316,325,386–388
Medag	Mesenteric oestrogen-dependent	Member of the sex-steroid regulated mesenteric	Cardiac fibroblasts “1”	Adipogenesis; glucose uptake; interacts with the	283,389,390

	adipogenesis protein	oestrogen-dependent adipogenesis proteins		fatty acid transporter CD36 that is involved in the uptake of apoptotic material	
Mef2a	Myocyte-specific enhancer factor 2A	Transcription factor of the MEF2 family	Cardiomyocytes, cardiac fibroblasts, endothelial cells, smooth muscle cells, macrophages and pericytes	Cardiogenesis; vasculogenesis	122,325,391,392
Mef2c	Myocyte-specific enhancer factor 2C or MADS box transcription enhancer factor 2	Transcription factor of the MEF2 family	Cardiomyocytes, cardiac fibroblasts, endothelial cells, smooth muscle cells, macrophages and pericytes	Cardiogenesis; vasculogenesis	20,29,122,281,282,325,393
Mesp1	Mesoderm Posterior Transcription Factor 1	Transcription factor of the basic helix-loop-helix family	Mesoderm	Development of cardiac mesoderm	18
Mrc1	Mannose receptor C-type 1 or CD206	Transmembrane glycoprotein	Macrophages (used as an M2 marker)	Mediates the endocytotic functions by macrophages and the DNA replication checkpoint	283,325,394–396
Ms4a4d	Membrane-spanning 4-domains subfamily A member 4D	Member of the membrane-spanning 4A (MS4A) family	Cardiac fibroblasts “1”, reported to be expressed in M2 macrophages	May have a role as an adaptor protein to facilitate intracellular protein–protein interactions. Its functionality is still not fully understood.	283,397,398
Myh6	Myosin heavy chain 6 or αMHC	Hexameric ATPase cellular motor protein	Predominantly atrial cardiomyocytes	Cardiogenesis; force generation and muscle contraction	399
Myl2	Myosin light chain 2	Hexameric ATPase cellular motor protein	Predominantly ventricular cardiomyocytes	Cardiogenesis; force generation	399

				and muscle contraction	
Nanog	Nanog Homeobox	Transcription factor of the Nanog homeobox family	Stem cells	Pluripotency; tumourigenicity	[400,401]
Ng2	Neuron-glial antigen 2 or chondroitin sulphate proteoglycan 4	Transmembrane proteoglycan	Pericytes, smooth muscle cells	Co-receptor in conjunction with PDGFRα; angiogenesis; cell survival and migration	[325,402–404]
Nkx2-5	NK2 homeobox 5	Transcription factor of the NK-2 homeobox family	Cardiomyocytes	Cardiogenesis	[325,405]
Nppa	Natriuretic Peptide A	The natriuretic peptide family	Predominantly atrial cardiomyocytes	Cardiac hormone involved in regulating blood volume and pressure and cardiovascular homeostasis	[406]
Pou5f1	Octamer-binding transcription factor 4 (Oct4) or POU class 5 homeobox 1	Transcription factor of the homeodomain POU (Pit-Oct-Unc) family.	Stem cells	Pluripotency; tumourigenicity	[407,408]
Pdgfrα	Platelet-derived growth factor receptor α	Receptor tyrosine kinase	Fibroblasts, defines the $SCA1^{+}SP^{+}$ population (CPCs)	Development of mesenchymal cell types; cardiogenesis	[122,325,409–411]
Pdgfrβ	Platelet-derived growth factor receptor β	Receptor tyrosine kinase	Pericytes, fibroblasts, endothelial cells, smooth muscle cells	Development of mesenchymal cell types; regulation of autophagic processes; cell proliferation and survival; adult mammalian cardiomyocyte proliferation; cardiogenesis	[325,411–418]
Plp1	Proteolipid protein 1	Myelin proteolipid protein	Schwann cells, endothelial cells, smooth muscle cells, pericytes	Myelination	[5,9,419]

			and macrophages		
Prg4	Proteoglycan 4	Mucinous glycoprotein	Cardiac fibroblasts “2”	Ligand for CD44 receptor, ECM constituent conferring compression resistance	283,420,421
Ptprc (*Cd45*)	Protein tyrosine phosphatase, receptor type, C	Transmembrane glycoprotein	Haematopoietic cells (except erythrocytes and plasma cells)	Haematopoietic cell activation and differentiation and immune Function	422–424
Ly6a	Stem cell antigen 1 (SCA1) or lymphocyte antigen 6 complex	Glycosyl phosphatidylinositol-anchored cell surface protein of the LY6 gene family	HSCs, fibroblasts, endothelial cells, CPCs	Tumourigenicity; cell migration; HSC self-renewal and fate determination	122,325,425–428
Tbx20	T-box 20	Transcription factor of the T-box family	Cardiomyocytes, cardiac pericytes and fibroblasts	Cardiogenesis	122,325
Tbx5	T-box 5	Transcription factor of the T-box family	Cardiomyocytes, cardiac fibroblasts	Cardiogenesis	20,281,282
Tcf21	Transcription factor 21	Transcription factor of the basic helix-loop-helix family	Epicardium, Cardiac fibroblasts “1”	Initiation of epicardial EMT for fibroblasts development; proepicardial cell specification	283,306,429
Tert	Telomerase reverse transcriptase	Member of the reverse transcriptase family	Stem and progenitor cells	Cellular immortalisation tumourigenicity; cell proliferation	430,431
Vim	Vimentin or fibroblast intermediate filament	Type III intermediate filament protein	Fibroblasts, endothelial cell, smooth muscle cells, Schwann cells	Maintenance of cellular integrity; EMT; protective role against nuclear rupture and DNA damage during cell migration.	298,325
Vwf	von Willebrand factor	Adhesive plasma glycoprotein	Endothelial cells	Platelet adhesion and aggregation	432
Wif1	WNT inhibitory factor 1	Lipid-binding protein	Cardiac fibroblasts “2”	Mesoderm segmentation; cardiogenesis	283,433

Wt1	Wilms tumour 1	Transcription factor with proline / glutamine- rich DNA- binding domain	Epicardium, fibroblasts, endothelial cells, macrophages	Epicardial EMT; vasculogenesis	[311–313,434,435]
Acta2	Alpha smooth muscle actin (αSMA) or Actin alpha 2	Member of the globular Actin proteins family	Smooth muscle cells, myofibroblasts, pericytes	Cell motility and contractility	[297,436]

Table 3.2 The growth factors assessed in cell conditioned media using antibody arrays and their relevant functions

Growth factor	Summary of relevant functions and references
Amphiregulin (AR)	• Member of the EGF family. • Promoted cardiac fibrosis after MI partly though activating the EGFR pathway[437]. • HIF2α induced AR to elicit cardioprotection following I/R injury[438].
bFGF	• Member of the FGF family. • Angiogenic functions[439]. • Showed cardioprotection following I/R injury[440]. • Repopulating engineered decellularised rat hearts containing immobilised bFGF using hESCs-derived CPCs enhanced cell retention and differentiation[441]. • Controlled release of bFGF improved CDC retention and cardiac function following MI[442].
EGF	• Member of the EGF family. • Overexpressed EGF in the MI border area in rabbit hearts exacerbated ventricular remodelling showing a pathophysiological role in MI[443].
GCSF	• Member of the haematopoietic colony stimulating factors growth factors family. • G-CSF/SCF therapy improved cardiac function when delivered following MI[444]. • Shown to induces M2 macrophage polarisation[445].
GM-CSF	• Member of the haematopoietic colony stimulating factors growth factors family. • Identified as contributor to the pathogenesis of MI by inducing M1 macrophage polarisation[343].
HGF	• Member of the HGF family. • MSCs genetically modified to overexpress IGF-1 and HGF promoted angiogenesis and reduced inflammation following MI[332]. • Intracoronary administration of IGF-1 and HGF during coronary reperfusion in a pig MI model improved cardiomyocyte survival and KIT^+ cell numbers, as well as reducing fibrosis[334]. • IGF-1 and HGF administration increased the retention of $SCA1^+$ cells, reduced infarct size, and attenuated post-MI remodelling, compared to transplantation of $SCA1^+$ cells alone[335].

IGF-I	• Member of the IGF family. • IGF-1 induced *in vitro* cardiogenesis of PSCs[333]. • Shown to improve cardiac remodelling after MI by targeting myeloid cells[446]. • Pro-angiogenic[447]. • See above studies with HGF.
IGF-II	• Member of the IGF family. • Implicated in cardiomyocyte proliferation and cardiac development in mice[448,449]. • Required for zebrafish cardiac regeneration[450]. • Pro-angiogenic[447].
IGFBPs	• Members of the IGFBP family regulate the bioavailability of IGFs by binding them. • IGFBP4, IGFBP5 and IGFBP6 shown to be anti-angiogenic, whereas IGFBP2 is pro-angiogenic. Contradictory roles for IGFBP3 have been described[447].
IL-2	• Member of the common γ-chain family. • Injection of IL-2-activated natural killer (NK) cells improved vascular remodelling and cardiac function following MI[451]. • Intravenous injection of IL-2 positively improved cardiac function by promoting angiogenesis through a process involving NK cells[452].
IL-7	• Member of the common γ-chain family. • Shown to promote the expansion of pro-inflammatory $CD4^{+}CD28^{null}$ T lymphocytes in MI. MI patients exhibiting expansion of $CD4^{+}CD28^{null}$ T lymphocytes have increased risk of recurrent MI and poorer prognosis[453].
M-CSF	• Member of the haematopoietic colony stimulating factors growth factors family. • Improved cardiac function following MI by promoting VEGF-A production and cardiomyocyte survival[454]. • Shown to induces M2 macrophage polarisation[455].
SCF	• Member of the SCF family. • Cardiomyocyte-specific overexpression of SCF decreased myocardial apoptosis and improved cardiac function following MI[456]. • As a ligand for KIT, it has been shown to induce homing of KIT^{+} cells at the border zone[457] and in situ expansion following MI[458].
VEGF-A	• Member of the VEGF family. • Regulator of angiogenesis and vascular permeability. • Improved angiogenesis and cardiac function following MI[459].
VEGF-D	• Member of the VEGF family. • Regulator of angiogenesis and lymphangiogenesis. • Closely related to VEGF-C, both structurally and functionally[460]. • Context-dependent requirement for Vegf-c/d -dependant lymphangiogenesis during zebrafish cardiac regeneration[461].
VEGF-R1	• Member of the tyrosine kinase receptor Flt/VEGFR Family. • Soluble VEGFR-1 shown to function as an antagonist to VEGF-A activity by binding it, thus suppressing angiogenesis[462–464].
VEGF-R3	• Member of the tyrosine kinase receptor Flt/VEGFR Family. • Soluble VEGFR-3 shown to function as an antagonist to VEGF-C/D activity by binding it, thus suppressing lymphangiogenesis[465–467].

CHAPTER 4

miR-210-transfected CTs show decreased apoptotic cell death and mitochondrial autophagy and fission

4 Results chapter 2

4.1 Introduction

4.1.1 Cell death pathways

In this thesis, in order to probe the mechanism by which miR-210 increased cell survival, cell death pathways were investigated. Cell death plays a key role in tissue development, and in homeostasis to eliminate unwanted, damaged, or harmful cells. The role of cell death in development was first recognized in 1842 when Karl Vogt demonstrated that the death of cells composing the notochord of the midwife toad allows the formation of vertebrae during metamorphosis[468,469]. However, death was still viewed as a passive end of cell life until in the 1960s when it was demonstrated that cells self-destruct in response to endogenous signalling cascades and the term programmed cell death (PCD) was introduced[469–471].

4.1.1.1 Apoptosis

Cells possess an intrinsic mechanism of self-destruction known as PCD, of which apoptosis is the most widely studied and a highly conserved form. It is mediated by two signalling pathways: intrinsic and extrinsic. Intrinsic apoptosis is initiated by different intracellular microenvironmental distresses such as reactive oxygen species (ROS)[472,473] and DNA damage[474]. The intrinsic pathway is demarcated by irreversible mitochondrial outer membrane permeabilisation (MOMP)[475–477], which is controlled by the BCL2 apoptosis regulator protein family. The BCL2 family comprises both pro- and anti-apoptosis proteins that share one to four BCL2 homology (BH) domains[478,479].

Extrinsic apoptosis is initiated by perturbations of the extracellular microenvironment. These are detected by plasma membrane receptors. Death receptors include: Fas cell surface death receptor (FAS; also known as CD95 or APO-1), and the tumour necrosis factor (TNF) receptor superfamily that are characterised by an intracellular domain known as the death domain.

Binding by the death receptors' corresponding ligands allows the assembly of a dynamic multiprotein complex at the intracellular tail of the receptor, known as "death-inducing signalling complex" (DISC). The extrinsic pathway is propagated by caspase-8 (or alternatively caspase-10), which is recruited to DISC to be cleaved and activated[480–482].

Both pathways culminate in the activation of caspases (cysteine aspartyl-specific proteases), inactive zymogens expressed in almost all cells[483,484]. This leads to the morphological changes that are characteristic of apoptosis and include nuclear fragmentation (karyorrhexis), chromatin condensation (pyknosis), cytoplasmic shrinkage, membrane blebbing and, subsequently, cell elimination with the formation of apoptotic bodies that are taken up by neighbouring cells with phagocytic activity to be degraded in lysosomes[482]. Caspases are classified as "initiators" including Dredd and Dronc in *D. melanogaster*, and caspases 1, 2, 4, 5, 8, 9, 10, 11 in mammals, or "executioners" including Ice (or Drice) and Dcp1 in *D. melanogaster*, and caspases 3, 6, 7 and 14 in mammals[469]. Figure 4.2 demonstrates the role of key players in both the intrinsic and extrinsic pathways of apoptosis.

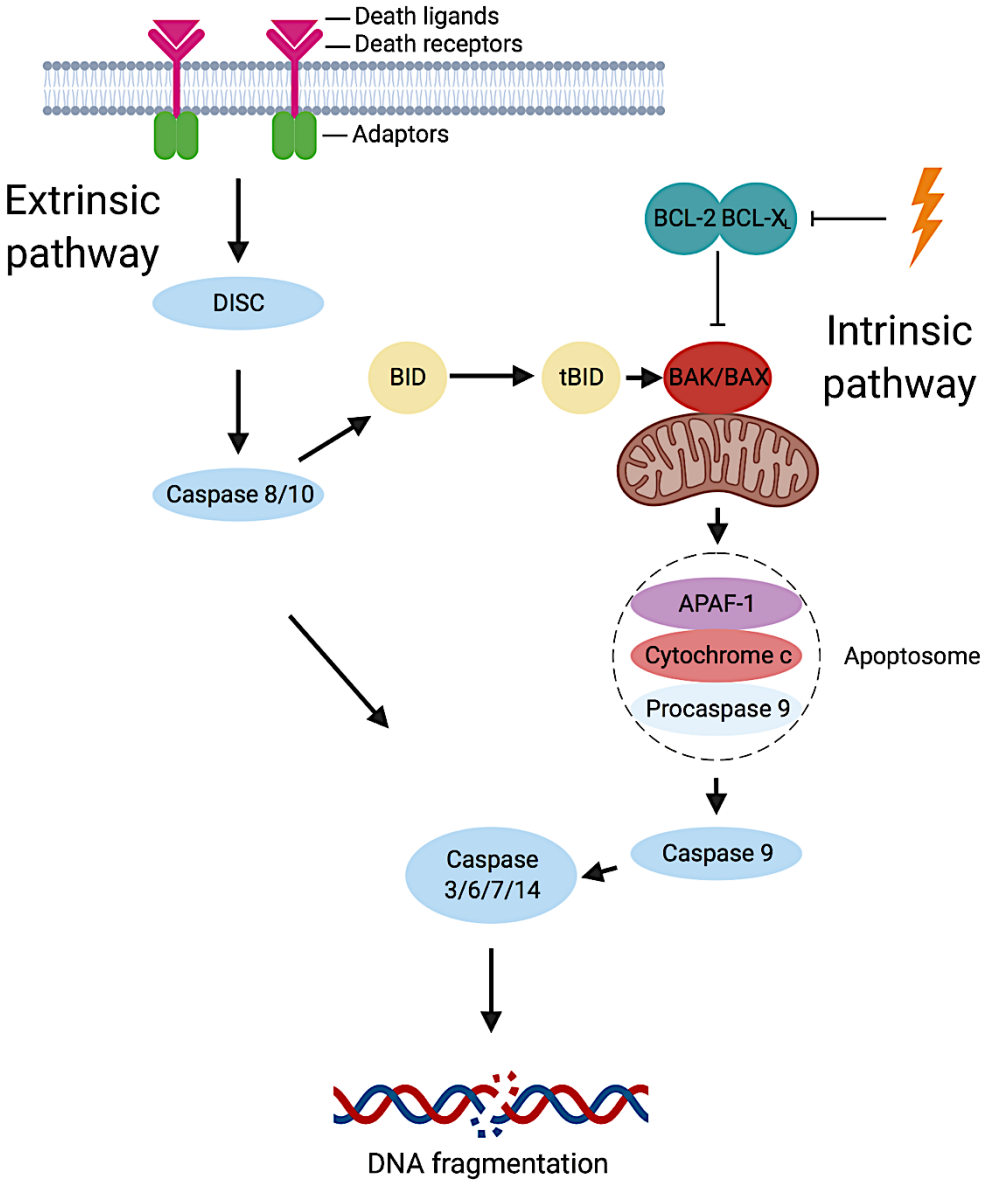


Figure 4.1 The extrinsic and intrinsic pathways of apoptosis

Simplified schematic of the apoptotic pathways. The extrinsic pathway is mediated by a variety of death receptor ligands, including the TNF and FAS ligands, that trigger apoptosis by binding to cell surface death receptors. This allows the assembly of a dynamic multiprotein complex at the intracellular tail of the receptor, DISC, and the consequent activation of caspase 8 from the zymogen procaspase 8. The intrinsic pathway is mediated by intracellular microenvironmental distresses that lead to irreversible MOMP, which is controlled by the BCL2 apoptosis regulator protein family comprising both pro- and anti-apoptosis proteins. MOMP results in the leakage of cytochrome c from mitochondria to the cytosol. Cytochrome c and APAF-1 (apoptotic protease activating factor 1) form the apoptosome that activates caspase 9. Crosstalk between the pathways exists via cleavage of BCL2 interacting domain (BID) by caspase 8 to form truncated Bid (tBID) that targets the BCL2 family. Both pathways culminate in the activation of the executioner caspases. (Adapted from[485] and [486])

4.1.1.2 Autophagy: death or an attempt at survival?

In 1955, Christian de Duve and colleagues discovered membrane-bound organelles containing hydrolytic enzymes and named them "lysosomes", Greek for "digestive bodies". This discovery led to the award of the Nobel Prize in Medicine or Physiology in 1974. In the 1960s, lysosomes were found to be involved in the digestion of extracellular material taken up by endocytosis and of intracellular material segregated by autophagy, when the terms "endocytosis" and "autophagy" were introduced[487,488].

Autophagy is an evolutionarily conserved cellular recycling process that maintains cellular quality control and homeostasis by turning over cytoplasmic components under conditions of stress such as nutrient deprivation[489]. Autophagy is initiated by the formation of a cup-shaped structure called the phagophore. The phagophore then undergoes expansion which involves the activation of the ATG8 proteins (in mammals: LC3, GABARAPs, and GATE-16) and their conjugation to membrane-resident phosphatidylethanolamine (PE) by ATG7 and ATG3. This converts the ATG8 proteins from diffuse forms to membrane-bound lipidated forms[490], allowing the phagophore to become the autophagosome. LC3 is frequently used as a mammalian autophagosomal membrane marker and its lipidated form is known as LC3-II. The autophagosome matures via the action of different components, including ATG4, and SNARE-mediated fusion with the lysosome occurs. This allows the autophagic cargo to be degraded by the lysosome and recovered components are recycled back into the cytoplasm[491].

Considering autophagy as a cell death mechanism has been controversial. Indeed, autophagy involves the recycling of multiple cytoplasmic components during standard physiological conditions and in response to different types of stress, such as starvation and hypoxia, to maintain cellular homeostasis. Autophagic dysfunction, either caused genetically or chemically, has been implicated in the progression of cancer[492], aging[493], immune diseases[494] and neurodegeneration[495]. The role of autophagy in the adaptation to early neonatal starvation

was demonstrated by showing that *Atg5* mutant mice appeared almost normal at birth but die within 1 day of birth[496]. Adult mice with cardiac-specific *Atg5* deficiency developed severe cardiac dysfunction following transverse aortic constriction accompanied by an increase in disorganised sarcomere structure and mitochondrial misalignment and aggregation[497]. Autophagy activation appears to be protective after MI. Indeed, pharmacological inhibition of autophagy exacerbates post-infarction cardiac remodelling and dysfunction[498].

The contribution of autophagy to cell death has also been documented. In the developing *D. melanogaster*, cell death during midgut degradation is marked by an increased expression of apoptosis-related genes and Atgs, and an accumulation of autophagosomes. Treatment with the pan-caspase inhibitor P35 and knockdown of caspases are not sufficient to disrupt midgut degradation. In contrast, midgut degradation is severely impaired in *Atg2* and *Atg18* mutants despite maintained caspase activity[499].

Autophagy has been observed in dying cells during mammalian development. For example, the regression of the corpus luteum, and the involution of the mammary and prostate glands[500,501]. Moreover, it has been suggested that ATGs are required for the execution of cell death when apoptotic pathways are blocked. Autophagic death in U937 monocyte and L929 fibrosarcoma cells require the genes *ATG7* and *Beclin 1* in response to caspase-8 inhibition[502]. In addition, *Bax*/*Bak*$^{-/-}$ MEFs undergo cell death accompanied by autophagy, which requires Beclin1 and is repressed by autophagy inhibitors[503].

The dynamics of autophagic interaction with cell death remain unclear. It has been suggested that autophagy contributes to cell death upon excessive activation of autophagy, or in a cell type and context dependant manner[501,504]. For example, in myocardial ischaemia, induction of autophagy is protective. However, autophagy has been shown to induce cardiomyocyte cell death in some models of ischaemia/reperfusion[505], doxorubicin-related cardiomyopathy[506], and hemodynamic stress[507,508]. Therefore, understanding these mechanisms is particularly

important for the therapeutic targeting of autophagy and cell death pathways in various diseases and conditions.

4.1.1.3 Mitophagy as a form of selective autophagy

Non-selective autophagy, often referred to as macroautophagy, involves random bulk uptake of cytoplasmic cargo and subsequent degradation, whereas selective autophagy is responsible for the sequestration of a specific cargo and is dependent upon LC3 interacting region (LIR)-containing receptors. Mitophagy is a classic example[509] where dysfunctional mitochondria are labelled for degradation at the autophagosome through the interaction of LC3 with receptor proteins at the OMM. These include BNIP3, NIX (also known as BNIP3L), FUNDC1 and cardiolipin. Another mechanism involves the Pink1-Parkin pathway and the ubiquitination of mitochondrial proteins, with P62 and NBR1 acting as LC3 interacting proteins.

The Pink1-Parkin pathway is the most well studied mechanism regulating mitophagy in mammalian cells. It was first identified in Parkinson's disease where it was shown to promote mitophagy. PINK1 (PTEN-induced putative kinase 1) is a serine/ threonine kinase. In healthy mitochondria, PINK1 undergoes continuous degradation following its import into the inner mitochondrial membrane (IMM), but it accumulates at the OMM in depolarised mitochondria. Once stabilised, PINK1 phosphorylates targets including mitofusin 2 (MFN2) and ubiquitin at the OMM, which leads to the recruitment of Parkin[510,511]. Parkin ubiquitinates multiple substrates, which promotes recruitment of the LC3 interacting proteins P62 and NBR1[512]. Thereby, allowing mitochondria to be engulfed and degraded by mitophagy.

NIX and BNIP3 are also important regulators of mitophagy. They are members of the BCL2 protein family and possess a BH3 domain with homology to the BH3-only pro-apoptotic members. They are therefore bi-functional in their ability to induce both mitophagy and/or cell death[513]. The role of NIX inducing mitophagy in mammalian cells was first demonstrated in erythroid cells eliminating their mitochondria as they differentiate into erythrocytes. The

authors showed that *Nix*$^{-/-}$ mice have a reduced number of mature erythrocytes, mitochondrial accumulation and defective sequestration of mitochondria by autophagosomes[514] (figure 4.3). BNIP3 shares high sequence similarity with NIX (~50% identical amino acids), including the LIR allowing interaction with LC3[515]. Both are transmembrane proteins located in the OMM[516]. Although both genes are targets of HIF1α[350,517], BNIP3 is induced to higher levels than NIX in response to hypoxia[518–520]. Moreover, their expression is tissue-specific as BNIP3 is more abundant in the heart and skeletal muscle, whereas NIX is more abundant in the haematopoietic system[521,522]. During mitophagy induction, BNIP3 binds to LC3 via phosphorylation on serine residues adjacent to the LIR motif. For BNIP3 and NIX to function as receptor proteins, dimerisation may be required[516].

How damaged mitochondria are recognised and specifically labelled, as opposed to healthy mitochondria, is not entirely understood. It has been suggested that mitochondrial depolarisation and fragmentation have a role in the activation of mitophagy regulators as they precede mitophagy[523–525]. Indeed, mitochondrial depolarisation induces PINK1 stabilisation at the OMM[526–528], and the degradation of the fusion protein OPA-1[529–531]. Mitochondrial fragmentation is associated with increased mitophagy possibly due to the reduction in the size of mitochondria facilitating their uptake by phagophores. In contrast, mitochondrial tubular network formation via fusion protects healthy mitochondria from degradation. However, it should be noted that programmed mitochondrial clearance occurs to eliminate unwanted mitochondria. An example of that would be the elimination of sperm mitochondria in the early zygote where mitochondria are ubiquitinated for clearance[516,532,533].

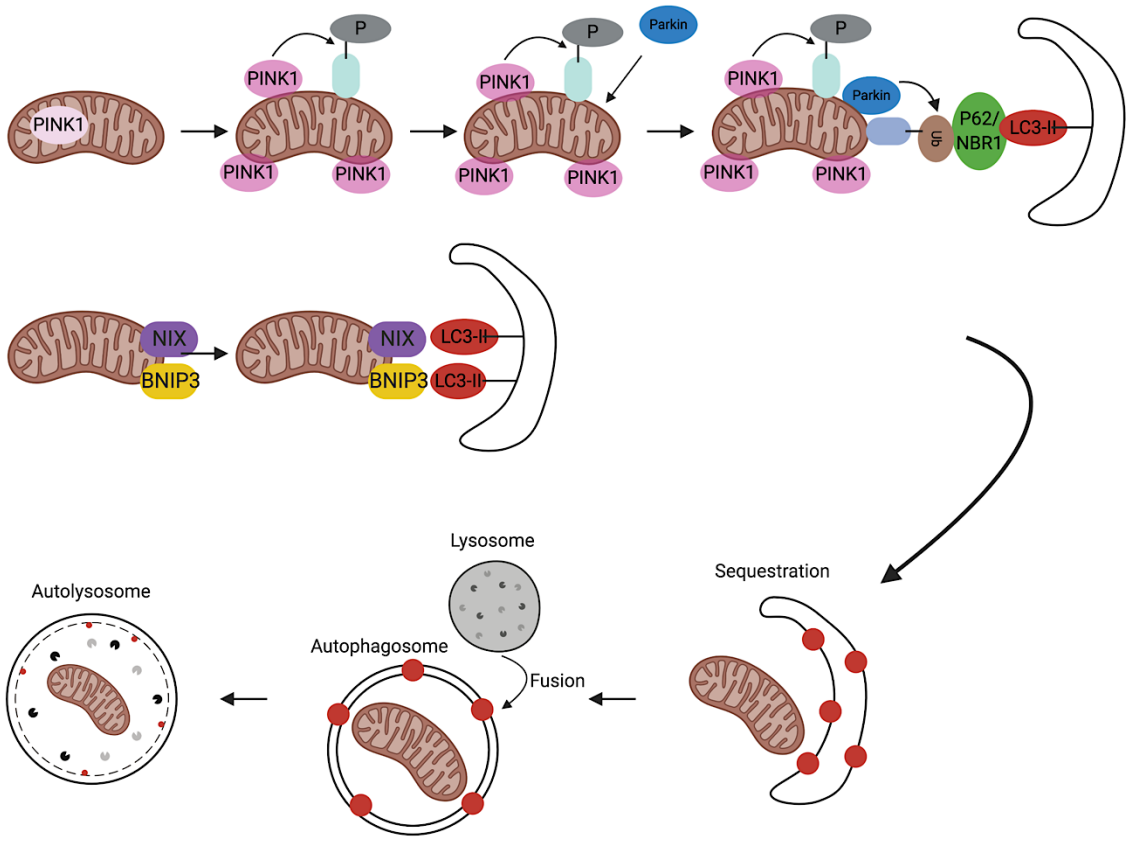


Figure 4.2 Mitophagy pathways

In healthy mitochondria, PINK1 undergoes continuous degradation following its import into the IMM. The PINK1/Parkin pathway is initiated upon accumulation of PINK1 on the OMM in depolarised mitochondria. PINK1 then phosphorylates its targets leading to the recruitment of Parkin, which ubiquitinates its substrates. The adaptor proteins P62 and NBR1 bind the ubiquitinated proteins and LC3-II on the autophagosome. The BNIP3/NIX pathway involves BNIP3 and NIX acting as receptor proteins at the OMM that directly bind LC3-II. Mitophagy involves the sequestration of mitochondria by autophagosomes, which fuse with lysosomes to form autolysosomes where mitochondrial degradation occurs. (Adapted from[534])

4.1.2 Aims

In this chapter, the overall aim was to explore mechanisms by which miR-210 may target cell death pathways in CTs. To facilitate this, I tested the use of NPs to deliver miR-210 into CTs and attempted to produce stable overexpression of miR-210 in CTs by retroviral transduction. Moreover, I investigated an anti-apoptotic role of miR-210 in CTs. Finally, as an hypoxia miRNA, miR-210 may have a role in targeting mitochondrial dynamics. Therefore, I examined the unexplored role of miR-210 in the regulation of mitophagy.

4.2 Results

4.2.1 Optimisation of miR-210 delivery into CTs

4.2.1.1 Intracellular release of miRNA using NP170

We tested whether NP170 could be used to internalise miR-210 in CTs more efficiently than the commercial transfection agent DharmaFECT formulation 1 (cationic lipid-mediated method) to optimise miRNA delivery. Previous work from the Carr group reported the use of biodegradable NP170s that have increasing capacity to efficiently release complexed miRNAs[535]. The NP170s were formed by poly(lactic acid-co-glycolic acid) PLGA encapsulating the fluorine-based compound PFCE (perfluoro-1,5-crown ether), which can be tracked noninvasively by MRI. NP170s complexed with miRNAs were found to accumulate within the endolysosomal compartment and interact in higher frequency with the AGO2 and GW182 proteins, which are involved in miRNA-mediated gene silencing. In contrast, commercial transfection reagents were found to result in the accumulation of miRNA in the cell cytoplasm. The NP170s were labelled with Rhodamine to enable fluorescence imaging.

S. Malandraki-Miller (thesis) attempted to deliver miR-210 to CTs using NP170 and assessed CT cell survival as an indication of miR-210's successful overexpression. This is because miR-210 has been shown to improve cell survival or inhibit cell apoptosis in previous studies[243,536–538]. Therefore, CTs were serum starved for 72 hours to induce apoptosis and cell number was used as a measure to evaluate miRNA capacity to improve cell survival. This was then compared to CTs transfected with miR-210 using the DharmaFECT reagent. No significant difference was observed between the different miRNA conditions with the NP170 method, whereas the DharmaFECT method showed a significant difference in cell numbers in miR-210-transfected CTs compared to the negative miRNA. This was attributed to NP170 suboptimal storage conditions. We therefore repeated the experiment with a different batch of NP170s as described in Methods 2.16. However, similar results were observed, as shown by a

significant difference between the miRNA groups using the DharmaFECT method (about 2-fold increase; starved Dh-neg, 31,833 ± 16,810; starved Dh-miR-210, 70,333 ± 19,502; $P < 0.05$; n=3) but not the NP170 method (starved NP-neg, 70,000 ± 5,000; starved NP-miR-210, 61,667 ± 12,583; $P = 0.44$; n=3) (figure 4.4).

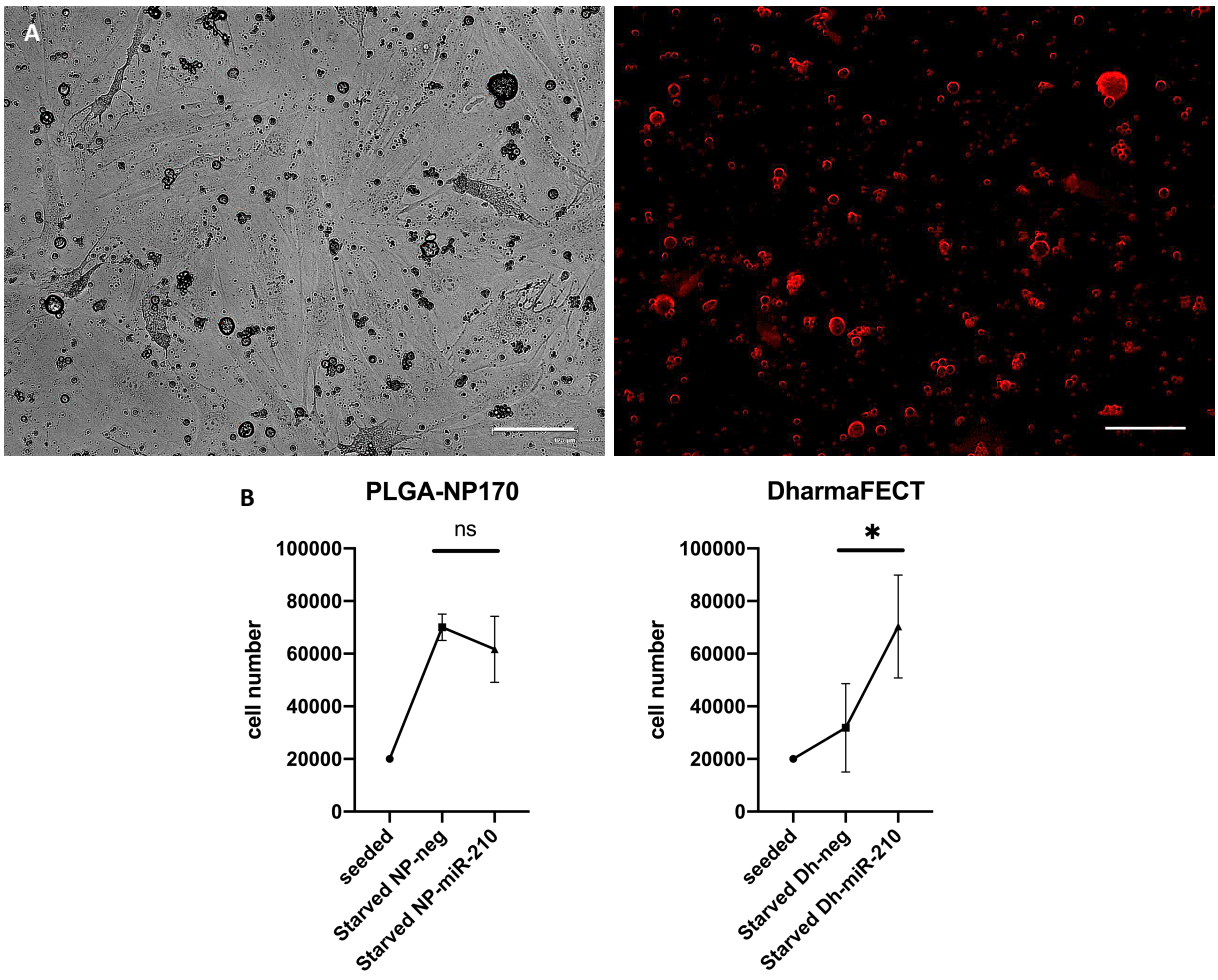


Figure 4.3 Delivery of miR-210 into CTs using NP170

(A) Representative images of CTs transfected with Rhodamine-labelled NP170 at 24-hours following transfection. Cells were imaged using an EVOS fluorescent microscope. Scale bar: 125µm. **(B)** The survival of CTs transfected with miR-210 using NP170 or DharmaFECT following 72-hour serum starvation, as assessed by cell counting. Analysed using a one-way ANOVA with Tukey's multiple comparisons test to determine statistical significance (n=3). Scale bar = 125µm.

4.2.1.2 Retroviral transduction of miR-210 in comparison to the DharmaFECT reagent

To obtain stable miR-210-overexpressing CTs, we attempted miR-210 overexpression by retroviral transduction. A miR-210 retroviral vector and a backbone vector, used in previous publications[539], were kindly provided by Fabio Martelli from the University of Milan. The pre-miR-210 sequence (MI0000286) was cloned between *BglII* and *HindIII* restriction sites, in pSUPER.retro.puro vector (pSUPER, Oligoengine). The retroviral transduction protocol is described in detail in Methods 2.17.

As the retroviral vector contained a puromycin resistance gene, we treated the cells with puromycin for 7 days to select for the cells that were successfully transduced with the vector. Figure 4.5 (A-C) shows the negative control cells where no vector was added, cells transduced with the backbone vector, and cells transduced with the miR-210 vector on the 7th day of puromycin treatment. As expected, the negative control cells died following puromycin treatment whereas cell survival was observed in the transduced cells indicating successful transduction.

Therefore, miR-210 qRT-PCR was performed to verify successful overexpression. miR-210 qRT-PCR was also performed on cells transfected using the DharmaFECT protocol (Methods 2.6). miR-210 was always prepared at the concentration of 100nM. Following the transfection or transduction protocol, the culture media was changed to CEM and cells were kept in culture for 72 hours prior to collection for total RNA extraction. Interestingly, there was no observed upregulation in miR-210 levels in the retroviral-transduced cells (neg – retroviral, 0.62 ± 0.14; miR-210 – retroviral, 0.67 ± 0.11; $P > 0.05$; n=3). However, a successful overexpression was obtained with DharmaFECT transfection (neg – DharmaFECT 100nM, 1.1 ± 0.47; miR-210 – DharmaFECT 100nM, 85 ± 13; $P < 0.0001$; n=3) (figure 4.5.D). Therefore, the DharmaFECT transfection method was selected for this thesis.

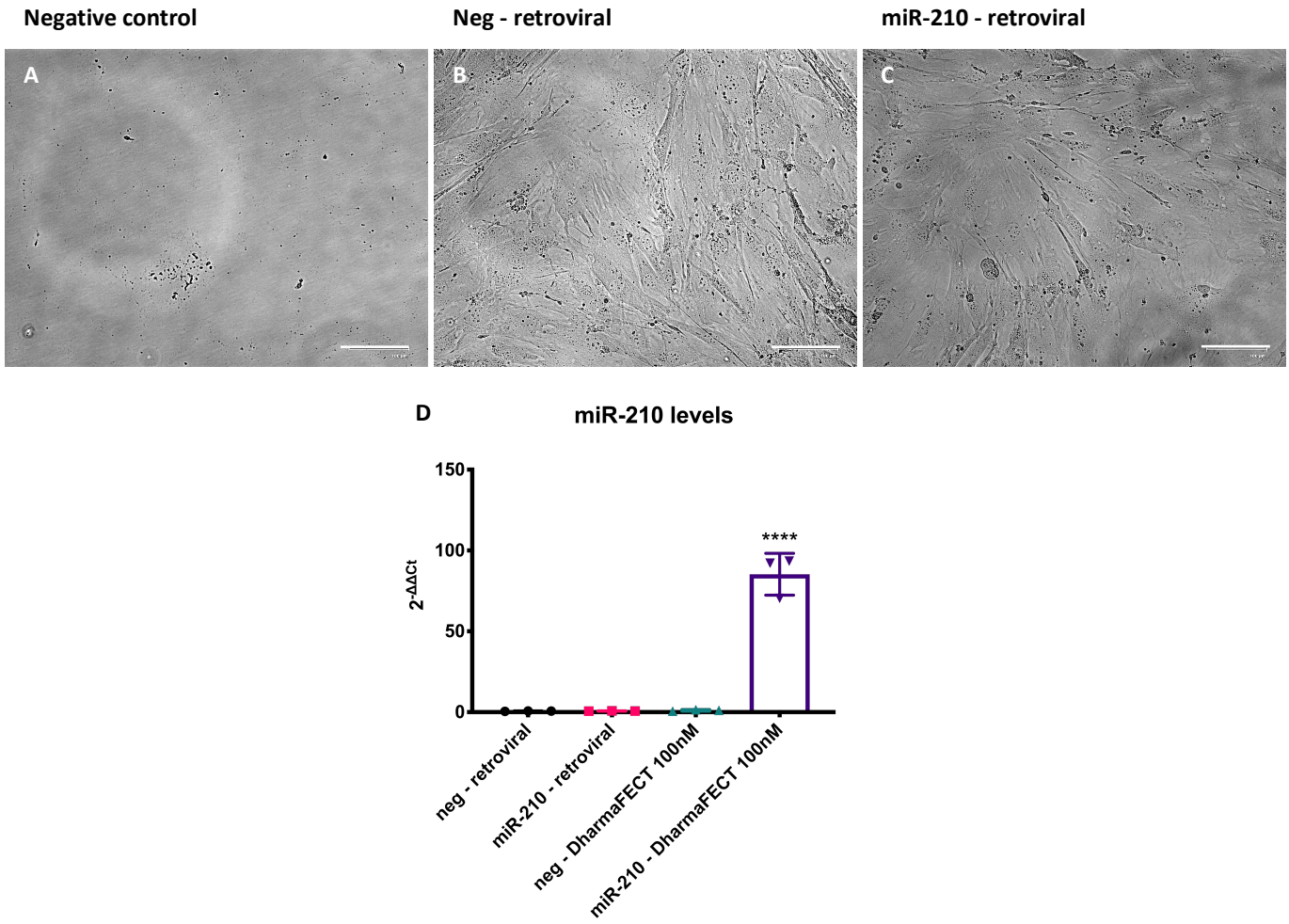


Figure 4.4 Retroviral transduction of miR-210 in comparison to the DharmaFECT reagent

Representative images of **(A)** negative control CTs that were not transduced with a retroviral vector, **(B)** transduced with a backbone retroviral vector or **(C)** transduced with a miR-210 retroviral vector on the 7th day of puromycin treatment. The negative control CTs (A) died following puromycin treatment whereas cell survival was observed in the transduced cells (B & C) indicating successful transduction. Cells were imaged using an EVOS fluorescent microscope. Scale bar: 125µm. **(D)** miR-210 levels in CTs measured by qRT-PCR at 72 hours following retroviral transduction or DharmaFECT transfection. Analysed using a one-way ANOVA with Tukey's multiple comparisons test to determine statistical significance (n=3). Scale bar = 125µm.

In addition to the 72-hour timepoint, miRNA levels were assessed at 24 and 48 hours following DharmaFECT transfection by both qRT-PCR and confocal imaging. The qRT-PCR results demonstrated that miR-210 levels were most upregulated at the 24-hour timepoint as they were significantly higher in comparison to the 48- and 72-hour timepoints (miR-210 – DharmaFECT 100nM (24h), 1.1 ± 0.49; miR-210 – DharmaFECT 100nM (48h), 0.27 ± 0.03; $P < 0.05$; miR-210 – DharmaFECT 100nM (72h), 0.23 ± 0.04; $P < 0.05$; n=3). No significant difference was detected between 48 and 72 hours (miR-210 – DharmaFECT 100nM (48h), 0.27 ± 0.03; miR-210 – DharmaFECT 100nM (72h), 0.23 ± 0.04; $P = 0.98$; n=3) (figure 4.6).

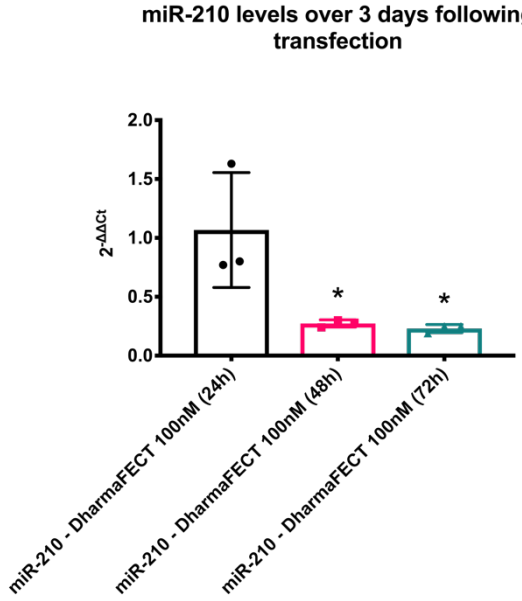


Figure 4.5 miR-210 levels in CTs over 3 days following transfection using the DharmaFECT reagent

miR-210 levels in CTs measured by qRT-PCR at 24, 48 or 72 hours following DharmaFECT transfection. Analysed using a one-way ANOVA with Tukey's multiple comparisons test to determine statistical significance (n=3).

As no fluorescently-labelled miR-210 could be obtained commercially, Dy547-labelled miRNA was used, a mimic negative control miRNA based on the *C. elegans* miRNA cel-miR-67 for monitoring delivery into human, mouse, and rat cells. Transfection of the Dy547-labelled miRNA was performed using the DharmaFECT reagent. Quantification of Dy547-labelled miRNA internalised by CTs was performed using confocal microscopy. Dy547-labelled miRNA levels were found to not significantly change over 72 hours (Dy547-miRNA – DharmaFECT (24h), 123,294 ± 74,837; Dy547-miRNA – DharmaFECT (48h), 62,741 ± 21,774; Dy547-miRNA – DharmaFECT (72h), 121,141 ± 15,999; $P > 0.05$; n=3) (figure 4.7). Measuring miRNA levels following the DharmaFECT transfection method enabled us to determine how long the delivered miRNA remained upregulated in CTs to select the timepoint by which the cells were processed for both the *in vitro* and *in vivo* parts of the study. Although no significant change was observed by imaging, the 24-hour timepoint showed significantly higher upregulation of the miRNA by qRT-PCR. However, the cells were allowed to recover for at least 48 hours following transfection as transfection can affect cell viability[540,541]. For the *in vitro* study, CTs were cultured for 72 hours in serum-free media following transfection to induce apoptotic cell death (as described in 3.2.4). For the *in vivo* study, cells were allowed to recover for 48 hours following transfection prior to injection into the MI mouse model.

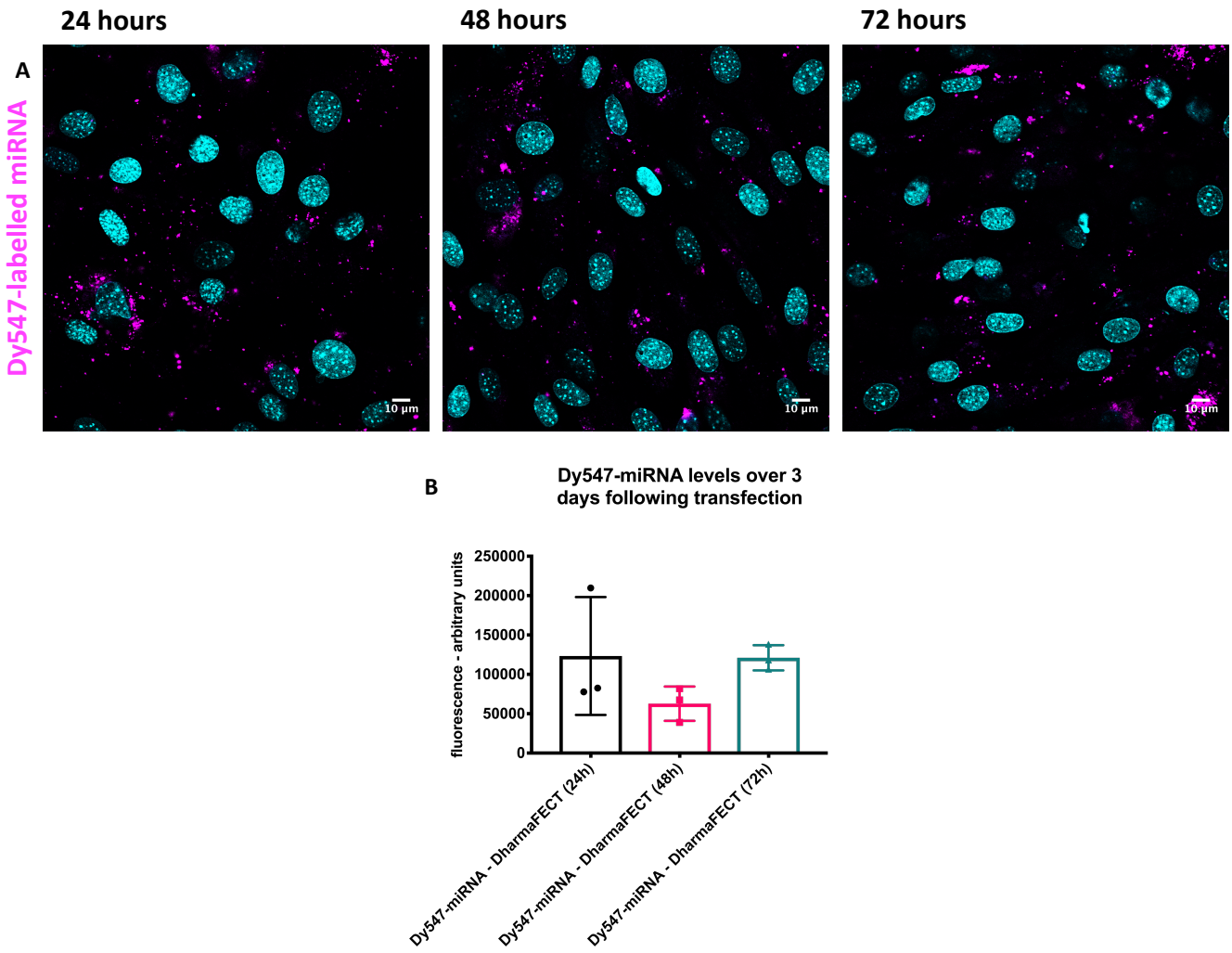


Figure 4.6 Dy547-miRNA levels in CTs over 3 days following transfection using the DharmaFECT reagent

(A) Representative images of CTs transfected with Dy547-miRNA using DharmaFECT at 24, 48 or 72 hours following transfection. Cells were imaged using an FV1000 confocal microscope. **(B)** Dy547-miRNA fluorescence intensity was quantified using Fiji software by assessing cells visualised in 3 random fields (described in Methods 2.13). Analysed using a one-way ANOVA with Tukey's multiple comparisons test to determine statistical significance (n=3). Scale bar = 10µm.

4.2.2 miR-210 inhibits apoptotic cell death and has a role in the regulation of mitochondrial fission and autophagy in CTs

4.2.2.1 miR-210 improves the survival of CTs by targeting apoptotic cell death following serum starvation

To further validate miR-210's pro-survival effect and confirm that it targets cell death pathways in CTs, multiple parameters were examined after 72 hours of serum starvation. *Casp8ap2* expression was analysed as it has been shown to be a direct target of miR-210 through which it mediates cytoprotection[249]. *Casp8ap2* encodes caspase 8 associated protein 2, a multifunctional protein that has been implicated in cell cycle regulation[542], transcriptional control[543] and the activation of caspase 8 during apoptosis[544]. *Casp8ap2* mRNA levels were significantly downregulated following miR-210 transfection in comparison to the negative miRNA (starved neg, 1.0 ± 0.09; starved miR-210, 0.81 ± 0.06; $P < 0.05$; n=3) (figure 4.8.A). Caspases are synthesized as catalytically inactive zymogens and must undergo activation through cleavage[545]. Therefore, a poly-caspase activity assay was performed to determine the levels of activated cleaved caspases following miRNA transfection and 72-hour serum starvation. The poly-caspase activity assay revealed significantly reduced overall activity of caspases following miR-210 transfection in comparison to the negative miRNA (starved neg, 41,800 ± 9,107; starved miR-210, 24,579 ± 3,059; $P < 0.05$; n=4) (figure 4.8.B).

Finally, downregulated apoptotic cell death was confirmed by measuring DNA fragmentation using a TUNEL assay (starved neg, 3.4 ± 1.4; starved miR-210, 0.35 ± 0.29; $P < 0.01$; n=5) (figure 4.9).

Figure 4.7 miR-210-transfected CTs show decreased Casp8ap2 mRNA levels and poly-caspase activity following serum starvation

(A) *Casp8ap2* mRNA levels (n=3) and **(B)** poly-caspase activity (n=4) in miR-210-transfected CTs following serum starvation, in comparison to CTs transfected with a negative miRNA. Analysed using a t-test to determine statistical significance.

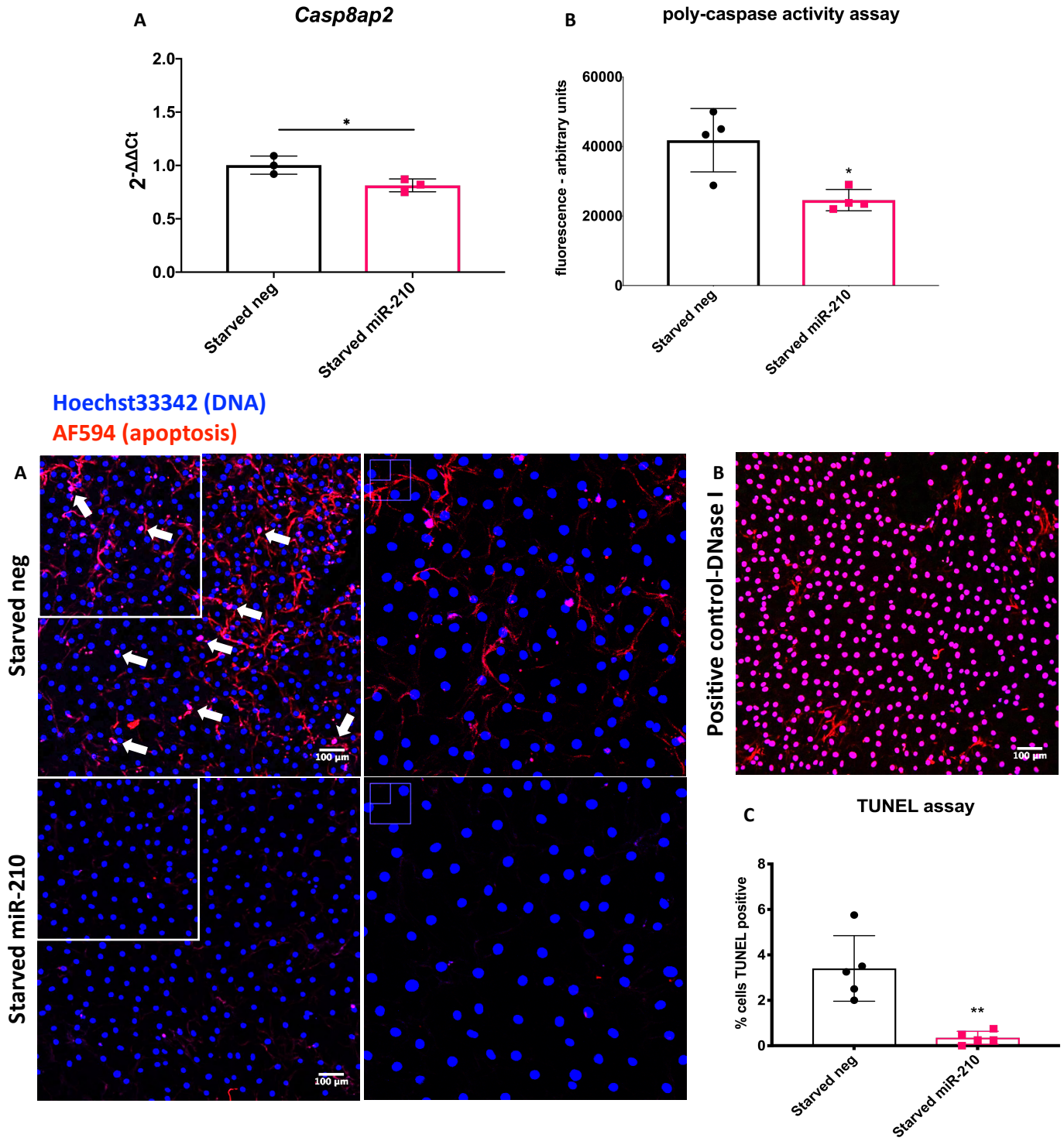


Figure 4.8 miR-210-transfected CTs show decreased TUNEL+ cells following serum starvation

(A) DNA fragmentation represented as TUNEL+ cells in miR-210-transfected CTs following serum starvation, in comparison to CTs transfected with a negative miRNA. Cells were imaged using an FV1000 confocal microscope. High power inserts are shown by white boxes. **(B)** DNase treatment was used as a TUNEL assay positive control **(C)** Quantification of the TUNEL assay (described in Methods 2.12). Analysed using a t-test to determine statistical significance (n=5). Scale bar = 100µm.

4.2.2.2 miR-210 downregulates the expression of glycerol-3-phosphate dehydrogenase 1-like (Gpd1l), a regulator of HIF1α stability

Due to the importance of miR-210 in the hypoxic response, the role of hypoxia in regulating mitochondrial dynamics and mitophagy[546,547], and the important crosstalk between mitochondrial dynamics and cell death pathways, the rest of this results chapter will therefore attempt to examine the relationship between miR-210, hypoxia and mitochondrial dynamics. It has been shown that miR-210 is not only downstream of HIF1α but also upstream of it by targeting *Gpd1l*[548,549]. GPD1L has homology to GPD1, a cytosolic enzyme involved in the glycerol phosphate shuttle of the glycolytic pathway. GPD1L catalyses the conversion of dihydroxyacetone phosphate to glycerol 3-phosphate and its mRNA is directly regulated by miR-210 at the 3' UTR. Destabilisation of GPD1L ultimately upregulates HIF1α, as GPD1L has a role in increasing prolyl hydroxylase (PHD)-dependent degradation of HIF1α[548,549].

To examine the possibility of miR-210 regulating HIF1α signalling via GPD1L in CTs, the mRNA levels of *Gpd1l* and *Hif1α* were assessed. HIF1α has been shown to be upregulated in response to certain treatments, e.g. doxorubicin[550] and nitric oxide[551], despite the cells being cultured in normoxia. Therefore, the experiment was performed under both normoxic and hypoxic (2% O_2) culture following serum starvation or culture in complete media. *Gpd1l* was found to be significantly downregulated in miR-210-overexpressing CTs in comparison to their respective negative miRNA group under all conditions, with the exception of the control hypoxic condition (normoxia: control neg, 1.0 ± 0.09; control miR-210, 0.50 ± 0.08; $P < 0.001$; starved neg, 1.2 ± 0.07; starved miR-210, 0.80 ± 0.05; $P < 0.001$; hypoxia: control neg, 1.0 ± 0.14; control miR-210, 0.54 ± 0.04; $P > 0.05$; starved neg, 2.9 ± 0.38; starved miR-210, 2.1 ± 0.37; $P < 0.05$; n=3) (figure 4.10.A). We also observed an upregulation in *Gpd1l* mRNA levels in response to serum starvation under all tested conditions (normoxia: control neg, 1.0 ± 0.09; starved neg, 1.2 ± 0.07; $P < 0.05$; control miR-210, 0.50 ± 0.08; starved miR-210, 0.80 ± 0.05;

$P < 0.01$; hypoxia: control neg, 1.0 ± 0.14; starved neg, 2.9 ± 0.38; $P < 0.001$; control miR-210, 0.54 ± 0.04; starved miR-210, 2.1 ± 0.37; $P < 0.001$; n=3). Similar to miR-210 overexpression, hypoxic culture significantly decreased *Gpd1l* levels (control neg - normoxia, 1.0 ± 0.09; control neg - hypoxia, 0.49 ± 0.07; $P < 0.01$; n=3) (supplementary figure 1, appendix A). Moreover, I attempted to examine HIF1α protein levels. Two antibodies against HIF1α were tested on CTs cultured under 2% O_2 for 16 hours, as a positive control for HIF1α. However, neither antibody showed any staining (figure 4.10.C). This may be attributed to the very short half-life of HIF1α[552].

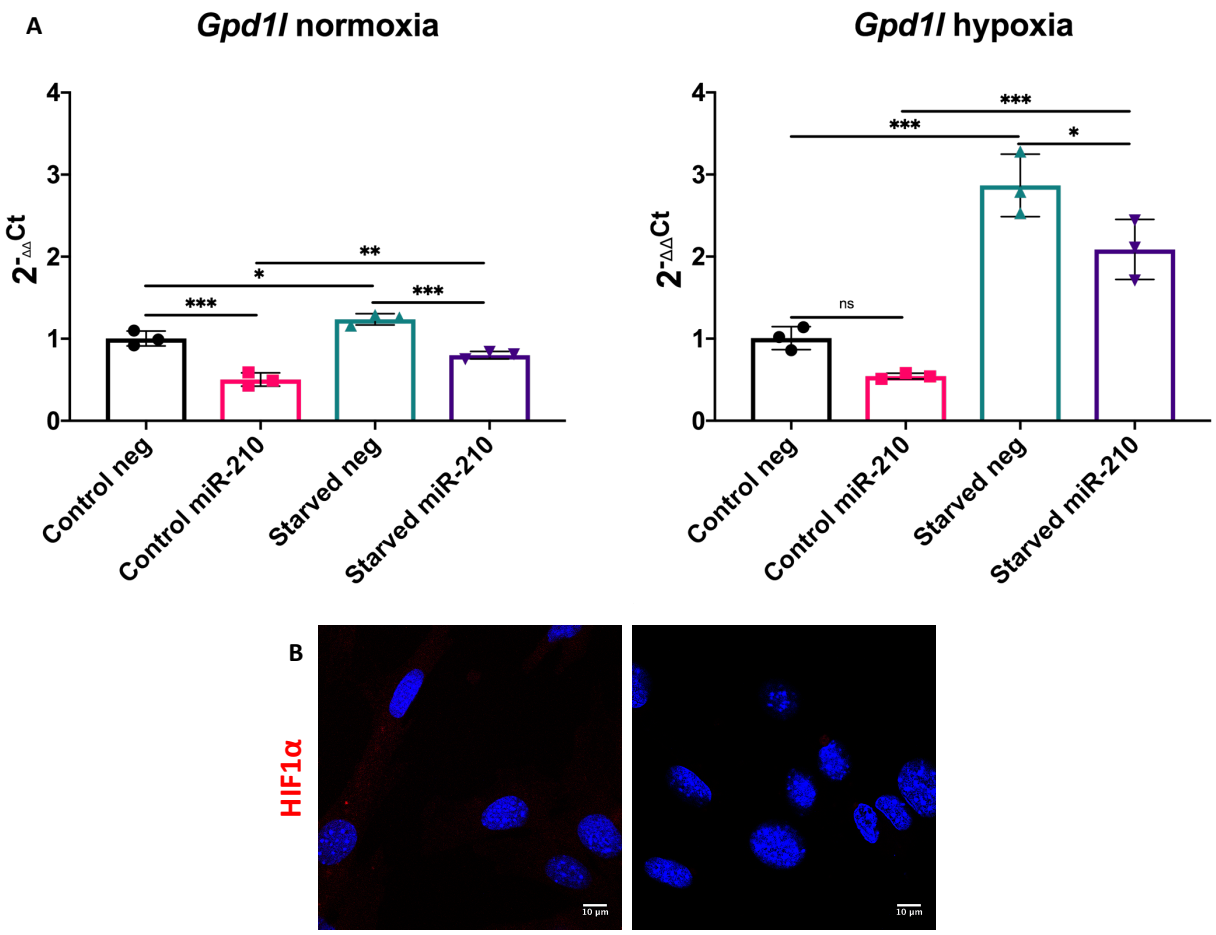


Figure 4.9 miR-210 downregulates the expression of glycerol-3-phosphate dehydrogenase 1-like (*Gpd1l*), a regulator of HIF1α stability

(A) *Gpd1l* mRNA levels in miR-210-transfected CTs, in comparison to CTs transfected with a negative miRNA, under the conditions shown: control media and normoxia, serum starvation and normoxia, control media and hypoxia, serum starvation and hypoxia. Analysed using a one-way ANOVA with Tukey's multiple comparisons test to determine statistical significance (n=3). **(B)** CTs stained with anti-HIF1α antibodies after culture under hypoxia for 16 hours. Cells were imaged using an FV1000 confocal microscope. Scale bar = 10μm.

4.2.2.3 miR-210 does not induce BNIP3 as an anti-apoptotic mechanism

To examine a potential relationship between miR-210, hypoxia and mitophagy, we examined the expression of mitophagy-associated genes in response to hypoxic culture and/or miR-210 overexpression. We firstly focused on *Bnip3* and *Nix* as they are both direct targets of HIF1α[350,517]. BNIP3 has been reported to induce apoptosis, necrosis, or autophagy depending on the cellular context[513] (see 4.1.2.3). The cytoprotective role of BNIP3-dependent mitophagy has been demonstrated in human primary epidermal keratinocytes[553]. Moreover, HIF1α has been shown to induce BNIP3-dependent mitophagy as an adaptive metabolic response to hypoxia to increase cell survival[547]. Therefore, based on the downregulation of *Gpd1l* expression, a HIF1α stability regulator, in response to miR-210 overexpression, we hypothesised that miR-210 may have a role in inducing BNIP3-dependent mitophagy for cytoprotection as observed in response to HIF1α. Indeed, we found that hypoxic culture increased the mRNA levels of *Bnip3* (control, 1.1 ± 0.54; 2% O_2 – 72h, 12 ± 2.00; $P < 0.0001$; n=3), *Nix* (control, 1.0 ± 0.17; 2% O_2 – 72h, 5 ± 1.50; $P < 0.01$; n=3) and *Atg4c* (control, 1.0 ± 0.23; 2% O_2 – 72h, 2.2 ± 0.50; $P < 0.01$; n=3) indicating enhanced mitophagy (figure 4.11).

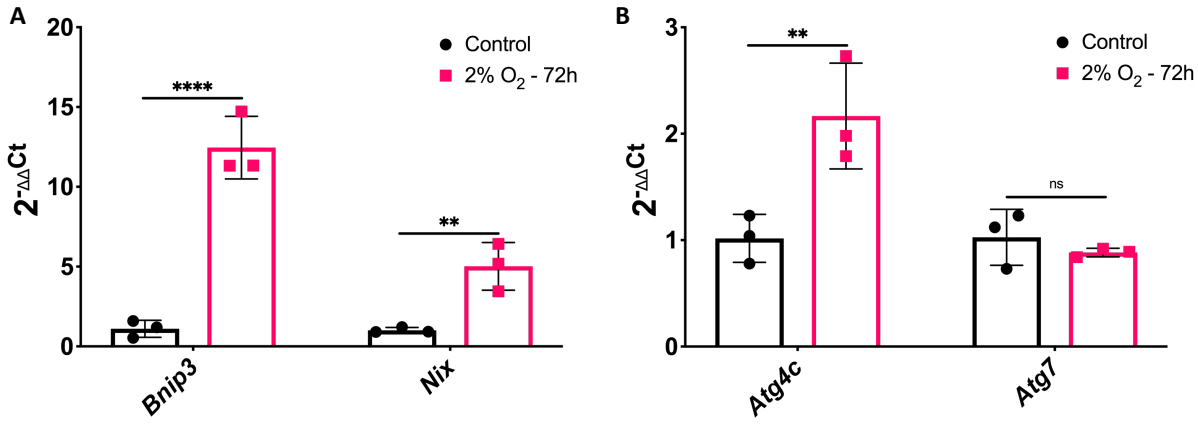


Figure 4.10 Hypoxic culture upregulates the mRNA levels of mitophagy-associated genes in CTs

(A) *Bnip3* and *Nix* and **(B)** *Atg4c* and *Atg7* mRNA levels in CTs cultured in hypoxia, in comparison to CTs cultured in normoxia. Analysed using a two-way ANOVA with Tukey's multiple comparisons test to determine statistical significance (n=3).

In an attempt to assess whether the cytoprotective role of miR-210 acted partly through BNIP3-dependent mitophagy, we knocked down the mRNA levels of *Bnip3* by siRNA and measured apoptosis. For *Bnip3* siRNA validation, two *Bnip3* siRNAs, a *Gapdh* siRNA positive control, and a scrambled negative control siRNA were used for transfection as described previously (Methods 2.6). *Bnip3* and *Gapdh* mRNA levels were assessed by qRT-PCR 48 hours post transfection. *Gapdh* mRNA levels were reduced at 100nM showing successful transfection (CNTRL, 1.0 ± 0.14; neg siR, 1.0 ± 0.17; pos siR – *Gapdh* 40nM, 0.71 ± 0.60; pos siR – *Gapdh* 100nM, 0.25 ± 0.03; $P < 0.05$; n=3). *Bnip3* siRNA 1 at 100nM showed the most reduction in *Bnip3* levels compared to siRNA 2 and combinations of siRNA 1 and 2 (CNTRL, 1.1 ± 0.19; neg siR, 1.2 ± 0.09; *Bnip3* siRNA 1 40nM, 0.11 ± 0.02; *Bnip3* siRNA 1 100nM, 0.09 ± 0.02; *Bnip3* siRNA 2 40nM, 0.63 ± 0.01; *Bnip3* siRNA 2 100nM, 0.42 ± 0.06; *Bnip3* siRNA 1+2 40nM, 0.18 ± 0.04; *Bnip3* siRNA 1+2 100nM, 0.35 ± 0.02; n=3) (figure 4.12). Therefore, siRNA 1 at 100nM was selected.

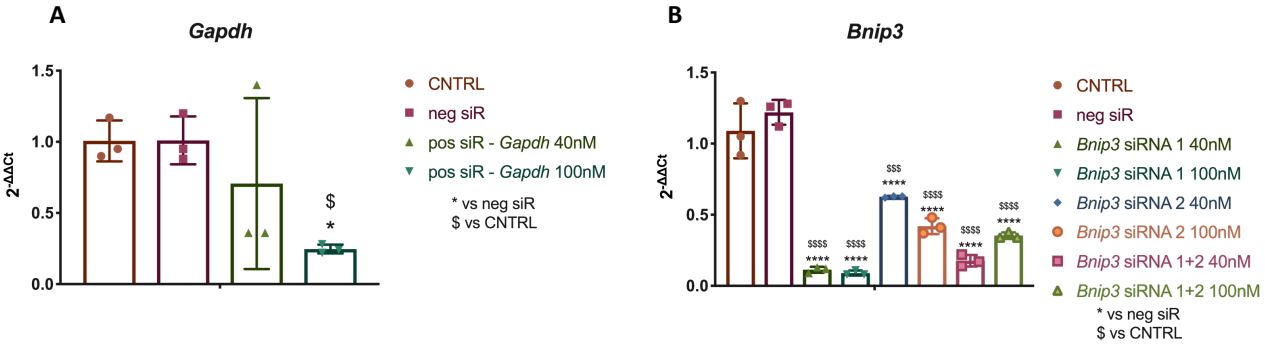


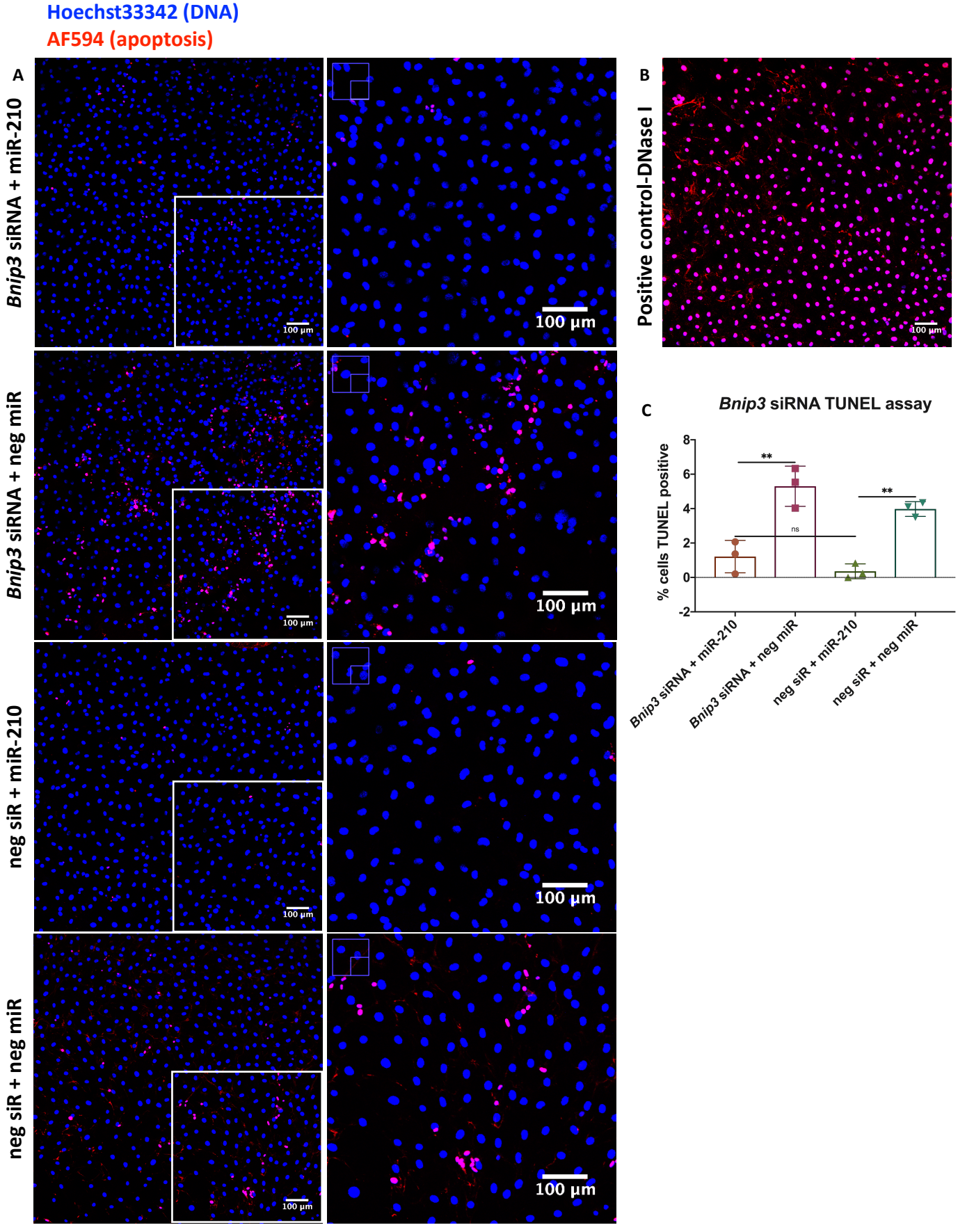
Figure 4.11 Validation of *Bnip3* siRNAs

(A) *Gapdh* mRNA levels following transfection of CTs with a positive control *Gapdh* siRNA **(B)** *Bnip3* mRNA levels following transfection of CTs with two different *Bnip3* siRNAs, individually or a combination of the two. Two concentrations of siRNAs were tested (40 and 100nM) in comparison to a negative siRNA and an untransfected control. Analysed using a one-way ANOVA with Tukey's multiple comparisons test to determine statistical significance (n=3).

CTs were transfected with *Bnip3* siRNA 1 and then starved for 72 hours. Apoptosis was assessed by measuring DNA fragmentation using a TUNEL assay as previously described. Appropriate control conditions were also used as shown in figure 4.13. *Bnip3* knockdown did not decrease miR-210's capacity to target apoptosis (*Bnip3* siRNA + miR-210, 1.2 ± 0.94; neg siR + miR-210, 0.36 ± 0.43; P = 0.59; n=3). This suggests that unlike the previously described role of HIF1α[547], miR-210 does not induce BNIP3 as an anti-apoptotic mechanism. A significant downregulation in apoptosis was observed in miR-210-transfected cells in comparison to their respective negative miRNA group in both *Bnip3* siRNA and negative siRNA conditions, which is consistent with miR-210's pro-survival effect (*Bnip3* siRNA + miR-210, 1.2 ± 0.94; *Bnip3* siRNA + neg miR, 5.3 ± 1.20; P < 0.01; neg siR + miR-210, 0.36 ± 0.43; neg siR + neg miR, 4.0 ± 0.43; P < 0.01; n=3).

Figure 4.12 *Bnip3* knockdown in miR-210-transfected CTs TUNEL assay

(A) DNA fragmentation represented as TUNEL$^+$ cells following serum starvation of CTs transfected with the following: *Bnip3* siRNA+miR-210, *Bnip3* siRNA+negative miRNA, negative siRNA+miR-210, negative siRNA+negative miRNA. Cells were imaged using an FV1000 confocal microscope. High power inserts are shown by white boxes. **(B)** DNase treatment was used as a TUNEL assay positive control (Scale bar = 10μm) **(C)** Quantification of the TUNEL assay (described in Methods 2.12). Analysed using a one-way ANOVA with Tukey's multiple comparisons test to determine statistical significance (n=3).


Hoechst33342 (DNA)
AF594 (apoptosis)
A
Bnip3 siRNA + miR-210
Bnip3 siRNA + neg miR
neg siR + miR-210
neg siR + neg miR
100 µm
B
Positive control-DNase I
C
Bnip3 siRNA TUNEL assay
% cells TUNEL positive
ns
Bnip3 siRNA + miR-210
Bnip3 siRNA + neg miR
neg siR + miR-210
neg siR + neg miR

Bnip3 and *Nix* mRNA levels were measured in miR-210-overexpressing CTs. We found that miR-210 did not significantly alter *Bnip3* mRNA levels (normoxia: control neg, 1.0 ± 0.20; control miR-210, 0.89 ± 0.12; starved neg, 1.0 ± 0.07; starved miR-210, 0.96 ± 0.09; hypoxia: control neg, 1.0 ± 0.25; control miR-210, 0.91 ± 0.32; starved neg, 0.35 ± 0.05; starved miR-210, 0.36 ± 0.07; $P > 0.05$; n=3) but downregulated *Nix* in CTs cultured in control conditions under hypoxia in comparison to their respective negative miRNA group (hypoxia: control neg, 1.0 ± 0.20; control miR-210, 0.62 ± 0.09; $P < 0.05$; n=3) (figure 4.14). Interestingly, *Nix* (hypoxia: control neg, 1.0 ± 0.20; starved neg, 0.60 ± 0.02; $P < 0.01$; n=3) and *Bnip3* (hypoxia: control neg, 1.0 ± 0.20; starved neg, 0.35 ± 0.05; $P < 0.05$; n=3) mRNA levels were decreased in response to serum starvation under hypoxia. In contrast, an increase in *Nix* mRNA was observed in response to serum starvation under normoxia (normoxia: control neg, 1.0 ± 0.26; starved neg, 1.5 ± 0.12; $P < 0.05$; n=3) and no significant change was observed with *Bnip3* mRNA levels (normoxia: control neg, 1.0 ± 0.20; starved neg, 1.0 ± 0.07; $P > 0.05$; n=3). Overall, this shows that, unlike hypoxia, miR-210 does not induce BNIP3-dependent mitophagy as an anti-apoptotic mechanism. In contrast, the reduction in *Nix* levels following miR-210 transfection of CTs under hypoxia suggested to us that there might be a reduction in mitophagy levels. Therefore, this was further investigated.

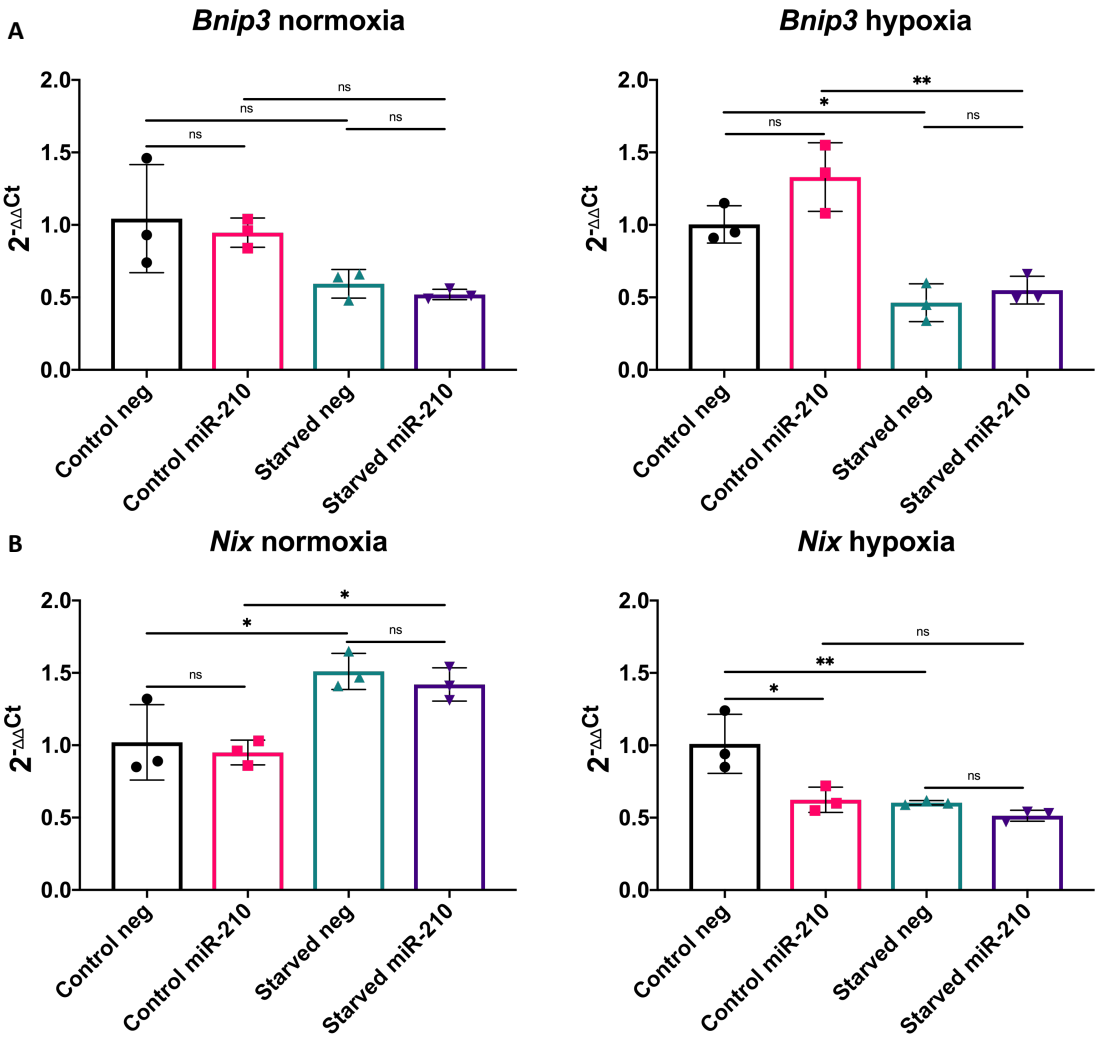


Figure 4.13 miR-210-transfected CTs show decreased *Nix*, but not *Bnip3*, mRNA levels

(A) *Bnip3* and **(B)** *Nix* mRNA levels in miR-210-transfected CTs, in comparison to CTs transfected with a negative miRNA, under the conditions shown: control media and normoxia, serum starvation and normoxia, control media and hypoxia, serum starvation and hypoxia. Analysed using a one-way ANOVA with Tukey's multiple comparisons test to determine statistical significance (n=3).

4.2.2.4 Mitophagy as a potential target of miR-210

To further validate the previous results, mRNA levels of the autophagy-associated genes *Atg4c*, and *Atg7* were assessed in response to miR-210 overexpression. *Atg4c* and *Atg7* were selected as they are computationally predicted to be direct targets of miR-210 by TargetScan and miRanda. Indeed, a luciferase assay was recently utilised to demonstrate the direct binding of miR-210 to the 3'UTR of *Atg7*[554]. Moreover, *Pink1* mRNA levels were also measured as the PINK1-Parkin pathway is the most widely studied mode of mitophagy. We found that *Pink1* was significantly downregulated in miR-210-overexpressing CTs in comparison to their respective negative miRNA group under all conditions, with the exception of the starved normoxic condition (normoxia: control neg, 1.0 ± 0.10; control miR-210, 0.71 ± 0.04; $P < 0.01$; starved neg, 1.5 ± 0.06; starved miR-210, 1.4 ± 0.10; $P > 0.05$; hypoxia: control neg, 1.0 ± 0.20; control miR-210, 0.65 ± 0.08; $P < 0.05$; starved neg, 1.6 ± 0.14; starved miR-210, 1.3 ± 0.09; $P < 0.05$; n=3). *Atg4c* was downregulated in miR-210-overexpressing CTs in comparison to their respective negative miRNA group in hypoxic conditions (hypoxia: control neg, 1.0 ± 0.22; control miR-210, 0.44 ± 0.15; $P < 0.01$; starved neg, 1.5 ± 0.08; starved miR-210, 1.0 ± 0.10; $P < 0.05$; n=3), whereas *Atg7* mRNA levels were not significantly altered (normoxia: control neg, 1.0 ± 0.39; control miR-210, 0.92 ± 0.09; starved neg, 1.3 ± 0.43; starved miR-210, 0.90 ± 0.07; hypoxia: control neg, 1.0 ± 0.14; control miR-210, 1.7 ± 0.57; starved neg, 0.85 ± 0.17; starved miR-210, 0.69 ± 0.08; $P > 0.05$; n=3) (figure 4.15). Overall, this suggested that mitophagy was reduced. Moreover, we observed an increase in *Pink1* mRNA levels in all conditions (normoxia: control neg, 1.0 ± 0.10; starved neg, 1.5 ± 0.06; $P < 0.001$; control miR-210, 0.71 ± 0.04; starved miR-210, 1.4 ± 0.10; $P < 0.0001$; hypoxia: control neg, 1.0 ± 0.20; starved neg, 1.6 ± 0.14; $P < 0.01$; control miR-210, 0.65 ± 0.08; starved miR-210, 1.3 ± 0.09; $P < 0.01$; n=3), and *Atg4c* in hypoxic conditions (hypoxia: control neg, 1.0 ± 0.22; starved neg, 1.5 ± 0.08; $P < 0.05$; control miR-210, 0.44 ± 0.15; starved miR-210, 1.0 ± 0.10; $P < 0.01$), in

response to serum starvation. Unlike miR-210 overexpression, hypoxic culture did not significantly alter *Pink1* levels (control neg - normoxia, 1.0 ± 0.10; control neg - hypoxia, 0.94 ± 0.18; $P > 0.05$; n=3) (supplementary figure 1, appendix A).

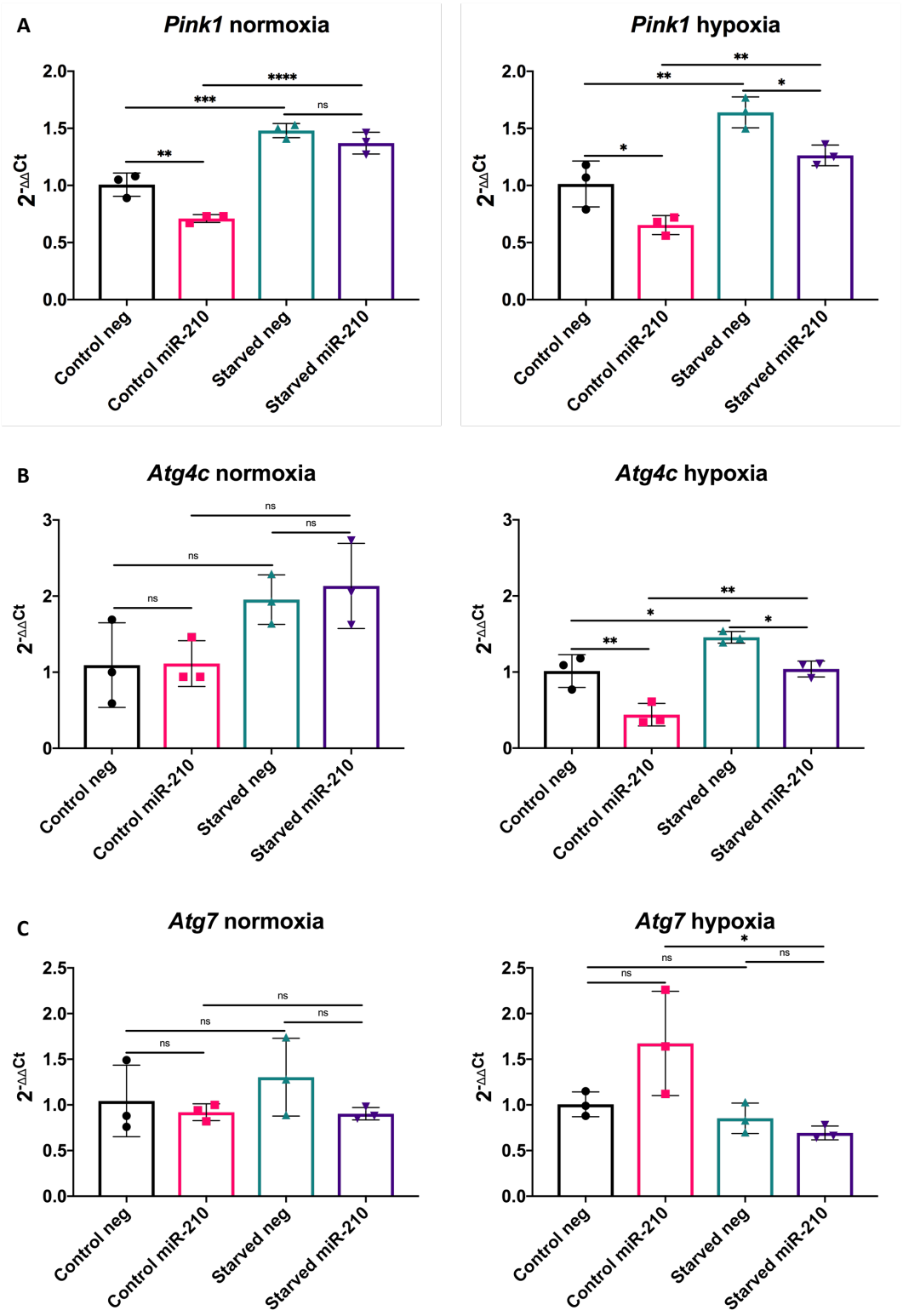


Figure 4.14 miR-210-transfected CTs show decreased mRNA levels of mitophagy-associated genes

(A) *Pink1*, **(B)** *Atg4c* and **(C)** *Atg7* mRNA levels in miR-210-transfected CTs, in comparison to CTs transfected with a negative miRNA, under the conditions shown: control media and normoxia, serum starvation and normoxia, control media and hypoxia, serum starvation and hypoxia. Analysed using a one-way ANOVA with Tukey's multiple comparisons test to determine statistical significance (n=3).

Mitophagy has been imaged by examining the co-localisation of mitochondrial probes with markers of the autophagic machinery and delivery of mitochondria to the lysosome[555]. Here, we attempted to measure mitophagy by quantifying the co-localisation of LC3-II autophagosomal puncta and MitoTracker Red CMXRos after serum starvation. Although MitoTracker Red CMXRos was used at the highest recommended concentration of 500nM, the dye was scarcely retained following staining with the LC3-II antibody. We also found high background noise with the LC3-II antibody making it difficult to quantify mitophagy (figure 4.16.A). Moreover, the experiment was repeated using an antibody against cytochrome c instead of the MitoTracker Red CMXRos dye to detect mitochondria. However, the cytochrome c antibody did not show an accurate representation of mitochondria as the staining was diffuse and did not co-localise well with the MitoTracker Red CMXRos dye (figure 4.16.B).

Finally, MEFs isolated from *RFP-MIT;EGFP-LC3* transgenic mice (Methods 2.3.5), kindly provided by the Poulton group (University of Oxford), were used to assess miR-210 induction of mitophagy. Interestingly, I did not observe EGFP-LC3 puncta in the cells following 72-hour serum starvation (not shown) or 24-hour treatment with the potent mitophagy inducer CCCP (figure 4.16.C), although mitochondrial fission was apparent. At a seminar in Oxford by Prof. Plun-Favreau, it was shown that the concentration of serum in the media alters CCCP's ability to depolarise mitochondria and induce mitophagy. The study suggested that 1μM of CCCP was sufficient to induce mitophagy in low-serum media, as opposed to the commonly used CCCP concentrations of >10μM. This was later published in 2019[556]. Therefore, the CCCP treatment was performed in serum-free media. Despite this, no EGFP-LC3 puncta were observed at both 1μM (not shown) and 10μM concentrations of CCCP.

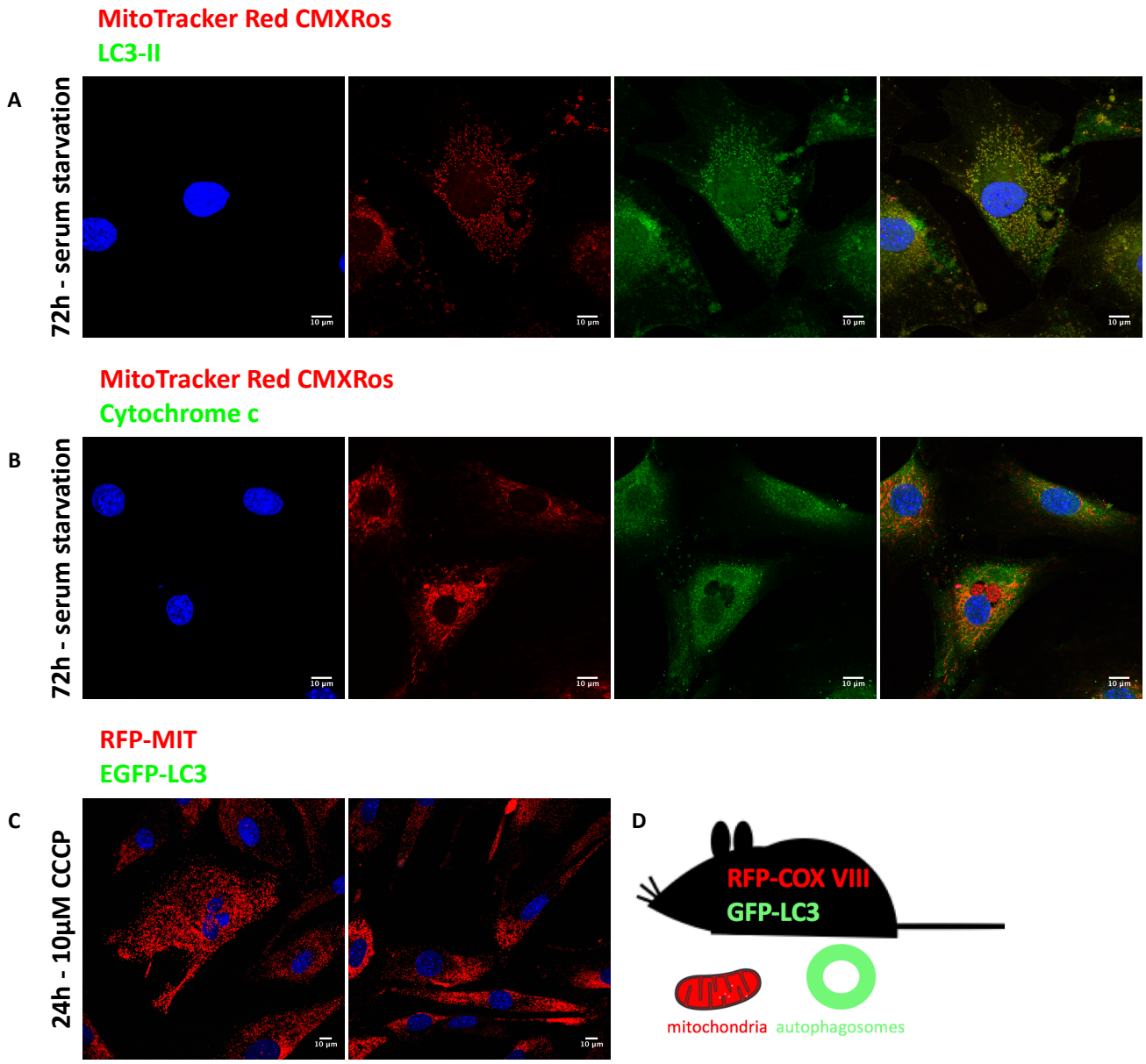


Figure 4.15 Attempts at visualising mitophagy using LC3 as a marker of autophagosomes

(A) CTs stained using an anti-LC3-II antibody and Mitotracker following serum starvation, representative of n=3. **(B)** CTs stained using an anti-cytochrome c antibody and Mitotracker following serum starvation, representative of n=1. **(C)** *RFP-MIT;EGFP-LC3* MEFs following 24-hour treatment with 10µM of CCCP, representative of n=2. Cells were imaged using an FV1000 confocal microscope. Scale bar = 10µm. **(D)** The *RFP-MIT;EGFP-LC3* mouse.

4.2.2.5 miR-210 enhances mitochondrial copy number and reduces mitochondrial fission in CTs

Alternative ways of assessing mitophagy include measuring mitochondrial membrane potential, and fission as they are considered mitophagy triggers[557] (see Introduction 4.1.2.3), as well as measuring mitochondrial copy number[558–560]. Fluorescent cationic probes are commonly used to assess mitochondrial membrane potential and in this study, we used Mitotracker CMXRos. We found an increase in Mitotracker CMXRos retention in miR-210-transfected CTs in comparison to the negative miRNA groups (normoxia: control neg, 933 ± 202; control miR-210, 1,639 ± 91; $P < 0.01$; starved neg, 1,044 ± 81; starved miR-210, 1,943 ± 276; $P < 0.01$; hypoxia: control neg, 1,027 ± 103; control miR-210, 1,497 ± 80; $P > 0.05$; starved neg, 997 ± 213; starved miR-210, 1,709 ± 415; $P < 0.05$; n=3) and no significant change in response to serum starvation (figure 4.17). However, as the fluorescence intensity cannot be normalised to mitochondrial number, it is difficult to conclude that the increased intensity is due to increased membrane potential rather than increased mitochondrial number.

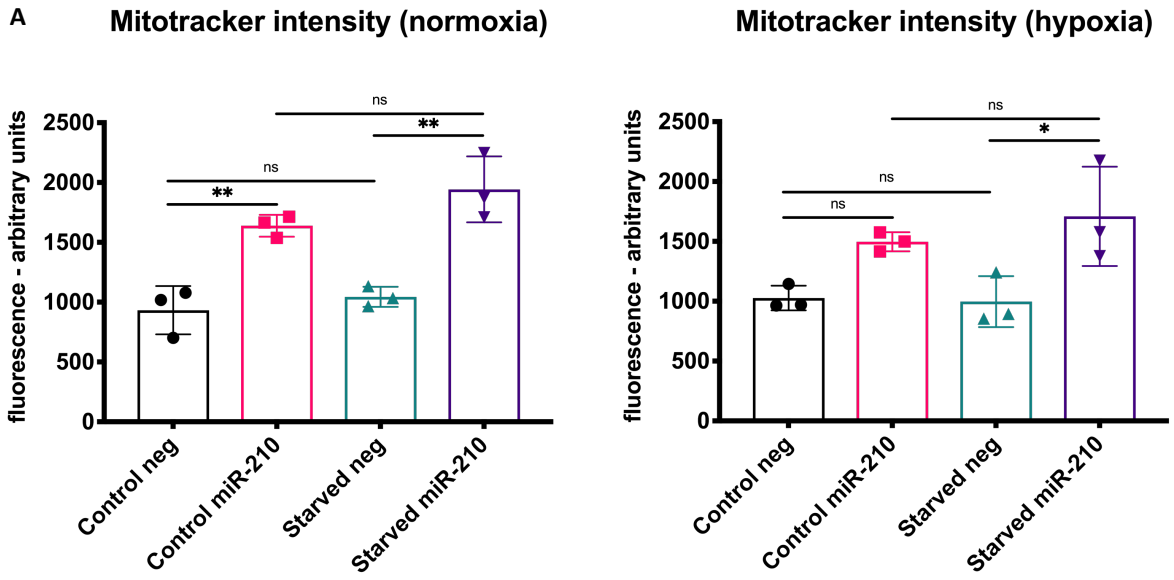
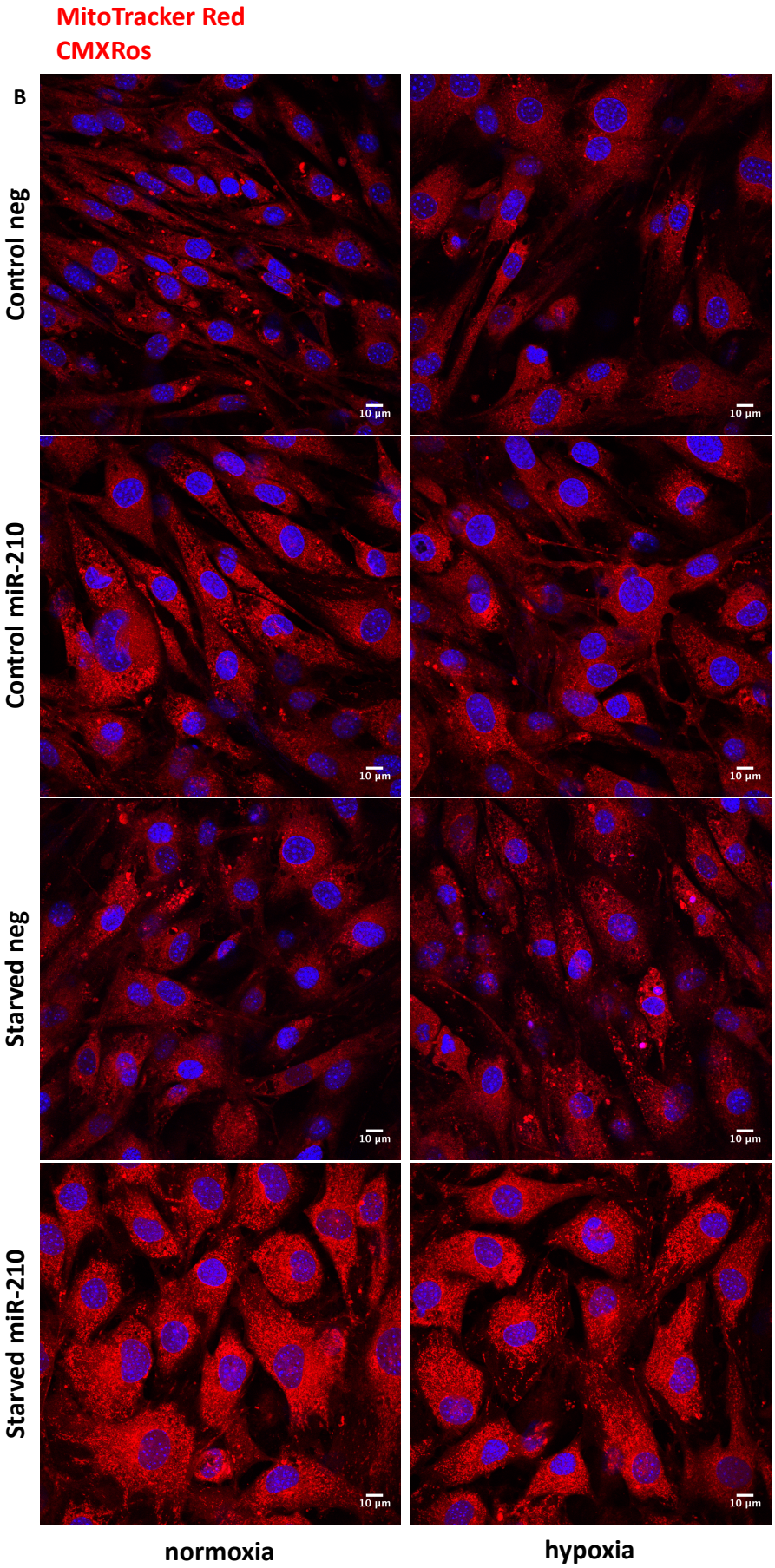


Figure 4.16 Mitotracker retention in miR-210-transfected CTs

(A) Quantification of the Mitotracker fluorescence intensity (described in Methods 2.12). Analysed using a one-way ANOVA with Tukey's multiple comparisons test to determine statistical significance (n=3). **(B)** Mitotracker staining of miR-210-transfected CTs, in comparison to CTs transfected with a negative miRNA, under the conditions shown: control media and normoxia, serum starvation and normoxia, control media and hypoxia, serum starvation and hypoxia. Cells were imaged using an FV1000 confocal microscope. Scale bar = 10μm.


MitoTracker Red
CMXRos
B
Control neg
Control miR-210
Starved neg
Starved miR-210
10 µm
normoxia
hypoxia

Mitochondrial copy number was also assessed by mitochondrial DNA/genomic DNA ratio qRT-PCR. We observed increased mitochondrial copy number in miR-210-transfected CTs in all conditions in comparison to their respective negative miRNA group (normoxia: control neg, 1.0 ± 0.09; control miR-210, 1.5 ± 0.18; $P < 0.05$; starved neg, 0.77 ± 0.15; starved miR-210, 1.3 ± 0.11; $P < 0.01$; hypoxia: control neg, 1.0 ± 0.22; control miR-210, 1.8 ± 0.08; $P < 0.001$; starved neg, 0.99 ± 0.09; starved miR-210, 1.6 ± 0.06; $P < 0.01$; n=3) (figure 4.18). No significant change was observed in mitochondrial copy number in response to serum starvation. Moreover, hypoxic culture significantly reduced mitochondrial copy number (control neg - normoxia, 1.0 ± 0.09; control neg - hypoxia, 0.65 ± 0.14; $P < 0.05$; n=3) but not Mitotracker CMXRos retention (control neg - normoxia, 933 ± 202; control neg - hypoxia, 1,027 ± 103; $P > 0.05$; n=3) (supplementary figure 2, appendix A).

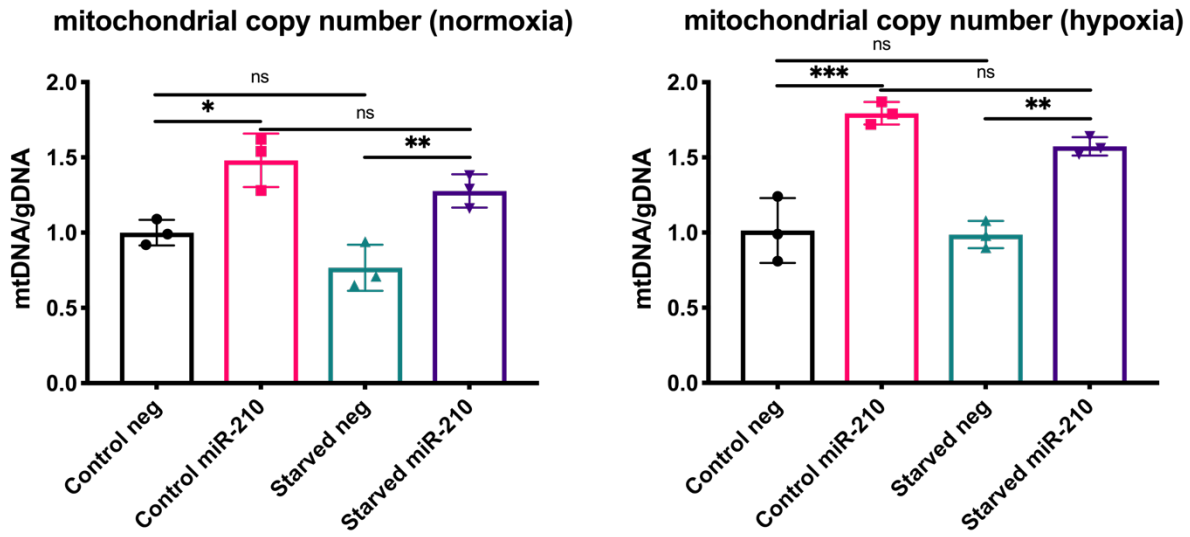


Figure 4.17 miR-210-transfected CTs show increased mitochondrial copy number

Mitochondrial copy number (mitochondrial DNA/ genomic DNA) in miR-210-transfected CTs, in comparison to CTs transfected with a negative miRNA, under the conditions shown: control media and normoxia, serum starvation and normoxia, control media and hypoxia, serum starvation and hypoxia. Analysed using a one-way ANOVA with Tukey's multiple comparisons test to determine statistical significance (n=3).

An increase in mitochondrial fission is favourable for mitophagy as it creates smaller-sized mitochondria, which can be more easily sequestered, whereas an increase in fusion hinders mitophagy[561]. We examined the mRNA levels of the fission factor *Drp1* in miR-210-overexpressing CTs. miR-210 decreased *Drp1* mRNA levels in some conditions indicating decreased mitochondrial fission (normoxia: control neg, 1.0 ± 0.31; control miR-210, 0.91 ± 0.22; $P > 0.05$; starved neg, 1.4 ± 0.10; starved miR-210, 0.88 ± 0.06; $P < 0.05$; hypoxia: control neg, 1.0 ± 0.07; control miR-210, 0.34 ± 0.05; $P < 0.05$; starved neg, 1.2 ± 0.23; starved miR-210, 1.1 ± 0.44; $P > 0.05$; n=3) (figure 4.19.A). A significant increase in *Drp1* levels in response to serum starvation in miR-210-transfected CTs cultured under hypoxia was observed. Unlike miR-210 overexpression, hypoxic culture did not significantly alter *Drp1* levels (control neg - normoxia, 1.0 ± 0.32; control neg - hypoxia, 1.0 ± 0.07; $P > 0.05$; n=3) (supplementary figure 1, appendix A). Figure 4.19.B shows representative images of *RFP-MIT;EGFP-LC3* MEFs displaying a fragmented mitochondrial phenotype in the negative miRNA group in comparison to miR-210-overexpressing CTs. Overall, these results are consistent with reduced mitophagy in response to miR-210 overexpression.

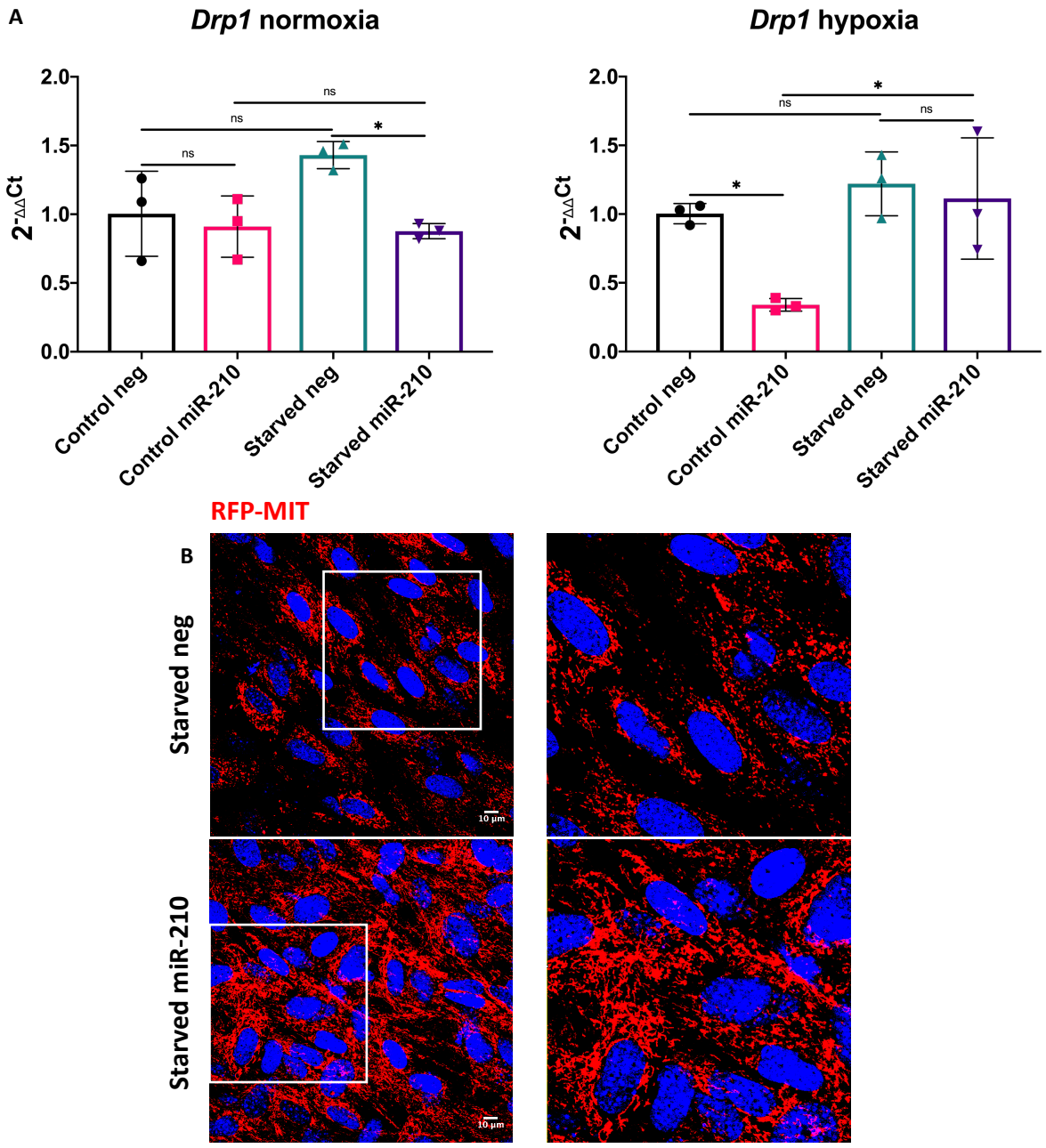


Figure 4.18 miR-210-transfected CTs show decreased mitochondrial fission

(A) *Drp1* mRNA levels in miR-210-transfected CTs, in comparison to CTs transfected with a negative miRNA, under the conditions shown: control media and normoxia, serum starvation and normoxia, control media and hypoxia, serum starvation and hypoxia. Analysed using a one-way ANOVA with Tukey's multiple comparisons test to determine statistical significance (n=3). **(B)** Imaging of mitochondrial networks in *RFP-MIT;EGFP-LC3* MEFs. Representative of n=3. Cells were imaged using an FV1000 confocal microscope. Scale bar = 10µm. High power inserts are shown by white boxes.

4.2.2.6 miR-210 increases glucose oxidation but not glycolysis in CTs

Mitophagy can act as a modulator of metabolism and cell fate[562]. Additionally, the degree of mitophagy has been shown to be dependent on the metabolic context[563]. We therefore examined the rates of glycolysis and glucose oxidation of miR-210-transfected CTs to examine if they are consistent with reduced mitophagy. As both of these measurements involved the use of radioactive material, they were performed in a radioactivity lab where only a normoxia incubator was available for use. Hence, the absence of data on CTs cultured under hypoxia. We found a significant increase in glucose oxidation rates in control miR-210-transfected CTs, measured in nMoles/ minute/ 10^5 cells, in comparison to their respective negative miRNA group, but not in starved conditions (control neg, 0.002 ± 0.001; control miR-210, 0.006 ± 0.004; $P < 0.05$; starved neg, 0.003 ± 0.001; starved miR-210, 0.004 ± 0.002; $P > 0.05$; n=6). No significant changes in glucose oxidation rates were observed in response to serum starvation. Moreover, no significant changes were detected in glycolytic rates (control neg, 0.11 ± 0.03; control miR-210, 0.13 ± 0.06; $P > 0.05$; starved neg, 0.07 ± 0.03; starved miR-210, 0.10 ± 0.04; $P > 0.05$; n=3) (figure 4.20).

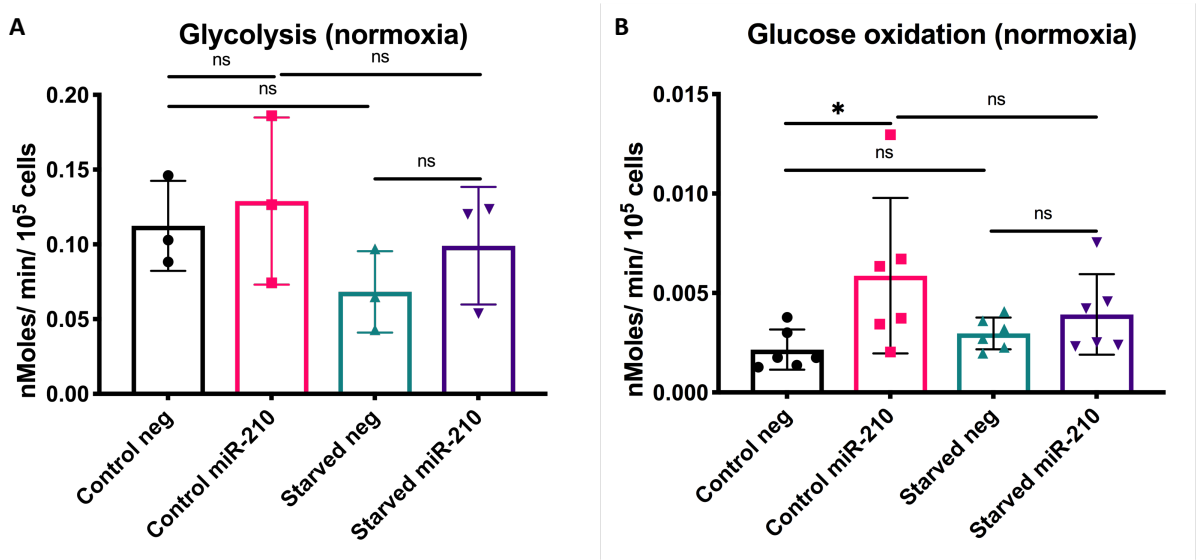


Figure 4.19 The effect of miR-210 on the metabolic profile of CTs

(A) Glycolytic (n=3) and **(C)** Glucose oxidation (n=6) rates measured as nMoles/ min/ 10^5 cells in miR-210-transfected CTs, in comparison to CTs transfected with a negative miRNA, under the conditions shown: control media and serum starvation. Analysed using a one-way ANOVA with Tukey's multiple comparisons test to determine statistical significance.

4.2.2.7 miR-210 and hypoxia

Although miR-210 is regarded as a hypoxamiR that is capable of upregulating HIF1α via targeting *Gpd1l*, our results indicated that unlike HIF1α, miR-210 may have a role in reducing mitophagy and enhancing oxidative metabolism. This warranted us to further explore the relationship between miR-210 and HIF1α by assessing the effect of miR-210 on the mRNA levels of the known HIF1α target pyruvate dehydrogenase kinase 1 (*Pdk1*)[564,565] as well as targets by which miR-210 has been shown to induce hypoxic adaptations. For example, research by the Harris lab showed that miR-210 targeted *Iscu*, which encodes the mitochondrial iron sulphur scaffold protein, to induce a glycolytic shift in human cancer cell lines[566]. Moreover, as we were not successful in directly quantifying the levels of HIF1α, we examined the mRNA levels of its stability regulators *Phd1* and *Phd3*.

We found that *Iscu1* was significantly downregulated in miR-210-overexpressing CTs in comparison to their respective negative miRNA group under all conditions (normoxia: control neg, 1.0 ± 0.12; control miR-210, 0.61 ± 0.08; $P < 0.01$; starved neg, 1.4 ± 0.05; starved miR-210, 0.94 ± 0.12; $P < 0.01$; hypoxia: control neg, 1.0 ± 0.24; control miR-210, 0.57 ± 0.04; $P < 0.05$; starved neg, 2.1 ± 0.18; starved miR-210, 1.2 ± 0.15; $P < 0.001$; n=3). *Iscu2* was downregulated in miR-210-overexpressing CTs in comparison to their respective negative miRNA group in starved hypoxic conditions (normoxia: control neg, 1.0 ± 0.13; control miR-210, 0.65 ± 0.14; $P > 0.05$; starved neg, 1.5 ± 0.16; starved miR-210, 1.2 ± 0.16; $P > 0.05$; hypoxia: control neg, 1.0 ± 0.33; control miR-210, 1.1 ± 0.52; $P > 0.05$; starved neg, 3.2 ± 0.51; starved miR-210, 1.9 ± 0.35; $P < 0.05$; n=3). Moreover, we observed an increase in *Iscu1* and *Iscu2* mRNA levels in almost all conditions in response to serum starvation (figure 4.21.A-B). Similar to miR-210 overexpression, hypoxic culture significantly decreased *Iscu1* (control neg - normoxia, 1.0 ± 0.12; control neg - hypoxia, 0.55 ± 0.13; $P < 0.05$; n=3) and *Iscu2* levels

(control neg - normoxia, 1.0 ± 0.13; control neg - hypoxia, 0.48 ± 0.15; $P < 0.01$; n=3) (supplementary figure 1, appendix A).

Pdk1 (hypoxia: control neg, 1.0 ± 0.15; control miR-210, 0.24 ± 0.14; $P > 0.001$; n=3), *Phd1* (normoxia: control neg, 1.0 ± 0.03; control miR-210, 0.76 ± 0.17; $P < 0.05$; n=3) and *Phd3* (normoxia: starved neg, 1.9 ± 0.13; starved miR-210, 1.5 ± 0.18; $P < 0.05$; n=3) were downregulated in miR-210-overexpressing CTs in comparison to their respective negative miRNA group in some conditions. Moreover, we observed an increase in *Pdk1* and *Phd3*, but not *Phd1*, mRNA levels in some conditions in response to serum starvation (figure 4.21.C-E). Unlike miR-210 overexpression, hypoxic culture significantly increased *Pdk1* (control neg - normoxia, 1.1 ± 0.63; control neg - hypoxia, 6.2 ± 0.89; $P < 0.01$; n=3)and *Phd3* levels (control neg - normoxia, 1.0 ± 0.03; control neg - hypoxia, 3.1 ± 0.98; $P < 0.05$; n=3) (supplementary figure 1, appendix A).

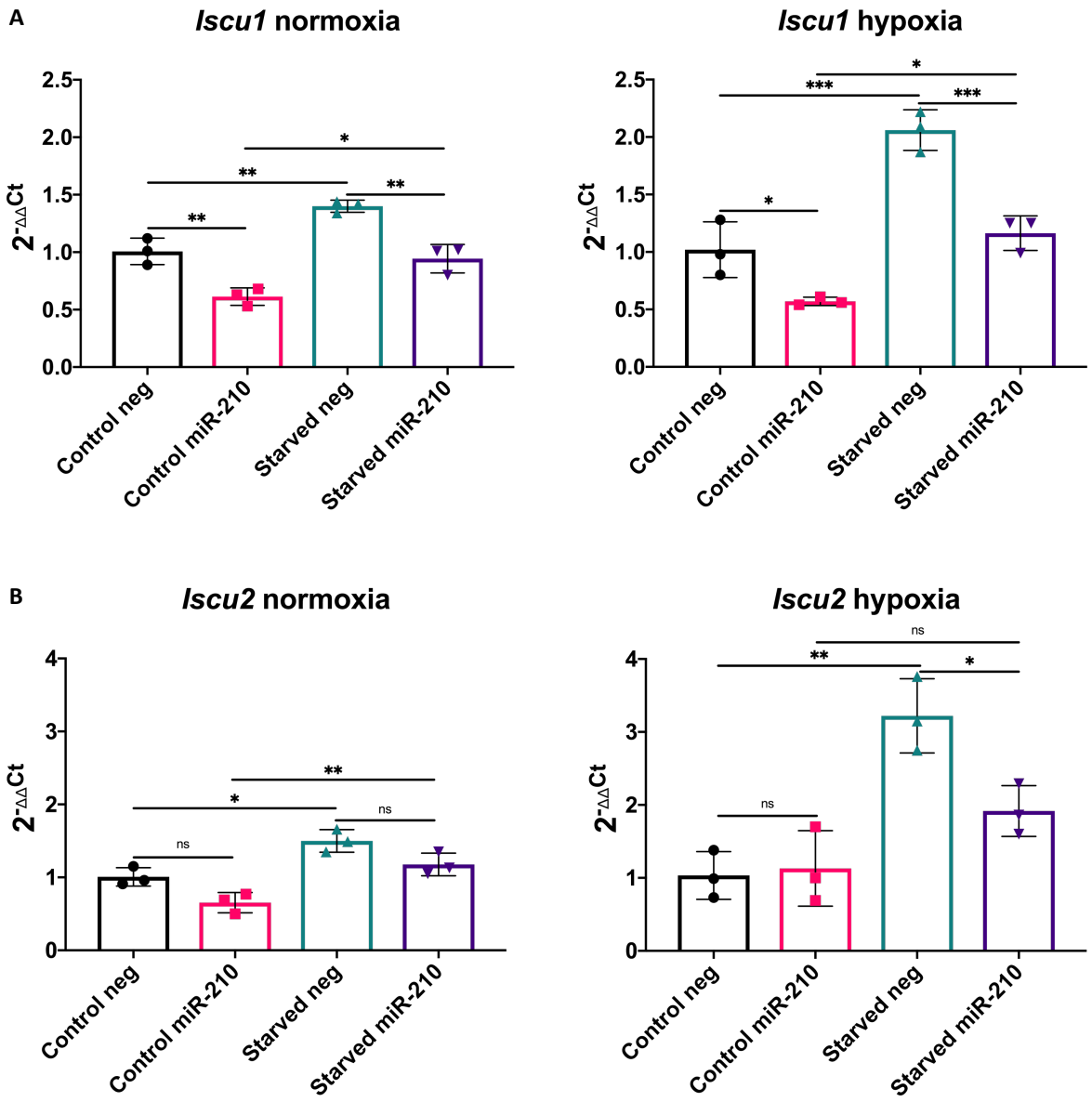
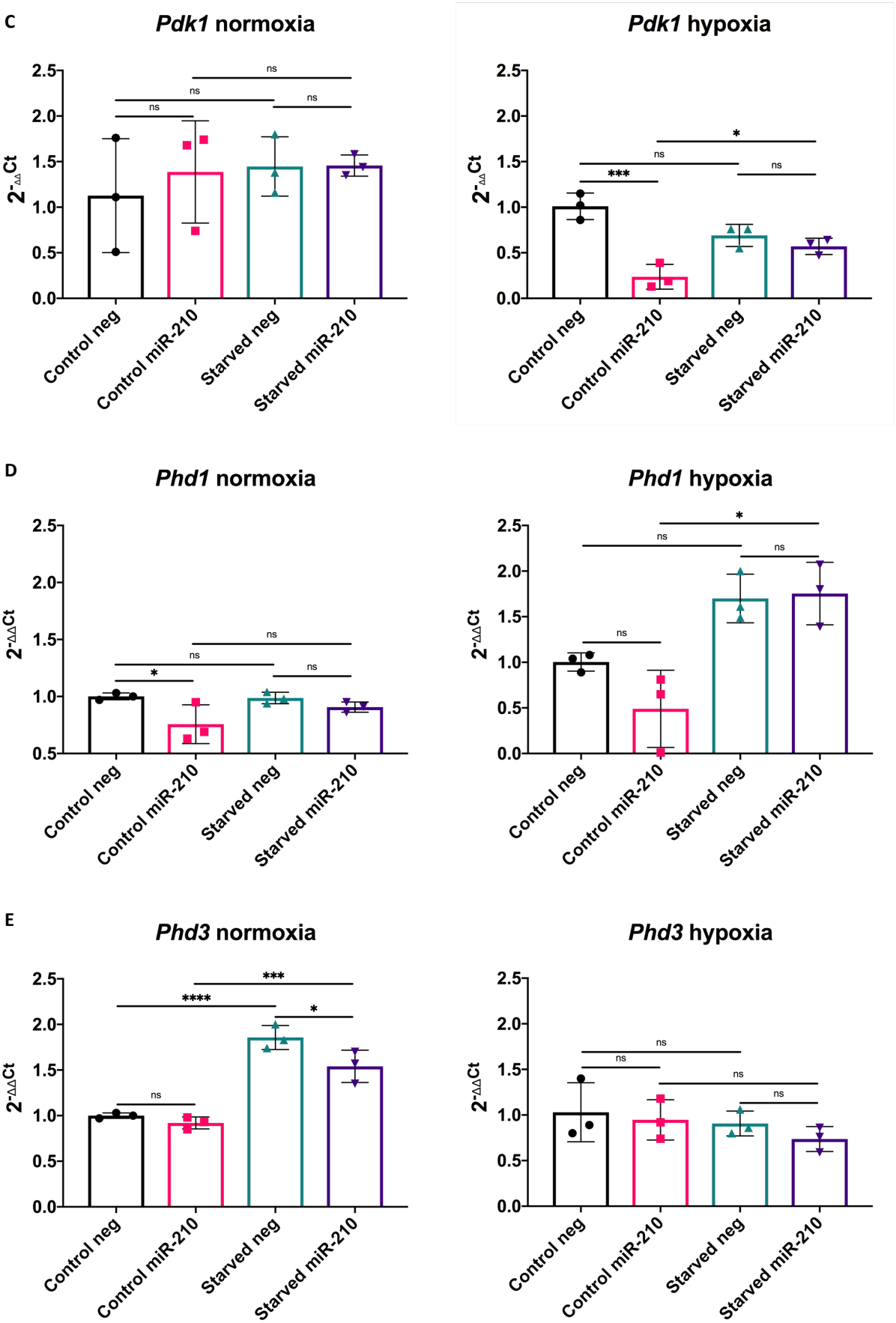


Figure 4.20 mRNA levels of hypoxia-associated genes in miR-210-transfected CTs

(A) *Iscu1*, **(B)** *Iscu2*, **(C)** *Pdk1*, **(D)** *Phd1*, **(E)** *Phd3* mRNA levels in miR-210-transfected CTs, in comparison to CTs transfected with a negative miRNA, under the conditions shown: control media and normoxia, serum starvation and normoxia, control media and hypoxia, serum starvation and hypoxia. Analysed using a one-way ANOVA with Tukey's multiple comparisons test to determine statistical significance (n=3).


C
Pdk1 normoxia
Pdk1 hypoxia
D
Phd1 normoxia
Phd1 hypoxia
E
Phd3 normoxia
Phd3 hypoxia
2-ΔΔCt
Control neg
Control miR-210
Starved neg
Starved miR-210
ns
*
***
****

4.3 Discussion

4.3.1 Optimisation of miR-210 delivery into CTs

We attempted to optimise miR-210 delivery into CTs using NP170s which have been shown to efficiently release complexed miRNAs in comparison to commercial transfection reagent in mouse endothelial cells and using retroviral transduction that would produce a stable overexpression of the miRNA. To test the NP170s, I repeated the same experiment performed by S. Malandraki-Miller (thesis) and found similar results where no significant difference in CT cell numbers was observed between the different miRNA conditions with the NP170 method, whereas the DharmaFECT method showed significantly higher cell numbers in miR-210-transfected CTs compared to the negative miRNA, following serum starvation. These NP170s are sent from our collaborators' lab in Portugal so this may be due to suboptimal storage or shipping conditions that affected the ability of NP170s to bind miRNAs. Moreover, the efficiency of NP-mediated delivery of miRNAs can be affected by the physicochemical properties of the NP, such as size, shape, and surface chemistry, in addition to cell type. Studies have shown that different cell types have a differential internalisation efficiency to NPs with different diameters[567]. However, S. Malandraki-Miller (thesis) showed that the NP170s were successfully internalised using flow cytometry. This successful internalisation of NP170s was also reported in our previous study in both CTs and CDCs[568]. Therefore, it seems that the internalisation itself was not compromised, but the conjugation of the NP170s with the miRNA. Moreover, we performed retroviral transduction using a miR-210 vector that contains a puromycin resistance gene. We observed successful transduction of the cells as shown after puromycin treatment, but no upregulation in miR-210 levels. This may be due to the selection of a colony that contained an incorrect or truncated DNA insert which can occur due to unstable DNA or DNA mutations that may have occurred during plasmid propagation in the transformed bacteria (ThermoFisher). Although we verified the size of the plasmid in our selected colony

by restriction digestion and gel electrophoresis, the gold standard is sequencing. This was not followed up as I was performing this experiment under the supervision of Dr. Tara Caffrey in the Wade-Martins lab who then left the group.

miR-210 transfection using the DharmaFECT reagent was successful as observed using qRT-PCR. We found that miR-210 transcript levels significantly dropped 24 hours post transfection. This was not observed by imaging a Dy547-labelled negative miRNA which showed us that miRNAs can remain upregulated for 3 days post transfection using the DharmaFECT reagent. However, the qRT-PCR results are more specific to miR-210. How long a miRNA may stay upregulated in the cell may be influenced by regulatory loops which can also be formed by their own targets[569,570].

4.3.2 miR-210 inhibits apoptotic cell death

The anti-apoptotic role of miR-210 in CTs was confirmed by assessing *Casp8ap2* expression, caspase activation and DNA fragmentation. We found that serum-starved CTs showed significantly decreased *Casp8ap2* mRNA levels, poly-caspase activity and DNA fragmentation when transfected with miR-210 in comparison to the negative miRNA indicating reduced apoptosis and superior survival potential. Both caspase activity and DNA fragmentation assays have been used widely to assess cell apoptosis, where the latter marks a later phase in the apoptotic process. Recent studies have uncovered nonapoptotic roles for caspases in fundamental cellular functions including cell proliferation, fate specification, metabolism and immune regulation[571–573]. Thus, it may be argued that examining caspase expression alone is not sufficient as an indicator of apoptosis.

Although a pro-apoptotic role for miR-210 via ROS induction has been described[574], miR-210 has been shown to inhibit apoptotic cell death by targeting *Casp8ap2*[249], *Ptp1b* and *Dapk1*[243]. Moreover, miR-210 promoted cardiomyocyte proliferation and inhibited apoptosis by targeting *Apc*, which encodes a cell cycle inhibitor[575]. miR-210 has also been shown to be enriched in

exosomes secreted by CDCs and that these exosomes have a cytoprotective role[178]. Moreover, miR-210 is upregulated in KIT^+ cell-derived exosomes subjected to hypoxia. These hypoxic exosomes improved cardiac function in a rat model of cardiac injury[576]. Contradictory roles of miRNAs have been described in the literature[577–580]. This may be attributed to the cell type and its gene expression profile and cellular microenvironment. It may also be a result of regulatory loops by the miRNA's own targets as a miRNA and its targets can form both feedback and feedforward loops[569,570]. Moreover, the ability to have multiple targets in various pathways is a miRNA characteristic, which may give them the potential to conduct different regulatory effects. In this study, we showed that miR-210 has an anti-apoptotic effect in CTs *in vitro*.

4.3.3 miR-210 has a role in the regulation of mitochondrial fission and autophagy in CTs

Due to the implication of miR-210 as an hypoxia miRNA, we examined its potential role in mitophagy under both normoxia and hypoxia and/or serum starvation. Table 4.1. provides a summary of the different parameters measured in response to miR-210 transfection, hypoxic culture and/or serum starvation.

We had initially hypothesised that miR-210 may have a role in inducing BNIP3-dependent mitophagy for cytoprotection, as observed with HIF1α which induces mitophagy as an adaptive metabolic response to hypoxia[547]. Indeed, we found that hypoxic culture induced an upregulation in the mRNA levels of *Bnip3*, *Nix* and *Atg4c* in CTs suggesting enhanced mitophagy. We also found that miR-210-transfected CTs displayed reduced *Gpd1l* mRNA levels, which has been shown to be a target of miR-210 that is capable of upregulating HIF1α downstream of miR-210[548,549,581]. Consistent with that, a reduction in *Gpd1l* mRNA levels was observed in CTs cultured under hypoxia. However, when we attempted to assess whether the cytoprotective role of miR-210 was partly through BNIP3-dependent mitophagy, we found that *Bnip3* knockdown by siRNA did not decrease miR-210's capacity to target apoptosis. Moreover, miR-210 did not significantly alter *Bnip3* mRNA levels but downregulated *Nix*

levels in CTs cultured in control conditions under hypoxia in comparison to their respective negative miRNA group. This suggested that, unlike hypoxia, miR-210 did not induce BNIP3-dependent mitophagy as an anti-apoptotic mechanism but may have downregulated mitophagy, as suggested by the decreased *Nix* levels following miR-210 transfection.

The potential downregulation of mitophagy by miR-210 in CTs was therefore followed up. We found that miR-210 overexpression in CTs significantly downregulated *Atg4c* and *Pink1* mRNA levels under some conditions suggesting reduced mitophagy. We attempted to corroborate these results by imaging the co-localisation of mitochondria with autophagosomal puncta as a measure of mitophagy. However, no LC3-II puncta were detected following serum starvation in MEFs isolated from *RFP-MIT;EGFP-LC3* transgenic mice. Moreover, no LC3-II puncta were detected even following a 24-hour treatment with the potent mitophagy inducer CCCP which has been shown to trigger complete conversion of LC3 from its cytosolic form LC3-I to its autophagy-related form LC3-II[582]. It may be argued that this is due to the utilisation of LC3-independent pathways of mitophagy, as these have been described in the literature where LC3 family members were shown to be nonessential for both PINK1-mediated mitophagy and macroautophagy[582–584]. A study has revealed a requirement for the GABARAP family in macroautophagy in hepatocytes and prostate cancer cells, whereas the LC3 family was dispensable for this process[585]. Therefore, recent studies have suggested that LC3 may have limited value as a marker of autophagy[586]. It remains to be determined how the roles orchestrated by LC3 and GABARAP families may differ depending on cell type and context[585]. Unfortunately, there is still no gold standard assay of autophagic processes. However, various assays and tools have been developed and using a combination of these tools can be sufficient to draw conclusions about the activation of autophagic processes. In the context of mitophagy, quantification assays include measuring mitochondrial membrane potential, and fission as they are considered mitophagy triggers[557], as well as measuring mitochondrial copy number[558–560].

In this study, we found that miR-210-transfected CTs displayed an upregulation in mitochondrial copy number regardless of the tested oxygen levels in culture and whether or not the CTs were cultured in control media or subjected to serum starvation. This was also true with MitoTracker Red CMXRos retention as a significant upregulation in fluorescent intensity was observed in miR-210-transfected CTs under almost all conditions, with the exception of control hypoxic conditions. Alternatively, CTs showed reduced mitochondrial copy number following hypoxic culture. Moreover, we observed a decrease in the mRNA levels of the fission factor *Drp1* in miR-210-transfected CTs under some conditions indicating reduced mitochondrial fission. This is in agreement with reduced mitophagy as fission creates smaller-sized mitochondria that can be more easily engulphed by the autophagy machinery[561].

Overall, our findings support a role for miR-210 in downregulating mitophagy. It may be argued that this is inconsistent with miR-210 being an hypoxia miRNA as the opposite effect is observed in hypoxia[547]. Indeed, this is what we had hypothesised at the beginning of the study. Although it has been shown that *Bnip3* is a direct target of miR-210 using luciferase reporter assays[587,588], which was in the context of a pro-apoptotic role for BNIP3 rather than its role in mitophagy, we did not observe a significant effect on *Bnip3* expression. This may be due to the experiment being underpowered.

A role for miR-210 in mitophagy has not been previously explored. However, our results showing decreased *Nix*, *Pink1*, and *Drp1* levels, and upregulated mitochondrial copy number and MitoTracker Red CMXRos retention in miR-210-transfected CTs support a role for miR-210 in mitophagy. A recent study in endothelial progenitor cells revealed that transfecting the progenitors with miR-210 enriched for miR-210 in their secreted exosomes[589]. Treatment of endothelial cells subjected to I/R injury using these exosomes increased ATP levels and mitochondrial membrane potential, as well as decreased mitochondrial fission[589]. This raises the question of whether mitophagy is a direct or indirect target of miR-210. A study reported

that fibroblasts lacking caspases 3 and 7 are resistant to loss in mitochondrial membrane potential[590]. Therefore, it can be argued that miR-210-induced caspase inhibition may be upstream of mitochondrial events. However, the downregulation of mitophagy in miR-210-transfected CTs is not confined to conditions of serum starvation where caspase activation is higher than control conditions.

Mitophagy has been classically viewed as a mitochondrial quality control mechanism but multiple reasons for mitochondrial elimination have been described. This is supported by observations ranging from programmed forms of mitophagy to basal mitophagy in different tissues demonstrating the complex and multi-factorial nature of mitophagy[591]. The existence of basal mitophagy may be regarded as a housekeeping mechanism but the levels of basal activation are heterogenous across tissues, and across different cells within the same tissue, highlighting context-dependant regulation that is yet unknown[592]. Indeed, it has been shown that levels of basal mitophagy depend on the metabolic context of the cell where greater levels are observed in highly metabolic cells such as cardiomyocytes and dopaminergic neurons[592]. Therefore, the observed downregulation in mitophagy is not necessarily linked to the pro-survival role that miR-210 played in CTs.

Moreover, programmed mitophagy describes instances where mitochondria are eliminated for developmental, physiological or metabolic purposes[593]. Cell fate determination and differentiation often involve metabolic reprogramming that implicate mitophagy. Cardiomyocyte maturation in the perinatal heart involves a switch in mitochondrial substrate preference from carbohydrates to fatty acids. Mitophagy is essential for the replacement of immature mitochondria by mature adult mitochondria that undergo fatty acid-driven metabolism[594]. A similar requirement for mitophagy is also observed in the reprogramming of somatic cells into pluripotent stem cells which are highly glycolytic[595–597]. In this study, we observed an increase in glucose oxidation in miR-210-transfected CTs cultured in control

conditions under normoxia concordant with reduced mitophagy. These results, in addition to the previous data, further support the notion that the observed downregulation in mitophagy is not necessarily linked to the pro-survival role of miR-210 and may be a distinct function to induce a metabolic switch.

It may be argued that the observed downregulation of mitophagy in miR-210-transfected CTs may be a reflection of a downregulation in macroautophagy in general as miR-210 has been shown to target macroautophagy. Indeed, *Atg7* and *Vmp1*, which encodes a critical transmembrane protein for phagophore formation, have been shown to be direct targets of miR-210[554,598], although we observed no significant change in *Atg7* expression. However, evidence of distinct regulation has been described between mitophagy and other forms of autophagy triggered under stress. For example, yeast are capable of blocking mitophagy even under severe starvation conditions, but not macroautophagy, if the carbon source makes mitochondrial metabolism essential[599].

It remains unclear why an hypoxia-inducible miRNA would upregulate mitochondrial networks. This is because the lack of oxygen would result in inefficient mitochondrial respiration stimulating a HIF1α-induced metabolic switch to upregulate glycolysis and mitophagy[547,591]. Studies have reported that miR-210 has a negative effect on mitochondrial respiration with direct targets including *Iscu1/2* (encoding iron-sulphur cluster assembly enzyme) and *Cox10* (encoding cytochrome c oxidase assembly protein), which are important factors of the mitochondria electron transport chain[255,548,600,601]. Indeed, we found a downregulation in *Iscu1/2* mRNA levels in miR-210-transfected CTs, similar to the downregulation observed in CTs cultured under hypoxia. However, to further elucidate the relationship between miR-210 and hypoxia, we examined *Pdk1* and *Phd1/3* and found opposing effects of miR-210 transfection and hypoxic culture on their mRNA levels. PHDs are oxygen sensors that use oxygen as a co-substrate to induce the hydroxylation of HIF1α and

subsequent polyubiquitination and proteasomal degradation[602]. Hypoxia, in turn, induces PHDs. This feedback loop leading to PHD accumulation has been explained as a mechanism to allow for rapid HIF1α degradation upon reoxygenation[603,604]. Moreover, HIF1α upregulates PDK1 to inactivate pyruvate dehydrogenase, thereby blocking the entry of pyruvate into the mitochondria for oxidative phosphorylation[605].

There is a possibility that miR-210 may function differently in oxygen levels lower than the one we used, which was 2%. However, 2% oxygen was sufficient to induce mitophagy according to both our qRT-PCR and mitochondrial copy number data. Moreover, the studies describing a negative effect of miR-210 on mitochondrial respiration were performed in normoxia further confirming that our observations were not due to not because oxygen levels were too high. In addition, lethal forms of mitophagy have been described. For example, ceramide mediates caspase-independent cell death via excessive activation of mitophagy[606]. Therefore, miR-210 may be downregulating mitophagy to protect against lethality of excessive mitophagy that may occur in hypoxic environments. Overall, our results suggest that the relationship between miR-210, HIF1α and hypoxia is not as straightforward as once thought and is an important topic to be investigated in future studies.

Furthermore, our data revealed an increase in the mRNA levels of *Pink1*, *Atg4c* and *Drp1* in serum starved CTs in comparison to their corresponding controls, which may be an indication of increased mitophagy. However, no significant changes were observed in MitoTracker Red CMXRos retention or mitochondrial copy number in response to serum starvation. This may be due to the experiment being underpowered as by performing t-tests a significant decrease in mitochondrial copy number can be observed in some conditions. In addition, ATG4c has another role that may be induced following starvation, which is macroautophagy. This may explain why only very small changes were observed in mitochondrial copy number as the mRNA changes may not be solely indicative of mitophagy. Interestingly, *Nix* mRNA levels

were increased in response to serum starvation under normoxia, but both *Nix* and *Bnip3* expression showed an opposite direction of change following serum starvation under hypoxia. BNIP3 and NIX share high sequence similarity and identical functionality has been described. They are therefore expected to follow the same pattern. Both genes are induced by HIF1α[350,517] but their expression needs to be tightly regulated as over expression induces cell death[607]. Hypoxic culture increased *Bnip3* and *Nix* mRNA levels and also showed a cytoprotective role in CTs. Therefore, the opposite direction of change in *Bnip3* and *Nix* mRNA levels following serum starvation under hypoxia in comparison to normoxia may be a mechanism by which hypoxia fine-tunes their levels to protect against cell death.

Other changes observed as a result of serum starvation include a consistent increase in *Gpd1l*, and *Iscu1/2* mRNA levels; and an increase in *Pdk1*, *Phd1* and *Phd3* in some conditions. These observed changes in response to serum starvation are contradictory as both components involved in inducing an hypoxic phenotype (*Pdk1*) and others involved in inducing oxidative metabolism (*Gpd1l*, *Iscu1/2*) are upregulated. Moreover, the upregulation in *Phd1/3* mRNA levels following serum starvation is similar to that observed following hypoxic culture. These changes do not appear to be differentially modulated in different conditions (i.e. neg- vs. miR-210-transfected CTs or CTs under normoxia vs. hypoxia). It is unclear why all of these components would be upregulated following serum starvation, although this may explain why no significant changes were observed in the metabolic rates of CTs following serum starvation. It has been previously shown that serum starvation alone induces mitochondrial fission[608], whereas eliminating glutamine or amino acids induces mitochondrial fusion suggesting that starvation conditions can differentially affect mitochondrial fission and fusion[524]. Moreover, human fibroblasts subjected to serum starvation showed a continuous decrease in cellular ATP levels[609]. Serum starvation has been shown to induce HIF1α as a pro-survival factor, even in normoxic cells[610,611]. All of these reports are consistent with enhanced mitophagy and increased

Pdk1 and *Phd1/3* mRNA levels, but contradict the increase observed in *Gpd1l* and *Iscu1/2* mRNA levels. Therefore, it is unclear how serum starvation may have affected the mitochondrial dynamics of CTs. The contradictory effects of serum starvation may explain why the effects of miR-210 transfection were more apparent in control conditions as opposed to starved conditions.

Overall, our results demonstrated a pro-survival role for miR-210 in CTs by showing that it downregulated apoptosis following serum starvation. Our results also indicated a role for miR-210 in downregulating mitophagy, which is contrary to hypoxia. There is no conclusive evidence to suggest that the observed downregulation in mitophagy is linked to the pro-survival role of miR-210 and whether mitophagy is a direct target of miR-210. The observed downregulation in mitophagy may be a mechanism by which miR-210 induces a metabolic shift. Whether or not the induced upregulation in mitochondrial dynamics by miR-210 is beneficial to the survival potential of transplanted CTs in ischaemic heart tissue may be revealed by *in vivo* cell survival and retention studies. miR-210-transfected MSCs showed enhanced engraftment at four days after transplantation in infarcted rat hearts[612]. However, examining mitophagy in miR-210-transfected cells following transplanting is required to assess if the same downregulatory effect is retained *in vivo*. Moreover, we found that miR-210 downregulated its known direct targets, *Gpd1l* and *Iscu1/2*, which are also downregulated in hypoxia. This may be an indication of the capability of miRNAs to conduct different regulatory functions due to their ability to have multiple targets in various pathways. As discussed earlier, this is similar to the reports of miR-210 being able to induce cell death despite having direct pro-apoptotic targets. Our findings therefore highlight that the relationship between miR-210, HIF1α and hypoxia is not as straightforward as once thought and warrant further investigation. Moreover, contradictory effects of serum starvation were observed in CTs. Although we found some changes that are consistent with other studies showing a shift towards an hypoxic

phenotype following serum starvation, contradictory effects on *Gpd1l* and *Iscu1/2* mRNA levels were also observed. It therefore remains ambiguous how serum starvation may have affected the mitochondrial dynamics of CTs.

Table 4.1 Summary of the different parameters measured in response to miR-210 transfection, hypoxic culture and/or serum starvation

Green represents changes in response to hypoxia or serum starvation that are in agreement with miR-210 transfection. Yellow represents the opposite. Red shows the differential effect of serum starvation on the mRNA levels of Nix under hypoxia in comparison to normoxia.

miR-210	-	-	-	+	+	+	+	**Notes**
Hypoxia	+	-	+	-	+	-	+	
Serum starvation	-	+	+	-	-	+	+	
Gpd1l	down	up	up	down	down	down	down	GPD1L increases proline hydroxylation of HIF1α
Bnip3	up	ns	down	ns	ns	ns	ns	*Bnip3* knockdown does not change miR-210's protective effect
Nix	up	up	down	ns	down	ns	ns	Mitophagy associated
Atg4c	up	up	up	ns	down	ns	down	Mitophagy associated
Pink1	ns	up	up	down	down	ns	down	Mitophagy associated
Mitotracker	ns	ns	ns	up	up	up	up	
Mitochondrial copy number	up	ns	ns	up	up	up	up	Decreased mitophagy associated with increased mitochondrial copy number
Drp1	ns	ns	ns	ns	down	down		Up in response to serum starvation in other conditions
Glycolysis	?	ns	?	ns	?	ns	?	
Glucose oxidation	?	ns	?	up	?	ns	?	
Iscu1	down	up	up	down	down	down	down	
Iscu2	down	up	up	ns	ns	ns	down	
Pdk1	up	ns	ns	ns	down	ns	ns	Up in response to serum starvation in other conditions
Phd1	ns	ns	ns	down	ns	ns	ns	Up in response to serum starvation in other conditions
Phd3	up	up	ns	ns	ns	down	ns	

CHAPTER 5

The effect of miR-210 overexpression on CT gene expression profile, paracrine potential and in vivo retention in an MI model

5 Results chapter 3

5.1 Introduction

5.1.1 Harnessing advances in the field of microRNA therapeutics for cell therapy

Clinical trials using different types of CPCs or cardiac stromal cells have demonstrated safety but limited efficacy. This has been attributed to low cell survival and retention, failure to differentiate into cardiomyocytes, or perhaps a suboptimal cell type. Following MI, harsh events such as ischaemia, oxidative stress, and increased inflammation limit the survival and engraftment of transplanted cells with studies reporting massive cell loss. Consequently, pro-survival strategies have been proposed to enhance the therapeutic potential of transplanted cells (see Introduction 1.5). Although CPCs display a lack of direct differentiation *in vivo*, the therapeutic effect of their paracrine signalling has been established. Therefore, enhancing the survival of the cells may provide a mechanism by which this window of beneficial paracrine signalling may be prolonged.

Due to the relative ease of the manufacture of miRNA mimics and overexpressing miRNAs in cells, miRNAs provide an attractive approach in cell therapy. Another unique advantage to miRNAs is their capability to target multiple components that often work in concert within a particular pathway. This allows the modulation of a phenotype using a single miRNA sequence[206,613]. For example, miR-497 has been shown to inhibit angiogenesis by targeting *Kdr*, *Vegf-a*, and *Aeg-1*[614,615]. Moreover, miRNAs have been used to enhance the survival and paracrine potential of transplanted cells in ischaemic tissue. In a model of hindlimb ischaemia, a previous PhD student in collaboration with the Carr group revealed that overexpressing miR-132 in endothelial cells augmented their survival and pro-angiogenic activity, thereby reducing tissue damage and enhancing blood perfusion[205]. Moreover, transducing $SCA1^{+}$ cardiac cells

with a pro-survival cocktail consisting of miR-21, miR-24, and miR-221 significantly improved cell retention and functional recovery in a mouse model of MI[242].

In studying miRNAs as a conditioning agent for cell therapy, one must consider their possible effect on the gene expression profile of the cells in question. Indeed, miRNAs have been implicated in cell fate determination, differentiation, and stem cell renewal[616,617]. A number of miRNAs have been shown to regulate TGFβ signalling-mediated fibrosis[618]. In addition, miRNAs can promote differentiation by inactivating transcriptional repressors and cell cycle regulators[617,619]. Therefore, miRNA overexpression may alter the phenotype of the cells which may be favourable in some cases, e.g. inducing pluripotent stem cells into a cardiac lineage, or may have a detrimental effect, e.g. inducing fibroblasts into the myofibroblast lineage.

5.1.2 Mouse heart LAD ligation as an MI model

Permanent ligation of the LAD coronary artery has been extensively used to replicate MI in animal models. Artificial occlusion of the LAD artery leads to ischaemia in a portion of the myocardium and subsequent cell death and scar formation, hence recapitulating MI events. In the mouse, variability of coronary artery anatomy and extent of collaterals can lead to variability in infarct size when using this technique[620]. This can result in the requirement of large animal numbers in MI studies. Another method of inducing an MI is cryoinjury where a cryoprobe cooled by liquid nitrogen is applied to the surface of the heart. This technique allows larger consistency in infarct size and location. In addition, the extent to which the infarct is transmural may be controlled by the duration of cryoprobe application[56]. However, it can be argued that cryoinjury is less physiologically relevant in comparison to LAD ligation. For example, it has been suggested that a diffuse border zone is formed following LAD ligation, similar to that seen in the clinical situation, whereas a more defined border is formed in a cryoinjury model[621]. Unlike LAD ligation, cryoinjury does not induce ischaemia and cell death is probably caused by ice crystal formation[621]. Moreover, LAD ligation has been used more

widely as a model of MI which provides the advantage of allowing the study to be more comparable to a greater number of published studies in the field. Temporary LAD ligation to allow reperfusion would be more representative of the clinical situation, in comparison to permanent ligation, as treatment of MI involves rapid reperfusion of the occluded vessel to restore blood perfusion. However, reperfusion in the mouse heart is technically challenging and requires an experienced surgeon to prevent additional unwanted trauma. We therefore adopted the permanent LAD ligation method.

A key consideration to make in MI studies is the method by which the presence of cardiac injury and its extent can be evaluated. Biomarkers such as cardiac troponins and creatine kinase have been used as an indication of injury[622]. Moreover, determining the degree of fibrosis by histology is one of the main methods by which the extent of the injury may be assessed. This can be achieved using dyes such as picrosirius red staining and wheat germ agglutinin which allow visualisation of collagen in tissue sections[623,624]. Echocardiography and MRI are forms of cardiac imaging that represent non-invasive methods to assess cardiac function. Although MRI is more expensive, it is more accurate and reproducible, and can be combined with late-gadolinium enhancement to highlight dead and fibrotic tissue, making it the gold standard for both clinical and rodent studies.

5.1.3 Aims

In this chapter, the aim was to explore how miR-210 may affect the gene expression and paracrine profile of CTs and if miR-210 would enhance the retention of CTs upon transplantation into a mouse MI model. Therefore, we assessed miR-210's effect on the gene expression profile of CTs by single-cell qRT-PCR. Moreover, we examined the cytoprotective and angiogenic potential of CT conditioned media following miR-210 overexpression on HL-1 cardiomyocytes and HUVECs, respectively. Finally, although most studies assess cell retention by histology, we investigated a more robust quantification for this study to meet our aim of quantifying cell retention. Therefore, a protocol of mouse heart single-cell dissociation followed by flow cytometric analysis was followed. Hence, the extent of cardiac injury was evaluated using serum cTnI ELISA and cardiac function using echocardiography rather than histological analysis. This was performed to give us an indication of the variability of the LAD ligation surgery and MI induction. MRI was not performed due to the high cost associated with it in comparison to echocardiography. Figure 5.1 shows the design of the *in vivo* experiment.

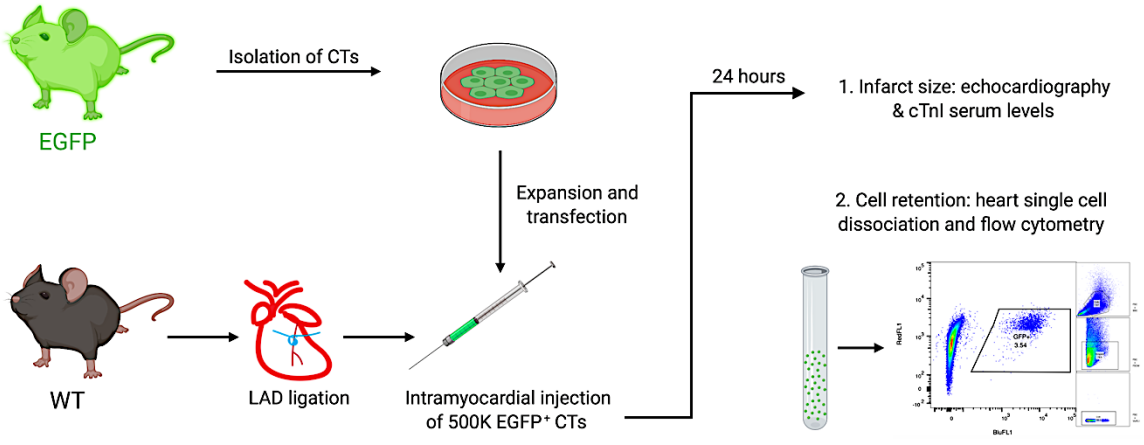


Figure 5.1 Overview of the in vivo experiment used to assess CT retention following miR-210 transfection in a mouse MI model

Schematic showing the steps involved in the *in vivo* experiment including the assessment of the infarct size and CT retention in mice following MI induction by LAD ligation.

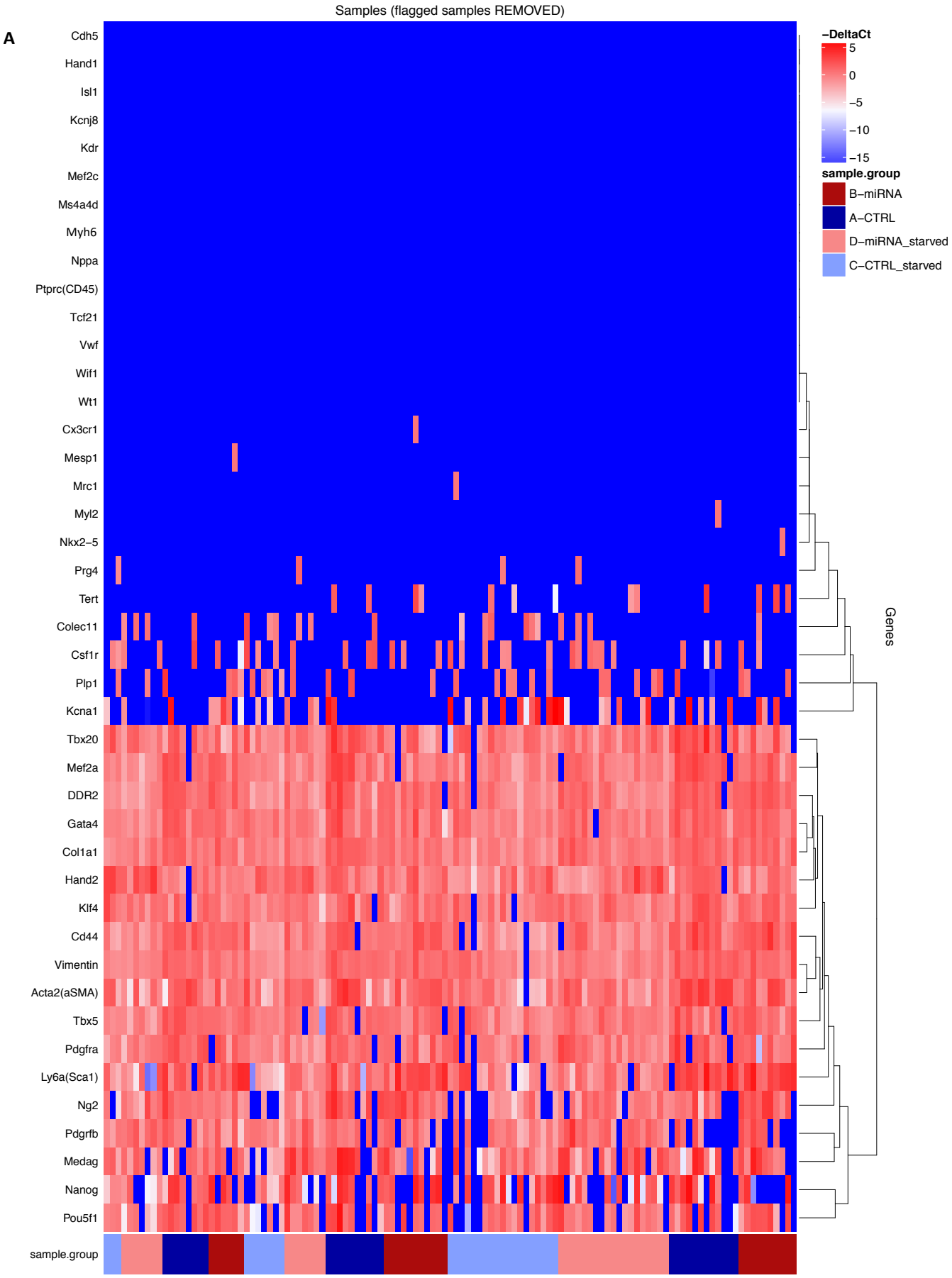
5.2 Results

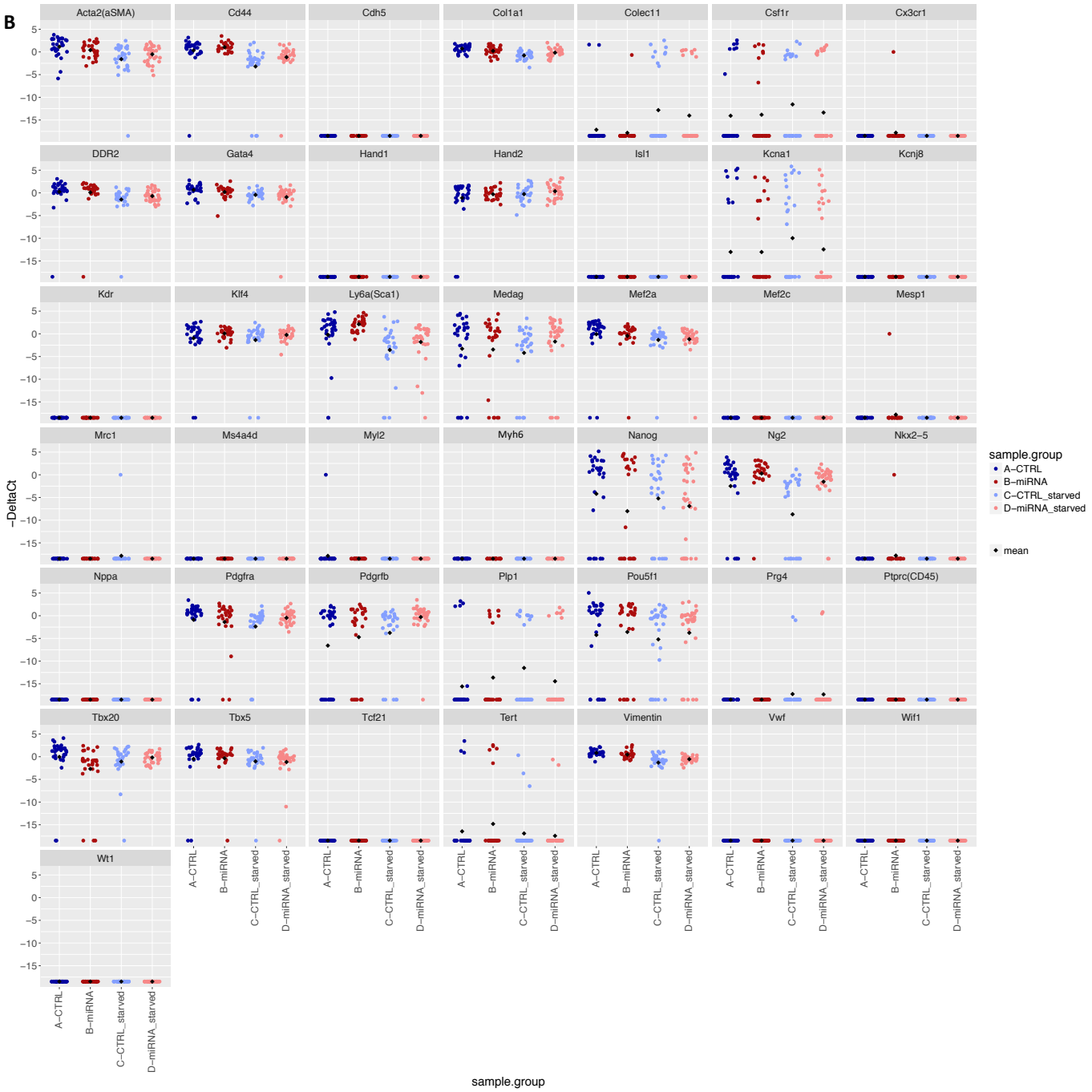
5.2.1 miR-210 transfection partially reversed the effect of serum starvation on the CT gene expression profile

To assess the effect of miR-210 overexpression and/or serum starvation on the heterogeneous population of CTs, gene expression was examined using single-cell qRT-PCR. Comparison of: control transfected with negative miRNA (A-CTRL), control transfected with miR-210 (B-miRNA), serum starved transfected with negative miRNA (C-CTRL_starved) and serum starved transfected with miR-210 (D-miRNA_starved) CT populations at passage 7 was performed. We tried to order the samples in the heatmap on the basis of cell type, as before, but that was not possible unfortunately due to technical difficulties with the R script used, which we are currently trying to resolve. This single-cell qRT-PCR experiment was performed at passage 7 as all the *in vitro* and *in vivo* data on miR-210 were also on passage 7 cells. Experiments were performed on passage 7 cells as I found that it is consistently the lowest passage number where I had sufficient cell numbers to perform the required assays. It is favourable to use low passage number cells due to possible phenotypic drift associated with prolonged *in vitro* culture. Interestingly, we found some changes in the gene expression profile of CTs at passage 7 in comparison to those at passage 3, which was discussed in the third chapter. In particular, expression *of Tcf21* and *Mrc1,* two of the genes that most clearly defined the CTs, was no longer detected. Almost uniform expression of *Tbx5* was observed in passage 7 CTs, which showed little to no expression in passage 3 CTs. Moreover, the heatmap suggested that passage 7 CTs were more homogenous than passage 3 CTs (figure 5.2.A).

Examining the expression of individual genes in figure 5.2.B showed an overall trend of rescue or reversal with miR-210 in the starved population (D-miRNA_starved) when compared to the starved transfected with negative miRNA (C-CTRL_starved) and control transfected with negative miRNA (A-CTRL) populations. This trend of rescue was apparent in the expression

of *Acta2, Cd44*, *Col1a1, Colec11, Csf1r, Kcna1, Ly6a, Ng2, and Pou5f1*. However, PCA did not reveal a separation in the clustering of the tested populations and did not show an apparent rescue with miR-210 (figure 5.2.C). Figure 5.3 demonstrates a statistical analysis of the above populations. Following starvation, there was a significant reduction in the expression of: *Ng2* ($P < 0.0001$), *Tbx5* ($P < 0.01$), *Gata4* ($P < 0.001$), *Ddr2* ($P < 0.0001$), *Cd44* ($P < 0.0001$), *Vim* ($P < 0.0001$), *Ly6a* ($P < 0.001$), *Mef2a* ($P < 0.0001$), *Col1a1* ($P < 0.0001$), *Pdgfrα* ($P < 0.001$), *Acta2* ($P < 0.0001$), and *Tbx20* ($P < 0.05$). Among these genes, the expression of *Ng2* ($P < 0.01$) was significantly increased in the starved miR-210 CTs in comparison to starved neg CTs suggesting a partial rescue of expression of *Ng2*. This explains the lack of resolution of the tested populations in the PCA in figure 5.2.C as only the rescue of one gene reached statistical significance. Although a significant change was not detected in the expression of *Pdgfrβ* following serum starvation, a significant increase in *Pdgfrβ* expression ($P < 0.05$) was noted in starved miR-210 CTs in comparison to control and starved neg CTs. In control conditions, miR-210 significantly reduced the expression of *Tbx20* ($P < 0.001$).


A
Samples (flagged samples REMOVED)
Cdh5
Hand1
Isl1
Kcnj8
Kdr
Mef2c
Ms4a4d
Myh6
Nppa
Ptprc(CD45)
Tcf21
Vwf
Wif1
Wt1
Cx3cr1
Mesp1
Mrc1
Myl2
Nkx2−5
Prg4
Tert
Colec11
Csf1r
Plp1
Kcna1
Tbx20
Mef2a
DDR2
Gata4
Col1a1
Hand2
Klf4
Cd44
Vimentin
Acta2(aSMA)
Tbx5
Pdgfra
Ly6a(Sca1)
Ng2
Pdgrfb
Medag
Nanog
Pou5f1
sample.group
−DeltaCt
5
0
−5
−10
−15
sample.group
B−miRNA
A−CTRL
D−miRNA_starved
C−CTRL_starved
Genes


B
Acta2(aSMA)
Cd44
Cdh5
Col1a1
Colec11
Csf1r
Cx3cr1
DDR2
Gata4
Hand1
Hand2
Isl1
Kcna1
Kcnj8
Kdr
Klf4
Ly6a(Sca1)
Medag
Mef2a
Mef2c
Mesp1
Mrc1
Ms4a4d
Myl2
Myh6
Nanog
Ng2
Nkx2−5
Nppa
Pdgfra
Pdgrfb
Plp1
Pou5f1
Prg4
Ptprc(CD45)
Tbx20
Tbx5
Tcf21
Tert
Vimentin
Vwf
Wif1
Wt1
−DeltaCt
5
0
−5
−10
−15
A−CTRL
B−miRNA
C−CTRL_starved
D−miRNA_starved
sample.group
sample.group
A−CTRL
B−miRNA
C−CTRL_starved
D−miRNA_starved
mean

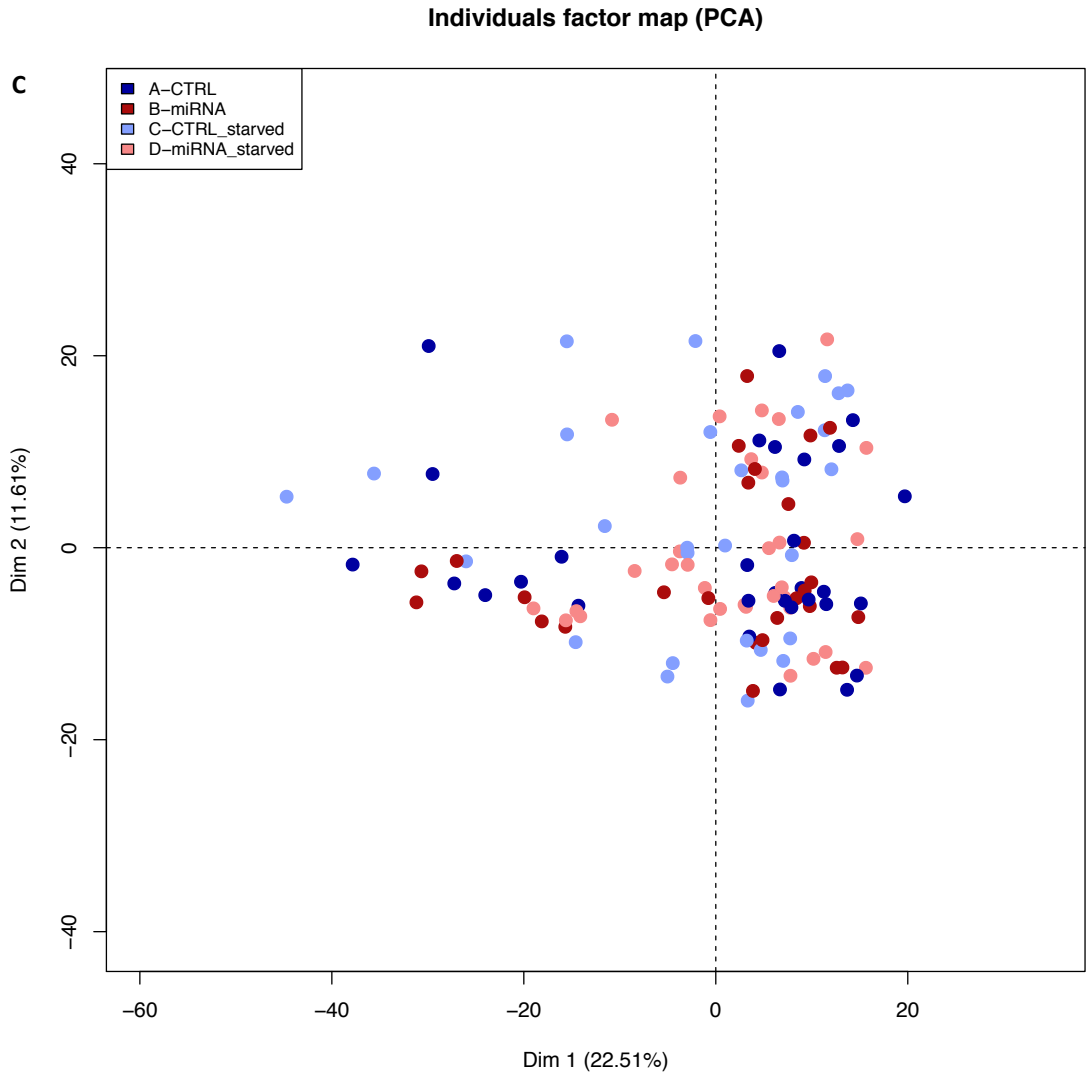


Figure 5.2 Single-cell gene expression profiles of CTs following miR-210 transfection and/or serum starvation

(A) Expression of 43 genes was analysed at the single-cell level in the four CT populations shown: control transfected with negative miRNA (A-CTRL; n=30), control transfected with miR-210 (B-miRNA; n=27), serum starved transfected with negative miRNA (C-CTRL_starved; n=29) and serum starved transfected with miR-210 (D-miRNA_starved; n=33) at passage 7. All four populations represent 3 biological replicates. The heatmap illustrates expression as -ΔCT values (blue is low or absent; red is high) and the genes were grouped by a hierarchical clustering algorithm based on the underlying co-expression pattern. **(B)** Single-cell expression of the tested 43 genes represented individually in the four cell populations shown. **(C)** PCA of the same four cell populations demonstrating no distinct separation between the populations.

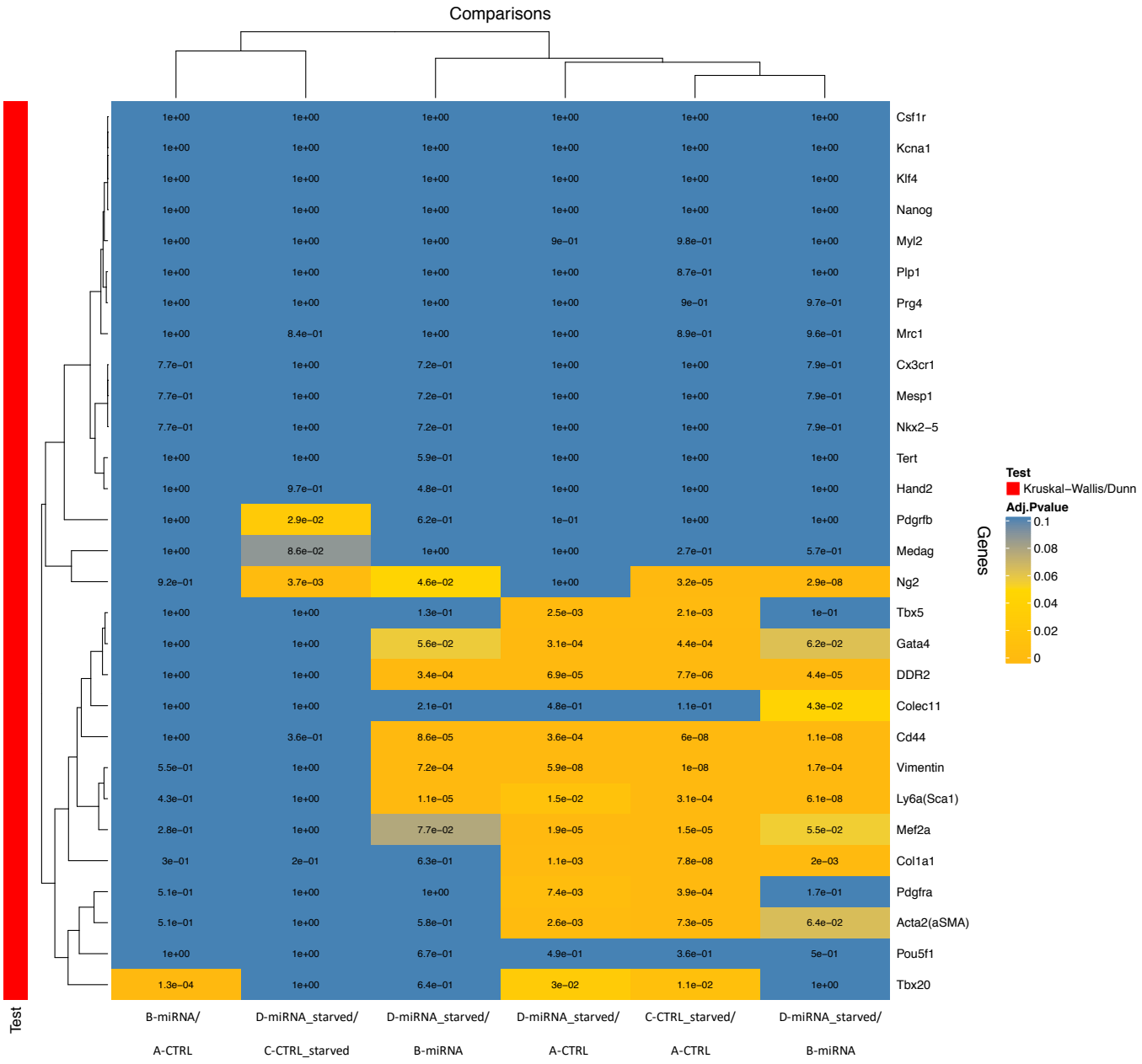


Figure 5.3 Statistical analysis of the single-cell qRT-PCR data

Statistical analysis of the four CT populations shown: control transfected with negative miRNA (A-CTRL; n=30), control transfected with miR-210 (B-miRNA; n=27), serum starved transfected with negative miRNA (C-CTRL_starved; n=29) and serum starved transfected with miR-210 (D-miRNA_starved; n=33) at passage 7. All four populations represent 3 biological replicates. The heatmap illustrates P values from 0 to 0.1 (orange to blue is low to high). The genes were grouped by a hierarchical clustering algorithm based on the underlying co-expression pattern.

Figure 5.4 shows a separate analysis performed using control untransfected, serum starved transfected with negative miRNA (C-CTRL_starved), and serum starved transfected with miR-210 (D-miRNA_starved) CT populations. This analysis differs from the previous analysis shown in figures 5.2 and 5.3 as it was performed prior to the acquisition of additional populations (A-CTRL, control transfected with negative miRNA; B-miRNA, control transfected with miR-210) and increasing sample numbers in populations C-CTRL_starved and D-miRNA_starved. PCA of only these three populations revealed a more apparent separation in the clustering of control CTs and starved negative CTs suggesting a shift in the expression profile of CTs following starvation. Starved miR-210 CTs clustered between the other two populations suggesting a partial rescue of the expression profile that occurred following starvation (figure 5.4.A). Statistical analysis of the above populations showed that the expression of *Vim*, *Ng2*, and *Ly6a* was significantly increased in the starved miR-210 CTs in comparison to starved neg CTs suggesting a partial rescue of expression. Although a significant change was not detected in the expression of *Pdgfrβ* (as described above) and *Medag* following serum starvation, a significant increase in *Pdgfrβ* and *Medag* expression was noted in starved miR-210 CTs in comparison to control and starved neg CTs (figure 5.4.B). The more apparent resolution of clustering in figure 5.4.A can be attributed to more genes rescued by miR-210 reaching statistical significance in comparison to the previous analysis (figures 5.2 and 5.3). This may be a result of the previous analysis being underpowered due to the use of four populations rather than just three. Another possibility is that the use of control untransfected CTs in this comparison rather than populations A-CTRL (control transfected with negative miRNA) and B-miRNA (control transfected with miR-210) may have affected the analysis. The use of control CTs transfected with negative miRNA is more appropriate than the use of control untransfected CTs as it overrules the possibility of the transfection itself altering gene expression.

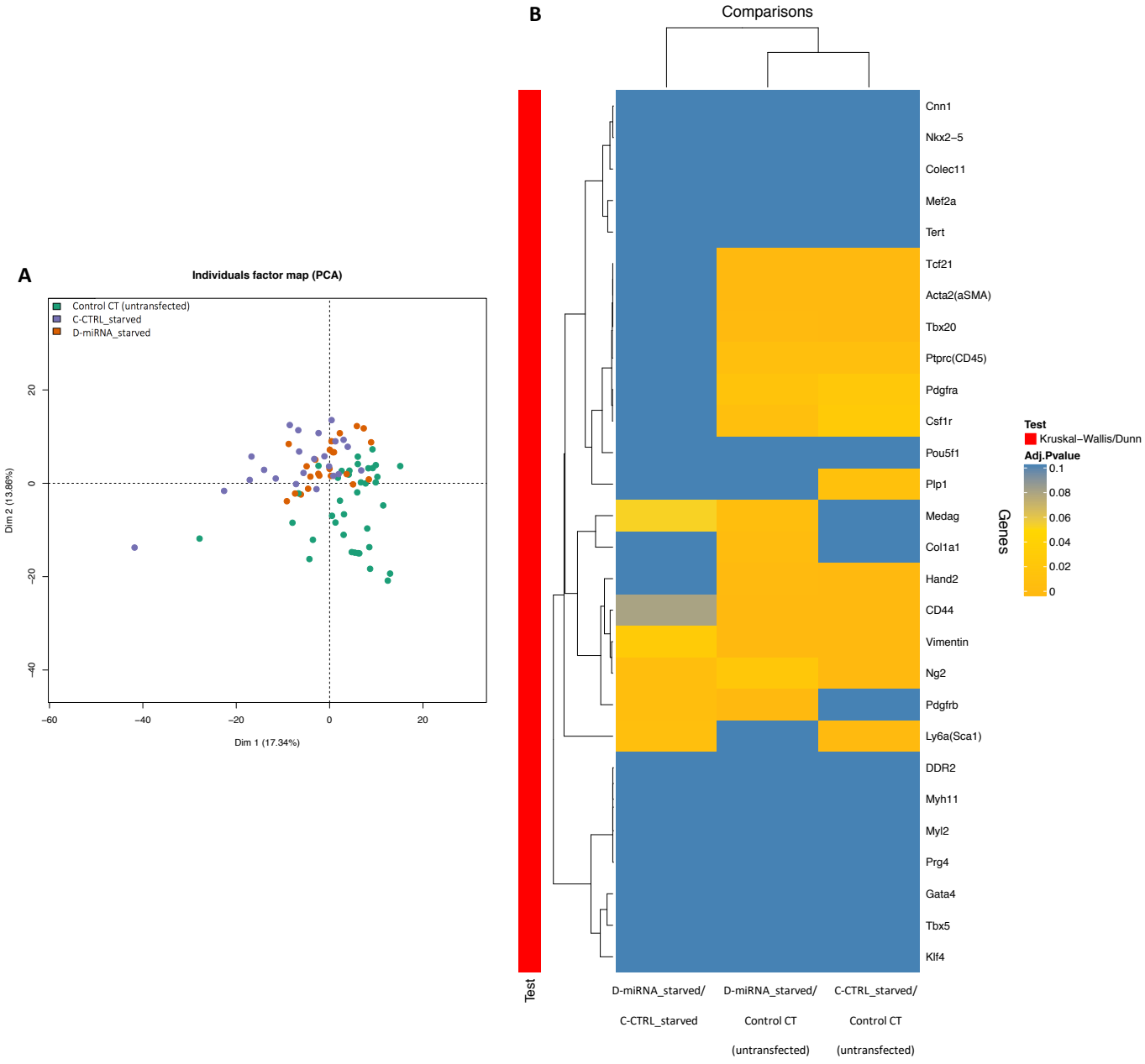


Figure 5.4 PCA and statistical analysis of serum starved CTs transfected with a negative miRNA or miR-210 in comparison to an untransfected control

(A) PCA of the three CT populations shown: control untransfected (n=37), serum starved transfected with negative miRNA (C-CTRL_starved; n=23) and serum starved transfected with miR-210 (D-miRNA_starved ; n=23) at passage 7. All four populations represent 3 biological replicates. Both Dim.1 and Dim.2 show the C-CTRL_starved populations clustering between the other two populations. **(B)** Statistical analysis of the same three populations. The heatmap illustrates P values from 0 to 0.1 (orange to blue is low to high). The genes were grouped by a hierarchical clustering algorithm based on the underlying co-expression pattern.

5.2.2 The effect of miR-210 on the paracrine potential of CTs

5.2.2.1 Measuring growth factor secretion from CTs following miR-210 overexpression

Due to the significant implication of paracrine signalling in the therapeutic effect of cell therapy on heart remodelling and regeneration (see Introduction 1.5), we assessed the ability of miR-210 to increase the secretion of beneficial growth factors from CTs. CTs were transfected with either a negative miRNA or miR-210, then cultured under normoxia or hypoxia in serum-free media (as required by the manufacturer) for 48 hours prior to collection of the conditioned media. The conditioned media was assessed by a mouse growth factor array that detects 20 growth factors, many of which had been implicated in cardiac repair (see table 3.2). When CTs were transfected with miR-210, an increase in SCF (CT neg conditioned media, 0.07 ± 0.01; CT miR-210 conditioned media, 0.11 ± 0.01; $P < 0.05$; n=3), IGF-1 (CT neg conditioned media, 0.61 ± 0.16; CT miR-210 conditioned media, 1.00 ± 0.04; $P < 0.05$; n=3) and IGFBP-2 (CT neg conditioned media, 0.48 ± 0.03; CT miR-210 conditioned media, 0.62 ± 0.02; $P < 0.01$; n=3) secretion was observed compared to the negative groups under normoxia. None of the factors were significantly differentially secreted under hypoxia (figure 5.5). However, IGF-2 showed a trend towards significance with a P value of 0.08 (CT neg 2% O_2 conditioned media, 0.17 ± 0.03; CT miR-210 2% O_2 conditioned media, 0.23 ± 0.04; n=3). When comparing CTs cultured under normoxia to CTs cultured under hypoxia, we found a significant increase in VEGF-A secretion only (CT neg conditioned media, 0.19 ± 0.04; CT neg 2% O_2 conditioned media, 0.30 ± 0.01; $P < 0.01$; n=3) (supplementary figure 3, appendix A).

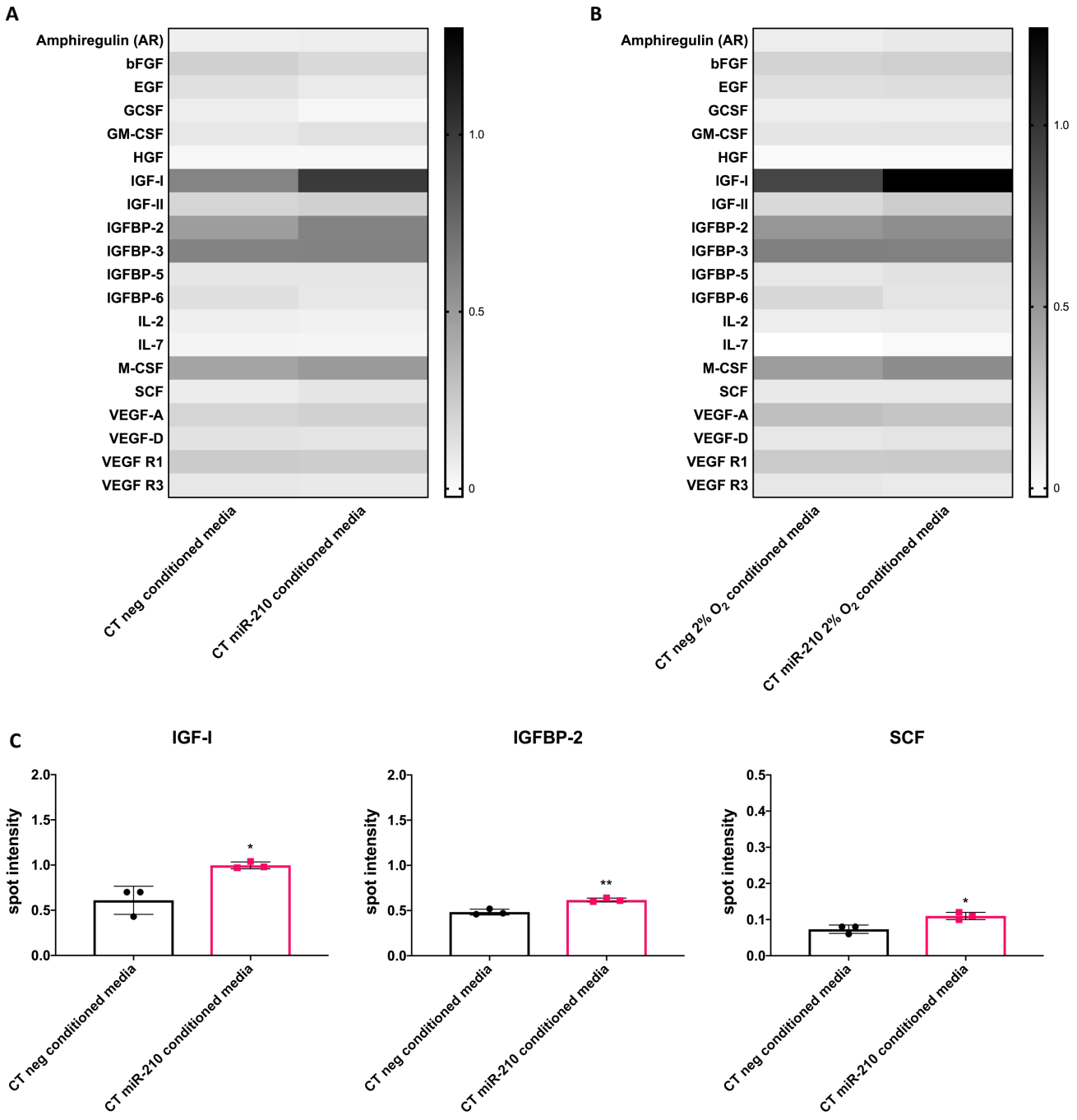


Figure 5.5 Growth factor array on the conditioned media of miR-210-transfected CTs

The secretion of 20 growth factors was assessed in the conditioned media of miR-210-transfected CTs, in comparison to CTs transfected with a negative miRNA using an array. Spot intensity of the samples was normalised to the average of the positive control spots of each array. The heatmap illustrates spot intensity (white is low or absent; black is high) of the assessed factors secreted from CTs cultured in normoxia **(A)** or hypoxia **(B)**. **(C)** Individual representation of growth factors that were significantly differentially secreted. Analysed using a t-test to determine statistical significance (n=3).

5.2.2.2 Conditioned media of normoxic miR-210-overexpressing CTs enhances HUVEC proliferation

HUVECs were used to evaluate the paracrine potential of CT conditioned media and whether miR-210 transfection enhanced this potential. HUVECs were switched to culture in 1:1 serum-free HUVEC media and conditioned media or unconditioned media as a negative control for 24 hours then harvested for cell counting. Conditioned media of CTs cultured under hypoxia, but not normoxia, enhanced the proliferation of HUVECs in comparison to the negative control (negative control, 133,333 ± 41,633; CT neg 2% O_2 conditioned media, 276,667 ± 75,056; $P < 0.05$; CT neg conditioned media, 176,667 ± 32,146; $P = 0.61$; n=3). Moreover, conditioned media of normoxic, but not hypoxic, miR-210-overexpressing CTs significantly enhanced the proliferation of HUVECs in comparison to that of CTs transfected with the negative miRNA (CT neg conditioned media, 176,667 ± 32,146; CT miR-210 conditioned media, 313,333 ± 77,675; $P < 0.05$; CT neg 2% O_2 conditioned media, 276,667 ± 75,056; CT miR-210 2% O_2 conditioned media, 176,667 ± 30,051; $P = 0.13$; n=3) (figure 5.6).

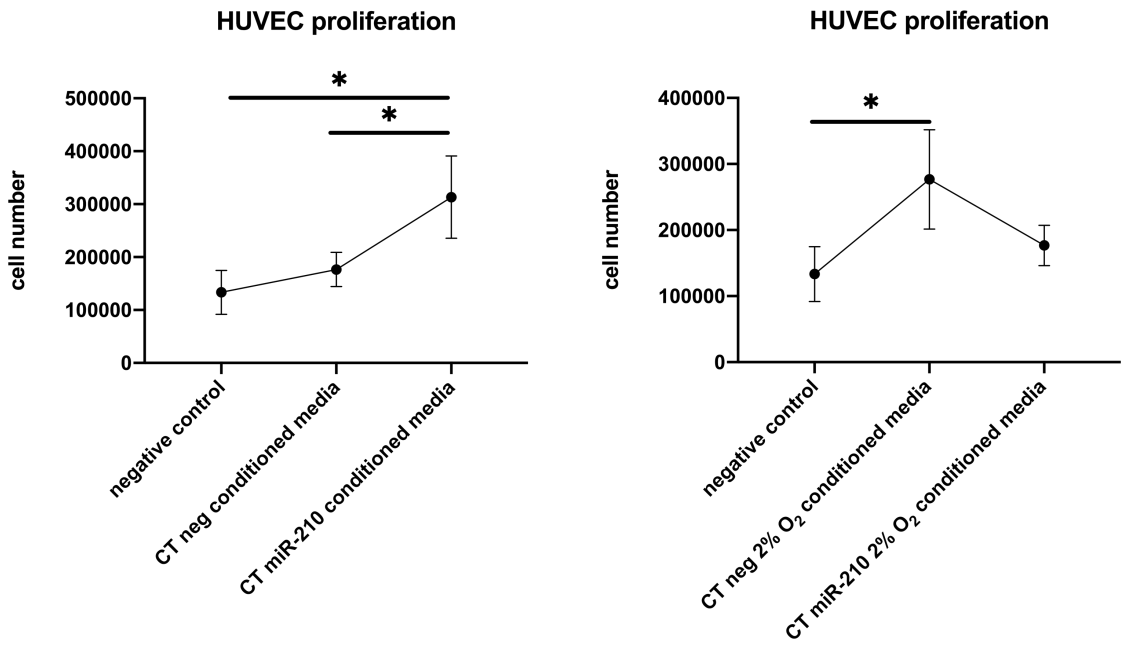


Figure 5.6 Conditioned media of normoxic miR-210-overexpressing CTs enhances HUVEC proliferation

HUVEC proliferation, as assessed by cell counting, after 24-hour culture in 1:1 serum-free HUVEC media and conditioned media or unconditioned media as a negative control. The conditioned media of miR-210-transfected CTs was compared to that of CTs transfected with a negative miRNA cultured in normoxia **(A)** or hypoxia **(B)**. Analysed using a two-way ANOVA with Tukey's multiple comparisons test to determine statistical significance (n=3).

5.2.2.3 Conditioned media of normoxic miR-210-overexpressing CTs has an anti-apoptotic effect in HL-1 cardiomyocytes subjected to simulated ischaemia/reperfusion

We next examined miR-210's ability to enhance the pro-survival effect of CT conditioned media on cultured cardiomyocytes. HL-1 cardiomyocytes were subjected to simulated ischaemia/reperfusion (I/R). This was performed by switching the cardiomyocytes to culture in serum- and glucose-free RPMI and hypoxia (1% O_2) to simulate ischaemia, then switched to culture in 1:1 serum-free RPMI media and conditioned media or unconditioned media as a negative control and normoxia for 24 hours to simulate reperfusion, then fixed for staining. To determine the required duration of simulated ischaemia, 4 different timepoints were tested: 3, 6, 12, and 24 hours (figure 5.7). Extremely low levels of apoptosis were detected at 3 hours (0.90 ± 0.36; n=3), and a large proportion of cells were $TUNEL^+$ at 12 (47 ± 0.47; n=3) and 24 hours (52 ± 3.7; n=3). Therefore the 6-hour timepoint was selected (9.6 ± 2.4; n=3). It was also noted that more cells died and de-attached with increased duration of simulated ischaemia as can be seen in the decreased confluency on the coverslips.

As described above, cardiomyocytes were subjected to simulated I/R and treatment with CT conditioned media and assessed for apoptotic cell death using a TUNEL assay. Conditioned media of CTs cultured under both normoxia and hypoxia decreased cardiomyocyte apoptosis under simulated I/R in comparison to the negative control (negative control, 8.6 ± 1.3; CT neg conditioned media, 3.9 ± 0.19; $P < 0.001$; CT neg 2% O_2 conditioned media 2.8 ± 2.5; $P < 0.05$; n=3). Moreover, conditioned media of normoxic miR-210-overexpressing CTs further decreased cardiomyocyte apoptosis in comparison to that of CTs transfected with the negative miRNA (CT neg conditioned media, 3.9 ± 0.19; CT miR-210 conditioned media 1.8 ± 0.20; $P < 0.05$; n=3) (figure 5.8).

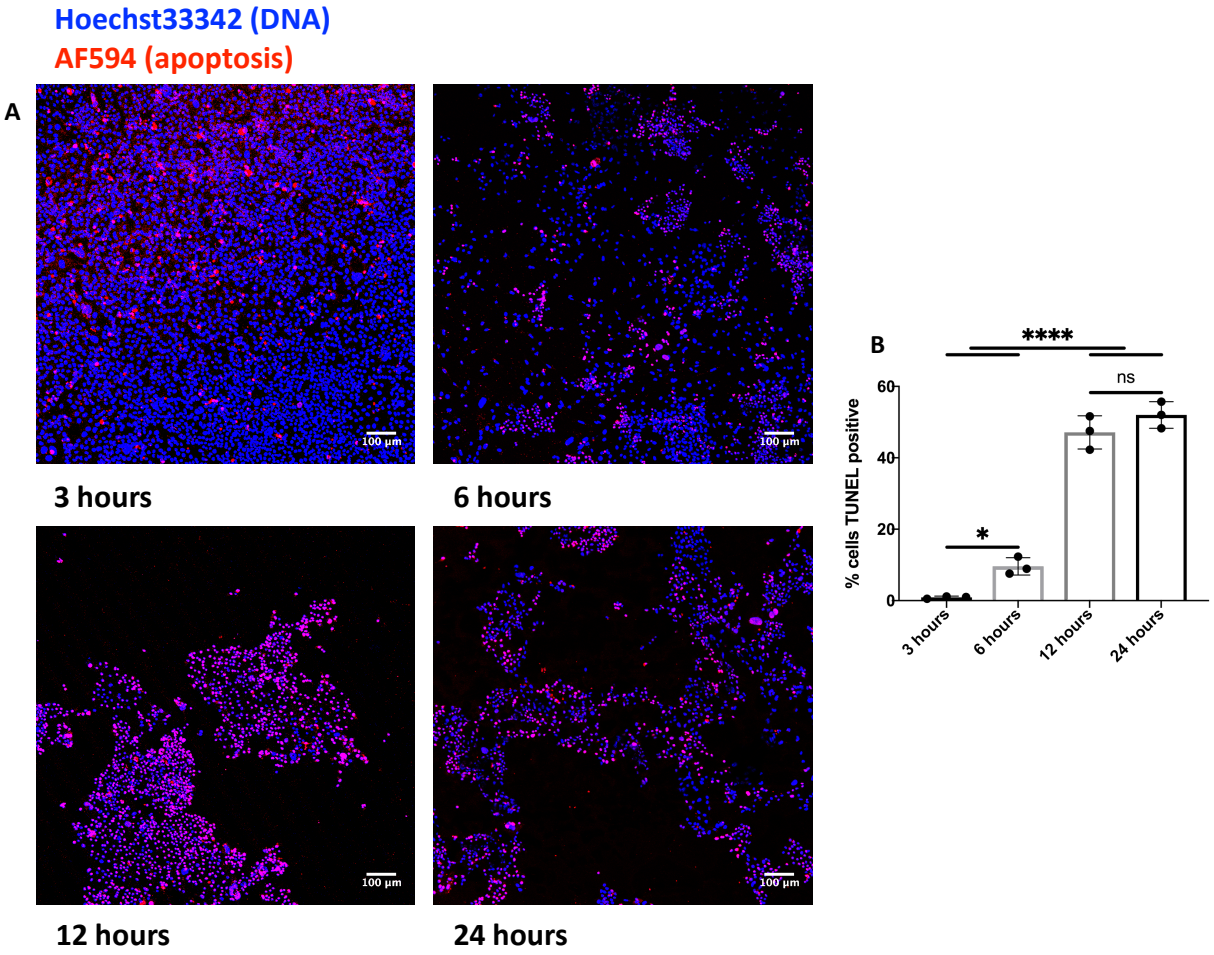


Figure 5.7 Optimisation of simulated ischaemia/reperfusion in HL-1 cardiomyocytes

HL-1 cardiomyocytes were switched to culture in serum- and glucose-free RPMI and hypoxia (1% O_2) to simulate ischaemia then switched to culture in 1:1 serum-free RPMI media and unconditioned IMDM media and normoxia for 24 hours to simulate reperfusion then fixed for a TUNEL assay. The shown four different durations of ischaemia were tested. **(A)** DNA fragmentation is represented as $TUNEL^+$ cells in HL-1 cardiomyocytes. Cells were imaged using an FV1000 confocal microscope. **(B)** Quantification of the TUNEL assay (described in Methods 2.12). Analysed using a one-way ANOVA with Tukey's multiple comparisons test to determine statistical significance (n=3).

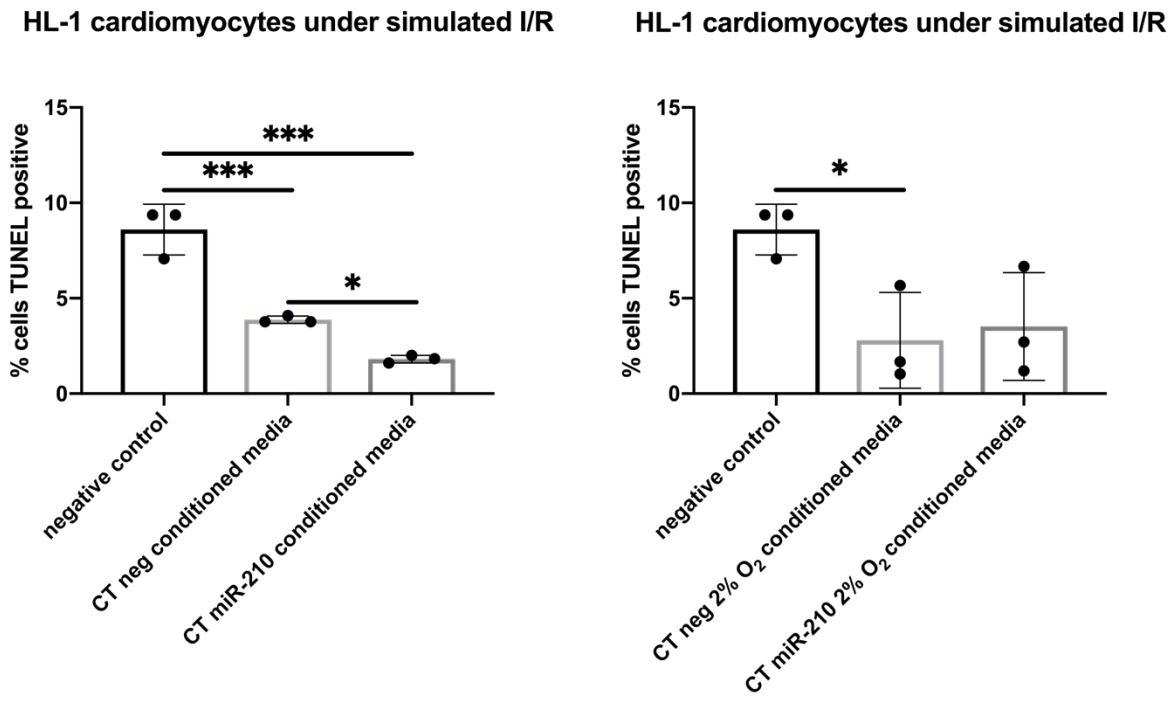
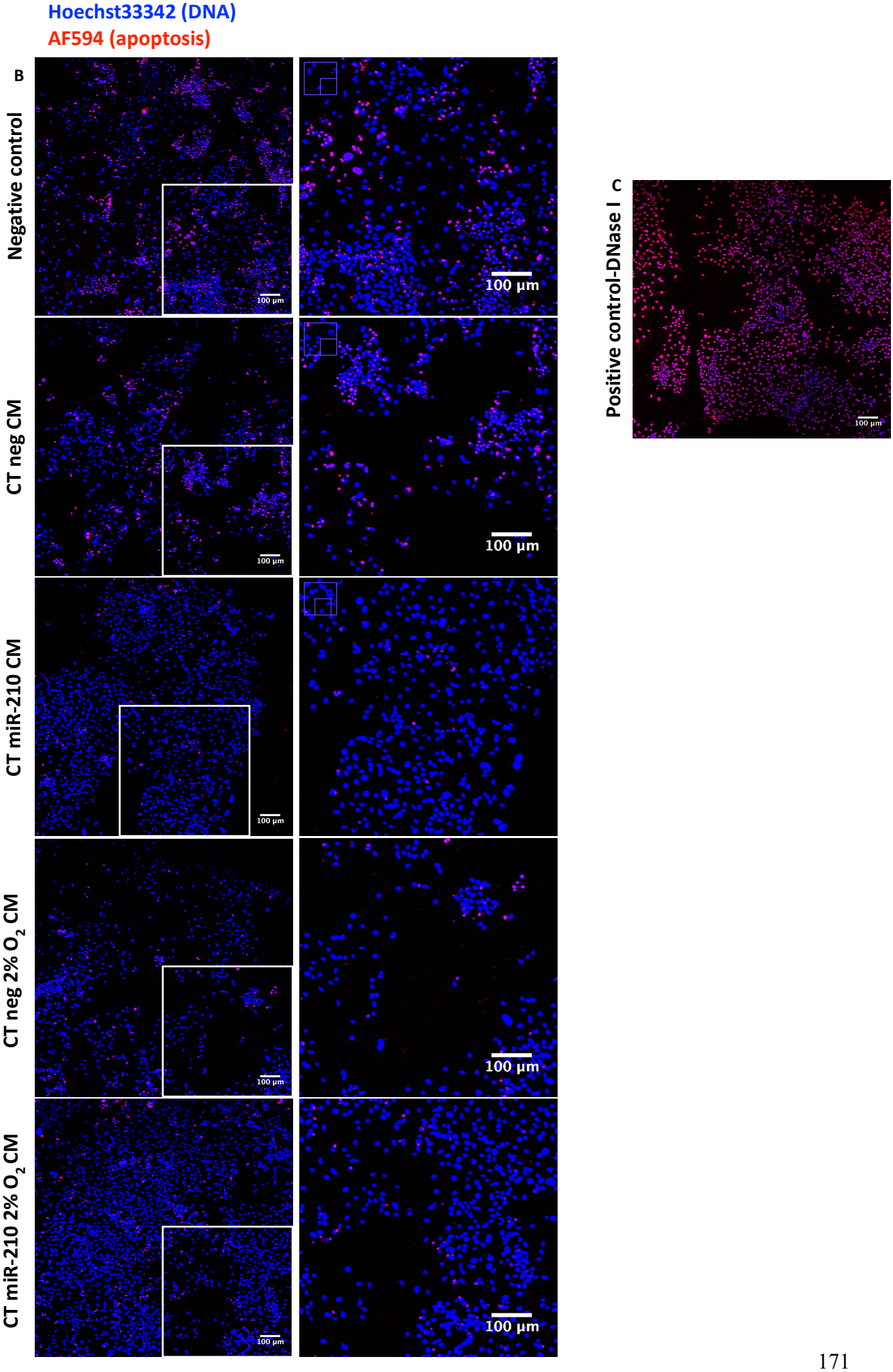


Figure 5.8 Conditioned media of normoxic miR-210-overexpressing CTs has an anti-apoptotic effect in HL-1 cardiomyocytes subjected to simulated ischaemia/reperfusion

(A) Quantification of the TUNEL assay (described in Methods 2.12). Analysed using a one-way ANOVA with Tukey's multiple comparisons test to determine statistical significance (n=3). **(B)** DNA fragmentation represented as $TUNEL^+$ cells in HL-1 cardiomyocytes after simulated I/R and treatment with CT conditioned media or unconditioned media as a negative control. The conditioned media of miR-210-transfected CTs was compared to that of CTs transfected with a negative miRNA cultured in normoxia or hypoxia. Cells were imaged using an FV1000 confocal microscope. High power inserts are shown by white boxes. **(C)** DNase treatment was used as a TUNEL assay positive control.


Hoechst33342 (DNA)
AF594 (apoptosis)
B
Negative control
CT neg CM
CT miR-210 CM
CT neg 2% O2 CM
CT miR-210 2% O2 CM
100 µm
C
Positive control-DNase I

5.2.3 The effect of miR-210 transfection on CT retention 24 hours post MI

To assess the ability of miR-210 to enhance the retention of CTs in a mouse MI model, $EGFP^+$ CTs were transfected with either a negative miRNA or miR-210 then switched to culture in CEM for 48 hours. On the day of surgery, CTs were harvested using trypsin then counted and resuspended at a concentration of 500,000 cells in 40µl of DPBS. The cell suspensions were kept in Eppendorf tubes on ice during surgery until the time of injection. MI was induced in mice by LAD ligation as described in Methods 2.19. Once the heart had settled for around a minute after ligation, cells were injected into the infarct region at one or two points using an insulin syringe (30G). A maximum of four mice underwent surgery and cell injection per day finishing with a total number of eight mice per group. The following day, the mice were imaged by echocardiography prior to heart and serum collection to be processed for flow cytometric analysis and cTnI ELISA, respectively. The hearts were dissociated into single cells, stained with the fixable viability dye Zombie Violet, then fixed to be run on the flow cytometer within 48 hours. Non-viable cells, which tend to have greater autofluorescence, and doublets increase false positives and therefore were excluded. Negative and single-colour flow controls were used as described in Methods 2.19. Three different comparisons were performed between hearts injected with CTs transfected with a negative miRNA or with miR-210 but no significant difference was found in any of the analyses: comparison of all 16 injected hearts with no omissions (CTs – neg, 0.12 ± 0.14; CTs – miR-210, 0.15 ± 0.14; P = 0.74; n=8), omission of hearts with an ejection fraction higher than 60% (CTs – neg, 0.12 ± 0.16, n=7; CTs – miR-210, 0.15 ± 0.14, n=8; P = 0.67) or omission of hearts where no $EGFP^+$ CTs were detected (CTs – neg, 0.12 ± 0.14, n=8; CTs – miR-210, 0.20 ± 0.12, n=6; P = 0.15) (figure 5.9). Omission of hearts with an ejection fraction higher than 60% was performed as ejection fraction in uninfarcted mouse hearts is typically around 60-80%[625,626]. Moreover, omitting hearts where zero $EGFP^+$ CTs were detected was performed based on the assumption that the cell injection

itself failed in these hearts. The original flow cytometry plots can be found in Appendix A (supplementary figure 4). By performing power calculations based on samples where $EGFP^+$ CTs were detected (CTs – neg, 0.12 ± 0.14; CTs – miR-210, 0.20 ± 0.12), we found that a difference would be detectable with a sample size of 25 (stat.ubc, $P < 0.05$, with power of 80%). One heart in the CTs – neg group retained at least twice as many cells as others in that group and may be skewing the data. However, more samples are needed before this could be considered as an outlier.

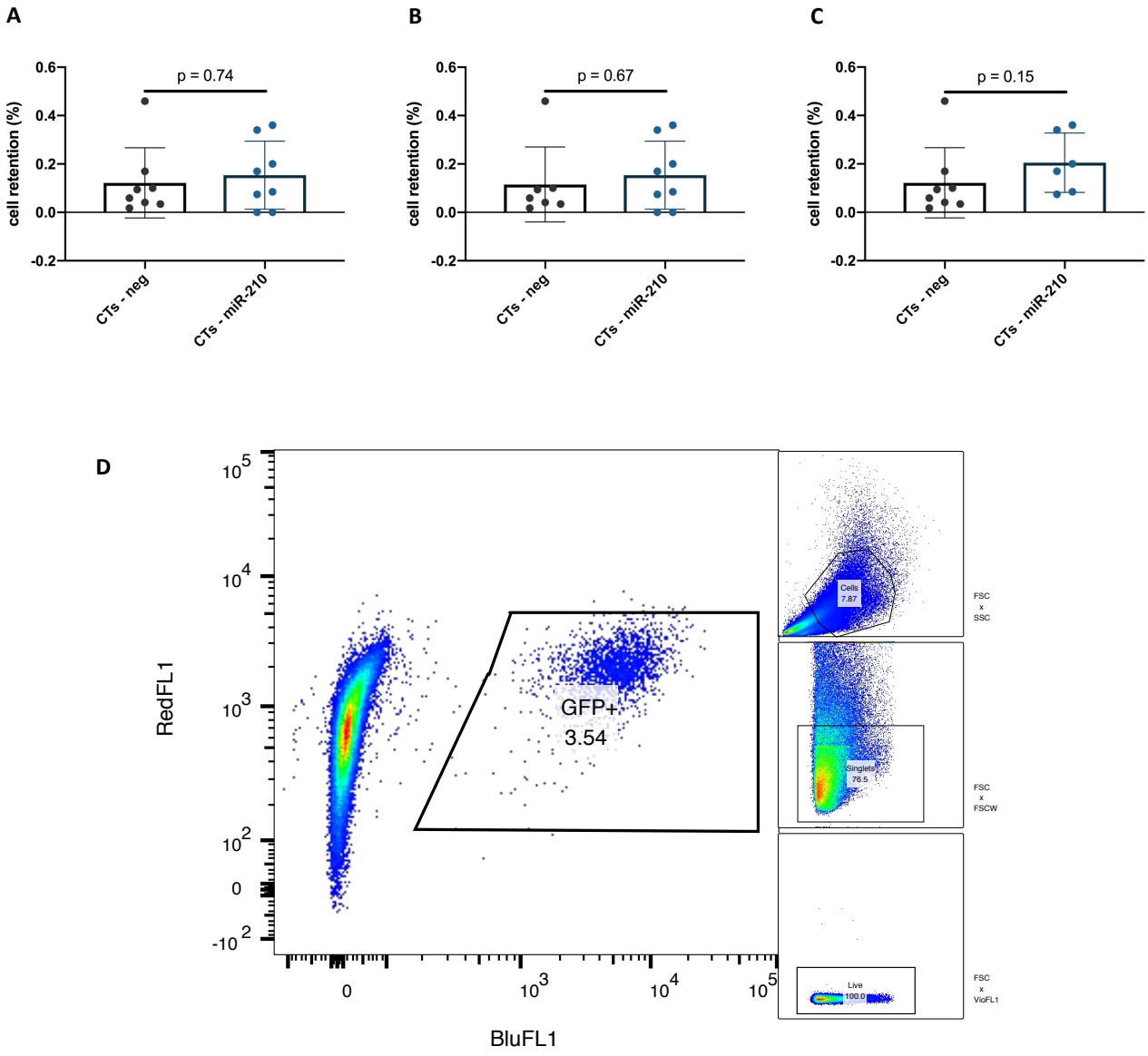


Figure 5.9 The effect of miR-210 transfection on CT retention 24 hours post MI

(A-C) Comparison of the retention of EGFP$^+$ CTs, as assessed by flow cytometry, that were either transfected with a negative miRNA or miR-210 24 hours after injection into infarcted mouse hearts (A) comparison of all 16 injected hearts with no omissions: CTs – neg, n=8; CTs – miR-210, n=8 (B) omission of the heart with an ejection fraction higher than 60%: CTs – neg, n=7; CTs – miR-210, n=8 (C) omission of hearts where no EGFP+ CTs were detected: CTs – neg, n=8; CTs – miR-210, n=6. Analysed using a Mann-Whitney test to determine statistical significance. **(D)** Representative image of the gating strategy used to quantify EGFP$^+$ CTs in each sample.

5.2.4 Echocardiography and serum cTnI levels 24 hours post MI

To examine the reproducibility of the LAD ligation surgery, cardiac function was evaluated by echocardiography (figure 5.10). Left ventricular ejection fraction and stroke volume were measured as an indication of cardiac function. Ejection fraction defines the blood fraction in diastole that is ejected in systole, whereas stroke volume refers to the total ejected blood volume per cycle. There was considerable variation in cardiac function with ejection fraction ranging from 24 to 79% and stroke volume ranging from 12 to 37µL . Although mice receiving sham surgery were not assessed, ejection fraction in uninfarcted mouse hearts is typically around 60-80%[625,626]. All mice used in this study had an ejection fraction below 60% with one exception. Moreover, serum cTnI levels, which peak between 24 and 48 hours[627], were assessed and revealed variability as well with values ranging from 48 to 81ng/mL (figure 5.11). Cardiac troponins, particularly the I and T isoforms, are well-established biomarkers of cardiac injury that are specific and sensitive for the assessment of the extent of myocardial death[628–630]. It has been shown that cTnI is a robust biomarker for MI development in mice and rats[627]. As the extent of cardiac injury may affect the degree of cell retention (see Discussion 5.3.3), we compared these parameters between hearts that were injected with CTs transfected with a negative miRNA or with miR-210 but observed no significant difference in ejection fraction (CTs – neg, 44.03 ± 15.48; CTs – miR-210, 40.19 ± 9.38; P = 0.56; n=8), stroke volume (CTs – neg, 21.68 ± 5.85; CTs – miR-210, 23.78 ± 8.23; P = 0.56; n=8) or serum cTnI levels (CTs – neg, 64.00 ± 11.36; CTs – miR-210, 67.84 ± 6.39; P = 0.42; n=8).

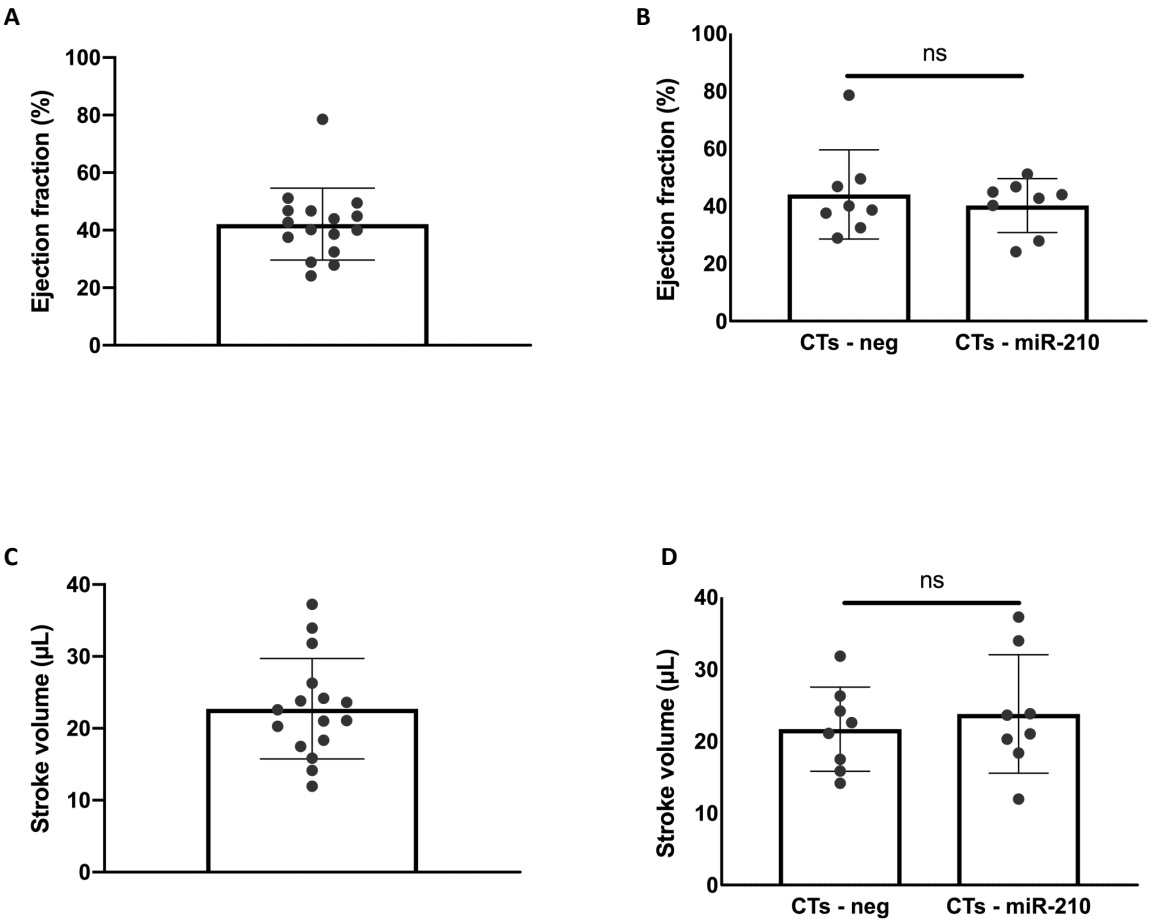


Figure 5.10 Echocardiography measurements in the infarcted mice used in this study

Echocardiography was used to assess cardiac function following MI induction using LAD ligation by measuring left ventricular ejection fraction **(A,B)** and stroke volume **(C,D)**. **(A,C)** Combined mouse data (n=16). **(B,D)** Comparison between hearts that were injected with CTs transfected with a negative miRNA (n=8) or with miR-210 (n=8).

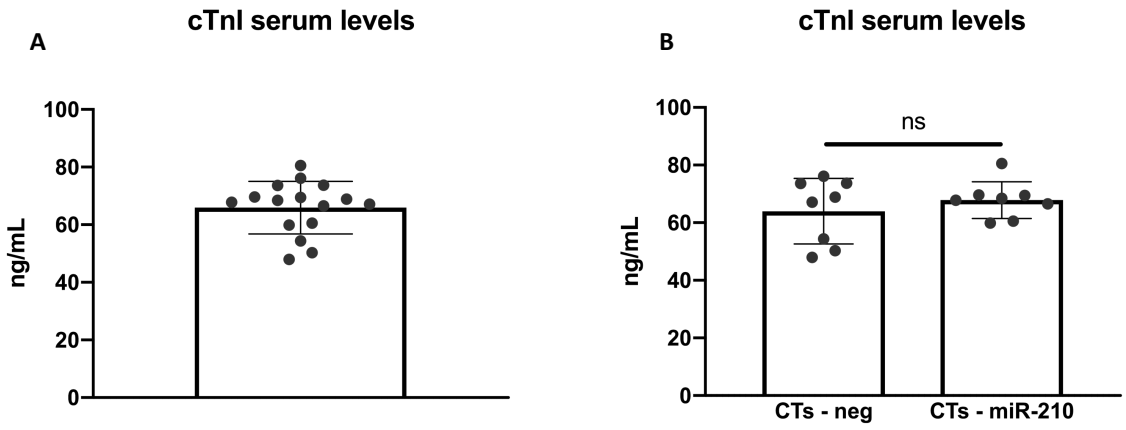


Figure 5.11 Serum cardiac troponin I levels in the infarcted mice used in this study

Serum cTnI levels was used to assess the extent of injury following MI induction using LAD ligation. **(A)** All mice used in this study (n=16). **(B)** Comparison between hearts that were injected with CTs transfected with a negative miRNA (n=8) or with miR-210 (n=8).

5.3 Discussion

5.3.1 miR-210 transfection partially reversed the effect of serum starvation on the CT gene expression profile

We assessed the effect of miR-210 overexpression and/or serum starvation on CTs using passage 7 cells as all the *in vitro* and *in vivo* experiments on miR-210 were also performed on passage 7 cells. The single-cell qRT-PCR data suggested a shift in the gene expression profile of CTs at passage 7 in comparison to passage 3. We did not directly compare these population but intend to perform this analysis soon. We found that the expression of some of the genes that gave the CTs a unique signature (*Tcf21* and *Mrc1*) at passage 3 were not present anymore. In contrast, *Tbx5* expression appeared to be upregulated. These data suggest that passage 7 CTs may more closely resemble passage 3 CDCs than do passage 3 CTs. As these data are relative rather than absolute values, the undetectable level of *Tbx5* expression in passage 3 CTs may be due to it being expressed at much higher levels in the CDCs and CFs. However, this is unlikely due to the changes observed in *Tcf21* expression as well, which was shown to have a strong negative correlation with *Tbx5*. Moreover, the CDCs undergo the additional step of cardiosphere formation and require longer time in culture to reach passage 3 in comparison CTs. Therefore, the CDCs may have undergone a similar switch in gene expression at an earlier stage. This phenomenon of changes in gene expression pattern with passaging and *in vitro* culture has been widely reported[631–633]. Indeed, this is one of the hurdles associated with cell therapy as *in vitro* expansion is required to acquire sufficient cells for therapy. How this may affect the functionality and the potential therapeutic benefit of CTs remains to be elucidated.

Although serum starvation did not affect the expression of all tested genes in CTs, the expression of 12 genes was significantly altered. This effect was not observed in genes associated with particular cell types but appeared more random and PCA of control negative, control miR-210, starved negative, and starved miR-210 CT populations did not show an

apparent separation in their clustering. Moreover, of these genes, only *Ng2* expression was significantly increased in the starved miR-210 CTs in comparison to starved neg CTs. However, PCA of control untransfected, starved negative, and starved miR-210 CT populations showed a transcriptional gradient in the gene expression profile of CTs, with a shift following starvation and a clustering of the starved miR-210 CT population between the control untransfected and starved negative CT populations suggesting a partial rescue of the gene expression profile that occurred following starvation. The more apparent resolution of clustering in this analysis may be attributed to more genes rescued by miR-210 reaching statistical significance in comparison to the previous analysis. Indeed, statistical analysis showed that miR-210 significantly increased *Vim*, *Ng2*, and *Ly6a* expression in the starved miR-210 CTs in comparison to starved neg CTs. This is consistent with miR-210 playing a pro-survival role in CTs.

Interestingly, a significant change was not detected in the expression of *Pdgfrβ* and *Medag* following serum starvation, though a significant increase in *Pdgfrβ* and *Medag* expression was noted in starved miR-210 CTs in comparison to control and starved neg CTs. This may be due to a functional role of PDGFRβ and MEDAG in a cellular process that miR-210 is a part of or regulates. For example, PDGFR signalling has been implicated in the regulation of autophagic processes, though conflicting effects have been described[413,414]. PDGFRβ is involved in cell proliferation and survival and has been recently shown to promote adult mammalian cardiomyocyte proliferation and regeneration[415,416]. MEDAG has been shown to have a role in glucose uptake and lipid accumulation[387]. Moreover, miR-210 significantly reduced the expression of *Tbx20* in control conditions. TBX20 is essential for normal cardiac development and adult cardiomyocyte function[634,635] and has also been shown to promote cardiomyocyte proliferation in adult mouse hearts[636]. This may suggest an effect of miR-210 on the cardiogenic potential of CTs.

Performing analysis on four populations masked some of the changes that occurred with miR-210 overexpression and/or serum starvation. Unfortunately, the analysis performed using three populations only did not have the most appropriate control which would be control negative rather than control untransfected. The use of control CTs transfected with negative miRNA is more appropriate than the use of control untransfected CTs as it overrules the possibility of the transfection itself altering gene expression. Therefore, we are currently repeating the analysis with the control negative population instead. In summary, although miRNAs have been implicated in cell fate and identity (see Introduction 5.1.1), there is no conclusive evidence to suggest a shift in the cell identity of CTs with miR-210 transfection. We did observe changes in *Pdgfrβ*, *Medag* and *Tbx20* expression levels in response to miR-210 overexpression but examining a wider array of genes (by e.g. single-cell RNA sequencing) is required to uncover a possible shift in cell identity. In addition, our results indicated that serum starvation altered the gene expression of CTs and that miR-210 was capable of partially rescuing some of the changes at the transcriptional level, which is consistent with its pro-survival effect.

5.3.2 The effect of miR-210 on the paracrine potential of CTs

In this study, we found that miR-210 improved CT paracrine function by increasing SCF, IGF-1 and IGFBP-2 secretion. SCF is a direct target of HIF1 and HIF2 and has been implicated in angiogenesis[637–640]. Cardiomyocyte-specific overexpression of SCF decreased myocardial apoptosis and improved cardiac function following MI[456]. Both IGF-1 and IGFBP-2 have been implicated in promoting angiogenesis. IGF-1 has also been shown to have a cytoprotective effect in the infarcted heart (more detail in 3.3.2.). This is concordant with the angiogenic effect of miR-210. Injection of a miR-210 vector injection into infarcted mouse hearts increased capillary density[243] and miR-210 has been demonstrated to target and repress *Efna3*, which encodes an inhibitor of angiogenesis[539]. *Efna3* repression by miR-210 in HUVECs is essential for the initiation of HUVEC tubulogenesis, revealing its vital role in angiogenesis[539].

Moreover, miR-210 overexpression in HUVECs stimulated cell migration and tubulogenesis, possibly through a Notch-dependant mechanism[251]. S. Malandraki-Miller (thesis) showed using ELISA that miR-210 increased VEGF-A secretion from CTs. However, this was not detected by our growth factor arrays. This may be due to reduced sensitivity of the VEGF-A antibody in the arrays in comparison to the ELISA. When comparing CTs cultured under normoxia to CTs cultured under hypoxia, we found a significant increase in VEGF-A secretion which is consistent with VEGF-A being a direct target of HIF1α. Our results show that miR-210 may have a role in regulating angiogenesis and/or cell survival by targeting IGF and SCF signalling. This is also consistent with miRNAs being capable of targeting multiple components that often work in concert within a particular pathway.

Due to the implication of miR-210 in angiogenesis and its positive effect on the CT paracrine profile, we sought to identify whether the conditioned media of CTs affected the angiogenic potential of HUVECs and if miR-210 transfection of CTs enhanced that effect. HUVEC proliferation has frequently been used as an assay of angiogenesis, and was used in our study[641–643]. We observed an increase in the proliferation of HUVECs following incubation in the conditioned media of CTs cultured under hypoxia, but not normoxia, compared to the negative control. This is similar to the effect of CDC conditioned media on HUVEC tubulogenesis[644] and studies reporting increased angiogenic paracrine signalling following hypoxic preconditioning of a variety of cell types[203,645–647]. Moreover, conditioned media of normoxic miR-210-overexpressing CTs enhanced the proliferation of HUVECs in comparison to that of CTs transfected with the negative miRNA, which is consistent with miR-210's pro-angiogenic roles. This effect may also be explained by an increase in the levels of pro-survival factors in the secretome of miR-210-transfected CTs which may have a positive effect on HUVEC proliferation. Therefore, additional assays such as migration and tubulogenesis are required for a more conclusive assessment of angiogenesis.

In addition to the beneficial effect of miR-210 transfection on the potential of the CT secretome to enhance HUVEC proliferation, we also investigated whether it also increased survival in HL-1 cardiomyocytes. HL-1 cardiomyocytes have been widely used for the analysis of mechanisms behind cardiac I/R injury[299]. We found that conditioned media of CTs cultured under both normoxia and hypoxia decreased cardiomyocyte apoptosis under simulated I/R in comparison to the negative control. Likewise, a cytoprotective role of $SCA1^+$ cell conditioned media has been demonstrated following hypoxic injury in HL-1 cardiomyocytes[648]. Moreover, we found that the conditioned media of normoxic miR-210-overexpressing CTs further decreased cardiomyocyte apoptosis in comparison to that of CTs transfected with the negative miRNA. This was also noted by observation of the confluency of cells on the coverslips but that would have been difficult to quantify and only the percentage of $TUNEL^+$ was taken into consideration. miR-210 has been shown to transfer to primary neonatal cardiomyocytes co-cultured with MSCs via Cx43 gap junctions, resulting in reduced expression of its pro-apoptotic target *Casp8ap2* and improved survival[612]. Moreover, injection of a miR-210 vector into infarcted mouse hearts reduced the percentage of $TUNEL^+$ cardiomyocytes[243]. We did not investigate the factor/s responsible for this anti-apoptotic effect of miR-210-transfected CT secretome in our experiment. It may be due to the secretion of miR-210 itself or the effect of other proteins or genetic material that may have been upregulated in the CT secretome.

An interesting observation was that miR-210 transfection had a positive impact on CT conditioned media under normoxia but not hypoxia as assessed by both HUVEC proliferation and HL-1 cardiomyocyte apoptosis. This is consistent with the results of the growth factor array where no significant increase in the secretion of any of the factors was detected under hypoxia. It is unclear why miR-210 may lose its effect on CT paracrine potential under hypoxia in comparison to normoxia. It may be due to the activation of hypoxia targets involved in angiogenesis and cell survival that attenuated miR-210 effects. Assessing cell death and

angiogenesis in CT-injected infarcted hearts would have been advantageous in examining the effect of miR-210 on the paracrine signalling of CTs in ischaemic tissue. Overall, our results suggest that miR-210 has the potential to enhance the paracrine signalling of CTs.

5.3.3 The effect of miR-210 transfection on CT retention 24 hours post MI

Cell therapy studies often assess cell retention using histological analysis[122,173], *in vivo* imaging[205] or qPCR[192,193,649–651]. All of these methods offer relative assessments of cell retention, though efforts have been made to develop strategies of measuring absolute cell numbers[193]. Most quantitative studies use qPCR to detect Y chromosome sequences where sex-mismatched cells are transplanted and their retention is extrapolated based on standard curves generated by serial dilutions of male genomic DNA[192,649]. The same principle applies to studies using the transplantation of human cells in animal models to assess cell retention[650,651]. Initially, we aimed to deliver miR-210 using NP170s, which can be tracked noninvasively by MRI and thus provide a relative evaluation of cell retention based on image intensity. However, as described in chapter 4, we were unable to use NP170s to overexpress miR-210 in CTs. In this study, cell retention was quantified using a flow cytometric approach where EGFP was used as a reporter for the transplanted CTs. The numbers reported were therefore the percentage of $EGFP^+$ CTs relative to the total of number of cells generated by single-cell dissociation of the heart. This is similar to a study that used flow cytometry to show improved cardiac cell retention with the use of curved, rather than straight, needles for cell injection[652].

Although we observed an anti-apoptotic effect of miR-210 in CTs *in vitro*, we did not find a significant increase in the retention of miR-210-transfected CTs *in vivo* in a mouse MI model. As we did not examine cell death *in vivo*, we could not ascertain any improvement in the viability of miR-210-transfected CTs post-transplantation. Cell retention was assessed at 24 hours as studies have reported that the majority of cells are lost within the first day either due to cell death or simply due to leakage during the injection or washout through circulation[191].

For example, a study reported that only 60% of transplanted cells were retained immediately following injection into recipient hearts[192]. One study reported that more than 75% of KIT^+ cells were lost within the first 24 hours after intramyocardial injection[193], although other groups reported even higher cell loss at 24 hours following transplantation of KIT^+ cells[194]. These reports also highlight the necessity for the development of strategies to enhance cell survival and retention, which is what we aimed to achieve in this study.

It may be argued that targeting cell death pathways in transplanted cells is not sufficient to combat the low survival observed in cell therapy and a combinatorial framework is needed where both cell death and cell loss are addressed. However, the use of anti-apoptotic miRNAs as a pro-survival strategy in cell therapy has been reported and shown to be an effective tool[205,242]. We observed a variability in a number of factors in our experiment which may have affected our outcome measures. There was considerable variability in MI development by LAD ligation as inferred by both the echocardiography measurements and serum cTnI levels. Unfortunately, this is not unusual in studies using the LAD occlusion method to induce MI. The environment of the host tissue can be a determinant of the fate of transplanted cells and the degree of cardiac injury has been shown to have an effect on cell retention[653,654]. This may be attributed to hypoxia which has a role in inducing growth factors implicated in cell trafficking and homing[202], or other factors such as inflammation and ECM activation which may affect cell homing and angiogenesis[654,655]. A variability in the cell numbers resulting from the heart dissociations and their viability, as indicated by Zombie Violet staining, was also observed. Although we tried to avoid that by using a standard dissociation kit, there was still some variation. Moreover, variability in the performance of the injection is inevitable. We therefore aim to increase animal numbers to reduce the possible effect of variables on our outcome measures.

CHAPTER 6

Conclusion

6 Conclusion

Cardiac cell therapy emerged about two decades ago with the hope to regenerate cardiac muscle following MI by replacing dead muscle tissue with *de novo* cardiomyocytes[112,656]. Various types of CPCs or cardiac stromal populations have been investigated and were shown to be effective in improving cardiac function in animal MI models. However, a lack of long-term retention and ability to generate *de novo* cardiomyocytes were also described. Despite this, and due to the mountain of evidence showing a therapeutic effect in pre-clinical studies, CPCs entered clinical trials and demonstrated safety. However, less consistency in the beneficial effect of CPCs was observed in clinical trials, especially as phase III data are lacking (see Introduction 1.4). Moreover, more recent evidence cast doubt on the identity of these cells as progenitors by showing that most adult mammalian cardiomyocyte renewal is achieved via cardiomyocyte proliferation rather than a progenitor cell type[40,186–189]. The therapeutic effect of these CPC populations has been attributed to paracrine signalling that can have anti-apoptotic, pro-angiogenic, anti-inflammatory and anti-fibrotic roles[657].

In this study, we attempted to investigate the identity of cardiac stromal populations isolated using different protocols from adult mouse hearts. These included the well-established CDCs, a slowly adhering population of unsorted cells isolated using a collagenase and trypsin protocol developed by our group (CTs), and a purchased CF population. This is the first study, to our knowledge, that examines the transcriptional profile of CDCs at the single-cell level. We demonstrated that CTs and CDCs showed expression of cardiogenic transcription factors, which can contribute to cardiac repair[281]. Our findings suggest that all three populations resembled a cardiac fibroblast phenotype with CTs being more closely related to CDCs than CFs and that CTs and CDCs appeared more homogenous than CFs. CTs were enriched for *Tcf21* and the macrophage-associated genes *Mrc1* and *Csf1r* and an interesting polarisation between *Tcf21* and *Tbx5* was observed. However, CTs started to more closely resemble CDCs

at later passages. Hybrid mesenchymal phenotypes have been previously described where fibroblast-associated genes are expressed in minor subpopulations of macrophages[283]. Macrophages have been shown to directly deposit collagen and contribute to fibrosis in both zebrafish and mouse hearts following injury[658]. It is unclear whether fibroblast subsets have the ability to upregulate macrophage-associated genes, which is the more likely scenario in CTs due to the lack of *Cd45* expression. It is therefore of interest to verify *Mrc1* and *Csf1r* expression in freshly isolated CTs to determine if this upregulation is a caveat of *in vitro* culture and to further investigate this *in vivo*. Furthermore, a transcriptional gradient was revealed highlighting the heterogeneity of cardiac fibroblasts which may reflect functional heterogeneity and how the isolation protocol may enrich for specific cell subpopulations even within the fibroblast population. This was reflected on their secretion of growth factors. Although all three populations showed a similar pattern in their secretion of the tested growth factors, differences in the levels of certain factors were detected between populations. Moreover, we found that CTs were more robust than CFs in response to *in vitro* serum starvation, which may be a reflection of their gene expression profile as a modest separation in clustering was revealed. This may be an indication of their *in vivo* behaviour following transplantation.

It may be argued that the gene expression profile of the cells may ultimately affect their therapeutic potential. However, studies comparing the therapeutic benefit of different CPC or cardiac stromal populations are lacking. In cell therapy, the optimal cell population would be a safe and robust population that is capable of exerting a therapeutic effect and can be isolated and expanded in a time- and cost-effective manner. Cardiac stromal populations have proven to be safe as no adverse effects directly linked to them have been reported in clinical trials of cardiac disease (see Introduction 1.4). Although PSC-derived cells have also provided a promising source, there are concerns about their safety due to possible tumourigenicity and

increased risk of arrythmias, as well as the need for long-term immunosuppression in the case of embryonic stem cells[659–662]. The use of PSCs also comes with the added cost of *in vitro* differentiation into a cardiac phenotype, as well as purification to eliminate undifferentiated cells that increase the risk of tumourigenicity[662]. Moreover, it has been argued that, as observed with stromal populations, the therapeutic benefit following transplantation of PSC-derived cells is attributed to paracrine mechanisms[663,664] and that they demonstrate a similar lack of long-term retention[662,663,665,666]. To address suboptimal retention of PSC-derived cardiomyocytes, co-transplantation with cardiac stromal cells such as epicardial cells[173] and biomaterials such as engineered heart tissue patches have been utilised. However, these patches also come with limitations including the lack of electromechanical coupling and insufficient vascularisation within the patch[667].

Although CTs secreted lower levels of certain growth factors in comparison to the CDCs and CFs, we showed that the CT protocol generated a population that resembled the already established CDCs in their gene expression profile and that they both expressed cardiogenic transcription factors at a higher level compared to CFs. CTs also demonstrated higher robustness *in vitro* compared to CFs. These findings, in addition to data from previous group members showing that the CT protocol is less variable in cell yield and expansion time compared to CDCs, suggested that the CTs possess characteristics of a promising cell type for therapy. An *in vivo* functional study is required to assess the utility of CTs as a therapeutic population for transplantation following MI.

In an effort to address the reduced retention of cells following transplantation, I investigated miR-210 as a pro-survival miRNA to overexpress in our population of our interest, the CTs. We found that miR-210 has an anti-apoptotic effect in CTs under serum starvation. I also attempted to understand additional mechanisms by which miR-210 may exert its pro-survival effect by examining mitophagy. Our results suggested a role for miR-210 in downregulating

mitochondrial autophagy and fission. However, it remains unclear if this is linked to the pro-survival role of miR-210 as it may be a distinct function to induce a metabolic switch. There are studies that implicated miR-210 in macroautophagy[554,598], direct targeting of *Bnip3* to repress its apoptotic functions[587,588], increasing mitochondrial ATP levels and membrane potential[589], and in inducing *Hif1α* expression[549] and repressing mitochondrial metabolism[255,548,600,601], which represent conflicting roles for miR-210. Our findings, in addition to these studies, highlight the necessity to further decipher the relationship between miR-210, HIF1α and hypoxia as evidence suggests that miR-210 does not always behave as a typical hypoxia miRNA. Whether or not the induced upregulation in mitochondrial dynamics by miR-210 is beneficial to the survival potential of transplanted CTs in ischaemic heart tissue may be revealed by *in vivo* CT cell survival and retention studies. It is of interest to further examine the role of miR-210 in regulating mitophagy *in vivo* using the previously described miR-210 gain-[261] or loss-of-function[256] mouse models. These models also represent useful tools to assess the function of miR-210 in MI and other ischaemic diseases. Moreover, consistent with its pro-survival effect, our data suggest that miR-210 was capable of partially rescuing the gene expression profile of CTs that shifted following serum starvation. miR-210 also had an effect on the expression of *Pdgfrβ* and *Tbx20* but there is no conclusive evidence to suggest a shift in the cell identity of CTs with miR-210 transfection as examining a wider array of genes is required to determine that.

We also utilised growth factor arrays and indirect co-culture systems with HL-1 cardiomyocytes and HUVECs to investigate the ability of miR-210 to enhance the paracrine potential of CTs. miR-210 was found to improve CT paracrine function by inducing SCF, IGF-1 and IGFBP-2 secretion and to enhance the pro-survival and pro-angiogenic effect of CT conditioned media. All of the above findings suggest an encouraging use of miR-210 as a conditioning agent for cardiac cell therapy (figure 6.1). Finally, we tested the ability of miR-

210 to enhance the retention of CTs *in vivo* in a mouse MI model but unfortunately did not find a significant improvement. This may be attributed to the variability in infarct size, cell numbers resulting from the heart dissociations for flow cytometry and their viability, and the performance of the injection. We are therefore planning to increase animal numbers soon to reduce the possible effect of variables on our outcome measures.

In conclusion, this study provides insights into the identity of cardiac stromal populations isolated from the adult mouse heart without sorting, the use of miR-210 to enhance the therapeutic potential of such populations for transplantation following cardiac injury, and the relationship between miR-210 and mitophagy that open the door for further studies to uncover the behaviour of miR-210 as an hypoxia miRNA.

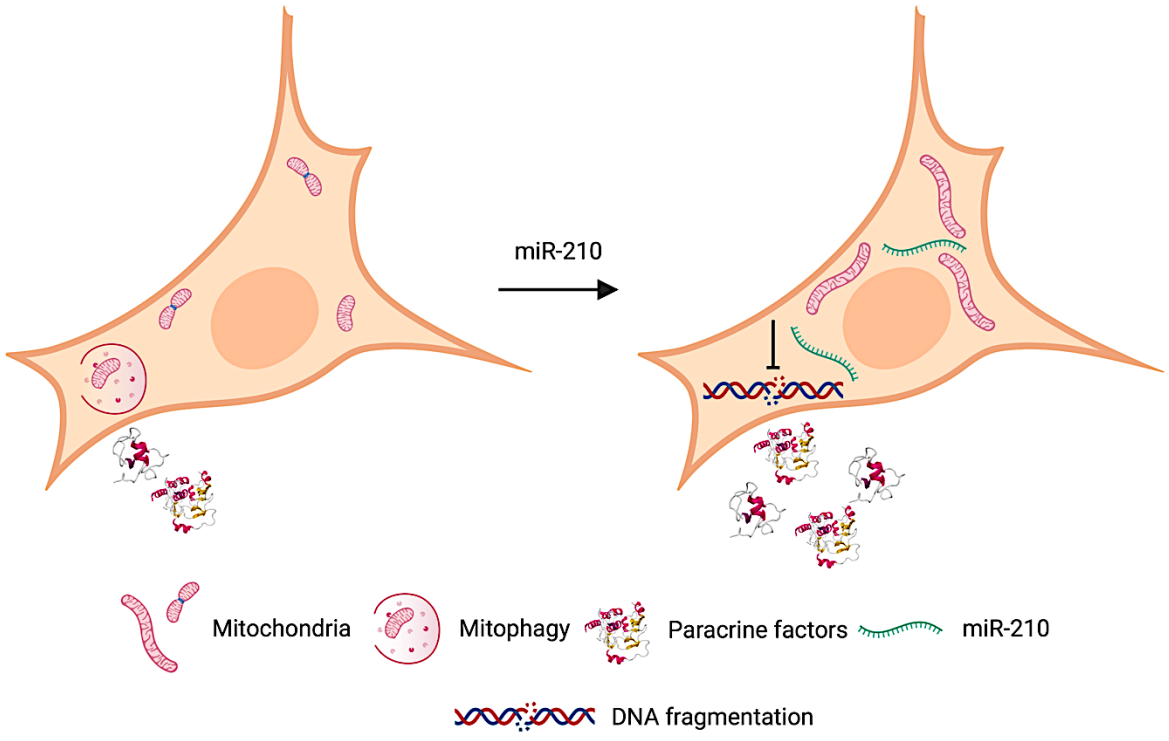


Figure 6.1 Overview of the effect of miR-210 overexpression on CTs

miR-210-transfected CTs showed downregulated apoptosis and mitochondrial autophagy and fission, as well as enhanced paracrine potential.

6.1 Study limitations and challenges

As with any research project, we faced some challenges that limited the scope of our study. Additional analysis of our single-cell qRT-PCR is required. Directly comparing passage 3 to passage 7 CTs would give us more understanding of the changes that occurred during passaging. As the CFs were purchased, we faced the limitation of only using technical replicates in our experiments rather than biological replicates. Moreover, we had technical difficulties with the R script for the analysis of the single-cell qRT-PCR data which resulted in the exclusion of some markers, such as smooth muscle cell markers and *Kit*, but we are currently trying to resolve them. In this study, we performed single-cell qRT-PCR rather than single-cell RNA sequencing as it is relatively more affordable. Single-cell RNA sequencing may have provided us with more conclusive characterisation of the three stromal cell populations as it would have allowed us to examine a much wider range of genes.

If time allowed, I would have liked to follow up on miR-210 overexpression in CTs using the NP170s or retroviral transduction as these would have given us the advantage of tracking the cells *in vivo* or stable overexpression, respectively. Additional treatment groups such as CTs transfected with an anti-miR-210 miRNA inhibitor to study the effect of miR-210 loss of function on apoptosis, mitophagy and CT retention in infarcted hearts would have complemented our study. Moreover, I tried to visualise autophagosomes engulfing mitochondria using LC3 as a marker. However, this was not achievable. Therefore, I would have liked to visualise autophagosomes engulfing mitochondria using electron microscopy to assess if this is reduced in miR-210-transfected CTs and corroborate our other data. Moreover, it would complement our story to have metabolic measurements of CTs transfected with either miR-210 or a negative miRNA under hypoxic culture. Unfortunately, that was not possible as an hypoxic incubator was not available in our radioactivity lab and I tried to locate a Seahorse machine that is enclosed in an hypoxia chamber but none were available for use at the time. In

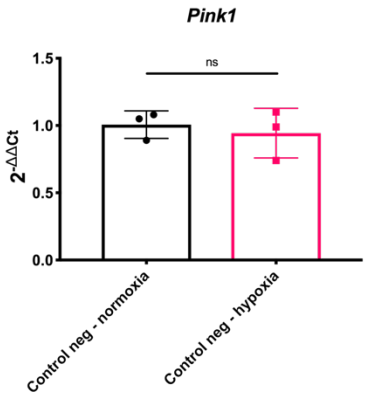
chapter 4, the majority of our data is assessing transcript levels of genes associated with mitophagy and hypoxic signalling to show a role for miR-210 in downregulating mitophagy. We realise that transcript levels do not always predict protein levels and ideally measuring protein levels in addition to our qRT-PCR results would have been more robust. However, other assessments such as mitochondrial copy number, MitoTracker Red CMXRos retention and glucose oxidation rates were consistent with our mRNA data. Moreover, changes in transcript levels of genes associated with mitophagy and hypoxic signalling in response to hypoxic culture were consistent with published studies which was reassuring in terms of using qRT-PCR. Other studies have used *Pink1* and *Atg* transcript levels as an assessment of mitophagy and showed changes that were concordant with other measures such as PINK1 protein levels, PINK1 co-localisation with mitochondria, imaging of autophagosomes engulfing mitochondria using electron microscopy, and autophagic flux using LC3-II reporters[668–670]. Gómez-Sánchez *et al*. showed that *Pink1* transcript levels increased following treatment with the mitochondrial uncoupler CCCP in a duration-dependent manner[671]. I believe that having bulk transcriptomic and/or proteomic data from CTs transfected with either miR-210 or a negative miRNA may have possibly given us more understanding of the relationship between miR-210, hypoxia and mitophagy.

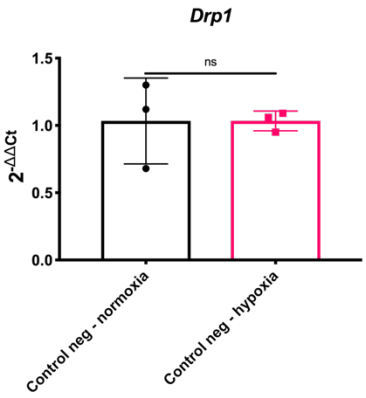
Our study was also limited by the use of the HL-1 cardiomyocyte cell line and HUVECs. Both cell types were more affordable and accessible than other alternatives. However, the use of primary cardiomyocytes in the single cell qRT-PCR experiment would have avoided the obstacle that we faced of some aberrant gene expression (e.g. *Kdr*, *Acta2* and *Vim* expression) and potential phenotypic drift and genomic instability. Primary adult ventricular cardiomyocytes would have served as a better cell model in the co-culture experiment since they are more representative of the myocardium injured following MI. Although HL-1 cardiomyocytes have been widely used for the analysis of mechanisms behind cardiac I/R

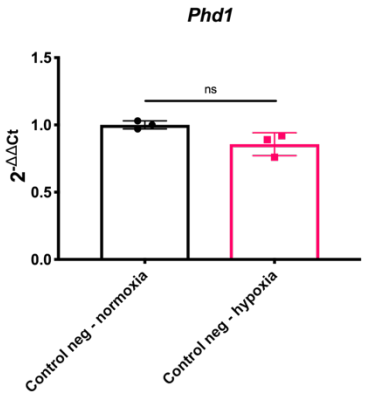
injury[299], they are atrial, resemble an embryonic phenotype[267] and have been shown to be more resistant to hypoxia and oxidative stress compared to H9c2 cells, an embryonic rat ventricular cardiomyocyte line[299]. Furthermore, HUVECs are widely used in angiogenesis assays due to their relative accessibility and their highly proliferative phenotype[672]. The use of mouse primary cardiac endothelial cells would have been a better representation of the *in vivo* setting. Finally, we faced challenges optimising LAD ligation, cell injections and heart dissociations. Although this was overcome eventually, it delayed the timeline of our *in vivo* study and obliged us to constrict it to examining cell retention alone. Ideally, we wanted to examine cell retention in more mice and to perform a long-term study, using MRI to examine cardiac function and infarct size, to see if CTs have a therapeutic effect following MI and if improvement in cell retention by miR-210 transfection would have increased that therapeutic effect. Moreover, due to the observed positive impact of miR-210 on the paracrine potential of CTs, it would have been advantageous to corroborate this observation by performing histology on additional CT-injected infarcted hearts to image cell death (e.g. using TUNEL assays) and angiogenesis. We could also have included further arms to the study where conditioned medium from neg miRNA- and miR-210- transfected CTs was administered rather than the cells themselves.

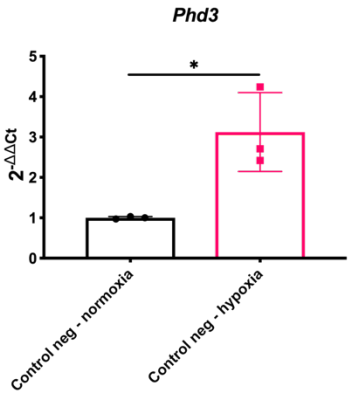
7 Appendices

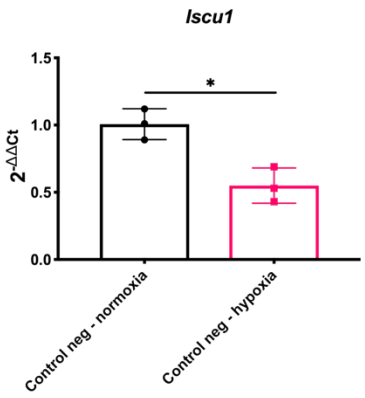
Appendix A. Supplementary results and figures

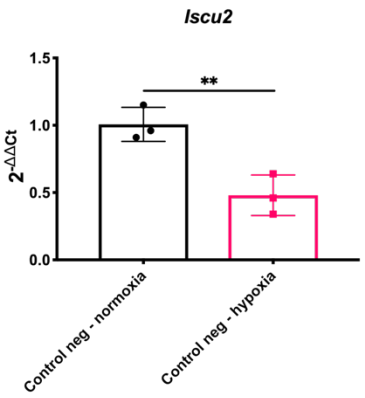


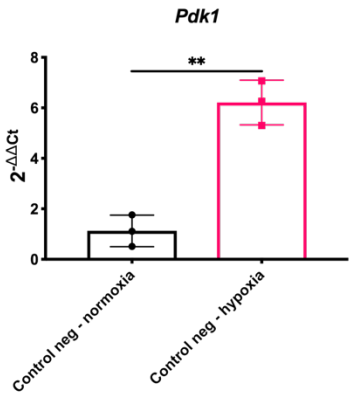


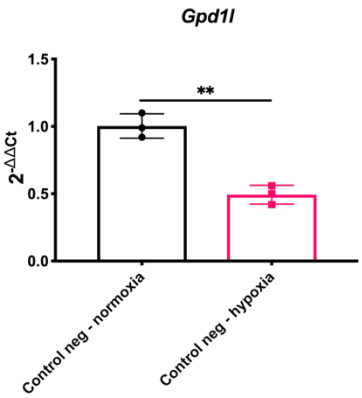






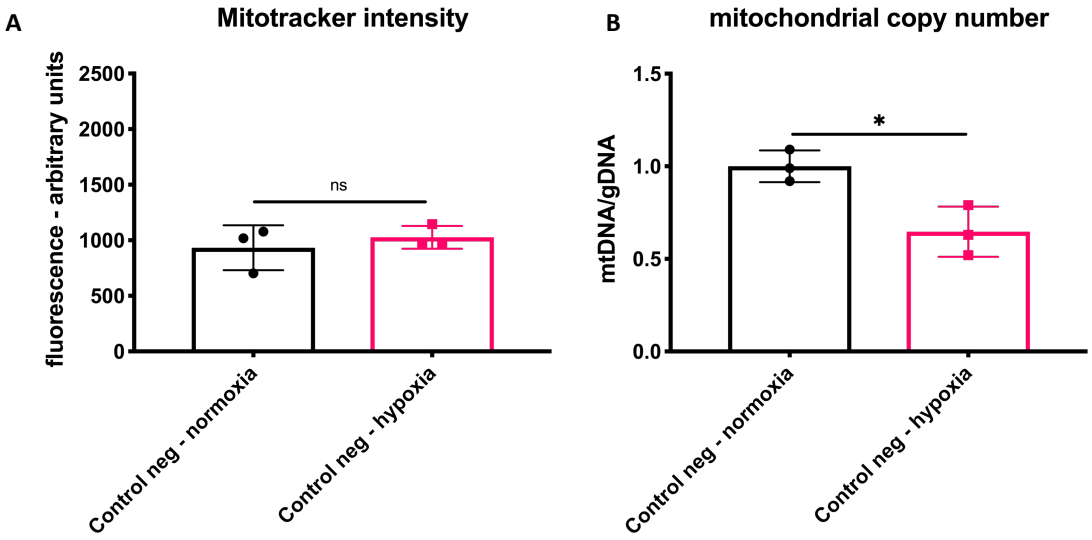






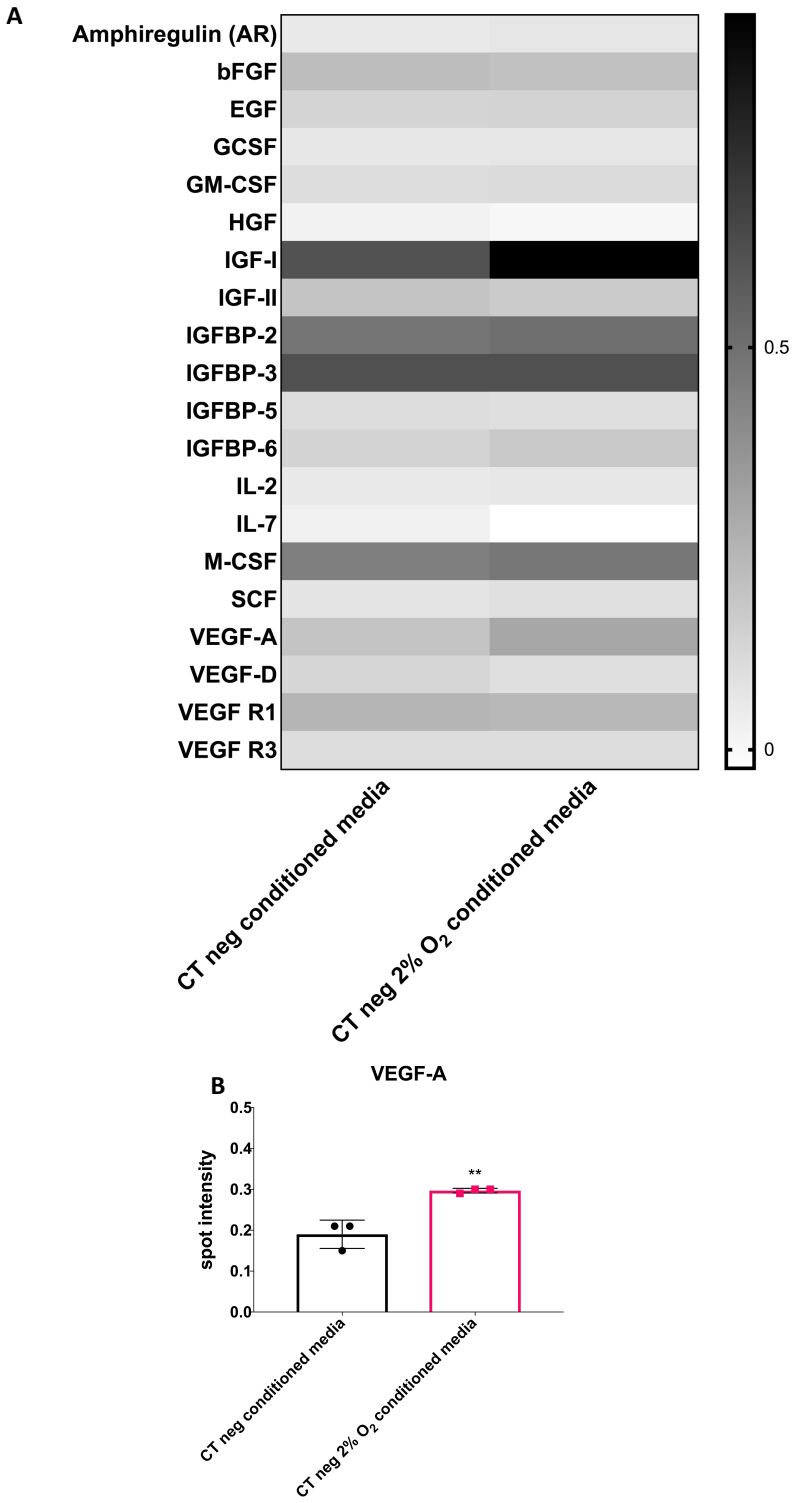
Supplementary figure 1 mRNA levels of additional mitophagy- and hypoxia-associated genes in CTs cultured in hypoxia

mRNA levels of additional mitophagy- and hypoxia-associated genes in CTs transfected with a negative miRNA and cultured in hypoxia, in comparison to CTs transfected with a negative miRNA and cultured in normoxia. The data are recycled from previous figures and were therefore added to the appendix. Analysed using a t-test to determine statistical significance (n=3).



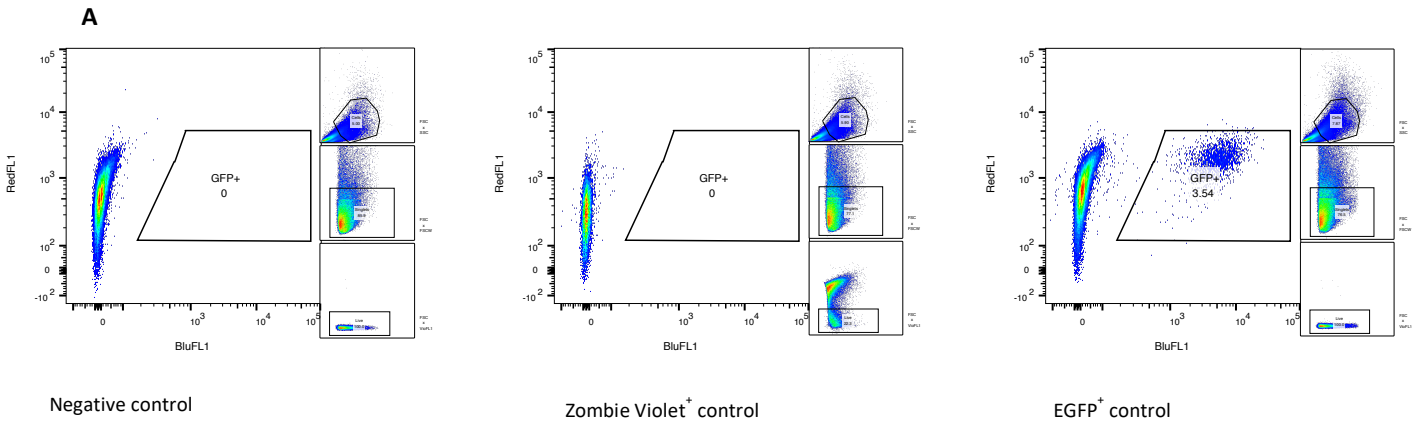
Supplementary figure 2 Mitotracker retention and mitochondrial copy number in CTs cultured in hypoxia

(A) Quantification of the Mitotracker fluorescence intensity (described in Methods 2.12) and **(B)** Mitochondrial copy number (mitochondrial DNA/ genomic DNA) in CTs transfected with a negative miRNA and cultured in hypoxia, in comparison to CTs transfected with a negative miRNA and cultured in normoxia. The data are recycled from previous figures and were therefore added to the appendix. Analysed using a t-test to determine statistical significance (n=3).



Supplementary figure 3 Growth factor array on the conditioned media of CTs cultured in hypoxia

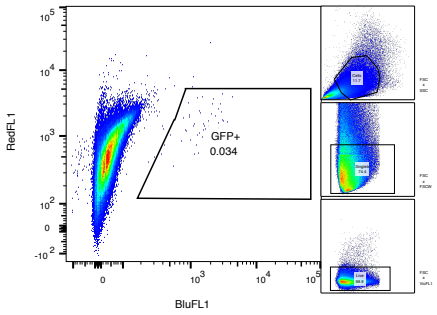
The secretion of 20 growth factors was assessed in the conditioned media of CTs transfected with a negative miRNA and cultured in hypoxia, in comparison to CTs transfected with a negative miRNA and cultured in normoxia using an array. Spot intensity of the samples was normalised to the average of the positive control spots of each array. **(A)** The heatmap illustrates spot intensity (white is low or absent; black is high). **(B)** Individual representation of growth factors that were significantly differentially secreted. The data are recycled from previous figures and were therefore added to the appendix. Analysed using a t-test to determine statistical significance (n=3).



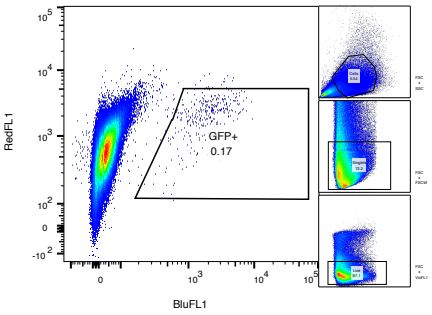
Supplementary figure 4 Flow cytometry plots of data assessing effect of miR-210 transfection on CT retention in MI hearts

Flow cytometry plots showing the gating strategy of **(A)** the negative and single-colour flow controls **(B)** $EGFP^+$ CTs transfected with a negative miRNA **(C)** $EGFP^+$ CTs transfected with miR-210.

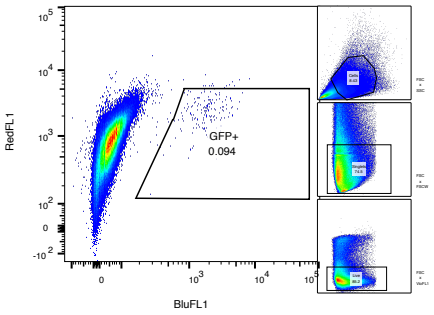
B



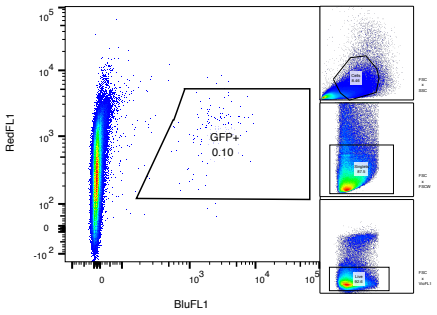
Mouse 1 25-JUN



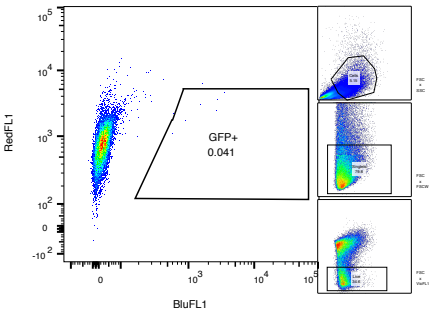
Mouse 1 04-JUL



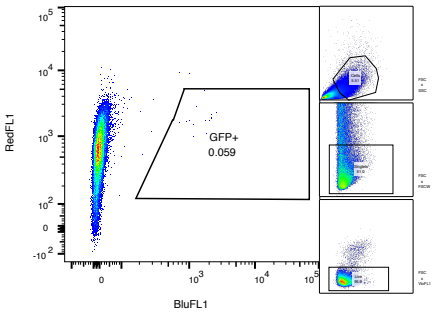
Mouse 30 04-JUL



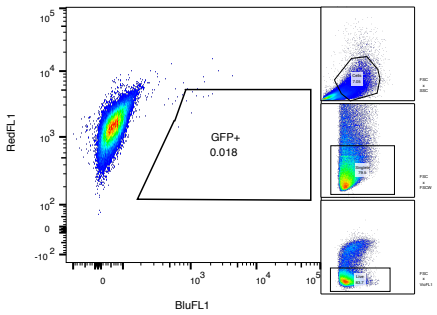
Mouse 10 08-JUL



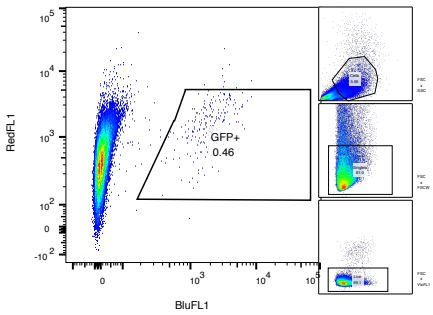
Mouse 1 23-SEP



Mouse 1 25-SEP

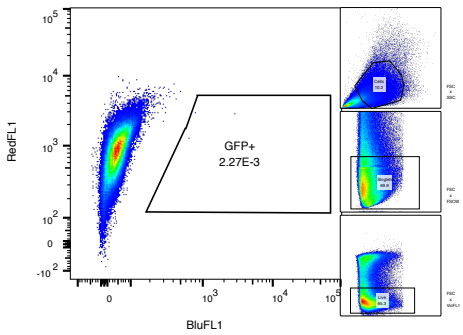


Mouse 30 23-SEP

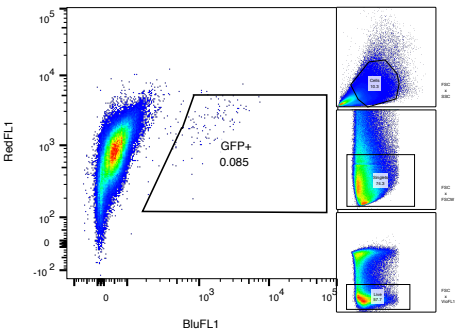


Mouse 30 25-SEP

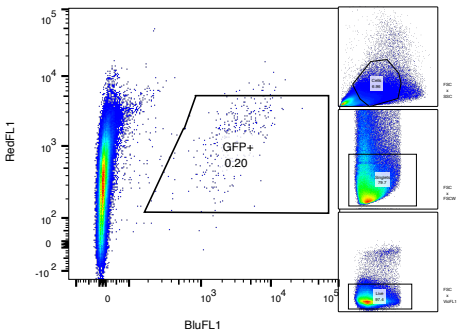
C



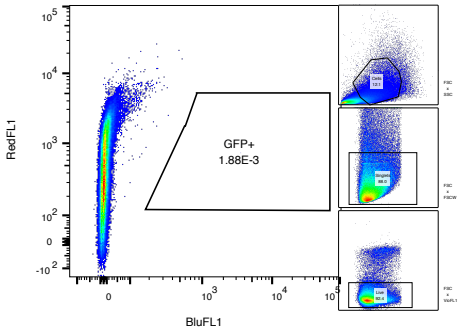
Mouse 3 04-JUL



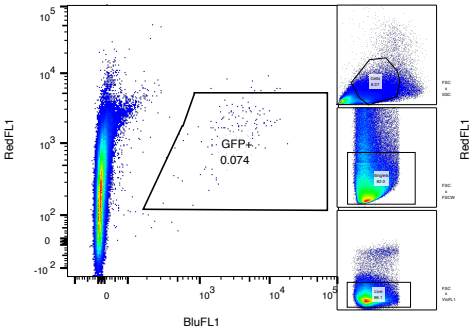
Mouse 10 04-JUL



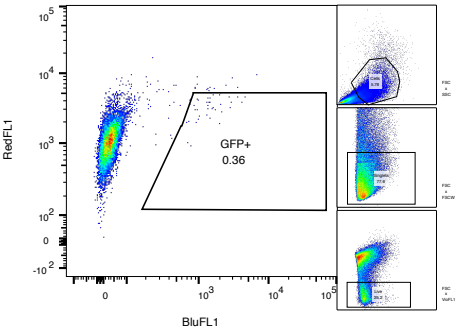
Mouse 3 08-JUL



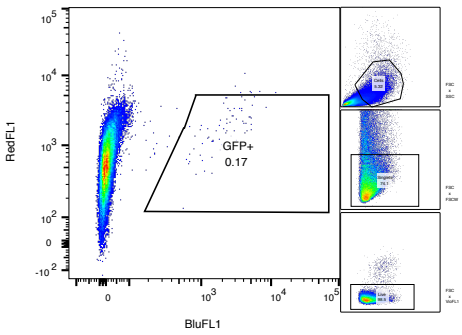
Mouse 30 08-JUL



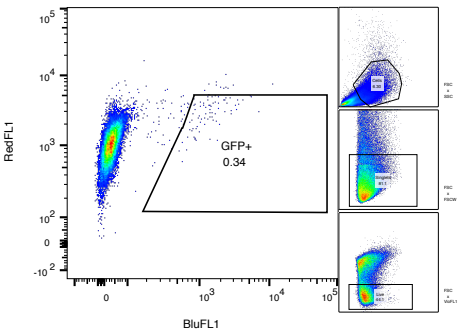
Mouse NC 08-JUL



Mouse 3 23-SEP



Mouse 3 25-SEP



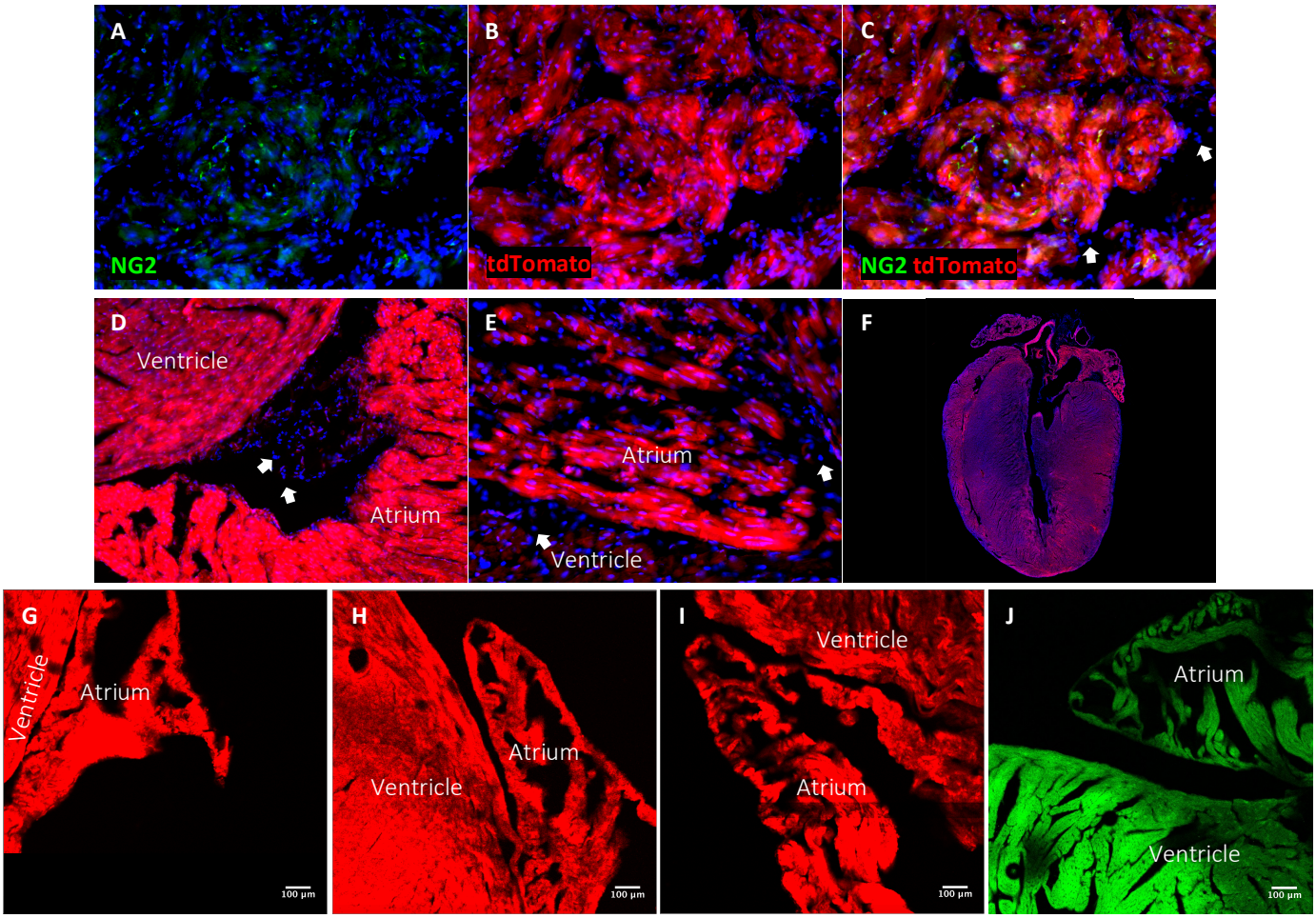
Mouse 10 23-SEP

Imaging of a Sarcolipin$^{Cre/+}$; R26R-tdTomato and Sarcolipin$^{Cre/+}$; R26R-EYFP mouse models

Sarcolipin (SLN) is a sarco(endo)plasmic reticulum (SR) membrane protein that is detected in atrial cardiomyocytes but undetectable in the ventricles of the mammalian heart[673,674]. *Sln* is also expressed in skeletal muscle[673]. Although an ISL1$^+$/SLN$^+$ progenitor cell population has been described in mouse embryos[674], whether or not *Sln* is expressed in stromal cell types in the atria of adult mouse hearts is still unknown. Therefore, we attempted to determine the co-expression of stromal cell markers with *Sln* by imaging the atria of *Sln$^{Cre/+}$; R26R-tdTomato* mice. The *Sln$^{Cre/+}$* mouse line was generated by Nakano *et al*.[264] by inserting *Cre* into the endogenous *Sln* locus by homologous recombination. Since heterozygous deletion of *Sln* maintains normal cardiac function[675], *Sln$^{Cre/+}$* can be utilized for atrium-specific gene targeting. The overarching aim of using this mouse model was to determine whether atrial stromal populations migrate to the site of injury following MI as it has been noted that KIT$^+$ and SCA1$^+$ populations preferentially distribute to the atria in comparison to the ventricles[291–293]. The mobilisation of KIT$^+$ cells to the injury site had been previously shown following growth factor administration[334,676].

However, upon imaging of the *Sln$^{Cre/+}$; R26R-tdTomato* mouse model, we found that the ventricles appeared red in the mouse model. We assumed that this was because tdTomato is an exceptionally bright red fluorescent protein[677] and might have reflected very low expression of *Sln*. Although some tdTomato$^-$ cells were detected as evident by DAPI staining, cells positive for NG2 appeared to be positive for tdTomato. NG2$^+$ cells were mostly perivascular consistent with a pericyte phenotype. We therefore repeated the imaging using an *R26R-EYFP* reporter line as previously described[678,679]. Despite this, we found that the EYFP was not specific to the atria (supplementary figure 5). The lack of specificity was surprising to us as atrial localisation was described in heart sections of adult and neonate *Sln$^{Cre/+}$; CAG-DsRed* mice as well as

neonate *Sln*$^{Cre/+}$*; R26R-EYFP* mice[679,680]. We decided not to investigate this further due to time constraints. Phenotypic inconsistencies in transgenic mouse models may be attributed to the genetic background[681]. However, all the *Sln*$^{Cre/+}$ studies were performed on a C57BL/6 background. Other considerations include genetic contamination, which may arise via a breeding error, and genetic drift, which describes the spontaneous arising of mutations in mouse colonies[682].



Supplementary figure 5 Imaging of heart sections in a *Sln*$^{Cre/+}$ mouse model

(A-J) Imaging of an adult *Sln*$^{Cre/+}$*;* R26R-tdTomato mouse model, representative of n=5. A-C shows atrial sections stained with an anti-NG2 antibody and DAPI, C is an overlay of A and B. D shows the atrioventricular groove stained with DAPI. E, H, I and J show the atrial appendage and the underlying ventricle stained with DAPI. F shows a whole heart section stained with DAPI. G shows CTs isolated from the mouse model. **(K)** Heart section of an adult *Sln*$^{Cre/+}$*; R26R-EYFP* mouse model, representative of n=3. Cells negative for tdTomato are highlighted by white arrows. A to G were imaged using a Leica DM6000 epifluorescent microscope whereas H to K were imaged using an FV1000 confocal microscope.

Appendix B. Immunochemistry antibodies

Antibody	Catalogue number	Host species	Dilution
PDGFRβ	Ab32570	rabbit	1:100
WT1	Ab89901	rabbit	1:50
Vimentin	Ab45939	rabbit	1:1000
CD44	Ab25340	rat	1:100
αSMA	Ab32575	rabbit	1:500
αSA	A7811	mouse	1:500
Cardiac troponin T	Ab8295	mouse	1:200
MYL2	Ab79935	rabbit	1:140
MYH6	Ab207926	mouse	1:100
HIF1α	NB100-105	mouse	1:50
HIF1α	Ab216842	rabbit	1:100
Cytochrome c	Ab13575	mouse	1:250
LC3B	NB100-2220	rabbit	1:150
Alexa Fluor 488	A-11006	goat anti-rat	1:200
Alexa Fluor 568	A-11011	goat anti-rabbit	1:200
Alexa Fluor 488	A-21202	donkey anti-mouse	1:200
Alexa Fluor 568	A-11004	goat anti-Mouse	1:200

Appendix C. SYBR green primer sequences

Target	Forward sequence	Reverse sequence	Reference
Hprt	TCAGTCAACGGGGGACATAA	GGGGCTGTACTGCTTAACCAG	[273]
Atg4c	GGAGCCTCTCTCGATTCTGC	CCAATATAAGTTCAAAGGGCGAGG	Designed. NCBI Reference Sequence: NM_001145967.1
Atg7	TGGAGTTCAGTGCTTTTGAC	GGTGTTGTGCAGGGTTCC	[683]
Bnip3	CAGCATGAATCTGGACGAAG	ATCTTCCTCAGACAGAGTGC	[684]
Casp8ap2	GATGTCTGTCCTGCCTCTCC	AACAGCACTGTCCAACCCAG	Designed. NCBI Reference Sequence: NM_001122978.2
Drp1	ATGCCAGCAAGTCCACAGAA	TGTTCTCGGGCAGACAGTTT	[685]
Gpd1l	CGGGCTGAAGCTAATCTCCG	TTGCTGCCAATGGTGGTCTC	Designed. NCBI Reference Sequence: NM_175380.5
Hif1α	GGTTCCAGCAGACCCAGTTA	AGGCTCCTTGGATGAGCTTT	[686]
Iscu1	ACCACAAGAAGGTTGTGGATCA	CACCAATCCGGTTCCAACAT	Designed. NCBI Reference Sequence: NM_025526.5

Iscu2	CGAACCATCGAGGGGACC	CATAATGATCCACAACCCGGAC	Designed. NCBI Reference Sequence: NM_001363317.1
Nix	CCTCGTCTTCCATCCACAAT	GTCCCTGCTGGTATGCATCT	687
Pdk1	GGCGGCTTTGTGATTTGTAT	ACCTGAATCGGGGGATAAAC	686
Phd1	TTGCCTGGGTAGAAGGTCAC	GCTCGATGTTGGCTACCACT	686
Phd2	AGCCATGGTTGCTTGTTACC	CTCGCTCATCTGCATCAAAA	686
Phd3	CAACTTCCTCCTGTCCCTCA	GGCTGGACTTCATGTGGATT	686
Pink1	GCTGGTGAGGTCACTGCTC	TCTTCAGGGCTAGAAGATGCTC	668
mt-Nd1	GAGCATCTTATCCACGCTTCC	GGTGGTACTCCCGCTGTAAA	688
B2m	CACAGTTCCACCCGCCTCACA	TGGGCTCGGCCATACTGGCA	688

Appendix D. Taqman probes used for single-cell qRT-PCR

Mesp1	Mm00801883_g1	*Nkx2-5*	Mm00657783_m1
Mef2c	Mm01340842_m1	*Myh11*	Mm00443013_m1
Mef2a	Mm01318990_m1	*Cnn1*	Mm00487032_m1
Hand1	Mm00433931_m1	*αSMA (Acta2)*	Mm01546133_m1
Islet1 (Isl1)	Mm00627860_m1	*Vim*	Mm01333430_m1
Tbx20	Mm00451515_m1	*Cd44*	Mm01277163_m1
Gata4	Mm00484689_m1	*Pdgfrβ*	Mm00435546_m1
Hand2	Mm00439247_m1	*Ng2*	Mm01283063_m1
Tbx5	Mm00803518_m1	*Ddr2*	Mm00445615_m1
Ly6a (Sca1)	Mm00726565_s1	*Medag*	Mm00551008_m1
Kit	Mm00445221_m1	*Ms4a4d*	Mm00656404_m1
Wt1	Mm00460570_m1	*Col1a1*	Mm00801666_g1
Klf4	Mm00516104_m1	*Prg4*	Mm01284582_m1
Pou5f1 (Oct4)	Mm03053917_g1	*Wif1*	Mm00442355_m1
Nanog	Mm02019550_s1	*Colec11*	Mm01289834_m1
Tert	Mm0352136_m1	*Kcnj8*	Mm00434620_m1
Kdr	Mm00440111_m1	*Mrc1*	Mm01329362_m1
Cdh5	Mm00486938_m1	*Cx3cr1*	Mm00438354_m1
Vwf	Mm00550376_m1	*Csf1 r*	Mm01266652_m1
Pdgfra	Mm01211685_m1	*Kcna1*	Mm00439977_s1
Tcf21	Mm00448961_m1	*Plp1*	Mm01297210_m1
Myl2	Mm00440384_m1	*Ptprc (Cd45)*	Mm01293577_m1
Myh6	Mm00440359_m1	*Ubc*	Mm01201237_m1
Nppa	Mm01255748_g1	*Hmbs*	Mm01143545_m1

Appendix E. Reagent catalogue numbers

Reagent/ kit	Manufacturer	Cat. number
Collagenase, Type II, Clostridium histolyticum	234155	Merck millipore – Calbiochem
Trypsin-EDTA (0.05%), phenol red	25300-054	ThermoFisher
Fibronectin from bovine plasma	F1141	Sigma-Aldrich
IMDM	21980-032	ThermoFisher
DMEM	11965084	ThermoFisher
DMEM, no glucose	A14430	ThermoFisher
Heat inactivated foetal bovine serum	10500	ThermoFisher
Penicillin-Streptomycin-Glutamine (100X)	10378016	ThermoFisher
Dulbecco's Phosphate Buffered Saline	D8537	Sigma-Aldrich
Primocin	ant-pm-2	InvivoGen
HUVECs in EGM-Plus	CC-2935	Lonza
EGM-Plus Endothelial Cell Growth Media-Plus BulletKit	CC-5035	Lonza
C57BL/6 Adult Mouse Primary Cardiac Fibroblasts (atrial only)	C57-6049	Cell Biologics
Complete Fibroblast Medium	M2267	Cell Biologics
HL-1 Cardiac Muscle Cell Line	SCC065	Sigma-Aldrich
Claycomb Medium	51800C	Sigma-Aldrich
Gelatin from bovine skin type B	G9391	Sigma-Aldrich
L-Ascorbic acid	A7506	Sigma-Aldrich
(±)-Norepinephrine (+)-bitartrate salt	A0937	Sigma-Aldrich
Multi Tissue Dissociation Kit 2	130-110-203	Miltenyi Biotec
DNeasy Blood & Tissue Kit	69504	Qiagen
RNeasy Mini Kit	74104	Qiagen
High-Capacity cDNA Reverse Transcription Kit	4368814	ThermoFisher
SYBR Green Master Mix	4309155	ThermoFisher
Mm_miR-210_2 miScript Primer Assay product no. 218300	MS00032564	ThermoFisher
Hs_SNORD68_11 miScript Primer Assay Product no. 218300	MS00033712	ThermoFisher
miRNeasy Mini Kit	217004	Qiagen
miScript SYBR Green PCR Kit	218073	ThermoFisher
miScript II RT Kit	218160	ThermoFisher
DharmaFECT 1 Transfection Reagent	T-2001-02	Dharmacon
miRIDIAN microRNA Mimic Transfection Control with Dy547	CP-004500-01	Dharmacon
mmu-miR-210-3p mirVana miRNA mimic ID: MC10516	4464066	ThermoFisher
mirVana miRNA Mimic, Negative Control	4464059	ThermoFisher
Silencer Select Pre-Designed siRNA Application Silencer Select Assay Id s63060	4390771	ThermoFisher
Silencer Select Pre-Designed siRNA Application Silencer Select Assay Id s63061	4390771	ThermoFisher

Silencer Select GAPDH Positive Control siRNA	4390849	ThermoFisher
Silencer Select Negative Control No. 2 siRNA	4390846	ThermoFisher
Mouse Growth Factor Array	AAM-GF-2	RayBiotech
High Sensitivity Mouse Cardiac Troponin-I ELISA Kit	CTNI-1-HS	Life Diagnostics
Paraformaldehyde solution 4% in PBS	Sc-281692	Santa Cruz Biotechnology
MitoTracker® Red CMXRos	M7512	ThermoFisher
Click-iT TUNEL Alexa Fluor 594 Imaging Assay	C10246	ThermoFisher
FAM-FLICA Poly-Caspase Assay Kit	ICT091	BIO-RAD
Zombie Violet Fixable Viability Kit	423113	Biolegend
CellsDirect One-Step qRT-PCR Kit	11753100	ThermoFisher
SUPERase	AM2694	ThermoFisher
TE Buffer	12090015	ThermoFisher
One Shot Stbl3 Chemically Competent *E. coli*	C7373-03	ThermoFisher
S.O.C. Medium	15544034	ThermoFisher
QIAprep Spin Miniprep Kit	27104	Qiagen
XhoI	R0146	New England BioLabs
PvuI-HF	R3150	New England BioLabs
CutSmart HF buffer	B7204	New England BioLabs
5x DNA Loading Buffer Blue	BIO-37045	Bioline
HyperLadder 1Kb	BIO-33053	Bioline
NucleoBond Xtra Maxi kit	740414.10	Macherey-Nagel
NucleoBond Finalizer Large Plus kit	740419.20	Macherey-Nagel
FuGENE HD Transfection Reagent	E2311	Promega
OptiMEM Reduced Serum Medium	31985070	ThermoFisher
pmaxGFP Vector	VVCA-1003	Lonza
Triton X-100	T8787	Sigma-Aldrich

8 Bibliography

1. Hammer, A. *Ein Fall von thrombotischem Verschlusse einer der Kranzarterien des Herzens am Krankenbette konstatirt*. (Druck der k. Wiener Zeitung, 1878).
2. Friedberg, C. K. & Horn, H. Acute myocardial infarction not due to coronary artery occlusion. *J. Am. Med. Assoc.* (1939). doi:10.1001/jama.1939.02800170021007
3. Denmark, K. T. *et al.* Fourth universal definition of myocardial infarction (2018). 237–269 (2019). doi:10.1093/eurheartj/ehy462
4. Jennings, R. B. & Ganote, C. E. Structural changes in myocardium during acute ischemia. *Circulation Research* (1974).
5. Virmani, R., Forman, M. B. & Kolodgie, F. D. Myocardial reperfusion injury. Histopathological effects of perfluorochemical. in *Circulation* (1990).
6. Frangogiannis, N. G. Regulation of the inflammatory response in cardiac repair. *Circulation Research* (2012). doi:10.1161/CIRCRESAHA.111.243162
7. Frangogiannis, N. G. The inflammatory response in myocardial injury, repair, and remodelling. *Nature Reviews Cardiology* (2014). doi:10.1038/nrcardio.2014.28
8. Timmers, L. *et al.* The innate immune response in reperfused myocardium. *Cardiovascular Research* (2012). doi:10.1093/cvr/cvs018
9. Willems, I. E. M. G., Havenith, M. G., De Mey, J. G. R. & Daemen, M. J. A. P. The ??-smooth muscle actin-positive cells in healing human myocardial scars. *Am. J. Pathol.* (1994).
10. Frangogiannis, N. G., Michael, L. H. & Entman, M. L. Myofibroblasts in reperfused myocardial infarcts express the embryonic form of smooth muscle myosin heavy chain (SMemb). *Cardiovasc. Res.* (2000). doi:10.1016/S0008-6363(00)00158-9
11. Zeisberg, E. M. *et al.* Endothelial-to-mesenchymal transition contributes to cardiac fibrosis. *Nat. Med.* (2007). doi:10.1038/nm1613

12. Hinz, B. *et al.* The myofibroblast: One function, multiple origins. *Am. J. Pathol.* (2007). doi:10.2353/ajpath.2007.070112

13. Möllmann, H. *et al.* Bone marrow-derived cells contribute to infarct remodelling. *Cardiovasc. Res.* (2006). doi:10.1016/j.cardiores.2006.06.013

14. Ikeuchi, M. *et al.* Inhibition of TGF-β signaling exacerbates early cardiac dysfunction but prevents late remodeling after infarction. *Cardiovasc. Res.* (2004). doi:10.1016/j.cardiores.2004.07.017

15. Fullerton, J. N., O'Brien, A. J. & Gilroy, D. W. Pathways mediating resolution of inflammation: When enough is too much. *Journal of Pathology* (2013). doi:10.1002/path.4232

16. Saga, Y. *et al.* MesP1 is expressed in the heart precursor cells and required for the formation of a single heart tube. *Development* (1999).

17. Van Vliet, P., Wu, S. M., Zaffran, S. & Pucéat, M. Early cardiac development: A view from stem cells to embryos. *Cardiovascular Research* (2012). doi:10.1093/cvr/cvs270

18. Kitajima, S., Takagi, A., Inoue, T. & Saga, Y. MesP1 and MesP2 are essential for the development of cardiac mesoderm. *Development* (2000).

19. Buckingham, M., Meilhac, S. & Zaffran, S. Building the mammalian heart from two sources of myocardial cells. *Nature Reviews Genetics* (2005). doi:10.1038/nrg1710

20. Xin, M., Olson, E. N. & Bassel-Duby, R. Mending broken hearts: Cardiac development as a basis for adult heart regeneration and repair. *Nature Reviews Molecular Cell Biology* (2013). doi:10.1038/nrm3619

21. Tyser, R. C. *et al.* Calcium handling precedes cardiac differentiation to initiate the first heartbeat. *Elife* **5**, 1–25 (2016).

22. Lie-Venema, H. *et al.* Origin, fate, and function of epicardium-derived cells (EPCDs) in normal and abnormal cardiac development. *TheScientificWorldJournal* (2007).

doi:10.1100/tsw.2007.294

23. Samsa, L. A., Yang, B. & Liu, J. Embryonic cardiac chamber maturation: Trabeculation, conduction, and cardiomyocyte proliferation. *Am. J. Med. Genet. Part C Semin. Med. Genet.* (2013). doi:10.1002/ajmg.c.31366

24. Waldo, K., Miyagawa-Tomita, S., Kumiski, D. & Kirby, M. L. Cardiac neural crest cells provide new insight into septation of the cardiac outflow tract: Aortic sac to ventricular septal closure. *Dev. Biol.* (1998). doi:10.1006/dbio.1998.8860

25. Yelbuz, T. M. *et al.* Shortened outflow tract leads to altered cardiac looping after neural crest ablation. *Circulation* (2002). doi:10.1161/01.CIR.0000023044.44974.8A

26. Smith, T. K. & Bader, D. M. Signals from both sides: Control of cardiac development by the endocardium and epicardium. *Seminars in Cell and Developmental Biology* (2007). doi:10.1016/j.semcdb.2006.12.013

27. Olson, E. N. Gene regulatory networks in the evolution and development of the heart. *Science* (2006). doi:10.1126/science.1132292

28. Black, B. L., Molkentin, J. D. & Olson, E. N. Multiple roles for the MyoD basic region in transmission of transcriptional activation signals and interaction with MEF2. *Mol. Cell. Biol.* **18**, 69–77 (1998).

29. Lin, Q., Schwarz, J., Bucana, C. & N. Olson, E. Control of Mouse Cardiac Morphogenesis and Myogenesis by Transcription Factor MEF2C. *Science (80-.).* **276**, 1404 LP – 1407 (1997).

30. Xu, H. *et al.* Tbx1 has a dual role in the morphogenesis of the cardiac outflow tract. *Development* (2004). doi:10.1242/dev.01174

31. Yamagishi, H. *et al.* Tbx1 is regulated by tissue-specific forkhead proteins through a common Sonic hedgehog-responsive enhancer. *Genes Dev.* (2003). doi:10.1101/gad.1048903

32. Takeuchi, J. K. *et al.* Tbx20 dose-dependently regulates transcription factor networks required for mouse heart and motoneuron development. *Development* (2005). doi:10.1242/dev.01827

33. Srivastava, D. Making or Breaking the Heart: From Lineage Determination to Morphogenesis. *Cell* (2006). doi:10.1016/j.cell.2006.09.003

34. Ahuja, P., Sdek, P. & MacLellan, W. R. Cardiac myocyte cell cycle control in development, disease, and regeneration. *Physiological Reviews* (2007). doi:10.1152/physrev.00032.2006

35. Quaini, F. *et al.* End-stage cardiac failure in humans is coupled with the induction of proliferating cell nuclear antigen and nuclear mitotic division in ventricular myocytes. *Circ. Res.* (1994). doi:10.1161/01.RES.75.6.1050

36. Kajstura, J. *et al.* Myocyte proliferation in end-stage cardiac failure in humans. *Proc. Natl. Acad. Sci.* **95**, 8801–8805 (1998).

37. Beltrami, A. P. *et al.* Evidence that human cardiac myocytes divide after myocardial infarction. *N. Engl. J. Med.* (2001). doi:10.1056/NEJM200106073442303

38. Bergmann, O. *et al.* Evidence for Cardiomyocyte Renewal in Humans. *Science (80-.).* **324**, 98–102 (2009).

39. Kajstura, J. *et al.* Cardiomyogenesis in the adult human heart. *Circ. Res.* (2010). doi:10.1161/CIRCRESAHA.110.223024

40. Senyo, S. E. *et al.* Mammalian heart renewal by pre-existing cardiomyocytes. *Nature* (2013). doi:10.1038/nature11682

41. Mollova, M. *et al.* Cardiomyocyte proliferation contributes to heart growth in young humans. *Proc. Natl. Acad. Sci. U. S. A.* (2013). doi:10.1073/pnas.1214608110

42. Poss, K. D., Wilson, L. G. & Keating, M. T. Heart regeneration in zebrafish. *Science (80-.).* (2002). doi:10.1126/science.1077857

43. Kikuchi, K. *et al.* Primary contribution to zebrafish heart regeneration by gata4+ cardiomyocytes. *Nature* (2010). doi:10.1038/nature08804

44. Jopling, C. *et al.* Zebrafish heart regeneration occurs by cardiomyocyte dedifferentiation and proliferation. *Nature* (2010). doi:10.1038/nature08899

45. González-Rosa, J. M. *et al.* Myocardial Polyploidization Creates a Barrier to Heart Regeneration in Zebrafish. *Dev. Cell* **44**, 433-446.e7 (2018).

46. Zhao, L., Ben-Yair, R., Burns, C. E. & Burns, C. G. Endocardial Notch Signaling Promotes Cardiomyocyte Proliferation in the Regenerating Zebrafish Heart through Wnt Pathway Antagonism. *Cell Rep.* **26**, 546-554.e5 (2019).

47. Kikuchi, K. *et al.* Retinoic Acid Production by Endocardium and Epicardium Is an Injury Response Essential for Zebrafish Heart Regeneration. *Dev. Cell* **20**, 397–404 (2011).

48. Puente, B. N. *et al.* The oxygen-rich postnatal environment induces cardiomyocyte cell-cycle arrest through DNA damage response. *Cell* **157**, (2014).

49. Wang, Z. *et al.* Mechanistic basis of neonatal heart regeneration revealed by transcriptome and histone modification profiling. *Proc. Natl. Acad. Sci.* 201905824 (2019). doi:10.1073/pnas.1905824116

50. Aurora, A. B. *et al.* Macrophages are required for neonatal heart regeneration. *J. Clin. Invest.* (2014). doi:10.1172/JCI72181

51. Ito, K. *et al.* Differential reparative phenotypes between zebrafish and medaka after cardiac injury. *Dev. Dyn.* (2014). doi:10.1002/dvdy.24154

52. Stockdale, W. T. *et al.* Heart Regeneration in the Mexican Cavefish. *Cell Rep.* **25**, 1997-2007.e7 (2018).

53. Porrello, E. R. *et al.* Transient regenerative potential of the neonatal mouse heart. *Science (80-.).* (2011). doi:10.1126/science.1200708

54. Haubner, B. J. *et al.* Complete cardiac regeneration in a mouse model of myocardial infarction. *Aging (Albany. NY).* (2012). doi:10.18632/aging.100526

55. Jesty, S. A. *et al.* C-kit + precursors support postinfarction myogenesis in the neonatal, but not adult, heart. *Proc. Natl. Acad. Sci. U. S. A.* (2012). doi:10.1073/pnas.1208114109

56. Strungs, E. G. *et al.* Cryoinjury models of the adult and neonatal mouse heart for studies of scarring and regeneration. *Methods Mol. Biol.* (2013). doi:10.1007/978-1-62703-505-7_20

57. Bryant, D. M. *et al.* A systematic analysis of neonatal mouse heart regeneration after apical resection. *J. Mol. Cell. Cardiol.* (2015). doi:10.1016/j.yjmcc.2014.12.011

58. Warthin, A. S. The myocardial lesions of diphtheria. *J. Infect. Dis.* **35**, 32–66 (1924).

59. Macmahon, H. E. Hyperplasia and Regeneration of the Myocardium in Infants and in Children. *Am. J. Pathol.* (1937).

60. Fratz, S. *et al.* Long-term myocardial scarring after operation for anomalous left coronary artery from the pulmonary artery. *Ann. Thorac. Surg.* (2011). doi:10.1016/j.athoracsur.2011.06.021

61. Haubner, B. J. *et al.* New Hypotheses in Clinical Medicine Functional Recovery of a Human Neonatal Heart After Severe Myocardial Infarction. 216–221 (2016). doi:10.1161/CIRCRESAHA.115.307017

62. Uygur, A. & Lee, R. T. Mechanisms of Cardiac Regeneration. *Developmental Cell* **36**, 362–374 (2016).

63. Goshima, J., Goldberg, V. M. & Caplan, A. I. Osteogenic potential of culture-expanded rat marrow cells as assayed in vivo with porous calcium phosphate ceramic. *Biomaterials* (1991). doi:10.1016/0142-9612(91)90209-S

64. Garikipati, V. N. S. *et al.* Isolation and characterization of mesenchymal stem cells

from human fetus heart. *PLoS One* **13**, e0192244 (2018).

65. Pilato, C. A. *et al.* Isolation and Characterization of Cardiac Mesenchymal Stromal Cells from Endomyocardial Bioptic Samples of Arrhythmogenic Cardiomyopathy Patients. *J. Vis. Exp.* (2018). doi:10.3791/57263

66. Khoury, M., Alcayaga-Miranda, F., Illanes, S. E. & Figueroa, F. E. The promising potential of menstrual stem cells for antenatal diagnosis and cell therapy. *Frontiers in Immunology* (2014). doi:10.3389/fimmu.2014.00205

67. Liu, C., Tsai, A. L., Li, P. C., Huang, C. W. & Wu, C. C. Endothelial differentiation of bone marrow mesenchyme stem cells applicable to hypoxia and increased migration through Akt and NFκB signals. *Stem Cell Res. Ther.* (2017). doi:10.1186/s13287-017-0470-0

68. Oswald, J. *et al.* Mesenchymal Stem Cells Can Be Differentiated Into Endothelial Cells In Vitro. *Stem Cells* (2004). doi:10.1634/stemcells.22-3-377

69. Guo, X. *et al.* Cardiomyocyte differentiation of mesenchymal stem cells from bone marrow: New regulators and its implications. *Stem Cell Research and Therapy* (2018). doi:10.1186/s13287-018-0773-9

70. Karnieli, O., Izhar-Prato, Y., Bulvik, S. & Efrat, S. Generation of Insulin-Producing Cells from Human Bone Marrow Mesenchymal Stem Cells by Genetic Manipulation. *Stem Cells* (2007). doi:10.1634/stemcells.2007-0164

71. Singaravelu, K. & Padanilam, B. J. In vitro differentiation of MSC into cells with a renal tubular epithelial-like phenotype. *Ren. Fail.* (2009). doi:10.1080/08860220902928981

72. Ryan, J. M., Barry, F. P., Murphy, J. M. & Mahon, B. P. Mesenchymal stem cells avoid allogeneic rejection. *J. Inflamm. (Lond).* **2**, 8 (2005).

73. Ankrum, J. A., Ong, J. F. & Karp, J. M. Mesenchymal stem cells: Immune evasive, not

immune privileged. *Nature Biotechnology* (2014). doi:10.1038/nbt.2816

74. Sipp, D., Robey, P. G. & Turner, L. Clear up this stem-cell mess. 8–10

75. Mendicino, M., Bailey, A. M., Wonnacott, K., Puri, R. K. & Bauer, S. R. MSC-based product characterization for clinical trials: An FDA perspective. *Cell Stem Cell* (2014). doi:10.1016/j.stem.2014.01.013

76. Dominici, M. *et al.* Minimal criteria for defining multipotent mesenchymal stromal cells. The International Society for Cellular Therapy position statement. *Cytotherapy* (2006). doi:10.1080/14653240600855905

77. Caplan, A. I. Mesenchymal stem cells: Time to change the name! *Stem Cells Transl. Med.* **6**, 1445–1451 (2017).

78. Yang, D. *et al.* The Relative Contribution of Paracine Effect versus Direct Differentiation on Adipose-Derived Stem Cell Transplantation Mediated Cardiac Repair. *PLoS One* **8**, 1–11 (2013).

79. Rehman, J. *et al.* Secretion of Angiogenic and Antiapoptotic Factors by Human Adipose Stromal Cells. *Circulation* **109**, 1292–1298 (2004).

80. Valina, C. *et al.* Intracoronary administration of autologous adipose tissue-derived stem cells improves left ventricular function, perfusion, and remodelling after acute myocardial infarction. *Eur. Heart J.* (2007). doi:10.1093/eurheartj/ehm426

81. Li, B. *et al.* Adipose tissue stromal cells transplantation in rats of acute myocardial infarction. *Coron. Artery Dis.* (2007). doi:10.1097/MCA.0b013e32801235da

82. Ward, M. R., Abadeh, A. & Connelly, K. A. Concise review: Rational use of mesenchymal stem cells in the treatment of ischemic heart disease. *Stem Cells Transl. Med.* **7**, 543–550 (2018).

83. Smith, C. L., Baek, S. T., Sung, C. Y. & Tallquist, M. D. Epicardial-derived cell epithelial-to-mesenchymal transition and fate specification require PDGF receptor

signaling. *Circ. Res.* (2011). doi:10.1161/CIRCRESAHA.110.235531

84. Mikawa, T. & Gourdie, R. G. Pericardial mesoderm generates a population of coronary smooth muscle cells migrating into the heart along with ingrowth of the epicardial organ. *Dev. Biol.* (1996). doi:10.1006/dbio.1996.0068

85. Fang, M., Xiang, F. L., Braitsch, C. M. & Yutzey, K. E. Epicardium-derived fibroblasts in heart development and disease. *Journal of Molecular and Cellular Cardiology* (2016). doi:10.1016/j.yjmcc.2015.12.019

86. Dettman, R. W., Denetclaw, W., Ordahl, C. P. & Bristow, J. Common epicardial origin of coronary vascular smooth muscle, perivascular fibroblasts, and intermyocardial fibroblasts in the avian heart. *Dev. Biol.* (1998). doi:10.1006/dbio.1997.8801

87. Perez-Pomares, J. M. *et al.* Origin of coronary endothelial cells from epicardial mesothelium in avian embryos. *Int. J. Dev. Biol.* (2002). doi:035083

88. Lighthouse, J. K. & Small, E. M. Transcriptional control of cardiac fibroblast plasticity. *Journal of Molecular and Cellular Cardiology* (2016). doi:10.1016/j.yjmcc.2015.12.016

89. Moore-Morris, T. *et al.* Resident fibroblast lineages mediate pressure overload-induced cardiac fibrosis. *J. Clin. Invest.* (2014). doi:10.1172/JCI74783

90. Von Gise, A. & Pu, W. T. Endocardial and epicardial epithelial to mesenchymal transitions in heart development and disease. *Circ. Res.* (2012). doi:10.1161/CIRCRESAHA.111.259960

91. Haudek, S. B. *et al.* Bone marrow-derived fibroblast precursors mediate ischemic cardiomyopathy in mice. *Proc. Natl. Acad. Sci.* (2006). doi:10.1073/pnas.0608799103

92. Ali, S. R. *et al.* Developmental heterogeneity of cardiac fibroblasts does not predict pathological proliferation and activation. *Circ. Res.* (2014). doi:10.1161/CIRCRESAHA.115.303794

93. Furtado, M. B., Nim, H. T., Boyd, S. E. & Rosenthal, N. A. View from the heart: Cardiac fibroblasts in development, scarring and regeneration. *Development (Cambridge)* (2016). doi:10.1242/dev.120576

94. Porter, K. E. & Turner, N. A. Cardiac fibroblasts: At the heart of myocardial remodeling. *Pharmacology and Therapeutics* (2009). doi:10.1016/j.pharmthera.2009.05.002

95. Vliegen, H. W., van der Laarse, A., Cornelisse, C. J. & Eulderink, F. Myocardial changes in pressure overload-induced left ventricular hypertrophy. A study on tissue composition, polyploidization and multinucleation. *Eur. Heart J.* (1991). doi:10.1093/oxfordjournals.eurheartj.a059928

96. Banerjee, I., Fuseler, J. W., Price, R. L., Borg, T. K. & Baudino, T. A. Determination of cell types and numbers during cardiac development in the neonatal and adult rat and mouse. *AJP Hear. Circ. Physiol.* (2007). doi:10.1152/ajpheart.00514.2007

97. Frangogiannis, N. G. The Functional Pluralism of Fibroblasts in the Infarcted Myocardium. *Circ. Res.* **119**, 1049–1051 (2016).

98. Abrial, M. *et al.* Cardiac fibroblasts protect cardiomyocytes against lethal ischemia-reperfusion injury. *J. Mol. Cell. Cardiol.* (2014). doi:10.1016/j.yjmcc.2014.01.005

99. Woodall, M. C., Woodall, B. P., Gao, E., Yuan, A. & Koch, W. J. Cardiac Fibroblast GRK2 Deletion Enhances Contractility and Remodeling Following Ischemia/Reperfusion Injury. *Circ. Res.* (2016). doi:10.1161/CIRCRESAHA.116.309538

100. Friedenstein, A. J., Petrakova, K. V, Kurolesova, A. I. & Frolova, G. P. Heterotopic of bone marrow. Analysis of precursor cells for osteogenic and hematopoietic tissues. *Transplantation* (1968). doi:10.1097/00007890-196803000-00009

101. Friedenstein, A. J., Chailakhjan, R. K. & Lalykina, K. S. THE DEVELOPMENT OF

FIBROBLAST COLONIES IN MONOLAYER CULTURES OF GUINEA-PIG BONE MARROW AND SPLEEN CELLS. *Cell Prolif.* (1970). doi:10.1111/j.1365-2184.1970.tb00347.x

102. Hematti, P. Mesenchymal stromal cells and fibroblasts: A case of mistaken identity? *Cytotherapy* (2012). doi:10.3109/14653249.2012.677822

103. Friedenstein, A. J., Chailakhyan, R. K., Latsinik, N. V., Panasyvk, A. F. & Keiliss-Borok, I. V. Stromal cells responsible for transferring the microenvironment of the hemopoietic tissues: Cloning in vitro and retransplantation in vivo. *Transplantation* (1974). doi:10.1097/00007890-197404000-00001

104. Alt, E. *et al.* Fibroblasts share mesenchymal phenotypes with stem cells, but lack their differentiation and colony-forming potential. *Biol. Cell* (2011). doi:10.1111/j.1768-322X.2011.tb01312.x

105. Denu, R. A. *et al.* Fibroblasts and Mesenchymal Stromal/Stem Cells Are Phenotypically Indistinguishable. *Acta Haematol.* (2016). doi:10.1159/000445096

106. Ghazanfari, R., Li, H., Zacharaki, D., Lim, H. C. & Scheding, S. Human Non-Hematopoietic CD271 ^{pos} /CD140a $^{low/neg}$ Bone Marrow Stroma Cells Fulfill Stringent Stem Cell Criteria in Serial Transplantations. *Stem Cells Dev.* (2016). doi:10.1089/scd.2016.0169

107. Soundararajan, M. & Kannan, S. Fibroblasts and mesenchymal stem cells: Two sides of the same coin? *Journal of Cellular Physiology* (2018). doi:10.1002/jcp.26860

108. Pauziene, N. *et al.* Neuroanatomy of the Pig Cardiac Ventricles. A Stereomicroscopic, Confocal and Electron Microscope Study. *Anat. Rec.* (2017). doi:10.1002/ar.23619

109. Dick, S. A. *et al.* Self-renewing resident cardiac macrophages limit adverse remodeling following myocardial infarction. *Nat. Immunol.* (2019). doi:10.1038/s41590-018-0272-2

110. Swirski, F. K. & Nahrendorf, M. Cardioimmunology: the immune system in cardiac homeostasis and disease. *Nature Reviews Immunology* (2018). doi:10.1038/s41577-018-0065-8

111. Forte, E., Furtado, M. B. & Rosenthal, N. The interstitium in cardiac repair: role of the immune–stromal cell interplay. *Nature Reviews Cardiology* (2018). doi:10.1038/s41569-018-0077-x

112. Hierlihy, A. M., Seale, P., Lobe, C. G., Rudnicki, M. A. & Megeney, L. A. The post-natal heart contains a myocardial stem cell population. *FEBS Lett.* **530**, 239–243 (2002).

113. Storms, R. W., Goodell, M. A., Fisher, A., Mulligan, R. C. & Smith, C. Hoechst dye efflux reveals a novel CD7+CD34-lymphoid progenitor in human umbilical cord blood. *Blood* (2000).

114. Asakura, A., Seale, P., Girgis-Gabardo, A. & Rudnicki, M. A. Myogenic specification of side population cells in skeletal muscle. *J. Cell Biol.* (2002). doi:10.1083/jcb.200202092

115. Iwatani, H. *et al.* Hematopoietic and nonhematopoietic potentials of Hoechst low /side population cells isolated from adult rat kidney. in *Kidney International* (2004). doi:10.1111/j.1523-1755.2004.00561.x

116. Clayton, H., Titley, I. & Vivanco, M. d. M. Growth and differentiation of progenitor/stem cells derived from the human mammary gland. *Exp. Cell Res.* (2004). doi:10.1016/j.yexcr.2004.03.029

117. Summer, R. *et al.* Side population cells and Bcrp1 expression in lung. *Am. J. Physiol. - Lung Cell. Mol. Physiol.* (2003).

118. Pfister, O. *et al.* CD31- but not CD31+ cardiac side population cells exhibit functional cardiomyogenic differentiation. *Circ. Res.* (2005).

doi:10.1161/01.RES.0000173297.53793.fa

119. Oh, H. *et al.* Cardiac progenitor cells from adult myocardium: homing, differentiation, and fusion after infarction. *Proc. Natl. Acad. Sci. U. S. A.* **100**, 12313–8 (2003).

120. Uchida, S. *et al.* Sca1-derived cells are a source of myocardial renewal in the murine adult heart. *Stem Cell Reports* **1**, 397–410 (2013).

121. Chong, J. J. H. *et al.* Adult cardiac-resident MSC-like stem cells with a proepicardial origin. *Cell Stem Cell* **9**, 527–540 (2011).

122. Noseda, M. *et al.* PDGFRα demarcates the cardiogenic clonogenic Sca1+ stem/progenitor cell in adult murine myocardium. *Nat. Commun.* **6**, 1–16 (2015).

123. Smits, A. M. *et al.* Human cardiomyocyte progenitor cells differentiate into functional mature cardiomyocytes: an in vitro model for studying human cardiac physiology and pathophysiology. *Nat. Protoc.* **4**, 232–243 (2009).

124. Sandstedt, J. *et al.* Left atrium of the human adult heart contains a population of side population cells. *Basic Res. Cardiol.* (2012). doi:10.1007/s00395-012-0255-7

125. Beltrami, A. P. *et al.* Adult cardiac stem cells are multipotent and support myocardial regeneration. *Cell* **114**, 763–776 (2003).

126. Li, M. *et al.* c-kit is required for cardiomyocyte terminal differentiation. *Circ. Res.* (2008). doi:10.1161/CIRCRESAHA.107.161737

127. Kubin, T. *et al.* Oncostatin M is a major mediator of cardiomyocyte dedifferentiation and remodeling. *Cell Stem Cell* (2011). doi:10.1016/j.stem.2011.08.013

128. Zhang, Y. *et al.* Dedifferentiation and proliferation of mammalian cardiomyocytes. *PLoS One* (2010). doi:10.1371/journal.pone.0012559

129. Tallini, Y. N. *et al.* c-kit expression identifies cardiovascular precursors in the neonatal heart. *Proc. Natl. Acad. Sci.* (2009). doi:10.1073/pnas.0808920106

130. Kubo, H. *et al.* Increased cardiac myocyte progenitors in failing human hearts.

Circulation (2008). doi:10.1161/CIRCULATIONAHA.107.761031

131. Linke, A. *et al.* Stem cells in the dog heart are self-renewing, clonogenic, and multipotent and regenerate infarcted myocardium, improving cardiac function. *Proc. Natl. Acad. Sci.* (2005). doi:10.1073/pnas.0502678102

132. Hosoda, T. *et al.* Clonality of mouse and human cardiomyogenesis in vivo. *Proc. Natl. Acad. Sci.* (2009). doi:10.1073/pnas.0903089106

133. Leri, A. *et al.* Human cardiac stem cells. in *Microscopy and Microanalysis* (2005). doi:10.1017/S1431927605507517

134. Bearzi, C. *et al.* Identification of a coronary vascular progenitor cell in the human heart. *Proc. Natl. Acad. Sci.* (2009). doi:10.1073/pnas.0907622106

135. Ellison, G. M. *et al.* Adult c-kitpos cardiac stem cells are necessary and sufficient for functional cardiac regeneration and repair. *Cell* **154**, (2013).

136. Berlo, J. H. Van *et al.* C-Kit 1 Cells Minimally Contribute. (2014). doi:10.1038/nature13309

137. Sultana, N. *et al.* Resident c-kit(+) cells in the heart are not cardiac stem cells. *Nat. Commun.* **6**, 8701 (2015).

138. Liu, Q. *et al.* Genetic lineage tracing identifies in situ Kit-expressing cardiomyocytes. *Cell Res.* **26**, 119–130 (2016).

139. Prall, O. W. J. *et al.* An Nkx2-5/Bmp2/Smad1 Negative Feedback Loop Controls Heart Progenitor Specification and Proliferation. *Cell* (2007). doi:10.1016/j.cell.2007.01.042

140. Cai, C. L. *et al.* Isl1 identifies a cardiac progenitor population that proliferates prior to differentiation and contributes a majority of cells to the heart. *Dev. Cell* (2003). doi:10.1016/S1534-5807(03)00363-0

141. Engleka, K. A. *et al.* Islet1 derivatives in the heart are of both neural crest and second

heart field origin. *Circ. Res.* (2012). doi:10.1161/CIRCRESAHA.112.266510

142. Moretti, A. *et al.* Multipotent Embryonic Isl1+ Progenitor Cells Lead to Cardiac, Smooth Muscle, and Endothelial Cell Diversification. *Cell* (2006). doi:10.1016/j.cell.2006.10.029

143. Laugwitz, K. L. *et al.* Postnatal isl1+ cardioblasts enter fully differentiated cardiomyocyte lineages. *Nature* (2005). doi:10.1038/nature03215

144. Weinberger, F. *et al.* Localization of islet-1-positive cells in the healthy and infarcted adult murine heart. *Circ. Res.* (2012). doi:10.1161/CIRCRESAHA.111.259630

145. Lam, J. T., Moretti, A. & Laugwitz, K. L. Multipotent progenitor cells in regenerative cardiovascular medicine. in *Pediatric Cardiology* (2009). doi:10.1007/s00246-009-9450-1

146. Weinberger, F. *et al.* No effect of thymosin beta-4 on the expression of the transcription factor Islet-1 in the adult murine heart. *Pharmacol. Res. Perspect.* (2018). doi:10.1002/prp2.407

147. Foo, K. S. *et al.* Human ISL1 + Ventricular Progenitors Self-Assemble into an In Vivo Functional Heart Patch and Preserve Cardiac Function Post Infarction. *Mol. Ther.* (2018). doi:10.1016/j.ymthe.2018.02.012

148. Menasché, P. *et al.* Transplantation of Human Embryonic Stem Cell–Derived Cardiovascular Progenitors for Severe Ischemic Left Ventricular Dysfunction. *J. Am. Coll. Cardiol.* (2018). doi:10.1016/j.jacc.2017.11.047

149. Messina, E. *et al.* Isolation and expansion of adult cardiac stem cells from human and murine heart. *Circ. Res.* (2004). doi:10.1161/01.RES.0000147315.71699.51

150. Smith, R. R. *et al.* Regenerative potential of cardiosphere-derived cells expanded from percutaneous endomyocardial biopsy specimens. *Circulation* (2007). doi:10.1161/CIRCULATIONAHA.106.655209

151. Lee, S.-T. *et al.* Intramyocardial injection of autologous cardiospheres or cardiosphere-derived cells preserves function and minimizes adverse ventricular remodeling in pigs with heart failure post-myocardial infarction. *J. Am. Coll. Cardiol.* **57**, 455–465 (2011).

152. Yee, K. *et al.* Allogeneic cardiospheres delivered via percutaneous transendocardial injection increase viable myocardium, decrease scar size, and attenuate cardiac dilatation in porcine ischemic cardiomyopathy. *PLoS One* **9**, e113805 (2014).

153. Aminzadeh, M. A. *et al.* Therapeutic efficacy of cardiosphere-derived cells in a transgenic mouse model of non-ischaemic dilated cardiomyopathy. *Eur. Heart J.* **36**, 751–762 (2015).

154. Gallet, R. *et al.* Cardiosphere-Derived Cells Reverse Heart Failure With Preserved Ejection Fraction in Rats by Decreasing Fibrosis and Inflammation. *JACC Basic to Transl. Sci.* **1**, 14–28 (2016).

155. Nana-Leventaki, E. *et al.* Cardiosphere-Derived Cells Attenuate Inflammation, Preserve Systolic Function, and Prevent Adverse Remodeling in Rat Hearts With Experimental Autoimmune Myocarditis. *J. Cardiovasc. Pharmacol. Ther.* **24**, 70–77 (2019).

156. Sun, Y. *et al.* Cadaveric cardiosphere-derived cells can maintain regenerative capacity and improve the heart function of cardiomyopathy. *Cell Cycle* **15**, 1248–1256 (2016).

157. Hosoyama, T. *et al.* Cardiosphere-derived cell sheet primed with hypoxia improves left ventricular function of chronically infarcted heart. *Am. J. Transl. Res.* **7**, 2738–2751 (2015).

158. Ye, J. *et al.* Sca-1+ cardiosphere-derived cells are enriched for Isl1-expressing cardiac precursors and improve cardiac function after myocardial injury. *PLoS One* **7**, e30329 (2012).

159. Martens, A. *et al.* Rhesus monkey cardiosphere-derived cells for myocardial restoration. *Cytotherapy* **13**, 864–872 (2011).

160. Carr, C. . *et al.* Cardiosphere-derived cells improve function in the infarcted rat heart for at least 16 weeks - an mri study. *PLoS One* **6**, (2011).

161. Chan, H. H. L. *et al.* Human Cardiosphere-Derived Cells from Patients with Chronic Ischaemic Heart Disease Can Be Routinely Expanded from Atrial but Not Epicardial Ventricular Biopsies. *J. Cardiovasc. Transl. Res.* **5**, 678–687 (2012).

162. Hsiao, L.-C. *et al.* Murine cardiosphere-derived cells are impaired by age but not by cardiac dystrophic dysfunction. *Stem Cells Dev.* **23**, 1027–36 (2014).

163. Perbellini, F. *et al.* Chronic High-Fat Feeding Affects the Mesenchymal Cell Population Expanded From Adipose Tissue but Not Cardiac Atria. *Stem Cells Transl. Med.* **4**, 1403–1414 (2015).

164. Malliaras, K. *et al.* Intracoronary cardiosphere-derived cells after myocardial infarction: Evidence of therapeutic regeneration in the final 1-year results of the CADUCEUS trial (CArdiosphere-derived aUtologous stem CElls to reverse ventricular dysfunction). *J. Am. Coll. Cardiol.* **63**, (2014).

165. Nakamura, K. & MacLellan, W. R. 41 - Stem Cell-Based and Gene Therapies in Heart Failure. in *Companion to Braunwald's Heart Disease* (eds. Felker, G. M. & Mann, D. L. B. T.-H. F. a C. to B. H. D. (Fourth E.) 599-607.e3 (Content Repository Only!, 2020). doi:https://doi.org/10.1016/B978-0-323-60987-6.00041-7

166. Lupu, I.-E., Redpath, A. N. & Smart, N. Spatiotemporal analysis reveals significant overlap of key proepicardial markers in the developing murine heart. *bioRxiv* (2019). doi:10.1101/666610

167. Smart, N., Dubé, K. N. & Riley, P. R. Epicardial progenitor cells in cardiac regeneration and neovascularisation. *Vascul. Pharmacol.* (2013).

doi:10.1016/j.vph.2012.08.001

168. Masters, M. & Riley, P. R. The epicardium signals the way towards heart regeneration. *Stem Cell Research* (2014). doi:10.1016/j.scr.2014.04.007

169. van Wijk, B., Gunst, Q. D., Moorman, A. F. M. & van den Hoff, M. J. B. Cardiac Regeneration from Activated Epicardium. *PLoS One* **7**, (2012).

170. Lepilina, A. *et al.* A Dynamic Epicardial Injury Response Supports Progenitor Cell Activity during Zebrafish Heart Regeneration. *Cell* (2006). doi:10.1016/j.cell.2006.08.052

171. Smart, N. *et al.* Thymosin β4 facilitates epicardial neovascularization of the injured adult heart. in *Annals of the New York Academy of Sciences* (2010). doi:10.1111/j.1749-6632.2010.05478.x

172. Smart, N. *et al.* De novo cardiomyocytes from within the activated adult heart after injury. *Nature* (2011). doi:10.1038/nature10188

173. Bargehr, J. *et al.* Epicardial cells derived from human embryonic stem cells augment cardiomyocyte-driven heart regeneration. *Nat. Biotechnol.* (2019). doi:10.1038/s41587-019-0197-9

174. Bujak, M. *et al.* Aging-Related Defects Are Associated With Adverse Cardiac Remodeling in a Mouse Model of Reperfused Myocardial Infarction. *J. Am. Coll. Cardiol.* (2008). doi:10.1016/j.jacc.2008.01.011

175. Cahill, T. J., Choudhury, R. P. & Riley, P. R. Heart regeneration and repair after myocardial infarction: Translational opportunities for novel therapeutics. *Nature Reviews Drug Discovery* (2017). doi:10.1038/nrd.2017.106

176. Ellison-Hughes, G. M. & Madeddu, P. Exploring pericyte and cardiac stem cell secretome unveils new tactics for drug discovery. *Pharmacology and Therapeutics* (2017). doi:10.1016/j.pharmthera.2016.11.007

177. Suzuki, E., Fujita, D., Takahashi, M., Oba, S. & Nishimatsu, H. Stem cell-derived exosomes as a therapeutic tool for cardiovascular disease. *World Journal of Stem Cells* (2016). doi:10.4252/wjsc.v8.i9.297

178. Barile, L. *et al.* Extracellular vesicles fromhuman cardiac progenitor cells inhibit cardiomyocyte apoptosis and improve cardiac function aftermyocardial infarction. *Cardiovasc. Res.* (2014). doi:10.1093/cvr/cvu167

179. Gallet, R. *et al.* Exosomes secreted by cardiosphere-derived cells reduce scarring, attenuate adverse remodelling, and improve function in acute and chronic porcine myocardial infarction. *Eur. Heart J.* (2017). doi:10.1093/eurheartj/ehw240

180. Aminzadeh, M. A. *et al.* Exosome-Mediated Benefits of Cell Therapy in Mouse and Human Models of Duchenne Muscular Dystrophy. *Stem cell reports* **10**, 942–955 (2018).

181. Lapchak, P. A., Boitano, P. D., de Couto, G. & Marban, E. Intravenous xenogeneic human cardiosphere-derived cell extracellular vesicles (exosomes) improves behavioral function in small-clot embolized rabbits. *Exp. Neurol.* **307**, 109–117 (2018).

182. Balbi, C. *et al.* Reactivating endogenous mechanisms of cardiac regeneration via paracrine boosting using the human amniotic fluid stem cell secretome. *Int. J. Cardiol.* (2019). doi:10.1016/j.ijcard.2019.04.011

183. Ibrahim, A. G. E., Cheng, K. & Marbán, E. Exosomes as critical agents of cardiac regeneration triggered by cell therapy. *Stem Cell Reports* (2014). doi:10.1016/j.stemcr.2014.04.006

184. Alrefai, M. *et al.* CARDIAC REPAIR USING STEM CELLS CONDITIONED MEDIA BASED THERAPY IN A RODENT MODEL OF MYOCARDIAL INFARCTION AND HEART FAILURE. *Can. J. Cardiol.* **33**, S1 (2017).

185. Vagnozzi, R. J. *et al.* An acute immune response underlies the benefit of cardiac stem-cell therapy. *Nature* (2019). doi:10.1038/s41586-019-1802-2

186. Eschenhagen, T. *et al.* Cardiomyocyte regeneration: A consensus statement. *Circulation* (2017). doi:10.1161/CIRCULATIONAHA.117.029343

187. Ali, S. R. *et al.* Existing cardiomyocytes generate cardiomyocytes at a low rate after birth in mice. *Proc. Natl. Acad. Sci. U. S. A.* (2014). doi:10.1073/pnas.1408233111

188. Kimura, W. *et al.* Hypoxia fate mapping identifies cycling cardiomyocytes in the adult heart. *Nature* (2015). doi:10.1038/nature14582

189. Li, Y. *et al.* Genetic Tracing Identifies Early Segregation of the Cardiomyocyte and Nonmyocyte Lineages. *Circ. Res.* (2019). doi:10.1161/circresaha.119.315280

190. Park, W. S., Ahn, S. Y., Sung, S. I., Ahn, J. Y. & Chang, Y. S. Strategies to enhance paracrine potency of transplanted mesenchymal stem cells in intractable neonatal disorders. *Pediatric Research* (2018). doi:10.1038/pr.2017.249

191. Laflamme, M. A. & Murry, C. E. Regenerating the heart. *Nat. Biotechnol.* (2005). doi:10.1038/nbt1117

192. Müller-Ehmsen, J. *et al.* Survival and development of neonatal rat cardiomyocytes transplanted into adult myocardium. *J. Mol. Cell. Cardiol.* (2002). doi:10.1006/jmcc.2001.1491

193. Hong, K. U. *et al.* A highly sensitive and accurate method to quantify absolute numbers of c-kit+ cardiac stem cells following transplantation in mice. *Basic Res. Cardiol.* (2013). doi:10.1007/s00395-013-0346-0

194. Hong, K. U. *et al.* c-kit+ cardiac stem cells alleviate post-myocardial infarction left ventricular dysfunction despite poor engraftment and negligible retention in the recipient heart. *PLoS One* (2014). doi:10.1371/journal.pone.0096725

195. Traverse, J. H. Using biomaterials to improve the efficacy of cell therapy following

acute myocardial infarction. *Journal of Cardiovascular Translational Research* (2012). doi:10.1007/s12265-011-9330-y

196. Araña, M. *et al.* Preparation and characterization of collagen-based ADSC-carrier sheets for cardiovascular application. *Acta Biomater.* (2013). doi:10.1016/j.actbio.2012.12.014

197. Davis, M. E. *et al.* Local myocardial insulin-like growth factor 1 (IGF-1) delivery with biotinylated peptide nanofibers improves cell therapy for myocardial infarction. *Proc. Natl. Acad. Sci. U. S. A.* (2006). doi:10.1073/pnas.0602877103

198. Laflamme, M. A. *et al.* Cardiomyocytes derived from human embryonic stem cells in pro-survival factors enhance function of infarcted rat hearts. *Nat. Biotechnol.* (2007). doi:10.1038/nbt1327

199. Lo, C. Y. *et al.* Cell surface glycoengineering improves selectin-mediated adhesion of mesenchymal stem cells (MSCs) and cardiosphere-derived cells (CDCs): Pilot validation in porcine ischemia-reperfusion model. *Biomaterials* (2016). doi:10.1016/j.biomaterials.2015.09.026

200. Hung, S. C. *et al.* Short-term exposure of multipotent stromal cells to low oxygen increases their expression of CX3CR1 and CXCR4 and their engraftment in vivo. *PLoS One* (2007). doi:10.1371/journal.pone.0000416

201. Wu, Y., Jin, A., Feng, C., Zhao, Y. & Liu, X. DFO and DMOG up-regulate the expression of CXCR4 in bone marrow mesenchymal stromal cells. *Pharmazie* (2013). doi:10.1691/ph.2013.3550

202. Ceradini, D. J. *et al.* Progenitor cell trafficking is regulated by hypoxic gradients through HIF-1 induction of SDF-1. *Nat. Med.* (2004). doi:10.1038/nm1075

203. Tan, S. C. *et al.* Preconditioning of cardiosphere-derived cells with hypoxia or prolyl-4-hydroxylase inhibitors increases stemness and decreases reliance on oxidative

metabolism. *Cell Transplant.* **25**, 35–53 (2016).

204. Llucià-Valldeperas, A. *et al.* Electromechanical Conditioning of Adult Progenitor Cells Improves Recovery of Cardiac Function After Myocardial Infarction. *Stem Cells Transl. Med.* (2017). doi:10.5966/sctm.2016-0079

205. Gomes, R. S. M. *et al.* Efficient pro-survival/angiogenic miRNA delivery by an MRI-detectable nanomaterial. *ACS Nano* **7**, (2013).

206. Lam, J. K. W., Chow, M. Y. T., Zhang, Y. & Leung, S. W. S. siRNA versus miRNA as therapeutics for gene silencing. *Molecular Therapy - Nucleic Acids* (2015). doi:10.1038/mtna.2015.23

207. Bartel, D. P. MicroRNA Target Recognition and Regulatory Functions. *Cell* **136**, 215–233 (2009).

208. Ha, M. & Kim, V. N. Regulation of microRNA biogenesis. *Nat Rev Mol Cell Biol* **15**, 509–524 (2014).

209. Lee, R. C. The C. elegans Heterochronic Gene lin-4 Encodes Small RNAs with Antisense Complementarity to &II-14. *Cell* **75**, 843–854 (1993).

210. Reinhart, B. J. *et al.* The 21-nucleotide let-7 RNA regulates developmental timing in Caenorhabditis elegans. *Nature* **403**, 901–906 (2000).

211. Cai, Y., Yu, X., Hu, S. & Yu, J. A Brief Review on the Mechanisms of miRNA Regulation. *Genomics, Proteomics Bioinforma.* **7**, 147–154 (2009).

212. Calin, G. A. & Croce, C. M. Chromosomal rearrangements and microRNAs: A new cancer link with clinical implications. *J. Clin. Invest.* **117**, 2059–2066 (2007).

213. Friedman, R. C., Farh, K. K. H., Burge, C. B. & Bartel, D. P. Most mammalian mRNAs are conserved targets of microRNAs. *Genome Res.* **19**, 92–105 (2009).

214. Lujambio, A. & Lowe, S. W. The microcosmos of cancer. *Nature* **482**, 347–355 (2012).

215. Im, H.-I. & Kenny, P. J. MicroRNAs in neuronal function and dysfunction. *Trends Neurosci.* **35**, 325–334 (2017).

216. Lee, Y. *et al.* The nuclear RNase III Drosha initiates microRNA processing. *Nature* **425**, 415–419 (2003).

217. Denli, A. M., Tops, B. B. J., Plasterk, R. H. A., Ketting, R. F. & Hannon, G. J. Processing of primary microRNAs by the Microprocessor complex. *Nature* **432**, 231–235 (2004).

218. Yi, R., Qin, Y., Macara, I. G. & Cullen, B. R. Exportin-5 mediates the nuclear export of pre-microRNAs and short hairpin RNAs. *Genes Dev.* **17**, 3011–3016 (2003).

219. Bohnsack, M. T., Czaplinski, K. & Gorlich, D. Exportin 5 is a RanGTP-dependent dsRNA-binding protein that mediates nuclear export of pre-miRNAs. *RNA* **10**, 185–91 (2004).

220. Hutvágner, G. *et al.* A Cellular Function for the RNA-Interference Enzyme Dicer in the Maturation of the let-7 Small Temporal RNA. *Science (80-.).* **293**, 834 LP – 838 (2001).

221. Ketting, R. F. *et al.* Dicer functions in RNA interference and in synthesis of small RNA involved in developmental timing in C. elegans. *Genes Dev.* **15**, 2654–2659 (2001).

222. Knight, S. W. & Bass, B. L. A Role for the RNase III Enzyme DCR-1 in RNA Interference and Germ Line Development in Caenorhabditis elegans. *Science* **293**, 2269–2271 (2001).

223. Hammond, S. M., Boettcher, S., Caudy, A. A., Kobayashi, R. & Hannon, G. J. Argonaute2, a Link Between Genetic and Biochemical Analyses of RNAi. *Science (80-.).* **293**, 1146 LP – 1150 (2001).

224. Tabara, H. *et al.* The rde-1 Gene, RNA Interference, and Transposon

Silencing in C. elegans. *Cell* **99**, 123–132 (2017).

225. Khvorova, A., Reynolds, A. & Jayasena, S. D. Functional siRNAs and miRNAs Exhibit Strand Bias. *Cell* **115**, 209–216 (2017).

226. Schwarz, D. S. *et al.* Asymmetry in the Assembly of the RNAi Enzyme Complex. *Cell* **115**, 199–208 (2017).

227. O'Brien, J., Hayder, H., Zayed, Y. & Peng, C. Overview of microRNA biogenesis, mechanisms of actions, and circulation. *Frontiers in Endocrinology* (2018). doi:10.3389/fendo.2018.00402

228. Riffo-Campos, Á. L., Riquelme, I. & Brebi-Mieville, P. Tools for sequence-based miRNA target prediction: What to choose? *International Journal of Molecular Sciences* (2016). doi:10.3390/ijms17121987

229. Zhao, Y. *et al.* Dysregulation of Cardiogenesis, Cardiac Conduction, and Cell Cycle in Mice Lacking miRNA-1-2. *Cell* (2007). doi:10.1016/j.cell.2007.03.030

230. Rao, P. K. *et al.* Loss of cardiac microRNA-mediated regulation leads to dilated cardiomyopathy and heart failure. *Circ. Res.* **105**, 585–594 (2009).

231. Xiao, Y., Zhao, J., Tuazon, J. P., Borlongan, C. V. & Yu, G. MicroRNA-133a and Myocardial Infarction. *Cell Transplant.* (2019). doi:10.1177/0963689719843806

232. Katz, M. G., Fargnoli, A. S., Kendle, A. P., Hajjar, R. J. & Bridges, C. R. The role of microRNAs in cardiac development and regenerative capacity. *American Journal of Physiology - Heart and Circulatory Physiology* (2016). doi:10.1152/ajpheart.00181.2015

233. Dorn, G. W., Matkovich, S. J., Eschenbacher, W. H. & Zhang, Y. A human 3′ miR-499 mutation alters cardiac mRNA targeting and function. *Circ. Res.* (2012). doi:10.1161/CIRCRESAHA.111.260752

234. Matkovich, S. J., Hu, Y., Eschenbacher, W. H., Dorn, L. E. & Dorn, G. W. Direct and

indirect involvement of MicroRNA-499 in clinical and experimental cardiomyopathy. *Circ. Res.* (2012). doi:10.1161/CIRCRESAHA.112.265736

235. Boon, R. A. & Dimmeler, S. MicroRNAs in myocardial infarction. *Nature Reviews Cardiology* (2015). doi:10.1038/nrcardio.2014.207

236. Hullinger, T. G. *et al.* Inhibition of miR-15 protects against cardiac ischemic injury. *Circ. Res.* **110**, 71–81 (2012).

237. Bernardo, B. C. *et al.* Therapeutic inhibition of the miR-34 family attenuates pathological cardiac remodeling and improves heart function. *Proc. Natl. Acad. Sci. U. S. A.* (2012). doi:10.1073/pnas.1206432109

238. Qian, L. *et al.* miR-24 inhibits apoptosis and represses Bim in mouse cardiomyocytes. *J. Exp. Med.* (2011). doi:10.1084/jem.20101547

239. Iaconetti, C. *et al.* Inhibition of miR-92a increases endothelial proliferation and migration in vitro as well as reduces neointimal proliferation in vivo after vascular injury. *Basic Res. Cardiol.* (2012). doi:10.1007/s00395-012-0296-y

240. Chen, J. J. & Zhou, S. H. Mesenchymal stem cells overexpressing MiR-126 enhance ischemic angiogenesis via the AKT/ERK-related pathway. *Cardiol. J.* (2011). doi:10.5603/CJ.2011.0032

241. Huang, F. *et al.* Mesenchymal stem cells modified with miR-126 release angiogenic factors and activate Notch ligand Delta-like-4, enhancing ischemic angiogenesis and cell survival. *Int. J. Mol. Med.* (2013). doi:10.3892/ijmm.2012.1200

242. Hu, S. *et al.* Novel MicroRNA prosurvival cocktail for improving engraftment and function of cardiac progenitor cell transplantation. *Circulation* (2011). doi:10.1161/CIRCULATIONAHA.111.017954

243. Hu, S. *et al.* MicroRNA-210 as a Novel Therapy for Treatment of Ischemic Heart Disease. *Circulation* **122**, S124–S131 (2010).

244. Kulshreshtha, R. *et al.* A MicroRNA Signature of Hypoxia . *Mol. Cell. Biol.* **27**, 1859–1867 (2007).

245. Huang, X., Le, Q.-T. & Giaccia, A. J. MiR-210, micromanager of the hypoxia pathway. *Trends Mol. Med.* **16**, 230–237 (2010).

246. Crosby, M. E., Kulshreshtha, R., Ivan, M. & Glazer, P. M. MicroRNA Regulation of DNA Repair Gene Expression in Hypoxic Stress. *Cancer Res.* **69**, 1221–1229 (2009).

247. Camps, C. *et al.* hsa-miR-210 Is Induced by Hypoxia and Is an Independent Prognostic Factor in Breast Cancer. *Clin. Cancer Res.* **14**, 1340 LP – 1348 (2008).

248. Huang, X. *et al.* Hypoxia inducible mir-210 regulates normoxic gene expression involved in tumor initiation. *Mol. Cell* **35**, 856–867 (2009).

249. Won Kim, H., Haider, H. K., Jiang, S. & Ashraf, M. Ischemic Preconditioning Augments Survival of Stem Cells via miR-210 Expression by Targeting Caspase-8-associated Protein 2. *J. Biol. Chem.* **284**, 33161–33168 (2009).

250. Zhang, Z. *et al.* MicroRNA miR-210 modulates cellular response to hypoxia through the MYC antagonist MNT. *Cell Cycle* **8**, 2756–2768 (2009).

251. Lou, Y.-L. *et al.* miR-210 activates notch signaling pathway in angiogenesis induced by cerebral ischemia. *Mol. Cell. Biochem.* **370**, 45–51 (2012).

252. Zeng, L. *et al.* MicroRNA-210 overexpression induces angiogenesis and neurogenesis in the normal adult mouse brain. *Gene Ther.* **21**, 37–43 (2014).

253. Wang, N. *et al.* Mesenchymal stem cells-derived extracellular vesicles, via miR-210, improve infarcted cardiac function by promotion of angiogenesis. *Biochim. Biophys. Acta - Mol. Basis Dis.* **1863**, 2085–2092 (2017).

254. Giannakakis, A. *et al.* miR-210 Links Hypoxia with Cell Cycle Regulation and Is Deleted in Human Epithelial Ovarian Cancer. *Cancer Biol. Ther.* **7**, 255–264 (2008).

255. Chan, S. Y. *et al.* MicroRNA-210 Controls Mitochondrial Metabolism during Hypoxia

by Repressing the Iron-Sulfur Cluster Assembly Proteins ISCU1/2. *Cell Metab.* **10**, 273–284 (2009).

256. Zaccagnini, G. *et al.* Hypoxia-Induced miR-210 Modulates Tissue Response to Acute Peripheral Ischemia. *Antioxid. Redox Signal.* **21**, 1177–1188 (2014).

257. Raitoharju, E. *et al.* MiR-21, miR-210, miR-34a, and miR-146a/b are up-regulated in human atherosclerotic plaques in the Tampere Vascular Study. *Atherosclerosis* **219**, 211–217 (2011).

258. Greco, S. *et al.* MicroRNA dysregulation in diabetic ischemic heart failure patients. *Diabetes* **61**, 1633–1641 (2012).

259. Biswas, S. *et al.* Hypoxia inducible microRNA 210 attenuates keratinocyte proliferation and impairs closure in a murine model of ischemic wounds. *Proc. Natl. Acad. Sci.* **107**, 6976–6981 (2010).

260. Boštjančič, E., Zidar, N. & Glavač, D. MicroRNA Microarray Expression Profiling in Human Myocardial Infarction. *Dis. Markers* **27**, 255–268 (2009).

261. Zaccagnini, G. *et al.* Overexpression of miR-210 and its significance in ischemic tissue damage. *Sci. Rep.* (2017). doi:10.1038/s41598-017-09763-4

262. Mok, Y. *et al.* MiR-210 Is Induced by Oct-2, Regulates B Cells, and Inhibits Autoantibody Production. *J. Immunol.* (2013). doi:10.4049/jimmunol.1301289

263. Okabe, M., Ikawa, M., Kominami, K., Nakanishi, T. & Nishimune, Y. 'Green mice' as a source of ubiquitous green cells. *FEBS Lett.* (1997). doi:10.1016/S0014-5793(97)00313-X

264. Nakano, H. *et al.* Cardiac origin of smooth muscle cells in the inflow tract. *J. Mol. Cell. Cardiol.* (2011). doi:10.1016/j.yjmcc.2010.10.009

265. Madisen, L. *et al.* A robust and high-throughput Cre reporting and characterization system for the whole mouse brain. *Nat. Neurosci.* (2010). doi:10.1038/nn.2467

266. Srinivas, S. *et al.* Cre reporter strains produced by targeted insertion of EYFP and ECFP into the ROSA26 locus. *BMC Dev. Biol.* (2001). doi:10.1186/1471-213X-1-4

267. Claycomb, W. C. *et al.* HL-1 cells: A cardiac muscle cell line that contracts and retains phenotypic characteristics of the adult cardiomyocyte. *Proc. Natl. Acad. Sci. U. S. A.* (1998). doi:10.1073/pnas.95.6.2979

268. Diot, A. *et al.* Validating the RedMIT/GFP-LC3 mouse model by studying mitophagy in autosomal dominant optic atrophy due to the OPA1Q285STOP mutation. *Front. Cell Dev. Biol.* (2018). doi:10.3389/fcell.2018.00103

269. Livak, K. J. & Schmittgen, T. D. Analysis of relative gene expression data using real-time quantitative PCR and the 2-ΔΔCT method. *Methods* (2001). doi:10.1006/meth.2001.1262

270. Bolte, S. & Cordelières, F. P. A guided tour into subcellular colocalization analysis in light microscopy. *Journal of Microscopy* (2006). doi:10.1111/j.1365-2818.2006.01706.x

271. Gavet, O. & Pines, J. Progressive activation of CyclinB1-Cdk1 coordinates entry to mitosis. *Dev. Cell* **18**, 533–543 (2010).

272. Collins, C. L., Bode, B. P., Souba, W. W. & Abcouwer, S. F. Multiwell 14CO2-capture assay for evaluation of substrate oxidation rates of cells in culture. *Biotechniques* (1998).

273. Malandraki-Miller, S. *et al.* Metabolic flux analyses to assess the differentiation of adult cardiac progenitors after fatty acid supplementation. *Stem Cell Res.* **38**, 101458 (2019).

274. Neely, J. R., Denton, R. M., England, P. J. & Randle, P. J. The effects of increased heart work on the tricarboxylate cycle and its interactions with glycolysis in the perfused rat heart. *Biochem. J.* (1972). doi:10.1042/bj1280147

275. Liedtke, A. J., Renstrom, B. & Nellis, S. H. Correlation between [5-3H]glucose and [U-14C]deoxyglucose as markers of glycolysis in reperfused myocardium. *Circ. Res.* (1992). doi:10.1161/01.RES.71.3.689

276. Heather, L. C. *et al.* Differential translocation of the fatty acid transporter, FAT/CD36, and the glucose transporter, GLUT4, coordinates changes in cardiac substrate metabolism during ischemia and reperfusion. *Circ. Hear. Fail.* (2013). doi:10.1161/CIRCHEARTFAILURE.112.000342

277. Barr, R. L. & Lopaschuk, G. D. Methodology for measuring in vitro/ex vivo cardiac energy metabolism. *J. Pharmacol. Toxicol. Methods* (2000). doi:10.1016/S1056-8719(00)00096-4

278. Bott, R. *A Handbook of Mouse Models of Cardiovascular Disease*. *Igarss 2014* (2014). doi:10.1007/s13398-014-0173-7.2

279. Caplan, A. I. All MSCs Are Pericytes? *Cell Stem Cell* (2008). doi:10.1016/j.stem.2008.08.008

280. Murray, I. R. & Péault, B. Q&A: Mesenchymal stem cells - where do they come from and is it important? *BMC Biol.* (2015). doi:10.1186/s12915-015-0212-7

281. Furtado, M. B. *et al.* Cardiogenic genes expressed in cardiac fibroblasts contribute to heart development and repair. *Circ. Res.* **114**, 1422–1434 (2014).

282. Furtado, M. B. *et al.* Microarray profiling to analyse adult cardiac fibroblast identity. *Genomics Data* (2014). doi:10.1016/j.gdata.2014.10.006

283. Skelly, D. A. *et al.* Single-Cell Transcriptional Profiling Reveals Cellular Diversity and Intercommunication in the Mouse Heart. *Cell Rep.* (2018). doi:10.1016/j.celrep.2017.12.072

284. Vicinanza, C. *et al.* Adult cardiac stem cells are multipotent and robustly myogenic: C-kit expression is necessary but not sufficient for their identification. *Cell Death Differ.*

(2017). doi:10.1038/cdd.2017.130

285. Gharaibeh, B. *et al.* Isolation of a slowly adhering cell fraction containing stem cells from murine skeletal muscle by the preplate technique. *Nat. Protoc.* **3**, 1501–1509 (2008).

286. Okada, M. *et al.* Human Skeletal Muscle Cells With a Slow Adhesion Rate After Isolation and an Enhanced Stress Resistance Improve Function of Ischemic Hearts. *Mol. Ther.* **20**, 138–145 (2012).

287. Goumans, M. J. *et al.* TGF-β1 induces efficient differentiation of human cardiomyocyte progenitor cells into functional cardiomyocytes in vitro. *Stem Cell Res.* (2008). doi:10.1016/j.scr.2008.02.003

288. Rota, M. *et al.* Local activation or implantation of cardiac progenitor cells rescues scarred infarcted myocardium improving cardiac function. *Circ. Res.* (2008). doi:10.1161/CIRCRESAHA.108.178525

289. Davis, D. R. *et al.* Isolation and expansion of functionally-competent cardiac progenitor cells directly from heart biopsies. *J. Mol. Cell. Cardiol.* (2010). doi:10.1016/j.yjmcc.2010.02.019

290. Bolli, R. *et al.* Cardiac stem cells in patients with ischaemic cardiomyopathy (SCIPIO): Initial results of a randomised phase 1 trial. *The Lancet* (2011). doi:10.1016/S0140-6736(11)61590-0

291. Urbanek, K. *et al.* Stem cell niches in the adult mouse heart. *Proc. Natl. Acad. Sci. U. S. A.* (2006). doi:10.1073/pnas.0600635103

292. Sanada, F. *et al.* C-kit-positive cardiac stem cells nested in hypoxic niches are activated by stem cell factor reversing the aging myopathy. *Circ. Res.* **114**, 41–55 (2014).

293. Saravanakumar, M. & Devaraj, H. Distribution and homing pattern of c-kit+ Sca-1+

CXCR4+ resident cardiac stem cells in neonatal, postnatal, and adult mouse heart. *Cardiovasc. Pathol.* **22**, 257–263 (2013).

294. Christoffels, V. M. *et al.* Formation of the venous pole of the heart from an Nkx2-5-negative precursor population requires Tbx18. *Circ. Res.* (2006). doi:10.1161/01.RES.0000227571.84189.65

295. Cañete, A. *et al.* A population of hematopoietic stem cells derives from GATA4-expressing progenitors located in the placenta and lateral mesoderm of mice. *Haematologica* (2017). doi:10.3324/haematol.2016.155812

296. Ravikanth, M., Soujanya, P., Manjunath, K., Saraswathi, T. R. & Ramachandran, C. R. Heterogenecity of fibroblasts. *J. Oral Maxillofac. Pathol.* (2011). doi:10.4103/0973-029X.84516

297. Rockey, D. C., Weymouth, N. & Shi, Z. Smooth muscle α actin (Acta2) and myofibroblast function during hepatic wound healing. *PLoS One* (2013). doi:10.1371/journal.pone.0077166

298. Patteson, A. E. *et al.* Vimentin protects the structural integrity of the nucleus and suppresses nuclear damage caused by large deformations. *bioRxiv* (2019). doi:10.1101/566174

299. Kuznetsov, A. V., Javadov, S., Sickinger, S., Frotschnig, S. & Grimm, M. H9c2 and HL-1 cells demonstrate distinct features of energy metabolism, mitochondrial function and sensitivity to hypoxia-reoxygenation. *Biochim. Biophys. Acta - Mol. Cell Res.* (2015). doi:10.1016/j.bbamcr.2014.11.015

300. Geraghty, R. J. *et al.* Guidelines for the use of cell lines in biomedical research. *Br. J. Cancer* (2014). doi:10.1038/bjc.2014.166

301. Motoike, T., Markham, D. W., Rossant, J. & Sato, T. N. Evidence for novel fate of Flk1+ progenitor: Contribution to muscle lineage. *Genesis* (2003).

doi:10.1002/gene.10175

302. Kattman, S. J., Huber, T. L. & Keller, G. M. M. Multipotent Flk-1+ Cardiovascular Progenitor Cells Give Rise to the Cardiomyocyte, Endothelial, and Vascular Smooth Muscle Lineages. *Dev. Cell* (2006). doi:10.1016/j.devcel.2006.10.002

303. Mekala, S. R. *et al.* Generation of cardiomyocytes from vascular adventitia-resident stem cells. *Circ. Res.* (2018). doi:10.1161/CIRCRESAHA.117.312526

304. Zampetaki, A., Kirton, J. P. & Xu, Q. Vascular repair by endothelial progenitor cells. *Cardiovascular Research* (2008). doi:10.1093/cvr/cvn081

305. Liu, Y., Beyer, A. & Aebersold, R. On the Dependency of Cellular Protein Levels on mRNA Abundance. *Cell* (2016). doi:10.1016/j.cell.2016.03.014

306. Acharya, A. *et al.* The bHLH transcription factor Tcf21 is required for lineagespecific EMT of cardiac fibroblast progenitors. *Dev.* (2012). doi:10.1242/dev.079970

307. Kanisicak, O. *et al.* Genetic lineage tracing defines myofibroblast origin and function in the injured heart. *Nat. Commun.* (2016). doi:10.1038/ncomms12260

308. Braitsch, C. M., Kanisicak, O., van Berlo, J. H., Molkentin, J. D. & Yutzey, K. E. Differential expression of embryonic epicardial progenitor markers and localization of cardiac fibrosis in adult ischemic injury and hypertensive heart disease. *J. Mol. Cell. Cardiol.* (2013). doi:10.1016/j.yjmcc.2013.10.005

309. Carmona, R., González-Iriarte, M., Pérez-Pomares, J. M. & Muñoz-Chápuli, R. Localization of the Wilms' tumour protein WT1 in avian embryos. *Cell Tissue Res.* (2001). doi:10.1007/s004410000307

310. Armstrong, J. F., Pritchard-Jones, K., Bickmore, W. A., Hastie, N. D. & Bard, J. B. L. The expression of the Wilms' tumour gene, WT1, in the developing mammalian embryo. *Mech. Dev.* (1993). doi:10.1016/0925-4773(93)90090-K

311. Duim, S. N., Kurakula, K., Goumans, M. J. & Kruithof, B. P. T. Cardiac endothelial

cells express Wilms' tumor-1. Wt1 expression in the developing, adult and infarcted heart. *J. Mol. Cell. Cardiol.* (2015). doi:10.1016/j.yjmcc.2015.02.007

312. Furtado, M. B. *et al.* Cardiogenic genes expressed in cardiac fibroblasts contribute to heart development and repair. *Circ. Res.* (2014). doi:10.1161/CIRCRESAHA.114.302530

313. Sanz-Morejón, A. *et al.* Wilms Tumor 1b Expression Defines a Pro-regenerative Macrophage Subtype and Is Required for Organ Regeneration in the Zebrafish. *Cell Rep.* (2019). doi:10.1016/j.celrep.2019.06.091

314. Webb, S. No role for Oct4 in regenerating adult tissues. *Nat. Reports Stem Cells* (2007). doi:10.1038/stemcells.2007.103

315. Zangrossi, S. *et al.* Oct-4 Expression in Adult Human Differentiated Cells Challenges Its Role as a Pure Stem Cell Marker. *Stem Cells* (2007). doi:10.1634/stemcells.2006-0611

316. Ghaleb, A. M. & Yang, V. W. Krüppel-like factor 4 (KLF4): What we currently know. *Gene* (2017). doi:10.1016/j.gene.2017.02.025

317. Ambady, S. *et al.* Expression of NANOG and NANOGP8 in a variety of undifferentiated and differentiated human cells. *Int. J. Dev. Biol.* (2011). doi:10.1387/ijdb.103192sa

318. Page, R. L. *et al.* Induction of stem cell gene expression in adult human fibroblasts without transgenes. *Cloning Stem Cells* (2009). doi:10.1089/clo.2009.0015

319. White, M. G. *et al.* Pluripotency-associated stem cell marker expression in proliferative cell cultures derived from adult human pancreas. *J. Endocrinol.* (2011). doi:10.1530/JOE-11-0123

320. Wang, G., Zhou, H., Gu, Z., Gao, Q. & Shen, G. Oct4 promotes cancer cell proliferation and migration and leads to poor prognosis associated with the

survivin/STAT3 pathway in hepatocellular carcinoma. *Oncol. Rep.* (2018). doi:10.3892/or.2018.6491

321. Sun, L. *et al.* Transient induction of telomerase expression mediates senescence and reduces tumorigenesis in primary fibroblasts. *Proc. Natl. Acad. Sci. U. S. A.* (2019). doi:10.1073/pnas.1907199116

322. Cannarile, M. A. *et al.* Colony-stimulating factor 1 receptor (CSF1R) inhibitors in cancer therapy. *Journal for ImmunoTherapy of Cancer* (2017). doi:10.1186/s40425-017-0257-y

323. Plein, A., Fantin, A., Denti, L., Pollard, J. W. & Ruhrberg, C. Erythro-myeloid progenitors contribute endothelial cells to blood vessels. *Nature* (2018). doi:10.1038/s41586-018-0552-x

324. Sinha, M. *et al.* Direct conversion of injury-site myeloid cells to fibroblast-like cells of granulation tissue. *Nat. Commun.* (2018). doi:10.1038/s41467-018-03208-w

325. Franzén, O., Gan, L. M. & Björkegren, J. L. M. PanglaoDB: a web server for exploration of mouse and human single-cell RNA sequencing data. *Database (Oxford).* (2019). doi:10.1093/database/baz046

326. Real, C., Glavieux-Pardanaud, C., Vaigot, P., Le Douarin, N. & Dupin, E. The instability of the neural crest phenotypes: Schwann cells can differentiate into myofibroblasts. *Int. J. Dev. Biol.* (2005). doi:10.1387/ijdb.041940cr

327. Petito, R. B. *et al.* Transforming growth factor-β1 may be a key mediator of the fibrogenic properties of neural cells in leprosy. *J. Neuropathol. Exp. Neurol.* (2013). doi:10.1097/NEN.0b013e31828bfc60

328. Bunge, M. B., Wood, P. M., Tynan, L. B., Bates, M. L. & Sanes, J. R. Perineurium originates from fibroblasts: Demonstration in vitro with a retroviral marker. *Science (80-.).* (1989). doi:10.1126/science.2492115

329. Selenius, L. A., Lundgren, M. W., Jawad, R., Danielsson, O. & Björnstedt, M. The cell culture medium affects growth, phenotype expression and the response to selenium cytotoxicity in A549 and Hepg2 cells. *Antioxidants* (2019). doi:10.3390/antiox8050130

330. Kleijkers, S. H. M. *et al.* Differences in gene expression profiles between human preimplantation embryos cultured in two different IVF culture media. *Hum. Reprod.* (2015). doi:10.1093/humrep/dev179

331. Arias, M. E., Ross, P. J. & Felmer, R. N. Culture medium composition affects the gene expression pattern and in vitro development potential of bovine somatic cell nuclear transfer (SCNT) embryos. *Biol. Res.* (2013). doi:10.4067/S0716-97602013000400016

332. Gómez-Mauricio, G. *et al.* Combined administration of mesenchymal stem cells overexpressing IGF-1 and HGF enhances neovascularization but moderately improves cardiac regeneration in a porcine model. *Stem Cell Res. Ther.* **7**, 94 (2016).

333. Engels, M. C. *et al.* Insulin-like growth factor promotes cardiac lineage induction in vitro by selective expansion of early mesoderm. *Stem Cells* (2014). doi:10.1002/stem.1660

334. Ellison, G. M. *et al.* Endogenous cardiac stem cell activation by insulin-like growth factor-1/hepatocyte growth factor intracoronary injection fosters survival and regeneration of the infarcted pig heart. *J. Am. Coll. Cardiol.* (2011). doi:10.1016/j.jacc.2011.05.013

335. Wang, X. *et al.* Intra-myocardial injection of both growth factors and heart derived Sca-1+/CD31- cells attenuates post-MI LV remodeling more than does cell transplantation Alone: Neither intervention enhances functionally significant cardiomyocyte regeneration. *PLoS One* **9**, 1–12 (2014).

336. Zhou, B. *et al.* Adult mouse epicardium modulates myocardial injury by secreting

paracrine factors. *J. Clin. Invest.* (2011). doi:10.1172/JCI45529

337. Ylä-Herttuala, S., Rissanen, T. T., Vajanto, I. & Hartikainen, J. Vascular Endothelial Growth Factors. Biology and Current Status of Clinical Applications in Cardiovascular Medicine. *Journal of the American College of Cardiology* (2007). doi:10.1016/j.jacc.2006.09.053

338. Gan, L. M. *et al.* Intradermal delivery of modified mRNA encoding VEGF-A in patients with type 2 diabetes. *Nat. Commun.* (2019). doi:10.1038/s41467-019-08852-4

339. Zangi, L. *et al.* Modified mRNA directs the fate of heart progenitor cells and induces vascular regeneration after myocardial infarction. *Nat. Biotechnol.* (2013). doi:10.1038/nbt.2682

340. Frantz, S. & Nahrendorf, M. Cardiac macrophages and their role in ischaemic heart disease. *Cardiovascular Research* (2014). doi:10.1093/cvr/cvu025

341. Van Amerongen, M. J., Harmsen, M. C., Van Rooijen, N., Petersen, A. H. & Van Luyn, M. J. A. Macrophage depletion impairs wound healing and increases left ventricular remodeling after myocardial injury in mice. *Am. J. Pathol.* (2007). doi:10.2353/ajpath.2007.060547

342. Zhang, Y. H., He, M., Wang, Y. & Liao, A. H. Modulators of the balance between M1 and M2 macrophages during pregnancy. *Front. Immunol.* (2017). doi:10.3389/fimmu.2017.00120

343. Anzai, A. *et al.* The infarcted myocardium solicits GM-CSF for the detrimental oversupply of inflammatory leukocytes. *J. Exp. Med.* (2017). doi:10.1084/jem.20170689

344. Vieira, J. M. *et al.* The cardiac lymphatic system stimulates resolution of inflammation following myocardial infarction. *J. Clin. Invest.* (2018). doi:10.1172/JCI97192

345. De Couto, G. *et al.* Macrophages mediate cardioprotective cellular postconditioning in

acute myocardial infarction. *J. Clin. Invest.* (2015). doi:10.1172/JCI81321

346. Chimenti, I. *et al.* Relative Roles of Direct Regeneration Versus Paracrine Effects of Human Cardiosphere-Derived Cells Transplanted Into Infarcted Mice. *Circ. Res.* **106**, 971 LP – 980 (2010).

347. Xing, Y. *et al.* microRNA-378 promotes mesenchymal stem cell survival and vascularization under hypoxic-ischemic conditions in vitro. *Stem Cell Res. Ther.* **5**, 130 (2014).

348. Lu, C. *et al.* Serum starvation induces H2AX phosphorylation to regulate apoptosis via p38 MAPK pathway. *FEBS Lett.* (2008). doi:10.1016/j.febslet.2008.06.051

349. King, T. C. Cell Injury, Cellular Responses to Injury, and Cell Death. in *Elsevier's Integrated Pathology* (2007). doi:10.1016/b978-0-323-04328-1.50007-3

350. Guo, K. *et al.* Hypoxia induces the expression of the pro-apoptotic gene BNIP3. *Cell Death Differ.* **8**, 367–376 (2001).

351. Azad, M. B. *et al.* Hypoxia induces autophagic cell death in apoptosis-competent cells through a mechanism involving BNIP3. *Autophagy* (2008). doi:10.4161/auto.5278

352. Kim, J. Y., Ahn, H. J., Ryu, J. H., Suk, K. & Park, J. H. BH3-only Protein Noxa Is a Mediator of Hypoxic Cell Death Induced by Hypoxia-inducible Factor 1α. *J. Exp. Med.* (2004). doi:10.1084/jem.20030613

353. Stempien-Otero, A. *et al.* Mechanisms of hypoxia-induced endothelial cell death: Role of p53 in apoptosis. *J. Biol. Chem.* **274**, 8039–8045 (1999).

354. Malandraki-Miller, S. *et al.* Metabolic flux analyses to assess the differentiation of adult cardiac progenitors after fatty acid supplementation. *Stem Cell Res.* (2019). doi:10.1016/j.scr.2019.101458

355. Potier, E. *et al.* Prolonged hypoxia concomitant with serum deprivation induces massive human mesenchymal stem cell death. *Tissue Eng.* (2007).

doi:10.1089/ten.2006.0325

356. Deschepper, M. *et al.* Survival and function of mesenchymal stem cells (MSCs) depend on glucose to overcome exposure to long-term, severe and continuous hypoxia. *J. Cell. Mol. Med.* (2011). doi:10.1111/j.1582-4934.2010.01138.x

357. Peng, L. *et al.* Comparative analysis of mesenchymal stem cells from bone marrow, cartilage, and adipose tissue. *Stem Cells Dev.* (2008). doi:10.1089/scd.2007.0217

358. Huang, Y. C. *et al.* Isolation of Mesenchymal stem cells from human placental decidua basalis and resistance to hypoxia and serum deprivation. *Stem Cell Rev. Reports* (2009). doi:10.1007/s12015-009-9069-x

359. Liberio, M. S., Sadowski, M. C., Soekmadji, C., Davis, R. A. & Nelson, C. C. Differential effects of tissue culture coating substrates on prostate cancer cell adherence, morphology and behavior. *PLoS One* (2014). doi:10.1371/journal.pone.0112122

360. Huebener, P. *et al.* CD44 Is Critically Involved in Infarct Healing by Regulating the Inflammatory and Fibrotic Response. *J. Immunol.* (2008). doi:10.4049/jimmunol.180.4.2625

361. Suleiman, M., Abdulrahman, N., Yalcin, H. & Mraiche, F. The role of CD44, hyaluronan and NHE1 in cardiac remodeling. *Life Sciences* (2018). doi:10.1016/j.lfs.2018.08.009

362. Sneath, R. J. S. & Mangham, D. C. The normal structure and function of CD44 and its role in neoplasia. *Journal of Clinical Pathology - Molecular Pathology* (1998). doi:10.1136/mp.51.4.191

363. Harris, E. S. & Nelson, W. J. VE-cadherin: At the front, center, and sides of endothelial cell organization and function. *Current Opinion in Cell Biology* (2010). doi:10.1016/j.ceb.2010.07.006

364. Pan, X., Chen, Z., Huang, R., Yao, Y. & Ma, G. Transforming Growth Factor β1 Induces the Expression of Collagen Type I by DNA Methylation in Cardiac Fibroblasts. *PLoS One* (2013). doi:10.1371/journal.pone.0060335

365. Selman, L. & Hansen, S. Structure and function of collectin liver 1 (CL-L1) and collectin 11 (CL-11, CL-K1). *Immunobiology* (2012). doi:10.1016/j.imbio.2011.12.008

366. Sandri, T. L. *et al.* Human collectin-11 (COLEC11) and its synergic genetic interaction with MASP2 are associated with the pathophysiology of Chagas Disease. *PLoS Negl. Trop. Dis.* (2019). doi:10.1371/journal.pntd.0007324

367. Sehgal, A. *et al.* The role of CSF1R-dependent macrophages in control of the intestinal stem-cell niche. *Nat. Commun.* (2018). doi:10.1038/s41467-018-03638-6

368. Lee, M., Lee, Y., Song, J., Lee, J. & Chang, S. Y. Tissue-specific role of CX3CR1 expressing immune cells and their relationships with human disease. *Immune Network* (2018). doi:10.4110/in.2018.18.e5

369. Zheng, J. *et al.* Chemokine receptor CX3CR1 contributes to macrophage survival in tumor metastasis. *Mol. Cancer* (2013). doi:10.1186/1476-4598-12-141

370. Helmke, A. *et al.* CX3CL1–CX3CR1 interaction mediates macrophage-mesothelial cross talk and promotes peritoneal fibrosis. *Kidney Int.* (2019). doi:10.1016/j.kint.2018.12.030

371. Leitinger, B. Discoidin domain receptor functions in physiological and pathological conditions. in *International Review of Cell and Molecular Biology* (2014). doi:10.1016/B978-0-12-800180-6.00002-5

372. Valiathan, R. R., Marco, M., Leitinger, B., Kleer, C. G. & Fridman, R. Discoidin domain receptor tyrosine kinases: New players in cancer progression. *Cancer and Metastasis Reviews* (2012). doi:10.1007/s10555-012-9346-z

373. Molkentin, J. D., Lin, Q., Duncan, S. A. & Olson, E. N. Requirement of the transcription factor GATA4 for heart tube formation and ventral morphogenesis. *Genes Dev.* (1997). doi:10.1101/gad.11.8.1061

374. Watt, A. J., Battle, M. A., Li, J. & Duncan, S. A. GATA4 is essential for formation of the proepicardium and regulates cardiogenesis. *Proc. Natl. Acad. Sci. U. S. A.* (2004). doi:10.1073/pnas.0400752101

375. McFadden, D. G. *et al.* The Hand1 and Hand2 transcription factors regulate expansion of the embryonic cardiac ventricles in a gene dosage-dependent manner. *Development* (2005). doi:10.1242/dev.01562

376. Tsuchihashi, T. *et al.* Hand2 function in second heart field progenitors is essential for cardiogenesis. *Dev. Biol.* (2011). doi:10.1016/j.ydbio.2010.12.023

377. Barnes, R. M. *et al.* Hand2 loss-of-function in hand1-expressing cells reveals distinct roles in epicardial and coronary vessel development. *Circ. Res.* (2011). doi:10.1161/CIRCRESAHA.110.233171

378. Thattaliyath, B. D., Livi, C. B., Steinhelper, M. E., Toney, G. M. & Firulli, A. B. HAND1 and HAND2 are expressed in the adult-rodent heart and are modulated during cardiac hypertrophy. *Biochem. Biophys. Res. Commun.* (2002). doi:10.1016/S0006-291X(02)02297-0

379. Glasscock, E. Kv1.1 channel subunits in the control of neurocardiac function. *Channels (Austin).* (2019). doi:10.1080/19336950.2019.1635864

380. Miki, T. *et al.* Mouse model of Prinzmetal angina by disruption of the inward rectifier Kir6.1. *Nat. Med.* (2002). doi:10.1038/nm0502-466

381. Zingman, L. V., Alekseev, A. E., Hodgson-Zingman, D. M. & Terzic, A. ATP-sensitive potassium channels: Metabolic sensing and cardioprotection. *Journal of Applied Physiology* (2007). doi:10.1152/japplphysiol.00747.2007

382. Tester, D. J. *et al.* Loss-of-function mutations in the KCNJ8-Encoded Kir6.1 KATP channel and sudden infant death syndrome. *Circ. Cardiovasc. Genet.* (2011). doi:10.1161/CIRCGENETICS.111.960195

383. Simons, M., Gordon, E. & Claesson-Welsh, L. Mechanisms and regulation of endothelial VEGF receptor signalling. *Nature Reviews Molecular Cell Biology* (2016). doi:10.1038/nrm.2016.87

384. Lennartsson, J. & Rönnstrand, L. Stem cell factor receptor/c-Kit: From basic Science to clinical implications. *Physiol. Rev.* (2012). doi:10.1152/physrev.00046.2011

385. Roberts, R. & Govender, D. Gene of the month: KIT. *J. Clin. Pathol.* (2015). doi:10.1136/jclinpath-2015-203207

386. Chiplunkar, A. R. *et al.* The Krüppel-like factor 2 and Krüppel-like factor 4 genes interact to maintain endothelial integrity in mouse embryonic vasculogenesis. *BMC Dev. Biol.* (2013). doi:10.1186/1471-213X-13-40

387. Zhang, Y. *et al.* Krüppel-Like Factor 4 Transcriptionally Regulates TGF-β1 and Contributes to Cardiac Myofibroblast Differentiation. *PLoS One* (2013). doi:10.1371/journal.pone.0063424

388. Zhang, P., Andrianakos, R., Yang, Y., Liu, C. & Lu, W. Kruppel-like factor 4 (Klf4) prevents embryonic stem (ES) cell differentiation by regulating Nanog gene expression. *J. Biol. Chem.* (2010). doi:10.1074/jbc.M109.077958

389. Zhang, H., Chen, X. & Sairam, M. R. Novel genes of visceral adiposity: Identification of mouse and human Mesenteric Estrogen-Dependent Adipose (MEDA)-4 gene and its adipogenic function. *Endocrinology* (2012). doi:10.1210/en.2011-2008

390. Stolzing, A. & Grune, T. Neuronal apoptotic bodies: phagocytosis and degradation by primary microglial cells. *FASEB J.* (2004). doi:10.1096/fj.03-0374fje

391. Subramanian, S. V. & Nadal-Ginard, B. Early expression of the different isoforms of

the myocyte enhancer factor-2 (MEF2) protein in myogenic as well as non-myogenic cell lineages during mouse embryogenesis. *Mech. Dev.* (1996). doi:10.1016/0925-4773(96)00542-4

392. Wang, L., Fan, C., Topol, S. E., Topol, E. J. & Wang, Q. Mutation of MEF2A in an Inherited Disorder with Features of Coronary Artery Disease. *Science (80-.).* (2003). doi:10.1126/science.1088477

393. Bi, W., Drake, C. J. & Schwarz, J. J. The transcription factor MEF2C-null mouse exhibits complex vascular malformations and reduced cardiac expression of angiopoietin 1 and VEGF. *Dev. Biol.* (1999). doi:10.1006/dbio.1999.9307

394. Roszer, T. Understanding the mysterious M2 macrophage through activation markers and effector mechanisms. *Mediators of Inflammation* (2015). doi:10.1155/2015/816460

395. Staines, K., Hunt, L. G., Young, J. R. & Butter, C. Evolution of an expanded mannose receptor gene family. *PLoS One* (2014). doi:10.1371/journal.pone.0110330

396. Komata, M., Bando, M., Araki, H. & Shirahige, K. The Direct Binding of Mrc1, a Checkpoint Mediator, to Mcm6, a Replication Helicase, Is Essential for the Replication Checkpoint against Methyl Methanesulfonate-Induced Stress. *Mol. Cell. Biol.* (2009). doi:10.1128/mcb.01934-08

397. Kuek, L. E., Leffler, M., Mackay, G. A. & Hulett, M. D. The MS4A family: Counting past 1, 2 and 3. *Immunology and Cell Biology* (2016). doi:10.1038/icb.2015.48

398. Martinez, F. O., Gordon, S., Locati, M. & Mantovani, A. Transcriptional Profiling of the Human Monocyte-to-Macrophage Differentiation and Polarization: New Molecules and Patterns of Gene Expression. *J. Immunol.* (2006). doi:10.4049/jimmunol.177.10.7303

399. England, J. & Loughna, S. Heavy and light roles: Myosin in the morphogenesis of the

heart. *Cellular and Molecular Life Sciences* (2013). doi:10.1007/s00018-012-1131-1

400. Mullin, N. & Chambers, I. The function of nanog in pluripotency. in *Nuclear Reprogramming and Stem Cells* (2012). doi:10.1007/978-1-61779-225-0_9

401. Gawlik-Rzemieniewska, N. & Bednarek, I. The role of NANOG transcriptional factor in the development of malignant phenotype of cancer cells. *Cancer Biology and Therapy* (2016). doi:10.1080/15384047.2015.1121348

402. Goretzki, L., Burg, M. A., Grako, K. A. & Stallcup, W. B. High-affinity binding of basic fibroblast growth factor and platelet- derived growth factor-AA to the core protein of the NG2 proteoglycan. *J. Biol. Chem.* (1999). doi:10.1074/jbc.274.24.16831

403. Fukushi, J. I., Makagiansar, I. T. & Stallcup, W. B. NG2 proteoglycan promotes endothelial cell motility and angiogenesis via engagement of Galectin-3 and α3β1 integrin. *Mol. Biol. Cell* (2004). doi:10.1091/mbc.E04-03-0236

404. Ampofo, E., Schmitt, B. M., Menger, M. D. & Laschke, M. W. The regulatory mechanisms of NG2/CSPG4 expression. *Cellular & molecular biology letters* (2017). doi:10.1186/s11658-017-0035-3

405. Tanaka, M., Chen, Z., Bartunkova, S., Yamasaki, N. & Izumo, S. The cardiac homeobox gene Csx/Nkx2.5 lies genetically upstream of multiple genes essential for heart development. *Development* (1999).

406. Song, W., Wang, H. & Wu, Q. Atrial natriuretic peptide in cardiovascular biology and disease (NPPA). *Gene* (2015). doi:10.1016/j.gene.2015.06.029

407. Zeineddine, D., Hammoud, A. A., Mortada, M. & Boeuf, H. The Oct4 protein: More than a magic stemness marker. *American Journal of Stem Cells* (2014).

408. Pan, G. J., Chang, Z. Y. I., Schöler, H. R. & Pei, D. Stem cell pluripotency and transcription factor Oct4. *Cell Research* (2002). doi:10.1038/sj.cr.7290134

409. Horikawa, S. *et al.* PDGFRα plays a crucial role in connective tissue remodeling. *Sci.*

Rep. (2015). doi:10.1038/srep17948

410. El-Rass, S. *et al.* Disruption of pdgfra alters endocardial and myocardial fusion during zebrafish cardiac assembly. *Biol. Open* (2017). doi:10.1242/bio.021212

411. Kim, J. *et al.* PDGF signaling is required for epicardial function and blood vessel formation in regenerating zebrafish hearts. *Proc. Natl. Acad. Sci.* **107**, 17206–17210 (2010).

412. Betsholtz, C. Insight into the physiological functions of PDGF through genetic studies in mice. *Cytokine Growth Factor Rev.* (2004). doi:10.1016/j.cytogfr.2004.03.005

413. Takeuchi, H., Kanzawa, T., Kondo, Y. & Kondo, S. Inhibition of platelet-derived growth factor signalling induces autophagy in malignant glioma cells. *Br. J. Cancer* (2004). doi:10.1038/sj.bjc.6601605

414. Wilkinson, S., O'Prey, J., Fricker, M. & Ryan, K. M. Hypoxia-selective macroautophagy and cell survival signaled by autocrine PDGFR activity. *Genes Dev.* (2009). doi:10.1101/gad.521709

415. Hsieh, P. C. H., Davis, M. E., Gannon, J., MacGillivray, C. & Lee, R. T. Controlled delivery of PDGF-BB for myocardial protection using injectable self-assembling peptide nanofibers. *J. Clin. Invest.* (2006). doi:10.1172/JCI25878

416. Yue, Z. *et al.* PDGFR-β Signaling Regulates Cardiomyocyte Proliferation and Myocardial Regeneration. *Cell Rep.* (2019). doi:10.1016/j.celrep.2019.06.065

417. Van Den Akker, N. M. S. *et al.* PDGF-B signaling is important for murine cardiac development: Its role in developing atrioventricular valves, coronaries, and cardiac innervation. *Dev. Dyn.* (2008). doi:10.1002/dvdy.21436

418. Peng, Y., Yan, S., Chen, D., Cui, X. & Jiao, K. Pdgfrb is a direct regulatory target of TGFβ signaling in atrioventricular cushion mesenchymal cells. *PLoS One* (2017). doi:10.1371/journal.pone.0175791

419. Grossi, S. *et al.* Molecular Genetic Analysis of the PLP1 Gene in 38 Families with PLP1-related disorders: Identification and Functional Characterization of 11 Novel PLP1 Mutations. *Orphanet J. Rare Dis.* (2011). doi:10.1186/1750-1172-6-40

420. Alquraini, A. *et al.* The autocrine role of proteoglycan-4 (PRG4) in modulating osteoarthritic synoviocyte proliferation and expression of matrix degrading enzymes. *Arthritis Res. Ther.* (2017). doi:10.1186/s13075-017-1301-5

421. Han, L., Grodzinsky, A. J. & Ortiz, C. Nanomechanics of the Cartilage Extracellular Matrix. *Annu. Rev. Mater. Res.* (2011). doi:10.1146/annurev-matsci-062910-100431

422. Dawes, R. *et al.* Combinations of CD45 Isoforms Are Crucial for Immune Function and Disease. *J. Immunol.* (2006). doi:10.4049/jimmunol.176.6.3417

423. Nakano, A., Harada, T., Morikawa, S. & Kato, Y. Expression of Leukocyte Common Antigen (CD45) on Various Human Leukemia/Lymphoma Cell Lines. *Pathol. Int.* (1990). doi:10.1111/j.1440-1827.1990.tb01549.x

424. Hermiston, M. L., Xu, Z. & Weiss, A. CD45: A Critical Regulator of Signaling Thresholds in Immune Cells. *Annu. Rev. Immunol.* (2003). doi:10.1146/annurev.immunol.21.120601.140946

425. Upadhyay, G. *et al.* Stem cell antigen-1 enhances tumorigenicity by disruption of growth differentiation factor-10 (GDF10)-dependent TGF-β signaling. *Proc. Natl. Acad. Sci. U. S. A.* (2011). doi:10.1073/pnas.1103441108

426. Batts, T. D. *et al.* Stem cell antigen-1 (Sca-1) regulates mammary tumor development and cell migration. *PLoS One* (2011). doi:10.1371/journal.pone.0027841

427. Bradfute, S. B., Graubert, T. A. & Goodell, M. A. Roles of Sca-1 in hematopoietic stem/progenitor cell function. *Exp. Hematol.* (2005). doi:10.1016/j.exphem.2005.04.001

428. Ito, C. Y., Li, C. Y. J., Bernstein, A., Dick, J. E. & Stanford, W. L. Hematopoietic

stem cell and progenitor defects in Sca-1/Ly-6A-null mice. *Blood* (2003). doi:10.1182/blood-2002-06-1918

429. Tandon, P., Miteva, Y. V., Kuchenbrod, L. M., Cristea, I. M. & Conlon, F. L. Tcf21 regulates the specification and maturation of proepicardial cells. *Dev.* (2012). doi:10.1242/dev.093385

430. Yuan, X., Larsson, C. & Xu, D. Mechanisms underlying the activation of TERT transcription and telomerase activity in human cancer: old actors and new players. *Oncogene* (2019). doi:10.1038/s41388-019-0872-9

431. Mattson, M. P., Fu, W. & Zhang, P. Emerging roles for telomerase in regulating cell differentiation and survival: A neuroscientist's perspective. *Mechanisms of Ageing and Development* (2001). doi:10.1016/S0047-6374(01)00221-4

432. Peyvandi, F., Garagiola, I. & Baronciani, L. Role of von Willebrand factor in the haemostasis. *Blood Transfusion* (2011). doi:10.2450/2011.002S

433. Lu, D. *et al.* WIF1 causes dysfunction of heart in transgenic mice. *Transgenic Res.* (2013). doi:10.1007/s11248-013-9738-z

434. Smits, A. M., Dronkers, E. & Goumans, M. J. The epicardium as a source of multipotent adult cardiac progenitor cells: Their origin, role and fate. *Pharmacological Research* (2018). doi:10.1016/j.phrs.2017.07.020

435. Zhao, L. *et al.* Notch signaling regulates cardiomyocyte proliferation during zebrafish heart regeneration. *Proc. Natl. Acad. Sci.* **111**, 1403–1408 (2014).

436. Schildmeyer, L. A. *et al.* Impaired vascular contractility and blood pressure homeostasis in the smooth muscle α-actin null mouse. *FASEB J.* (2000). doi:10.1096/fj.99-0927com

437. Liu, L. *et al.* Amphiregulin enhances cardiac fibrosis and aggravates cardiac dysfunction in mice with experimental myocardial infarction partly through activating

EGFR-dependent pathway. *Basic Res. Cardiol.* (2018). doi:10.1007/s00395-018-0669-y

438. Koeppen, M. *et al.* Hypoxia-inducible factor 2-alpha-dependent induction of amphiregulin dampens myocardial ischemia-reperfusion injury. *Nat. Commun.* (2018). doi:10.1038/s41467-018-03105-2

439. Cross, M. J. & Claesson-Welsh, L. FGF and VEGF function in angiogenesis: Signalling pathways, biological responses and therapeutic inhibition. *Trends in Pharmacological Sciences* (2001). doi:10.1016/S0165-6147(00)01676-X

440. House, S. L. *et al.* Fibroblast growth factor 2 is an essential cardioprotective factor in a closed-chest model of cardiac ischemia-reperfusion injury. *Physiol. Rep.* (2015). doi:10.14814/phy2.12278

441. Rajabi, S. *et al.* Human embryonic stem cell-derived cardiovascular progenitor cells efficiently colonize in bFGF-tethered natural matrix to construct contracting humanized rat hearts. *Biomaterials* (2018). doi:10.1016/j.biomaterials.2017.10.054

442. Takehara, N. *et al.* Controlled Delivery of Basic Fibroblast Growth Factor Promotes Human Cardiosphere-Derived Cell Engraftment to Enhance Cardiac Repair for Chronic Myocardial Infarction. *J. Am. Coll. Cardiol.* (2008). doi:10.1016/j.jacc.2008.06.052

443. Ushikoshi, H. *et al.* Local overexpression of HB-EGF exacerbates remodeling following myocardial infarction by activating noncardiomyocytes. *Lab. Investig.* (2005). doi:10.1038/labinvest.3700282

444. Kanellakis, P., Slater, N. J., Du, X. J., Bobik, A. & Curtis, D. J. Granulocyte colony-stimulating factor and stem cell factor improve endogenous repair after myocardial infarction. *Cardiovasc. Res.* (2006). doi:10.1016/j.cardiores.2006.01.005

445. Wen, Y. T., Huang, T. L., Huang, S. P., Chang, C. H. & Tsai, R. K. Early applications

of granulocyte colony-stimulating factor (G-CSF) can stabilize the blood-optic-nerve barrier and ameliorate inflammation in a rat model of anterior ischemic optic neuropathy (rAION). *DMM Dis. Model. Mech.* (2016). doi:10.1242/dmm.025999

446. Heinen, A. *et al.* IGF1 Treatment Improves Cardiac Remodeling after Infarction by Targeting Myeloid Cells. *Mol. Ther.* (2019). doi:10.1016/j.ymthe.2018.10.020

447. Bach, L. A. Endothelial cells and the IGF system. *Journal of Molecular Endocrinology* (2015). doi:10.1530/JME-14-0215

448. Brade, T. *et al.* Retinoic acid stimulates myocardial expansion by induction of hepatic erythropoietin which activates epicardial Igf2. *Development* (2011). doi:10.1242/dev.054239

449. Li, P. *et al.* IGF signaling directs ventricular cardiomyocyte proliferation during embryonic heart development. *Development* (2011). doi:10.1242/dev.054338

450. Huang, Y. *et al.* Igf Signaling is Required for Cardiomyocyte Proliferation during Zebrafish Heart Development and Regeneration. *PLoS One* (2013). doi:10.1371/journal.pone.0067266

451. Bouchentouf, M. *et al.* Induction of Cardiac Angiogenesis Requires Killer Cell Lectin-Like Receptor 1 and α4β7 Integrin Expression by NK Cells. *J. Immunol.* (2010). doi:10.4049/jimmunol.1001888

452. Bouchentouf, M. *et al.* Interleukin-2 enhances angiogenesis and preserves cardiac function following myocardial infarction. *Cytokine* (2011). doi:10.1016/j.cyto.2011.09.023

453. Dumitriu, I. E., Bullenkamp, J., Chhetri, I. & Kaski, J. C. P275The expansion of pro-inflammatory CD4+CD28null T lymphocytes in myocardial infarction is driven by homeostatic cytokines interleukin-7 (IL-7) and IL-15 and not by inflammatory cytokines. *Cardiovasc. Res.* **114**, S70–S71 (2018).

454. Okazaki, T. *et al.* Macrophage colony-stimulating factor improves cardiac function after ischemic injury by inducing vascular endothelial growth factor production and survival of cardiomyocytes. *Am. J. Pathol.* (2007). doi:10.2353/ajpath.2007.061191

455. Hamilton, T. A., Zhao, C., Pavicic, P. G. & Datta, S. Myeloid colony-stimulating factors as regulators of macrophage polarization. *Front. Immunol.* (2014). doi:10.3389/fimmu.2014.00554

456. Xiang, F. L. *et al.* Cardiomyocyte-specific overexpression of human stem cell factor improves cardiac function and survival after myocardial infarction in mice. *Circulation* (2009). doi:10.1161/CIRCULATIONAHA.108.839068

457. Ishikawa, K. *et al.* Stem cell factor gene transfer improves cardiac function after myocardial infarction in swine. *Circ. Hear. Fail.* (2015). doi:10.1161/CIRCHEARTFAILURE.114.001711

458. Yaniz-Galende, E. *et al.* Stem cell factor gene transfer promotes cardiac repair after myocardial infarction via in situ recruitment and expansion of c-kit+ cells. *Circ. Res.* (2012). doi:10.1161/CIRCRESAHA.111.263830

459. Carlsson, L. *et al.* Biocompatible, Purified VEGF-A mRNA Improves Cardiac Function after Intracardiac Injection 1 Week Post-myocardial Infarction in Swine. *Mol. Ther. - Methods Clin. Dev.* (2018). doi:10.1016/j.omtm.2018.04.003

460. Holmes, D. I. R. & Zachary, I. The vascular endothelial growth factor (VEGF) family: Angiogenic factors in health and disease. *Genome Biology* (2005). doi:10.1186/gb-2005-6-2-209

461. Vivien, C. J. *et al.* Vegfc/d-dependent regulation of the lymphatic vasculature during cardiac regeneration is influenced by injury context. *npj Regen. Med.* (2019). doi:10.1038/s41536-019-0079-2

462. Barleon, B. *et al.* Soluble VEGFR-1 secreted by endothelial cells and monocytes is

present in human serum and plasma from healthy donors. *Angiogenesis* (2001). doi:10.1023/A:1012245307884

463. Bruegmann, E., Gruemmer, R., Neulen, J. & Motejlek, K. Regulation of soluble vascular endothelial growth factor receptor 1 secretion from human endothelial cells by tissue inhibitor of metalloproteinase 1. *Mol. Hum. Reprod.* (2009). doi:10.1093/molehr/gap053

464. Ito, T. K. *et al.* Degradation of soluble VEGF receptor-1 by MMP-7 allows VEGF access to endothelial cells. *Blood* (2009). doi:10.1182/blood-2008-08-172742

465. Singh, N. *et al.* Soluble vascular endothelial growth factor receptor 3 is essential for corneal alymphaticity. *Blood* (2013). doi:10.1182/blood-2012-08-453043

466. Emami-Naeini, P. *et al.* Soluble vascular endothelial growth factor receptor-3 suppresses allosensitization and promotes corneal allograft survival. *Graefe's Arch. Clin. Exp. Ophthalmol.* (2014). doi:10.1007/s00417-014-2749-5

467. Yang, H. *et al.* Soluble vascular endothelial growth factor receptor-3 suppresses lymphangiogenesis and lymphatic metastasis in bladder cancer. *Mol. Cancer* (2011). doi:10.1186/1476-4598-10-36

468. Vogt, C. I. *Untersuchungen über die Entwicklungsgeschichte der Geburtshelferkröte (Alytes obstetricans).* (Jent, 1842).

469. Fuchs, Y. & Steller, H. Live to die another way: Modes of programmed cell death and the signals emanating from dying cells. *Nat. Rev. Mol. Cell Biol.* **16**, 329–344 (2015).

470. Lockshin, R. A. & Williams, C. M. Programmed cell death—II. Endocrine potentiation of the breakdown of the intersegmental muscles of silkmoths. *J. Insect Physiol.* **10**, 643–649 (1964).

471. Tata, J. R. Requirement for RNA and protein synthesis for induced regression of the tadpole tail in organ culture. *Dev. Biol.* **13**, 77–94 (1966).

472. Redza-Dutordoir, M. & Averill-Bates, D. A. Activation of apoptosis signalling pathways by reactive oxygen species. *Biochim. Biophys. Acta - Mol. Cell Res.* **1863**, 2977–2992 (2016).

473. Gibson, S. B. Investigating the role of reactive oxygen species in regulating autophagy. *Methods Enzymol.* **528**, 217–235 (2013).

474. Roos, W. P., Thomas, A. D. & Kaina, B. DNA damage and the balance between survival and death in cancer biology. *Nat. Rev. Cancer* **16**, 20–33 (2015).

475. Guido Kroemer, L. G. A. C. B. Mitochondrial Membrane Permeabilization in Cell Death. *Physiol. Rev.* **87**, 99–163 (2007).

476. Tait, S. W. G. & Green, D. R. Mitochondria and cell death: outer membrane permeabilization and beyond. *Nat. Rev. Mol. Cell Biol.* **11**, 621–632 (2010).

477. Galluzzi, L., Kepp, O. & Kroemer, G. Mitochondrial regulation of cell death: a phylogenetically conserved control. *Microb. Cell* **3**, 101–108 (2016).

478. Czabotar, P. E., Lessene, G., Strasser, A. & Adams, J. M. Control of apoptosis by the BCL-2 protein family: Implications for physiology and therapy. *Nature Reviews Molecular Cell Biology* **15**, 49–63 (2014).

479. Shamas-Din, A., Kale, J., Leber, B. & Andrews, D. W. Mechanisms of action of Bcl-2 family proteins. *Cold Spring Harb. Perspect. Biol.* **5**, 1–21 (2013).

480. Curtin, J. F. & Cotter, T. G. Live and let die: Regulatory mechanisms in Fas-mediated apoptosis. *Cellular Signalling* **15**, 983–992 (2003).

481. Schmitz, I., Kirchhoff, S. & Krammer, P. H. Regulation of death receptor-mediated apoptosis pathways. *International Journal of Biochemistry and Cell Biology* **32**, 1123–1136 (2000).

482. Galluzzi, L. *et al.* Molecular mechanisms of cell death: recommendations of the Nomenclature Committee on Cell Death 2018. *Cell Death Differ.* (2018).

doi:10.1038/s41418-017-0012-4

483. Thornberry, N. A. & Lazebnik, Y. Caspases: Enemies within. *Science* **281**, 1312–1316 (1998).

484. Hengartner, M. O. The biochemistry of apoptosis. *Nature* **407**, 770–776 (2000).

485. Parrino, J., Hotchkiss, R. S. & Bray, M. Prevention of immune cell apoptosis as potential therapeutic strategy for severe infections. *Emerg. Infect. Dis.* **13**, 191–198 (2007).

486. Derakhshan, A., Chen, Z. & Van Waes, C. Therapeutic small molecules target inhibitor of apoptosis proteins in cancers with deregulation of extrinsic and intrinsic cell death pathways. *Clin. Cancer Res.* **23**, 1379–1387 (2017).

487. de Duve, C., Pressman, B. C., Gianetto, R., Wattiaux, R. & Appelmans, F. Tissue fractionation studies. 6. Intracellular distribution patterns of enzymes in rat-liver tissue. *Biochem. J.* **60**, 604–617 (1955).

488. de Duve, C. The lysosome turns fifty. *Nat. Cell Biol.* **7**, 847 (2005).

489. He, C. & Klionsky, D. J. Regulation Mechanisms and Signaling Pathways of Autophagy. *Annu. Rev. Genet.* (2009). doi:10.1146/annurev-genet-102808-114910

490. Hamasaki, M. *et al.* Autophagosomes form at ER-mitochondria contact sites. *Nature* (2013). doi:10.1038/nature11910

491. Dikic, I. & Elazar, Z. Mechanism and medical implications of mammalian autophagy. *Nature Reviews Molecular Cell Biology* **19**, 349–364 (2018).

492. White, E. The role for autophagy in cancer. *J. Clin. Invest.* **125**, 42–46 (2015).

493. Lamming, D. W., Ye, L., Sabatini, D. M. & Baur, J. A. Rapalogs and mTOR inhibitors as anti-aging therapeutics. *J. Clin. Invest.* **123**, 980–989 (2013).

494. Zhou, X.-J. & Zang, H. Autophagy in immunity: Implications in etiology of autoimmune/autoinflammatory diseases. *Autophagy* **8**, 1286–1299 (2012).

495. Menzies, F. M. *et al.* Autophagy and Neurodegeneration: Pathogenic Mechanisms and Therapeutic Opportunities. *Neuron* **93**, 1015–1034 (2017).

496. Kuma, A. *et al.* The role of autophagy during the early neonatal starvation period. *Nature* **432**, 1032 (2004).

497. Nakai, A. *et al.* The role of autophagy in cardiomyocytes in the basal state and in response to hemodynamic stress. *Nat. Med.* **13**, 619 (2007).

498. Wu, X. *et al.* Impaired Autophagy Contributes to Adverse Cardiac Remodeling in Acute Myocardial Infarction. *PLoS One* **9**, e112891 (2014).

499. Denton, D. *et al.* Autophagy, not apoptosis, is essential for midgut cell death in Drosophila. *Curr. Biol.* **19**, 1741–1746 (2009).

500. Clarke, P. G. H. Developmental cell death: morphological diversity and multiple mechanisms. *Anat. Embryol. (Berl).* **181**, 195–213 (1990).

501. Das, G., Shravage, B. V. & Baehrecke, E. H. Regulation and function of autophagy during cell survival and cell death. *Cold Spring Harb. Perspect. Biol.* **4**, 1–14 (2012).

502. Yu, L. *et al.* Regulation of an ATG7-beclin 1 Program of Autophagic Cell Death by Caspase-8. *Science (80-.).* **304**, 1500 LP – 1502 (2004).

503. Shimizu, S. *et al.* Role of Bcl-2 family proteins in a non-apoptotic programmed cell death dependent on autophagy genes. *Nat. Cell Biol.* **6**, 1221 (2004).

504. Liu, B. *et al.* Quantitative assessment of cell fate decision between autophagy and apoptosis. *Sci. Rep.* **7**, 17605 (2017).

505. Matsui, Y. *et al.* Distinct roles of autophagy in the heart during ischemia and reperfusion: Roles of AMP-activated protein kinase and beclin 1 in mediating autophagy. *Circ. Res.* (2007). doi:10.1161/01.RES.0000261924.76669.36

506. Kobayashi, S. *et al.* Transcription factor GATA4 inhibits doxorubicin-induced

autophagy and cardiomyocyte death. *J. Biol. Chem.* (2010). doi:10.1074/jbc.M109.070037

507. Zhu, H. *et al.* Cardiac autophagy is a maladaptive response to hemodynamic stress. *J. Clin. Invest.* **117**, 1782–1793 (2007).

508. Nah, J., Fernández, Á. F., Kitsis, R. N., Levine, B. & Sadoshima, J. Does Autophagy Mediate Cardiac Myocyte Death during Stress? *Circulation Research* (2016). doi:10.1161/CIRCRESAHA.116.309765

509. Chourasia, A. H., Boland, M. L. & Macleod, K. F. Mitophagy and cancer. *Cancer and Metabolism* **3**, (2015).

510. Chen, Y. & Dorn, G. W. PINK1-phosphorylated mitofusin 2 is a parkin receptor for culling damaged mitochondria. *Science (80-.).* (2013). doi:10.1126/science.1231031

511. Pickles, S., Vigié, P. & Youle, R. J. Mitophagy and Quality Control Mechanisms in Mitochondrial Maintenance. *Current Biology* (2018). doi:10.1016/j.cub.2018.01.004

512. Ding, W. X. & Yin, X. M. Mitophagy: Mechanisms, pathophysiological roles, and analysis. *Biological Chemistry* (2012). doi:10.1515/hsz-2012-0119

513. Zhang, J. & Ney, P. A. Role of BNIP3 and NIX in cell death, autophagy, and mitophagy. *Cell Death and Differentiation* (2009). doi:10.1038/cdd.2009.16

514. Sandoval, H. *et al.* Essential role for Nic in autophagic maturation of erythroid cells. *Nature* **454**, 232–235 (2009).

515. Matsushima, M. *et al.* Isolation, mapping, and functional analysis of a novel human cDNA (BNIP3L) encoding a protein homologous to human NIP3. *Genes Chromosom. Cancer* (1998). doi:10.1002/(SICI)1098-2264(199803)21:3<230::AID-GCC7>3.0.CO;2-0

516. Ney, P. A. Mitochondrial autophagy: Origins, significance, and role of BNIP3 and NIX. *Biochim. Biophys. Acta - Mol. Cell Res.* **1853**, 2775–2783 (2015).

517. Bruick, R. K. Expression of the gene encoding the proapoptotic Nip3 protein is induced by hypoxia. *Proc. Natl. Acad. Sci. U. S. A.* **97**, 9082–7 (2000).

518. Kasper, L. H. *et al.* Two transactivation mechanisms cooperate for the bulk of HIF-1-responsive gene expression. *EMBO J.* **24**, 3846–3858 (2005).

519. Dayan, F., Roux, D., Brahimi-Horn, M. C., Pouyssegur, J. & Mazure, N. M. The oxygen sensor factor-inhibiting hypoxia-inducible factor-1 controls expression of distinct genes through the bifunctional transcriptional character of hypoxia-inducible factor-1α. *Cancer Res.* **66**, 3688–3698 (2006).

520. Pouysségur, J., Dayan, F. & Mazure, N. M. Hypoxia signalling in cancer and approaches to enforce tumour regression. *Nature* **441**, 437–443 (2006).

521. Diwan, A. *et al.* Unrestrained erythroblast development in Nix-/- mice reveals a mechanism for apoptotic modulation of erythropoiesis. *Proc. Natl. Acad. Sci. U. S. A.* **104**, 6794–9 (2007).

522. Gálvez, A. S. *et al.* Distinct pathways regulate proapoptotic Nix and BNip3 in cardiac stress. *J. Biol. Chem.* **281**, 1442–1448 (2006).

523. Gomes, L. C., Benedetto, G. Di & Scorrano, L. During autophagy mitochondria elongate, are spared from degradation and sustain cell viability. *Nat. Cell Biol.* **13**, 589–598 (2011).

524. Rambold, A. S., Kostelecky, B., Elia, N. & Lippincott-Schwartz, J. Tubular network formation protects mitochondria from autophagosomal degradation during nutrient starvation. *Proc. Natl. Acad. Sci.* **108**, 10190–10195 (2011).

525. Twig, G. *et al.* Fission and selective fusion govern mitochondrial segregation and elimination by autophagy. *EMBO J.* **27**, 433–446 (2008).

526. Vives-Bauza, C. *et al.* PINK1-dependent recruitment of Parkin to mitochondria in mitophagy. *Proc. Natl. Acad. Sci.* **107**, 378–383 (2010).

527. Narendra, D. P. *et al.* PINK1 is selectively stabilized on impaired mitochondria to activate Parkin. *PLoS Biol.* **8**, (2010).

528. Matsuda, N. *et al.* PINK1 stabilized by mitochondrial depolarization recruits Parkin to damaged mitochondria and activates latent Parkin for mitophagy. *J. Cell Biol.* **189**, 211–221 (2010).

529. Ehses, S. *et al.* Regulation of OPA1 processing and mitochondrial fusion by m-AAA protease isoenzymes and OMA1. *J. Cell Biol.* **187**, 1023–1036 (2009).

530. Head, B., Griparic, L., Amiri, M., Gandre-Babbe, S. & Van Der Bliek, A. M. Inducible proteolytic inactivation of OPA1 mediated by the OMA1 protease in mammalian cells. *J. Cell Biol.* **187**, 959–966 (2009).

531. Chourasia, A. H., Boland, M. L. & Macleod, K. F. Mitophagy and cancer. 1–11 (2015). doi:10.1186/s40170-015-0130-8

532. Sutovsky, P. *et al.* Ubiquitin tag for sperm mitochondria. *Nature* **402**, 371–372 (1999).

533. Sato, M. & Sato, K. Degradation of paternal mitochondria by fertilization-triggered autophagy in C. elegans embryos. *Science (80-.).* **334**, 1141–1144 (2011).

534. Moyzis, A. G., Sadoshima, J. & Gustafsson, Å. B. Mending a broken heart: the role of mitophagy in cardioprotection. *Am. J. Physiol. - Hear. Circ. Physiol.* **308**, H183–H192 (2015).

535. Shiba, Y. *et al.* Allogeneic transplantation of iPS cell-derived cardiomyocytes regenerates primate hearts. *Nature* 1–16 (2016). doi:10.1038/nature19815

536. Qin, Q., Furong, W. & Baosheng, L. Multiple functions of hypoxia-regulated miR-210 in cancer. *J. Exp. Clin. Cancer Res.* **33**, 50 (2014).

537. Tse, A. C.-K., Li, J.-W., Chan, T.-F., Wu, R. S.-S. & Lai, K.-P. Hypoxia induces miR-210, leading to anti-apoptosis in ovarian follicular cells of marine medaka Oryzias melastigma. *Aquat. Toxicol.* **165**, 189–196 (2015).

538. Biswas, S. *et al.* Hypoxia inducible microRNA 210 attenuates keratinocyte proliferation and impairs closure in a murine model of ischemic wounds. *Proc. Natl. Acad. Sci. U. S. A.* **107**, 6976–81 (2010).

539. Fasanaro, P. *et al.* MicroRNA-210 modulates endothelial cell response to hypoxia and inhibits the receptor tyrosine kinase ligand ephrin-A3. *J. Biol. Chem.* **283**, 15878–15883 (2008).

540. Jensen, K., Anderson, J. A. & Glass, E. J. Comparison of small interfering RNA (siRNA) delivery into bovine monocyte-derived macrophages by transfection and electroporation. *Vet. Immunol. Immunopathol.* (2014). doi:10.1016/j.vetimm.2014.02.002

541. Antczak, C., Mahida, J., Singh, C., Calder, P. & Djaballah, H. A High Content Assay to Assess Cellular Fitness. *Comb. Chem. High Throughput Screen.* (2014). doi:10.2174/13862073113169990056

542. Kiriyama, M., Kobayashi, Y., Saito, M., Ishikawa, F. & Yonehara, S. Interaction of FLASH with Arsenite Resistance Protein 2 Is Involved in Cell Cycle Progression at S Phase. *Mol. Cell. Biol.* (2009). doi:10.1128/mcb.00289-09

543. Alm-Kristiansen, A. H. *et al.* FLASH acts as a co-activator of the transcription factor c-Myb and localizes to active RNA polymerase II foci. *Oncogene* (2008). doi:10.1038/onc.2008.105

544. Imai, Y. *et al.* The CED-4-homologous protein FLASH is involved in Fas-mediated activation of caspase-8 during apoptosis. *Nature* (1999). doi:10.1038/19709

545. Shi, Y. Caspase activation, inhibition, and reactivation: a mechanistic view. *Protein Sci.* **13**, 1979–1987 (2004).

546. Thomas, L. W. & Ashcroft, M. Exploring the molecular interface between hypoxia-inducible factor signalling and mitochondria. *Cellular and Molecular Life Sciences*

(2019). doi:10.1007/s00018-019-03039-y

547. Zhang, H. *et al.* Mitochondrial Autophagy Is an HIF-1-dependent Adaptive Metabolic Response to Hypoxia. *J. Biol. Chem.* **283**, 10892–10903 (2008).

548. Fasanaro, P. *et al.* An Integrated Approach for Experimental Target Identification of Hypoxia-induced miR-210. *J. Biol. Chem.* **284**, 35134–35143 (2009).

549. Kelly, T. J., Souza, A. L., Clish, C. B. & Puigserver, P. A Hypoxia-Induced Positive Feedback Loop Promotes Hypoxia-Inducible Factor 1α Stability through miR-210 Suppression of Glycerol-3-Phosphate Dehydrogenase 1-Like . *Mol. Cell. Biol.* **31**, 2696–2706 (2011).

550. Cao, Y. *et al.* Tumor Cells Upregulate Normoxic HIF-1α in Response to Doxorubicin. *Cancer Res.* **73**, 6230–6242 (2013).

551. Kimura, H. *et al.* Hypoxia response element of the human vascular endothelial growth factor gene mediates transcriptional regulation by nitric oxide: control of hypoxia-inducible factor-1 activity by nitric oxide. *Blood* **95**, 189 LP – 197 (2000).

552. Heikal, L., Ghezzi, P., Mengozzi, M. & Ferns, G. Assessment of HIF-1α expression and release following endothelial injury in-vitro and in-vivo. *Mol. Med.* (2018). doi:10.1186/s10020-018-0026-5

553. Moriyama, M. *et al.* BNIP3 upregulation via stimulation of ERK and JNK activity is required for the protection of keratinocytes from UVB-induced apoptosis. *Cell Death Dis.* (2017). doi:10.1038/cddis.2017.4

554. Wang, C. *et al.* MiR-210 facilitates ECM degradation by suppressing autophagy via silencing of ATG7 in human degenerated NP cells. *Biomed. Pharmacother.* **93**, 470–479 (2017).

555. Dolman, N. J., Chambers, K. M., Mandavilli, B., Batchelor, R. H. & Janes, M. S. Tools and techniques to measure mitophagy using fluorescence microscopy.

Autophagy **9**, 1653–1662 (2013).

556. Soutar, M. P. M. *et al.* FBS/BSA media concentration determines CCCP's ability to depolarize mitochondria and activate PINK1-PRKN mitophagy. *Autophagy* **15**, 2002–2011 (2019).

557. Dolman, N. J., Chambers, K. M., Mandavilli, B., Batchelor, R. H. & Janes, M. S. Tools and techniques to measure mitophagy using fluorescence microscopy. *Autophagy* **9**, 1653–1662 (2013).

558. Feng, Y.-M. *et al.* Decreased mitochondrial DNA copy number in the hippocampus and peripheral blood during opiate addiction is mediated by autophagy and can be salvaged by melatonin. *Autophagy* **9**, 1395–1406 (2013).

559. Liao, C. *et al.* Dysregulated mitophagy and mitochondrial organization in optic atrophy due to OPA1 mutations. *Neurology* **88**, 131–142 (2017).

560. Lodge, T. *et al.* Defects in mitochondrial DNA (mtDNA) replication cause mtDNA depletion, increased mtDNA turnover and increased mitophagy. *Neuromuscul. Disord.* **27**, S23–S24 (2017).

561. Diot, A. *et al.* Modulating mitochondrial quality in disease transmission: towards enabling mitochondrial DNA disease carriers to have healthy children. *Biochem. Soc. Trans.* **44**, 1091–1100 (2016).

562. Esteban-Martínez, L., Sierra-Filardi, E. & Boya, P. Mitophagy, metabolism, and cell fate. *Mol. Cell. Oncol.* **4**, e1353854 (2017).

563. McWilliams, T. G. *et al.* Basal Mitophagy Occurs Independently of PINK1 in Mouse Tissues of High Metabolic Demand. *Cell Metab.* (2018). doi:10.1016/j.cmet.2017.12.008

564. Kim, J. W., Tchernyshyov, I., Semenza, G. L. & Dang, C. V. HIF-1-mediated expression of pyruvate dehydrogenase kinase: A metabolic switch required for cellular

adaptation to hypoxia. *Cell Metab.* (2006). doi:10.1016/j.cmet.2006.02.002

565. Papandreou, I., Cairns, R. A., Fontana, L., Lim, A. L. & Denko, N. C. HIF-1 mediates adaptation to hypoxia by actively downregulating mitochondrial oxygen consumption. *Cell Metab.* (2006). doi:10.1016/j.cmet.2006.01.012

566. Favaro, E. *et al.* MicroRNA-210 regulates mitochondrial free radical response to hypoxia and krebs cycle in cancer cells by targeting iron sulfur cluster protein ISCU. *PLoS One* (2010). doi:10.1371/journal.pone.0010345

567. Xiao, Y., Shi, K., Qu, Y., Chu, B. & Qian, Z. Engineering Nanoparticles for Targeted Delivery of Nucleic Acid Therapeutics in Tumor. *Molecular Therapy - Methods and Clinical Development* (2019). doi:10.1016/j.omtm.2018.09.002

568. Constantinides, C. *et al.* Improved cellular uptake of perfluorocarbon nanoparticles for in vivo murine cardiac 19F MRS/MRI and temporal tracking of progenitor cells. *Nanomedicine Nanotechnology, Biol. Med.* 1–11 (2018). doi:S1549963418305525

569. Seoudi, A. M., Lashine, Y. A. & Abdelaziz, A. I. MicroRNA-181a - A tale of discrepancies. *Expert Reviews in Molecular Medicine* (2012). doi:10.1017/S1462399411002122

570. Tsang, J., Zhu, J. & van Oudenaarden, A. MicroRNA-Mediated Feedback and Feedforward Loops Are Recurrent Network Motifs in Mammals. *Mol. Cell* (2007). doi:10.1016/j.molcel.2007.05.018

571. Nakajima, Y. I. & Kuranaga, E. Caspase-dependent non-apoptotic processes in development. *Cell Death and Differentiation* (2017). doi:10.1038/cdd.2017.36

572. Kuranaga, E. & Miura, M. Nonapoptotic functions of caspases: caspases as regulatory molecules for immunity and cell-fate determination. *Trends in Cell Biology* (2007). doi:10.1016/j.tcb.2007.01.001

573. Pradelli, L. A., Villa, E., Zunino, B., Marchetti, S. & Ricci, J. E. Glucose metabolism

is inhibited by caspases upon the induction of apoptosis. *Cell Death Dis.* (2014). doi:10.1038/cddis.2014.371

574. Tagscherer, K. E. *et al.* MicroRNA-210 induces apoptosis in colorectal cancer via induction of reactive oxygen. *Cancer Cell Int.* **16**, 1–12 (2016).

575. Arif, M. *et al.* MicroRNA-210-mediated proliferation, survival, and angiogenesis promote cardiac repair post myocardial infarction in rodents. *J. Mol. Med.* (2017). doi:10.1007/s00109-017-1591-8

576. Gray, W. D. *et al.* Identification of therapeutic covariant microRNA clusters in hypoxia-treated cardiac progenitor cell exosomes using systems biology. *Circ. Res.* (2015). doi:10.1161/CIRCRESAHA.116.304360

577. Kwon, J. J., Factora, T. D., Dey, S. & Kota, J. A Systematic Review of miR-29 in Cancer. *Molecular Therapy - Oncolytics* (2019). doi:10.1016/j.omto.2018.12.011

578. Cao, R. Y. *et al.* The emerging role of MicroRNA-155 in cardiovascular diseases. *BioMed Research International* (2016). doi:10.1155/2016/9869208

579. Si, W., Shen, J., Zheng, H. & Fan, W. The role and mechanisms of action of microRNAs in cancer drug resistance. *Clinical Epigenetics* (2019). doi:10.1186/s13148-018-0587-8

580. Yang, C., Tabatabaei, S. N., Ruan, X. & Hardy, P. The Dual Regulatory Role of MiR-181a in Breast Cancer. *Cellular Physiology and Biochemistry* (2017). doi:10.1159/000485351

581. Magenta, A., Greco, S., Gaetano, C. & Martelli, F. Oxidative stress and microRNAs in vascular diseases. *Int. J. Mol. Sci.* **14**, 17319–17346 (2013).

582. Rakovic, A. *et al.* PINK1-dependent mitophagy is driven by the UPS and can occur independently of LC3 conversion. *Cell Death Differ.* (2019). doi:10.1038/s41418-018-0219-z

583. Ra, E., Lee, S. & Park, B. Possible roles of LC3-independent autophagy in elimination of Shigella in human colon cells (INC4P.343). *J. Immunol.* **194**, 125.22 LP-125.22 (2015).

584. Engedal, N. & Seglen, P. O. Autophagy of cytoplasmic bulk cargo does not require LC3. *Autophagy* (2016). doi:10.1080/15548627.2015.1076606

585. Szalai, P. *et al.* Autophagic bulk sequestration of cytosolic cargo is independent of LC3, but requires GABARAPs. *Exp. Cell Res.* (2015). doi:10.1016/j.yexcr.2015.02.003

586. Orhon, I. & Reggiori, F. Assays to Monitor Autophagy Progression in Cell Cultures. *Cells* **6**, 20 (2017).

587. Diao, H. *et al.* MicroRNA-210 alleviates oxidative stress-associated cardiomyocyte apoptosis by regulating BNIP3. *Biosci. Biotechnol. Biochem.* (2017). doi:10.1080/09168451.2017.1343118

588. Wang, F. *et al.* MiR-210 suppresses BNIP3 to protect against the apoptosis of neural progenitor cells. *Stem Cell Res.* (2013). doi:10.1016/j.scr.2013.04.005

589. Ma, X. *et al.* Loading MiR-210 in Endothelial Progenitor Cells Derived Exosomes Boosts Their Beneficial Effects on Hypoxia/Reoxygeneation-Injured Human Endothelial Cells via Protecting Mitochondrial Function. *Cell. Physiol. Biochem.* **46**, 664–675 (2018).

590. Lakhani, S. A. *et al.* Caspases 3 and 7: Key mediators of mitochondrial events of apoptosis. *Science (80-.).* (2006). doi:10.1126/science.1115035

591. Montava-Garriga, L. & Ganley, I. G. Outstanding Questions in Mitophagy: What We Do and Do Not Know. *Journal of Molecular Biology* (2019). doi:10.1016/j.jmb.2019.06.032

592. McWilliams, T. G. *et al.* Basal Mitophagy Occurs Independently of PINK1 in Mouse

Tissues of High Metabolic Demand. *Cell Metab.* **27**, 439-449.e5 (2018).

593. Rodger, C. E., McWilliams, T. G. & Ganley, I. G. Mammalian mitophagy – from in vitro molecules to in vivo models. *FEBS Journal* (2018). doi:10.1111/febs.14336

594. Gong, G. *et al.* Parkin-mediated mitophagy directs perinatal cardiac metabolic maturation in mice. *Science (80-.).* (2015). doi:10.1126/science.aad2459

595. Folmes, C. D. L. *et al.* Somatic oxidative bioenergetics transitions into pluripotency-dependent glycolysis to facilitate nuclear reprogramming. *Cell Metab.* (2011). doi:10.1016/j.cmet.2011.06.011

596. Zhong, X. *et al.* Mitochondrial Dynamics Is Critical for the Full Pluripotency and Embryonic Developmental Potential of Pluripotent Stem Cells. *Cell Metab.* (2019). doi:10.1016/j.cmet.2018.11.007

597. Xiang, G. *et al.* BNIP3L-dependent mitophagy accounts for mitochondrial clearance during 3 factors-induced somatic cell reprogramming. *Autophagy* (2017). doi:10.1080/15548627.2017.1338545

598. Ying, Q. *et al.* Hypoxia-inducible MicroRNA-210 augments the metastatic potential of tumor cells by targeting vacuole membrane protein 1 in hepatocellular carcinoma. *Hepatology* (2011). doi:10.1002/hep.24614

599. Kanki, T. & Klionsky, D. J. Mitophagy in yeast occurs through a selective mechanism. *J. Biol. Chem.* (2008). doi:10.1074/jbc.M802403200

600. Chen, Z., Li, Y., Zhang, H., Huang, P. & Luthra, R. Hypoxia-regulated microRNA-210 modulates mitochondrial function and decreases ISCU and COX10 expression. *Oncogene* (2010). doi:10.1038/onc.2010.193

601. Qiao, A. *et al.* MicroRNA-210 decreases heme levels by targeting ferrochelatase in cardiomyocytes. *J. Am. Heart Assoc.* **2**, 1–12 (2013).

602. Fong, G. H. & Takeda, K. Role and regulation of prolyl hydroxylase domain proteins.

Cell Death and Differentiation (2008). doi:10.1038/cdd.2008.10

603. D'Angelo, G., Duplan, E., Boyer, N., Vigne, P. & Frelin, C. Hypoxia up-regulates prolyl hydroxylase activity. A feedback mechansim that limits HIF-1 responses during reoxygenation. *J. Biol. Chem.* (2003). doi:10.1074/jbc.M302244200

604. Marxsen, J. H. *et al.* Hypoxia-inducible factor-1 (HIF-1) promotes its degradation by induction of HIF-α-prolyl-4-hydroxylases. *Biochem. J.* (2004). doi:10.1042/BJ20040620

605. Majmundar, A. J., Wong, W. J. & Simon, M. C. Hypoxia-Inducible Factors and the Response to Hypoxic Stress. *Molecular Cell* (2010). doi:10.1016/j.molcel.2010.09.022

606. Sentelle, R. D. *et al.* Ceramide targets autophagosomes to mitochondria and induces lethal mitophagy. *Nat. Chem. Biol.* (2012). doi:10.1038/nchembio.1059

607. Burton, T. R. & Gibson, S. B. The role of Bcl-2 family member BNIP3 in cell death and disease: NIPping at the heels of cell death. *Cell Death and Differentiation* (2009). doi:10.1038/cdd.2008.185

608. Yao, C. H. *et al.* Mitochondrial fusion supports increased oxidative phosphorylation during cell proliferation. *Elife* (2019). doi:10.7554/eLife.41351

609. Song, S. & Hwang, E. A Rise in ATP, ROS, and Mitochondrial Content upon Glucose Withdrawal Correlates with a Dysregulated Mitochondria Turnover Mediated by the Activation of the Protein Deacetylase SIRT1. *Cells* (2018). doi:10.3390/cells8010011

610. Shi, Y. *et al.* Role and mechanism of hypoxia-inducible factor-1 in cell growth and apoptosis of breast cancer cell line MDA-MB-231. *Oncol. Lett.* (2010). doi:10.3892/ol_00000115

611. Thomas, R. & Kim, M. H. HIF-1α: A key survival factor for serum-deprived prostate cancer cells. *Prostate* (2008). doi:10.1002/pros.20808

612. Kim, H. W., Jiang, S., Ashraf, M. & Haider, K. H. Stem cell-based delivery of

Hypoxamir-210 to the infarcted heart: Implications on stem cell survival and preservation of infarcted heart function. *J. Mol. Med.* (2012). doi:10.1007/s00109-012-0920-1

613. Mack, G. S. MicroRNA gets down to business. *Nature Biotechnology* (2007). doi:10.1038/nbt0607-631

614. Yan, J. J. *et al.* MiR-497 suppresses angiogenesis and metastasis of hepatocellular carcinoma by inhibiting VEGFA and AEG-1. *Oncotarget* (2015). doi:10.18632/oncotarget.5012

615. Tu, Y. *et al.* Overexpression of miRNA-497 inhibits tumor angiogenesis by targeting VEGFR2. *Sci. Rep.* (2015). doi:10.1038/srep13827

616. Ribeiro, A., Schoof, C., Izzotti, A., Pereira, L. & Vasques, L. MicroRNAs: Modulators of Cell Identity, and their Applications in Tissue Engineering. *MicroRNA* (2014). doi:10.2174/2211536603666140522003539

617. Gangaraju, V. K. & Lin, H. MicroRNAs: Key regulators of stem cells. *Nature Reviews Molecular Cell Biology* (2009). doi:10.1038/nrm2621

618. Kang, H. Role of micrornas in TGF-β signaling pathway-mediated pulmonary fibrosis. *International Journal of Molecular Sciences* (2017). doi:10.3390/ijms18122527

619. Ivey, K. N. & Srivastava, D. MicroRNAs as regulators of differentiation and cell fate decisions. *Cell Stem Cell* (2010). doi:10.1016/j.stem.2010.06.012

620. Chen, J., Ceholski, D. K., Liang, L., Fish, K. & Hajjar, R. J. Variability in coronary artery anatomy affects consistency of cardiac damage after myocardial infarction in mice. *Am. J. Physiol. - Hear. Circ. Physiol.* (2017). doi:10.1152/ajpheart.00127.2017

621. Mitsos, S., Katsanos, K., Dougeni, E., Koletsis, E. N. & Dougenis, D. A critical appraisal of open- and closed-chest models of experimental myocardial ischemia. *Lab Animal* (2009). doi:10.1038/laban0509-167

622. Lindsey, M. L. *et al.* Guidelines for experimental models of myocardial ischemia and infarction. *Am. J. Physiol. Circ. Physiol.* **314**, H812–H838 (2018).

623. Whittaker, P., Kloner, R. A., Boughner, D. R. & Pickering, J. G. Quantitative assessment of myocardial collagen with picrosirius red staining and circularly polarized light. *Basic Res. Cardiol.* (1994). doi:10.1007/BF00788278

624. Pandya, K., Kim, H. S. & Smithies, O. Fibrosis, not cell size, delineates β-myosin heavy chain reexpression during cardiac hyperthrophy and normal aging in vivo. *Proc. Natl. Acad. Sci. U. S. A.* (2006). doi:10.1073/pnas.0607700103

625. Richards, D. A. *et al.* Distinct Phenotypes Induced by Three Degrees of Transverse Aortic Constriction in Mice. *Sci. Rep.* (2019). doi:10.1038/s41598-019-42209-7

626. Weinheimer, C. J., Lai, L., Kelly, D. P. & Kovacs, A. Novel mouse model of left ventricular pressure overload and infarction causing predictable ventricular remodelling and progression to heart failure. *Clin. Exp. Pharmacol. Physiol.* (2015). doi:10.1111/1440-1681.12318

627. Frobert, A. *et al.* Prognostic value of troponin I for infarct size to improve preclinical myocardial infarction small animal models. *Front. Physiol.* (2015). doi:10.3389/fphys.2015.00353

628. Hallén, J. Troponin for the estimation of infarct size: What have we learned? *Cardiology* (2012). doi:10.1159/000337113

629. Thygesen, K. *et al.* Recommendations for the use of cardiac troponin measurement in acute cardiac care. *European Heart Journal* (2010). doi:10.1093/eurheartj/ehq251

630. Hall, T. S. *et al.* Cardiac troponin i for prediction of clinical outcomes and cardiac function through 3-month follow-up after primary percutaneous coronary intervention for ST-segment elevation myocardial infarction. *Am. Heart J.* (2015). doi:10.1016/j.ahj.2014.10.015

631. Zaitseva, M., Vollenhoven, B. J. & Rogers, P. A. W. In vitro culture significantly alters gene expression profiles and reduces differences between myometrial and fibroid smooth muscle cells. *Mol. Hum. Reprod.* (2006). doi:10.1093/molehr/gal018

632. Neumann, E. *et al.* Cell culture and passaging alters gene expression pattern and proliferation rate in rheumatoid arthritis synovial fibroblasts. *Arthritis Res. Ther.* (2010). doi:10.1186/ar3010

633. Januszyk, M. *et al.* Evaluating the Effect of Cell Culture on Gene Expression in Primary Tissue Samples Using Microfluidic-Based Single Cell Transcriptional Analysis. *Microarrays* (2015). doi:10.3390/microarrays4040540

634. Shen, T. *et al.* Tbx20 regulates a genetic program essential to adult mouse cardiomyocyte function. *J. Clin. Invest.* (2011). doi:10.1172/JCI59472

635. Singh, M. K. *et al.* Tbx20 is essential for cardiac chamber differentiation and repression of Tbx2. *Development* (2005). doi:10.1242/dev.01854

636. Xiang, F. L., Guo, M. & Yutzey, K. E. Overexpression of Tbx20 in adult cardiomyocytes promotes proliferation and improves cardiac function after myocardial infarction. *Circulation* (2016). doi:10.1161/CIRCULATIONAHA.115.019357

637. Han, Z. B. *et al.* Hypoxia-inducible factor (HIF)-1α directly enhances the transcriptional activity of stem cell factor (SCF) in response to hypoxia and epidermal growth factor (EGF). *Carcinogenesis* (2008). doi:10.1093/carcin/bgn066

638. Wang, X. *et al.* HIF-2-dependent expression of stem cell factor promotes metastasis in hepatocellular carcinoma. *Cancer Lett.* (2017). doi:10.1016/j.canlet.2017.01.032

639. Kim, K. L. *et al.* SCF (Stem Cell Factor) and cKIT modulate pathological ocular neovascularization. *Arterioscler. Thromb. Vasc. Biol.* (2019). doi:10.1161/ATVBAHA.119.313179

640. Matsui, J., Wakabayashi, T., Asada, M., Yoshimatsu, K. & Okada, M. Stem Cell

Factor/c-kit Signaling Promotes the Survival, Migration, and Capillary Tube Formation of Human Umbilical Vein Endothelial Cells. *J. Biol. Chem.* (2004). doi:10.1074/jbc.M311643200

641. Goodwin, A. M. In vitro assays of angiogenesis for assessment of angiogenic and anti-angiogenic agents. *Microvascular Research* (2007). doi:10.1016/j.mvr.2007.05.006

642. Norton, K. A. & Popel, A. S. Effects of endothelial cell proliferation and migration rates in a computational model of sprouting angiogenesis. *Sci. Rep.* (2016). doi:10.1038/srep36992

643. Wang, S. *et al.* Control of endothelial cell proliferation and migration by VEGF signaling to histone deacetylase 7. *Proc. Natl. Acad. Sci. U. S. A.* (2008). doi:10.1073/pnas.0802857105

644. Chimenti, I. *et al.* Relative roles of direct regeneration versus paracrine effects of human cardiosphere-derived cells transplanted into infarcted mice. *Circ. Res.* (2010). doi:10.1161/CIRCRESAHA.109.210682

645. Hsiao, S. T. *et al.* Hypoxic conditioning enhances the angiogenic paracrine activity of human adipose-derived stem cells. *Stem Cells Dev.* (2013). doi:10.1089/scd.2012.0602

646. Fierro, F. A. *et al.* Hypoxic pre-conditioning increases the infiltration of endothelial cells into scaffolds for dermal regeneration pre-seeded with mesenchymal stem cells. *Front. Cell Dev. Biol.* (2015). doi:10.3389/fcell.2015.00068

647. Bader, A. M. *et al.* Hypoxic preconditioning increases survival and pro-Angiogenic capacity of human cord blood mesenchymal stromal cells in vitro. *PLoS One* (2015). doi:10.1371/journal.pone.0138477

648. Park, C. Y. *et al.* Cardiac stem cell secretome protects cardiomyocytes from hypoxic injury partly via monocyte chemotactic protein-1-dependent mechanism. *Int. J. Mol. Sci.* **17**, 1–17 (2016).

649. Tang, Y. L. *et al.* Improved graft mesenchymal stem cell survival in ischemic heart with a hypoxia-regulated heme oxygenase-1 vector. *J. Am. Coll. Cardiol.* (2005). doi:10.1016/j.jacc.2005.05.079

650. Creane, M., Howard, L., O'Brien, T. & Coleman, C. M. Biodistribution and retention of locally administered human mesenchymal stromal cells: Quantitative polymerase chain reaction–based detection of human DNA in murine organs. *Cytotherapy* (2017). doi:10.1016/j.jcyt.2016.12.003

651. Tang, J. *et al.* Heart Repair Using Nanogel-Encapsulated Human Cardiac Stem Cells in Mice and Pigs with Myocardial Infarction. *ACS Nano* (2017). doi:10.1021/acsnano.7b01008

652. Behfar, A. *et al.* Optimized delivery system achieves enhanced endomyocardial stem cell retention. *Circ. Cardiovasc. Interv.* (2013). doi:10.1161/CIRCINTERVENTIONS.112.000422

653. Schächinger, V. *et al.* Pilot trial on determinants of progenitor cell recruitment to the infarcted human myocardium. *Circulation* (2008). doi:10.1161/CIRCULATIONAHA.108.777102

654. Lautamäki, R. *et al.* Perfusion defect size predicts engraftment but not early retention of intra-myocardially injected cardiosphere-derived cells after acute myocardial infarction. *Basic Res. Cardiol.* (2011). doi:10.1007/s00395-011-0197-5

655. Lu, L., Zhang, J. Q., Ramires, F. J. & Sun, Y. Molecular and cellular events at the site of myocardial infarction: From the perspective of rebuilding myocardial tissue. *Biochem. Biophys. Res. Commun.* (2004). doi:10.1016/j.bbrc.2004.06.034

656. Honold, J., Assmus, B., Lehman, R., Zeiher, A. M. & Dimmeler, S. Stem cell therapy of cardiac disease: An update. *Nephrology Dialysis Transplantation* (2004). doi:10.1093/ndt/gfh140

657. Hodgkinson, C. P., Bareja, A., Gomez, J. A. & Dzau, V. J. Emerging Concepts in Paracrine Mechanisms in Regenerative Cardiovascular Medicine and Biology. *Circulation Research* (2016). doi:10.1161/CIRCRESAHA.115.305373

658. Simões, F. C. *et al.* Macrophages directly contribute collagen to scar formation during zebrafish heart regeneration and mouse heart repair. *Nat. Commun.* (2020). doi:10.1038/s41467-019-14263-2

659. Liu, Y. W. *et al.* Human embryonic stem cell-derived cardiomyocytes restore function in infarcted hearts of non-human primates. *Nat. Biotechnol.* (2018). doi:10.1038/nbt.4162

660. Chong, J. J. H. *et al.* Human embryonic-stem-cell-derived cardiomyocytes regenerate non-human primate hearts. *Nature* (2014). doi:10.1038/nature13233

661. Sverdlov, E. D. & Mineev, K. Mutation rate in stem cells: An underestimated barrier on the way to therapy. *Trends in Molecular Medicine* (2013). doi:10.1016/j.molmed.2013.01.004

662. Wysoczynski, M. & Bolli, R. A realistic appraisal of the use of embryonic stem cell-based therapies for cardiac repair. *Eur. Heart J.* 1–10 (2019). doi:10.1093/eurheartj/ehz787

663. Bellamy, V. *et al.* Long-term functional benefits of human embryonic stem cell-derived cardiac progenitors embedded into a fibrin scaffold. *J. Hear. Lung Transplant.* (2015). doi:10.1016/j.healun.2014.10.008

664. Kervadec, A. *et al.* Cardiovascular progenitor-derived extracellular vesicles recapitulate the beneficial effects of their parent cells in the treatment of chronic heart failure. *J. Hear. Lung Transplant.* (2016). doi:10.1016/j.healun.2016.01.013

665. Templin, C. *et al.* Transplantation and tracking of human-induced pluripotent stem cells in a pig model of myocardial infarction: Assessment of cell survival, engraftment,

and distribution by hybrid single photon emission computed tomography/computed tomography of sodium iod. *Circulation* (2012). doi:10.1161/CIRCULATIONAHA.111.087684

666. Zhu, K. *et al.* Lack of Remuscularization Following Transplantation of Human Embryonic Stem Cell-Derived Cardiovascular Progenitor Cells in Infarcted Nonhuman Primates. *Circ. Res.* (2018). doi:10.1161/CIRCRESAHA.117.311578

667. Jabbour, R. J., Owen, T. J., Pandey, P. & Harding, S. E. Future potential of engineered heart tissue patches for repairing the damage caused by heart attacks. *Expert Rev. Med. Devices* 1–3 (2019). doi:10.1080/17434440.2020.1700793

668. Audesse, A. J. *et al.* FOXO3 directly regulates an autophagy network to functionally regulate proteostasis in adult neural stem cells. *PLoS Genet.* (2019). doi:10.1371/journal.pgen.1008097

669. Zhang, C. *et al.* PINK1/Parkin-mediated mitophagy was activated against 1,4-enzoquinone-induced apoptosis in HL-60 cells. *Toxicol. Vitr.* **50**, 217–224 (2018).

670. Soutar, M. P. M. *et al.* AKT signalling selectively regulates PINK1 mitophagy in SHSY5Y cells and human iPSC-derived neurons. *Sci. Rep.* **8**, 1–11 (2018).

671. Gómez-Sánchez, R. *et al.* Mitochondrial impairment increases FL-PINK1 levels by calcium-dependent gene expression. *Neurobiol. Dis.* (2014). doi:10.1016/j.nbd.2013.10.021

672. Brown, M. D. & Park, J.-Y. Effects of In Vitro Laminar Shear Stress as an Exercise Mimetic on Endothelial Cell Health. in (2015). doi:10.1007/978-3-319-17076-3_7

673. Minamisawa, S. *et al.* Atrial chamber-specific expression of sarcolipin is regulated during development and hypertrophic remodeling. *J. Biol. Chem.* **278**, 9570–9575 (2003).

674. Vangheluwe, P. *et al.* Sarcolipin and phospholamban mRNA and protein expression in

cardiac and skeletal muscle of different species. *Biochem. J.* **389**, 151–159 (2005).

675. Shimura, D. *et al.* Heterozygous deletion of sarcolipin maintains normal cardiac function. *Am. J. Physiol. - Hear. Circ. Physiol.* (2016). doi:10.1152/ajpheart.00411.2015

676. Tang, J. M. *et al.* VEGF/SDF-1 promotes cardiac stem cell mobilization and myocardial repair in the infarcted heart. *Cardiovasc. Res.* (2011). doi:10.1093/cvr/cvr053

677. Shaner, N. C. *et al.* Improved monomeric red, orange and yellow fluorescent proteins derived from Discosoma sp. red fluorescent protein. *Nat Biotech* **22**, 1567–1572 (2004).

678. Shimura, D., Nakano, A. & Minamisawa, S. Sarcolipin in atrium-specific gene targeting. *Cardiovasc. Regen. Med.* 1–8 (2016). doi:10.14800/crm.1297

679. Sung, K. *et al.* Simplified three-dimensional tissue clearing and incorporation of colorimetric phenotyping. *Sci. Rep.* **6**, 30736 (2016).

680. Nakashima, Y. *et al.* Nkx2-5 suppresses the proliferation of atrial myocytes and conduction system. *Circ. Res.* (2014). doi:10.1161/CIRCRESAHA.114.303219

681. Montagutelli, X. Effect of the genetic background on the phenotype of mouse mutations. *Journal of the American Society of Nephrology* (2000).

682. Professor of Molecular Biology Lee M Silver, P. D. & Silver, L. M. *Mouse Genetics: Concepts and Applications*. (Oxford University Press, 1995).

683. Lévy, J. *et al.* Intestinal inhibition of Atg7 prevents tumour initiation through a microbiome-influenced immune response and suppresses tumour growth. *Nat. Cell Biol.* **17**, 1062 (2015).

684. Ghosh, M. C. *et al.* Deletion of iron regulatory protein 1 causes polycythemia and pulmonary hypertension in mice through translational derepression of HIF2α. *Cell*

Metab. (2013). doi:10.1016/j.cmet.2012.12.016

685. Chung, E. *et al.* Maternal exercise upregulates mitochondrial gene expression and increases enzyme activity of fetal mouse hearts. *Physiol. Rep.* (2017). doi:10.14814/phy2.13184

686. Nytko, K. J. *et al.* Vitamin C is dispensable for oxygen sensing in vivo. *Blood* **117**, 5485–5493 (2011).

687. Ha, S. D. *et al.* Mitochondrial proteins Bnip3 and Bnip3L are involved in anthrax lethal toxin-induced macrophage cell death. *J. Biol. Chem.* (2007). doi:10.1074/jbc.M703668200

688. Gold, W. A. *et al.* Mitochondrial dysfunction in the skeletal muscle of a mouse model of Rett syndrome (RTT): Implications for the disease phenotype. *Mitochondrion* **15**, 10–17 (2014).